

A DESIGN PROGRAMME FOR DILUTE PHASE PNEUMATIC CONVEYORS



KARSTEN H.K. WODRICH

Thesis presented in partial fulfillment of the requirements for the degree of Master of
Engineering at the University of Stellenbosch

Thesis supervisor: Prof. T.W. von Backström

Department of Mechanical Engineering

University of Stellenbosch

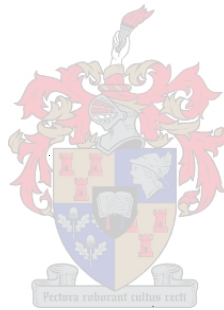
October 1997

DECLARATION

I the undersigned hereby declare that the work contained in this thesis is my own original work and has not previously, in its entirety or in part, been submitted at any university for a degree.

K. Wodri

Signature of candidate



10th day of November 19 97

'n Rekenaarprogram vir die ontwerp van pneumatiese vervoer stelsels vir vaste stowwe word aangebied. Dit behels beide positiewe druk en vakuum pneumatiese vervoer. Die karakteristieke eienskappe van twee-fase vloeï soos die druk en digtheid van die vervoergas, die interpartikulêre en gemiddelde lugsnelheid, partikelsnelheid en pyp volume fraksie ingeneem deur die lug word bereken deur integrasie van vyf beherende differensiaalvergelykings. Die vloeï word in hierdie model as een-dimensioneel langs die pypas benader. Digtheids- en versnellingseffekte word in ag geneem. Die integrasie proses word deur 'n Runge-Kutta-Fehlberg roetine uitgevoer en gee die verloop van die karakteristieke eienskappe langs die volle lengte van die pyplyn.

'n Nuwe metode vir die berekening van die vaste stof wrywingskoëffisient uit die bewegingsvergelyking van die partikels word voorgestel. Vergeleke met metodes wat tot dusver gebruik is laat dit 'n meer akkurate voorspelling van die partikelspoed toe. Die resultate van die simulasië program word met eksperimentele resultate vir sement- en ysvervoer vergelyk en toon 'n goeie ooreenkoms met betrekking tot die uittree veranderlikes.

Die teorie vir die skalering en berekening van die karakteristieke vir Roots-waaïers word gegee. 'n Roots-waaiër seleksie program implementeer die teorie as 'n gedeelte van die ontwerpprogram en word gebruik om die lugtoevoerstelsel vir 'n pneumatiese vervoerder te kies.

'n Vinnige, gebruikersvriendelike skakelvlak in terme van pyplyn geometrie definisie, simulasië en visualisering van die uittree data vir 'n pneumatiese vervoerder is geskep. Die visuele skakelvlak maak gebruik van objek georiënteerde programmering in die programeringstaal DELPHI.

A computer programme for the simulation of dilute phase pneumatic conveying of solids is presented. This includes positive pressure and vacuum pneumatic conveying. The characteristic conveying parameters such as the conveying absolute pressure, conveying air density, interstitial and average air velocity, particle velocity and voidage are calculated by integrating five differential equations that govern two-phase flow. The two-phase flow is approximated as one-dimensional along the pipe axis. Density and acceleration effects are accounted for. The integration is carried out by means of the Runge-Kutta-Fehlberg method yielding conveying parameter traces along the length of the pipeline.

A new method is presented for the determination of the solids friction coefficient from the solids motion equation. This allows for a more accurate determination of the solids velocity in the pipeline when compared to currently used methods. The computer model results are compared to experimental results for cement and ice conveying yielding good correlation for the main output parameters.

The theory for the scaling and calculation of Roots blower performance characteristics is presented. This is implemented in a Roots blower selection programme as an integral part of determining the prime air mover for the design of a pneumatic conveyor.

The aim of providing a fast, user-friendly interface in terms of pipeline geometry input, simulation and data visualisation has been achieved by using the advantages of object orientated programming and the visual user interface of the DELPHI programming language.

Ein Rechnerprogramm zum Entwurf von pneumatischen Dünnstomförderanlagen wird vorgestellt. Dieses beinhaltet beide Druck- und Vakuumförderanlagen. Die Parameter die berechnet werden sind der Druck, die Trägergasdichte, die durchschnittliche Gasgeschwindigkeit sowie die Gasgeschwindigkeit zwischen den Partikeln, die Partikelgeschwindigkeit und der Volumenbruchteil des Gases in der Rohrleitung. Die Parameter werden durch Integration der fünf für die Zweifasenströmung verantwortlichen Differentialgleichungen berechnet. Der Förderstrom wird als eindimensional längs der Rohrachse betrachtet. Dichte und Beschleunigungseffekte werden berücksichtigt. Die numerische Integration wird durch eine Runge-Kutta-Fehlberg Methode vorgenommen. Die Ergebnisse sind Förderparameterspuren die entlang der gesamten Rohrlänge gegeben werden.

Eine neue Methode zur Berechnung des Reibungskoeffizienten aus der Bewegungsgleichung für den festen Stoff wird gegeben. Diese erlaubt eine genauere Berechnung der Partikelgeschwindigkeit im Vergleich mit gebräuchlichen Methoden. Die Resultate des Rechnermodells werden mit experimentellen Resultaten für Zement- und Eisförderung verglichen und zeigen eine gute Übereinstimmung. Die Theorie und Skalierungsmethoden für Drehkolbengebläse werden präsentiert. Diese Berechnungen werden im Rahmen eines kompletten Entwurfes einer pneumatischen Förderanlage als eigenständiges Rechnerprogrammteil zur Selektion von Drehkolbenebläsen verwendet.

Das Ziel eines gebraucherfreundlichen Rechnerprogrammes mit Hinsicht auf die Eingabe der Rohrleitungsgeometrie, Simulation und anschließender Visualisierung der Resultate wird durch die Verwendung von Objektorientierter Programmierung mit Hilfe der DELPHI Programmiersprache erreicht.

ACKNOWLEDGEMENTS

My thanks are extended to Prof. T.W. von Backström for his guidance, assistance and help in solving many of the obstacles that were encountered during the course of the project. His confidence in allowing me to tackle a subject, both in the undergraduate project and the post-graduate thesis, which has not previously been part of the work done at the Department of Mechanical Engineering at the University of Stellenbosch is appreciated.

My gratitude must also be extended to Dr. J.D. Buys of the Mathematics Department for suggesting the method of solution for the two-phase flow differential equations and supplying the references for the computer code.

Mr. H. Schuster was always helpful in his support when programming problems arose and supplied one of the custom written objects used in the user interface of the simulation programme.

Most importantly the support of my parents is greatly appreciated, for without it these studies would not have been possible.

TABLE OF CONTENTS

OPSOMMING	i
ABSTRACT	ii
ZUSAMMENFASSUNG	iii
ACKNOWLEDGEMENTS	iv
TABLE OF CONTENTS	v
LIST OF TABLES	x
LIST OF FIGURES	xii
LIST OF SYMBOLS	xv
CHAPTER ONE:	
1. INTRODUCTION	1
1.1 Introduction to pneumatic conveying	1
1.2 Report structure	3
1.3 Literature review	4
1.3.1 Performance curves for pneumatic conveyors	4
1.3.2 Differential equations governing two phase flow	10
1.3.3 Acceleration pressure drop	10
1.3.4 Bend pressure drop	11
1.3.5 Air alone pressure drop	15
1.3.6 Combined friction pressure loss for air and solid particles	16
1.3.7 Friction coefficient correlation for horizontal flow	18
1.3.8 Particle shape definition	21
1.3.9 The influence of particle shape on the drag coefficient	22
1.3.10 The influence of voidage on the drag coefficient	24
1.3.11 Free fall velocity of particles	24
1.3.12 Methods of pneumatic conveyor design	25
1.4 Discussion and conclusion	28
1.5 Objectives of this thesis	28

CHAPTER TWO:

2. CONVEYING PIPE LAYOUT	30
2.1 Introduction	30
2.2 Chapter contents	30
2.3 Programme requirements	30
2.4 Theory and programme implementation	31
2.4.1 Introduction	31
2.4.2 Aligning a line in three-dimensional space with a coordinate axis	32
2.4.3 Adding components	34
2.4.4 Transforming a line segment from the x-axis back into 3-D space	36
2.4.5 Three-dimensional graphics representation	36
2.5 Component data file	40
2.6 DXF file format	40
2.7 Discussion and conclusion	40

CHAPTER THREE:

3. TWO-PHASE FLOW THEORY	41
3.1 Introduction	41
3.2 Chapter contents	41
3.3 Derivation of the two-phase flow differential equations	41
3.3.1 Continuity equation for the gaseous phase	42
3.3.2 Continuity equation for the solid phase	43
3.3.3 Pressure drop equation	44
3.3.4 Derivation of the equation of motion	49
3.3.5 Equation of state	50
3.4 Derivation of single-phase flow equations	51
3.5 Derivation of the bend friction coefficient	51
3.6 Model for expansions	54
3.7 Conclusion	55

CHAPTER FOUR:

4. SOLUTION METHOD FOR DIFFERENTIAL EQUATIONS	56
4.1 Introduction	56
4.2 Chapter contents	56

4.3 Runge-Kutta-Fehlberg algorithm for solving differential equations	56
4.4 Integration programme verification	58
4.5 Initial conditions and the influence on the final solution	58
4.6 Single to two-phase flow switchover	60
4.7 The difference in pressure and vacuum conveying	61
4.8 Discussion and conclusion	61
CHAPTER FIVE:	
5 SIMULATION RESULTS	64
5.1 Introduction	64
5.2 Chapter contents	64
5.3 Differential equations and friction coefficients	65
5.3.1 Introduction	65
5.3.2 Friction coefficient representation for bend flow	66
5.3.3 Summary of the differential equations used	66
5.4 Comparison of experimental and simulation results for cement	68
5.4.1 Introduction	68
5.4.2 Initial conditions	69
5.4.3 Results for cement using λ_{tot} and λ_s^*	70
5.4.4 Results for cement using λ_{tot} and λ_s'	70
5.4.5 Discussion	75
5.5 The simulated non-dimensional and normalised state diagram for cement	75
5.6 Comparison of experimental and simulation results for tube ice	77
5.6.1 Introduction	77
5.6.2 Air leakage at the feed point	78
5.6.3 Initial conditions for tube ice	79
5.6.4 Bend friction coefficient	79
5.6.5 Results for tube ice conveying using λ_{tot} and λ_s'	80
5.6.6 Discussion	83
5.7 The simulated non-dimensional and normalised state diagram for tube ice	84
5.8 Discussion of the overall results	85
5.9 Conclusion	87
5.10 Recommendation	87

CHAPTER SIX:

6 POSITIVE DISPLACEMENT BLOWERS	89
6.1 Introduction to Roots blowers	89
6.2 Chapter contents	89
6.3 Application to pneumatic conveying	89
6.4 Theory	90
6.4.1 Blower performance calculation	90
6.5 Method for determining leakage coefficient and swept volume	95
6.5.1 Introduction	95
6.5.2 Method	95
6.5.3 Results	96
6.6 Manufacturers performance curve transformation	98
6.6.1 Dimensional analysis and scaling of performance data	98
6.6.2 Comparison of the calculation and transformation method	99
6.7 Application to the pneumatic conveyor design programme	102
6.8 Discussion and conclusion	102

CHAPTER SEVEN

7. CONCLUSION	104
7.1 Introduction	104
7.2 Chapter contents	104
7.3 Friction coefficient implementation	104
7.4 Application to horizontal flow	105
7.5 Application to vertical flow	105
7.6 Bend flow model	105
7.7 Expansion model	106
7.8 Calculation of particle drag coefficients	106
7.9 Blower selection calculations	106
7.10 Design programme implementation	107
7.11 Summary with reference to the objectives of the thesis	107
7.12 Recommendation for future work	108

REFERENCES:

APPENDICES:

APPENDIX A: PIPE LAYOUT DATA FILE FORMAT	A1
APPENDIX B: ADDITIONAL EQUATION DERIVATION	B1
B.1 Alternate representation of the governing equations for two-phase flow	B1
B.2 Equation for flow of particles along a bend wall	B5
APPENDIX C: CALCULATION METHODS AND SAMPLE CALCULATIONS	C1
C.1 Sphericity determination for cement	C1
C.2 Cement friction coefficient correlation method	C2
C.3 Sphericity determination for tube ice	C11
C.4 Ice friction coefficient correlation method	C12
C.5 Roots blower sample calculations	C18
APPENDIX D: SIMULATION DATA	D1
D.1 Initial condition for cement conveying	D1
D.2 Results for the conveying simulations with cement using λ_{tot} and λ_s^*	D2
D.3 Results for the conveying simulations with cement using λ_{tot} and λ_s'	D8
D.4 State diagram data for cement	D14
D.5 Initial conditions for tube ice conveying	D16
D.6 Bend friction coefficient data	D16
D.7 Results for the conveying simulations with tube using λ_{tot} and λ_s'	D17
D.8 State diagram data for tube ice	D23
APPENDIX E: PROGRAMME USER MANUAL	E1
APPENDIX F: DIRECTORY STRUCTURE AND PROGRAMME	
FLOWCHART	F1
F.1 File directory structure	F1
APPENDIX G: RUNGE-KUTTA-FEHLBERG PROGRAMME LISTING	G1

 LIST OF TABLES

CHAPTER 1

Tab. 1.1 Expressions for solids and total friction coefficients for horizontal dilute phase flows	19
Tab. 1.2 Sphericity data	22

CHAPTER 4

Tab. 4.1 Comparison of the solutions to the Blasius flat-plate flow differential equations	62
--	----

APPENDIX A

Tab. A.1: Sample data file for pipe layout in figure A.1	A4
--	----

APPENDIX C

Tab. C.1 Data used for the friction coefficient correlation for cement	C15
Tab. C.2 Determination of leakage coefficient and swept volume: HIBON XN 4.5	C24
Tab. C.3 Roots blower performance prediction: HIBON XN 4.5	C25
Tab. C.4 Scaled and calculated blower performance prediction: HIBON XN 4.5	C26

APPENDIX D

Tab. D.1.1 Pressure ratio vs. initial solids Froude number for cement using λ_{tot} and λ_s^*	D1
Tab. D.1.2 Pressure ratio vs. initial solids Froude number for cement using λ_{tot} and λ_s'	D1
Tab. D.2.1 Results for cement conveying at $\dot{G} = 273$ kg/h with λ_{tot} and λ_s^*	D2
Tab. D.2.2 Results for cement conveying at $\dot{G} = 723$ kg/h with λ_{tot} and λ_s^*	D3
Tab. D.2.3 Results for cement conveying at $\dot{G} = 1002$ kg/h with λ_{tot} and λ_s^*	D4
Tab. D.2.4 Results for cement conveying at $\dot{G} = 1423$ kg/h with λ_{tot} and λ_s^*	D5
Tab. D.3.1 Results for cement conveying at $\dot{G} = 273$ kg/h with λ_{tot} and λ_s'	D8
Tab. D.3.2 Results for cement conveying at $\dot{G} = 723$ kg/h with λ_{tot} and λ_s'	D9
Tab. D.3.3 Results for cement conveying at $\dot{G} = 1002$ kg/h with λ_{tot} and λ_s'	D10
Tab. D.3.4 Results for cement conveying at $\dot{G} = 1423$ kg/h with λ_{tot} and λ_s'	D11

Tab. D. 4.1 Normalised and non-dimensional state diagram data for cement using λ_{tot} and λ_s^*	D14
Tab. D. 4.2 Normalised and non-dimensional state diagram data for cement using λ_{tot} and λ_s'	D15
Tab. D.5.1 Pressure ratio vs. initial solids Froude number for tube ice using λ_{tot} and λ_s'	D16
Tab. D.6.1 Sliding friction coefficients for bend flow in a 136 mm diameter uPVC pipe	D16
Tab. D.7.1 Results for tube ice conveying at $\dot{G} = 9360$ kg/h using λ_{tot} and λ_s'	D17
Tab. D.7.2 Results for tube ice conveying at $\dot{G} = 13100$ kg/h using λ_{tot} and λ_s'	D18
Tab. D.7.3 Results for tube ice conveying at $\dot{G} = 16200$ kg/h using λ_{tot} and λ_s'	D19
Tab. D.7.4 Results for tube ice conveying at $\dot{G} = 22300$ kg/h using λ_{tot} and λ_s'	D20
Tab. D.8.1 Normalised and non-dimensional simulated state diagram for ice using λ_{tot} and λ_s'	D23

 LIST OF FIGURES

CHAPTER	PAGE:
CHAPTER 1	
Fig. 1.1 Types of pneumatic conveying systems	2
Fig. 1.2 Flow patterns for fine particles in dilute phase horizontal conveying	5
Fig. 1.3 General state diagram for horizontal conveying	5
Fig. 1.4 General state diagram for polyethylene pellets	6
Fig. 1.5 Zenz and Othmer state diagram for polyethylene pellets	7
Fig. 1.6 Dimensionless state diagram for polyethylene pellets	8
Fig. 1.7 Conveying characteristics for cement	9
Fig. 1.8 Definition of bend geometry angles for a bend in the vertical plane	13
Fig. 1.9 Bend pressure drop determination	14
CHAPTER 2	
Fig. 2.1 Line segment end coordinate transformation	33
Fig. 2.2 Adding a bend segment	35
Fig. 2.3 Coordinate system transformation	37
Fig. 2.4 Coordinate system notation	38
Fig. 2.5 Example of the pipe layout generation interface	39
CHAPTER 3	
Fig. 3.1 Model of two-phase flow	42
Fig. 3.2 Particle velocity and distance relationship	45
Fig. 3.3 Buoyancy and gravity forces on a single particle	46
Fig. 3.4 Particle flow in a bend in the vertical plane	52
Fig. 3.5 Definition of bend angles for bends in a vertical plane	53
CHAPTER 4	
Fig. 4.1 Influence of the initial solids velocity on the simulation solution	60
CHAPTER 5	
Fig. 5.1 Pipe layout used for cement conveying experiments and simulation	68
Fig. 5.2 Pressure ratio vs. initial solids Froude number for cement using λ_{tot} and λ_s^*	69

Fig. 5.3 Pressure ratio vs. initial solids Froude number for cement using λ_{tot} and λ_s'	70
Fig. 5.4 Comparison of experimental and simulated data for cement at $\dot{G} = 273$ kg/h	71
Fig. 5.5 Comparison of experimental and simulated data for cement at $\dot{G} = 723$ kg/h	71
Fig. 5.6 Comparison of experimental and simulated data for cement at $\dot{G} = 1002$ kg/h	72
Fig. 5.7 Comparison of experimental and simulated data for cement at $\dot{G} = 1432$ kg/h	72
Fig. 5.8 Comparison of experimental and simulated data for cement $\dot{G} = 273$ kg/h	73
Fig. 5.9 Comparison of experimental and simulated data for cement $\dot{G} = 723$ kg/h	73
Fig. 5.10 Comparison of experimental and simulated data for cement $\dot{G} = 1002$ kg/h	74
Fig. 5.11 Comparison of experimental and simulated data for cement $\dot{G} = 1432$ kg/h	74
Fig. 5.12 Simulated non-dimensional state diagram for cement	76
Fig. 5.13 Simulated normalised state diagram for cement	77
Fig. 5.14 Pipe layout used for ice conveying experiments and simulation	78
Fig. 5.15 Pressure ratio vs. initial solids Froude number for tube ice using λ_{tot} and λ_s'	79
Fig. 5.16 Comparison of experimental and simulated data for tube ice $\dot{G} = 9360$ kg/h	81
Fig. 5.17 Comparison of experimental and simulated data for tube ice $\dot{G} = 13100$ kg/h	81
Fig. 5.18 Comparison of experimental and simulated data for tube ice $\dot{G} = 16200$ kg/h	82
Fig. 5.19 Comparison of experimental and simulated data for tube ice $\dot{G} = 22300$ kg/h	82
Fig. 5.20 Simulated non-dimensional state diagram for tube ice	84
Fig. 5.21 Simulated normalised state diagram for tube ice	85
 CHAPTER 6	
Fig. 6.1 Physical and analytic Roots blower configuration	91
Fig. 6.2 Blower performance prediction: inlet volume flow rate	97
Fig. 6.3 Blower performance prediction: exhaust temperature	97
Fig. 6.4 Blower performance prediction: shaft power	98
Fig. 6.5 Roots blower performance curve transformation: inlet volume flow rate	100
Fig. 6.6 Roots blower performance curve transformation: exhaust temperature	101
Fig. 6.7 Roots blower performance curve transformation: shaft power	101
 APPENDIX A	
Figure A.1 Sample pipe layout	A4
 APPENDIX B	
Figure B.1 Bend geometry variable definition	B6

APPENDIX C

Fig. C.1 Correlation of the total friction coefficient for cement	C9
Fig. C.2 Correlation of the solids impact and friction coefficient for cement	C10
Fig. C.3 Correlation of the alternative solids impact and friction coefficient for cement	C11
Fig. C.4 Correlation of the total friction coefficient for tube ice	C13
Fig. C.5 Correlation of the alternative solids impact and friction coefficient for tube ice	C14

APPENDIX D

Fig. D.2.1 Cement conveying error plot for the pressure	D6
Fig. D.2.2 Cement conveying error plot for the average air velocity	D6
Fig. D.2.3 Cement conveying error plot for the solids velocity	D7
Fig. D.3.1 Cement conveying error plot for the pressure	D12
Fig. D.3.2 Cement conveying error plot for the average air velocity	D12
Fig. D.3.3 Cement conveying error plot for the solids velocity	D13
Fig. D.7.1 Tube ice conveying error plot for the pressure	D21
Fig. D.7.2 Tube ice conveying error plot for the average air velocity	D21
Fig. D.7.3 Tube ice conveying error plot for the solids velocity	D22

APPENDIX E

Fig. E.1 Pipeline Layout Design screen	E2
Fig. E.2 Example of a completed pipe layout	E4
Fig. E.3 Saving the pipeline geometry as a DXF file	E4
Fig. E.4 Conveying Conditions and Material Properties screen	E5
Fig. E.5 Adding a conveying material to the database	E7
Fig. E.6 Conveyor Simulation Progress screen	E9
Fig. E.7 Displaying numerical conveyor results	E10
Fig. E.8 Graphical display of the solids velocity and air velocities	E11
Fig. E.9 Blower main menu screen	E12
Fig. E.10 Defining blower characteristics	E13
Fig. E.11 Entering the required blower performance data	E15
Fig. E.12 Selecting a blower	E12

APPENDIX F

Fig. F.2 Flow diagram for two-phase flow simulation procedure STARTANALYSIS	F4
---	----

LIST OF SYMBOLS

A	Area	m^2
A_{sv}	Surface area of a sphere with an equivalent volume of a non-spherical particle	m^2
$A_{s,ns}$	Surface area of a non-spherical particle	m^2
A_{ss}	Specific surface area	m^2/kg
a	Acceleration	m/s^2
C_d	Drag coefficient of a single particle at an infinite dilution	dimensionless
$C_{d,c}$	Drag coefficient of a single particle in a cloud of particles	dimensionless
$C_{d,ns}$	Drag coefficient of a single non-spherical particle at an infinite dilution	dimensionless
$C_{d,s}$	Drag coefficient of a single spherical particle at an infinite dilution	dimensionless
C_p	Constant pressure specific heat	J/kgK
c	Particle velocity	m/s
c_o	Initial solids velocity	m/s
D	Bend diameter	m
d	Pipe inner diameter	m
d_{avg}	Average particle diameter determined by mesh screening	m
d_s	Particle diameter	m
E	Energy	J
e	Voidage or gas volume fraction	dimensionless
F	Force	$N, kgm/s^2$
f	Sliding friction coefficient	dimensionless
\dot{G}	Solids mass flow rate	kg/s
g	Gravitational constant	m/s^2
\dot{H}	Heat transfer rate	J/s
h	Enthalpy	J/kgK
k	Blower leakage coefficient	m^2
L_a	Acceleration length	m
L_b	Bend length	m
L_{horiz}	Length of horizontal pipeline	m
L_{tot}	Total pipe length	m

L_{vert}	Length of vertical pipeline	m
l	Length	m
Δl	Increment of length	m
\bar{m}	Average mass	kg
n	Speed of revolution	rpm
n_s	Number of particles	dimensionless
P	Pressure	N/m ²
ΔP	Pressure differential or pressure drop	N/m ²
Q	Gas volume flow rate	m ³ /s
\dot{Q}	Gas mass flow rate	kg/s
R	Gas constant for air	J/kgK
r	Radius	m
r_c	Average radius	m
r_o	Bend radius to outer pipe wall	m
rp	Pressure ratio	dimensionless
s_x	Scaling factor in the x-axis direction	dimensionless
s_y	Scaling factor in the y-axis direction	dimensionless
T	Temperature	K
t	Time	s
t_x	Translation distance in the x-axis direction	m
t_y	Translation distance in the y-axis direction	m
V	Volume	m ³
V_p	Blower swept volume	m ³ /rev
V_s	Volume of a particle	m ³
v	Average gas velocity	m/s
v_e	Interstitial gas velocity	m/s
\dot{W}	Power	J/s
ΔW	Increment of work	Nm
w_s	Free fall or terminal velocity of a single particle in an infinite dilution	m/s
$w_{s,c}$	Free fall or terminal velocity of a single particle in a cloud of particles	m/s
$w_{s,s}$	Free fall or terminal velocity of a single spherical particle in	m/s

	an infinite dilution	
$w_{s,ns}$	Free fall or terminal velocity of a single non-spherical particle in an infinite dilution	m/s
x	Coordinate point in the x-axis direction	m
y	Coordinate point in the y-axis direction	m
Z	Particle shape factor	dimensionless
z	Coordinate point in the z-axis direction	m
Δz	Increment in z-direction	m
Greek symbols		
α	Turning angle or orientation angle	degrees
β	Pipe elevation angle	degrees
ε	Pipe roughness	m
ϕ	Particle size distribution parameter	dimensionless
γ	Specific heat ratio or coefficient of restitution	dimensionless
η_{vol}	Volumetric efficiency	dimensionless
λ_g	Gas friction coefficient	dimensionless
λ_s	Solids friction coefficient	dimensionless
λ_s^*	Solids impact and friction coefficient	dimensionless
λ_s'	Alternative solids impact and friction coefficient	dimensionless
λ_{s1-3}	Definition 1 to 3 for the solids friction coefficient (see appendix B)	dimensionless
λ_{tot}	Total friction coefficient	dimensionless
μ	Mass flow ratio	dimensionless
μ'	Dynamic gas viscosity	kg/ms
Π	Dimensionless group	dimensionless
θ	Angle	degrees
ρ	Density	kg/m ³
ρ_g	Gas density	kg/m ³
ρ_s	True particle density	kg/m ³
ψ	Sphericity	dimensionless

First subscript

<i>a</i>	acceleration
<i>b</i>	buoyancy or bend
<i>cv</i>	control volume
<i>e</i>	exit
<i>dyn</i>	dynamic
<i>g</i>	gas
<i>i</i>	inlet
<i>l</i>	leakage
<i>n</i>	normal
<i>r</i>	radial
<i>res</i>	resultant
<i>s</i>	solids
<i>t</i>	tangential
<i>th</i>	theoretical
<i>tot</i>	total

Second subscript

<i>avg</i>	average
<i>d</i>	drag
<i>e</i>	exit
<i>f</i>	friction
<i>w_d</i>	wall drag
<i>g</i>	gravity
<i>i</i>	inlet or interface
<i>l</i>	lift
<i>p</i>	pressure

Dimensionless numbers

<i>De</i>	$De = Re_d \left(\frac{d}{2r_b} \right)^2$	Dean number	dimensionless
<i>Fr</i>	$Fr = \frac{v^2}{gd}$	Froude number	dimensionless

Fr_e	$Fr_e = \frac{v_e^2}{gd}$	Froude number	dimensionless
Fr_{co}	$Fr_e = \frac{c_o^2}{gd_s}$	Froude number	dimensionless
Fr_t	$Fr_t = \frac{w_s}{gd}$	Froude number	dimensionless
Re_d	$Re_d = \frac{\rho_g v d}{\mu'}$	Reynolds number	dimensionless
Re_{ds}	$Re_{ds} = \frac{\rho_g v d_s}{\mu'}$	Reynolds number	dimensionless
Re_{ws}	$Re_{ws} = \frac{\rho_g w_s d_s}{\mu'}$	Reynolds number	dimensionless
Sz		Impact number	dimensionless

INTRODUCTION

1.1 Introduction to pneumatic conveying

Pneumatic conveying can be described as the transport of granular and powder material by means of a gas stream in a pipeline. Pneumatic conveying of solids is widespread in the mining, chemical, food, plastics, power generation and wood treatment industries. Examples of this type of conveying are the unloading of dry cement powder from cement trucks into silos on building construction sites or the unloading of flour into silos at bakeries.

Four types of pneumatic conveying systems can be identified. In vacuum or negative pressure conveying the pressure in the conveying pipeline is below atmospheric pressure and the functioning is similar to that of a household vacuum cleaner. The advantages of vacuum conveying are twofold. It is often used to convey hazardous material as no leakage of the conveying gas or material can occur to the atmosphere during conveying. Secondly multiple feeding points are easily set into a single pipeline. A disadvantage of vacuum conveying system is that it is limited to a pressure differential of about 40 kPa.

The more common method of pneumatic conveying is that of positive pressure conveying. Material is fed into a pipeline by means of an air lock system making use of either rotary vane feeders, tandem flap valves or a blow vessel. The prime air mover supplies the conveying air at the required pressure and the material is conveyed down the pipeline to the receiver at a pressure above atmospheric. Here the solids are separated from the conveying gas. This is accomplished by using cyclones, filters or a combination of the two. The advantages of positive pressure conveying are that pressure differentials up to 1000 kPa [90MA1] can be attained and hence longer conveying distances are possible. Furthermore multiple discharge points can be incorporated where diverter valves are used to direct the flow to the required discharge point.

Hybrid systems of combinations of vacuum and positive pressure systems are also in use. Explosive goods can be transported in a closed loop system with an inert conveying gas such as nitrogen. The closed loop system is used where the loss of conveying gas to the atmosphere

is to be minimised. Figure 1.1 shows the typical layout of vacuum, positive pressure, hybrid and closed loop conveying system.

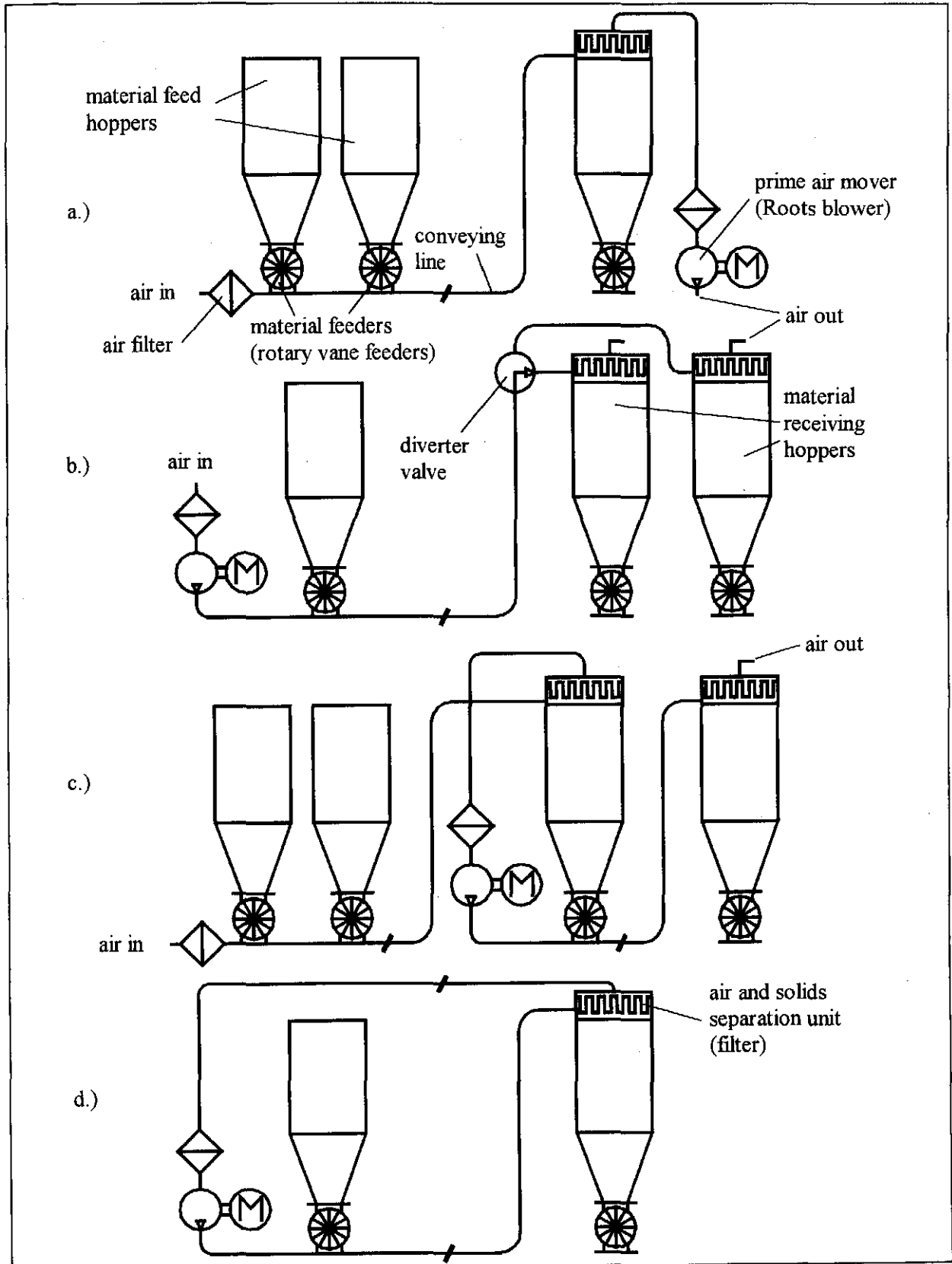


Fig. 1.1 Types of pneumatic conveying systems a: Vacuum conveying system, b: Positive pressure conveying system, c: Hybrid conveying system, d: Closed loop conveying system

Three distinct zones constitute a pneumatic conveyor [90MA1]. The first is the feeding, mixing and acceleration zone where the material is fed into the conveying pipeline, the particles mixed with the conveying gas and accelerated to a constant conveying velocity. The material is transported through the pipeline to its destination in the conveying zone. At the destination the material must be separated from the conveying air as discussed earlier. This is known as the gas and solids separation zone.

A further definition used in pneumatic conveying is the subdivision of the conveying mode into dilute and dense phase conveying. Dilute phase conveying is generally defined as conveying with a mass flow ratio less than 15 while in dense phase conveying the mass flow ratio is greater than 15 [89LA1, 90MA1].

In pneumatic conveyor design the most important design variables that have to be determined are the system pressure loss and the air mass flow rate required to sustain a given material mass flow rate. These two variables determine the size of the prime air mover and ultimately the power consumption of the system. It is important that the design seeks to optimise the conveying conditions so as to minimise the power consumption and hence the running costs. It is generally known that pneumatic conveyors are expensive to run. This is offset in part by the lower capital costs of the system when compared for example with a belt conveying system.

1.2 Report structure

Chapter one presents a summary of the literature survey as relevant to this project. A discussion of the merits and applicability of the subjects discussed in the literature survey follows. Section 1.5 defines the objectives of this thesis.

Chapter two introduces the theory and methods used to create the data input file for the pneumatic conveyor design programme in terms of the pipeline geometry.

The theory for two-phase flow and the derivation of the five differential equations governing the flow is given in the first part of chapter three. The single-phase flow theory is derived directly from the two-phase flow equations. The bend flow model follows in section 3.5 while the model for expansions from a smaller diameter pipe to a larger diameter pipe for use in stepped pipeline design is given in section 3.6.

The solution method for the differential equations derived in chapter three by means of a Runge-Kutta-Fehlberg integration algorithm is presented in chapter four together with the method of testing the code. The method for determining the initial conditions required to initialise the integration procedure is given in section 4.5. The switching from single-phase flow

to two-phase flow at the material feeding point and the difference in implementation of the programme for pressure and vacuum conveying is also discussed in this chapter.

Chapter five is introduced with a discussion and presentation of the friction coefficients used in the differential equations. Subsequently the simulation results for the conveying of Portland cement and tube ice are presented. A discussion on the overall results and the merits of the bend flow model follows.

Chapter six introduces the theory for determining the performance characteristics of a Roots blower both analytically and by means of scaling the performance curves. This is subsequently implemented in a Roots blower selection computer programme as part of the pneumatic conveyor design programme package.

A final summary of the results and insights gained throughout the work presented in previous chapters is given in chapter seven.

The bibliography follows chapter seven after which the appendices are presented. These contain data file formats, additional equation derivations, sample calculations, tables of results, programme flow charts and in conclusion a programme user manual for the pneumatic conveyor design programme PNEUSIM.

1.3 Literature review

1.3.1 Performance curves for pneumatic conveyors

i.) The Zenz and Othmer State Diagram

The state diagram was first introduced by Zenz and Othmer [60ZE1] as a useful tool for determining the flow characteristics in pneumatic conveying. The diagram represents a plot of the logarithm of the pressure drop per unit length of pipeline versus the logarithm of the superficial or average air velocity in the conveying pipe for a range of material mass flow rates. The Zenz and Othmer state diagram is a progression of the general state diagram proposed by Meyers, Marcus and Rizk [85ME1]. The flow patterns corresponding to figure 1.2 can be identified on the general state diagram as shown in figure 1.3.

As the average air velocity is decreased for a constant material mass flow rate, the solids loading ratio increases and the observed flow patterns change. The minimum point of a curve of constant material mass flow rate is the pressure minimum. A tangent can be constructed to the minima of the curves of different solids mass flow rate and the intersections connected to create the pressure minimum curve (line iii in figure 1.3).

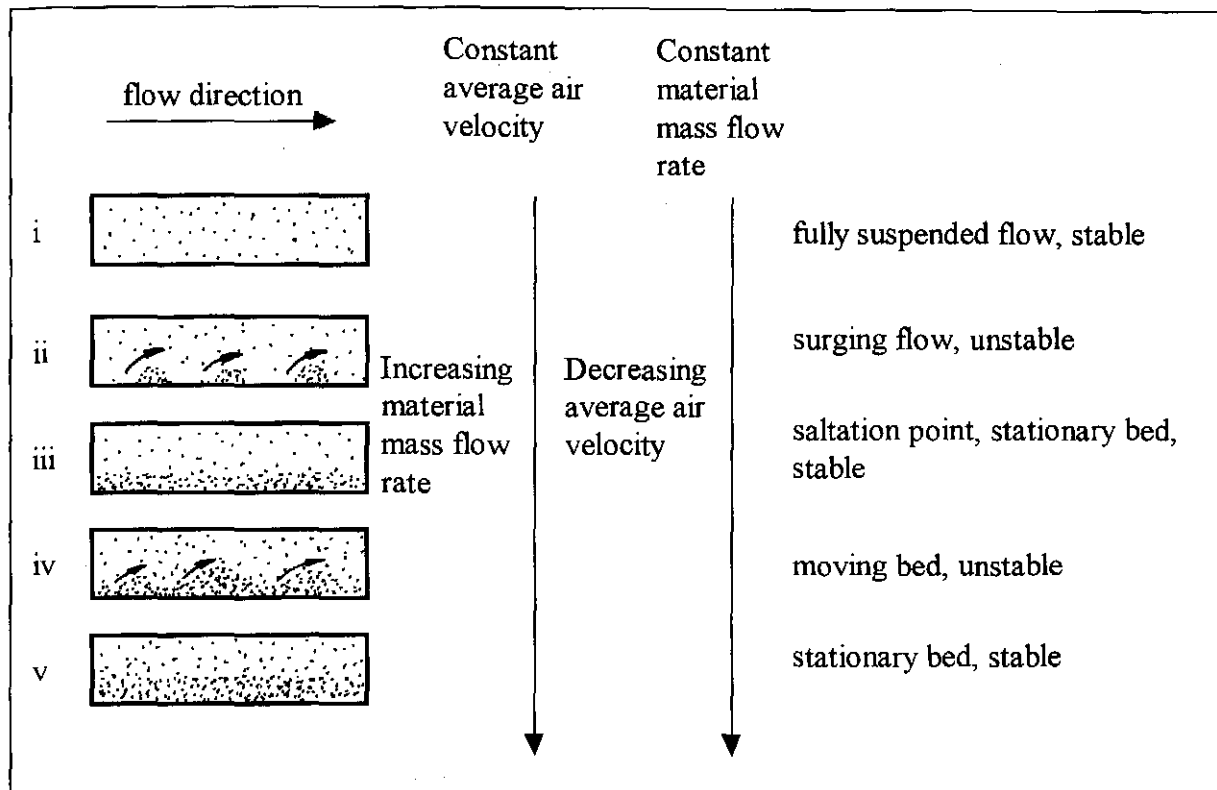


Fig. 1.2 Flow patterns for fine particles in dilute phase horizontal conveying [85ME1, 90MA1]

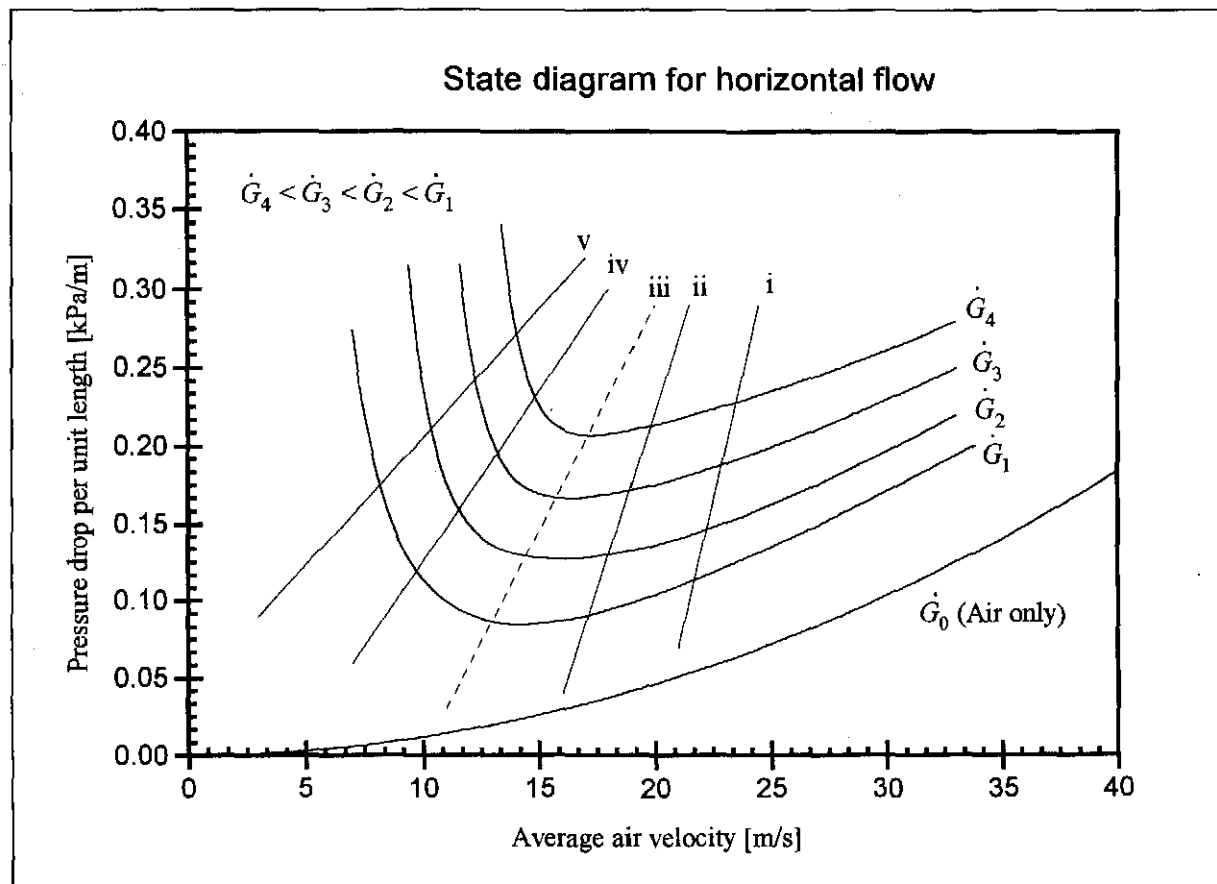


Fig. 1.3 General state diagram for horizontal conveying

For coarse particles the pressure minimum is that point where particles start settling out (line iii in figure 1.3) and on further reduction of the air velocity the flow moves into an unstable

conveying flow pattern. Further to the left of the pressure minimum curve the flow moves into the dense phase conveying condition which is often associated with pipe blockages.

For fine particles Meyers, Marcus and Rizk [85ME1] point out that the saltation velocity does not coincide with the pressure minimum curve as it does for coarse particles. The fine particles tend to settle out before the pressure minimum point is reached (line ii in figure 1.3).

An example of a state diagram for polyethylene pellets with a particle size of 3.66 mm is shown in figure 1.4. This general state diagram can be replotted in form of the Zenz and Othmer state

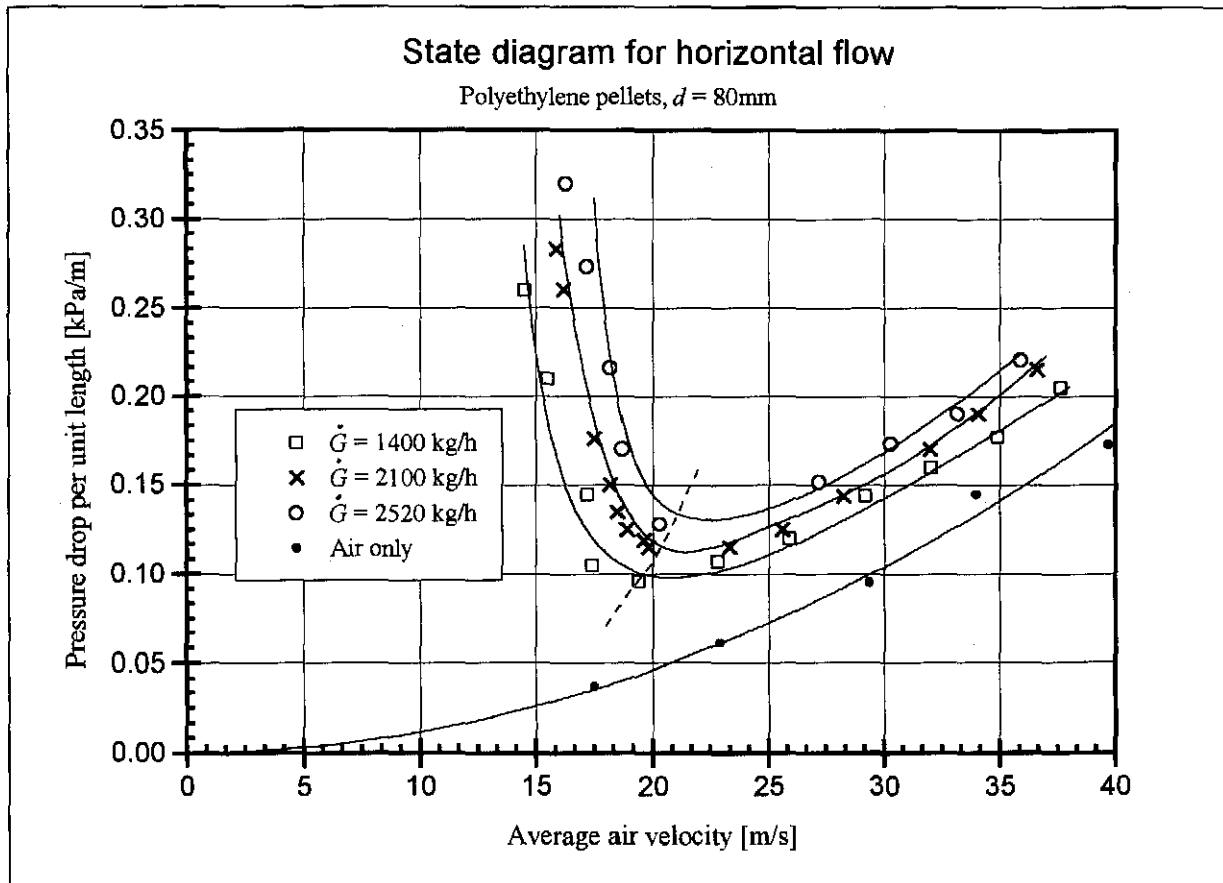


Fig. 1.4 General state diagram for polyethylene pellets [92OT1]

diagram shown in figure 1.5. Zenz and Othmer [60ZE1] point out that the discontinuity in the state diagram is as a result of the particles settling out at the pressure minimum point, where particles form a bed on the bottom of the pipeline. Unstable conveying conditions occur in this region and the pressure drop increases until a stable stationary bed conveying condition represented by line iii in figure 1.3 is attained.

In a study of the pneumatic conveying of large rock particles, Möhlmann [85MÖ1] notes that the Zenz and Othmer state diagram is not truly representative of the conveying conditions as the superficial air velocity is dependent on the position of the measuring section within a conveying setup due to the influence of the air density. Comparing the general state diagram

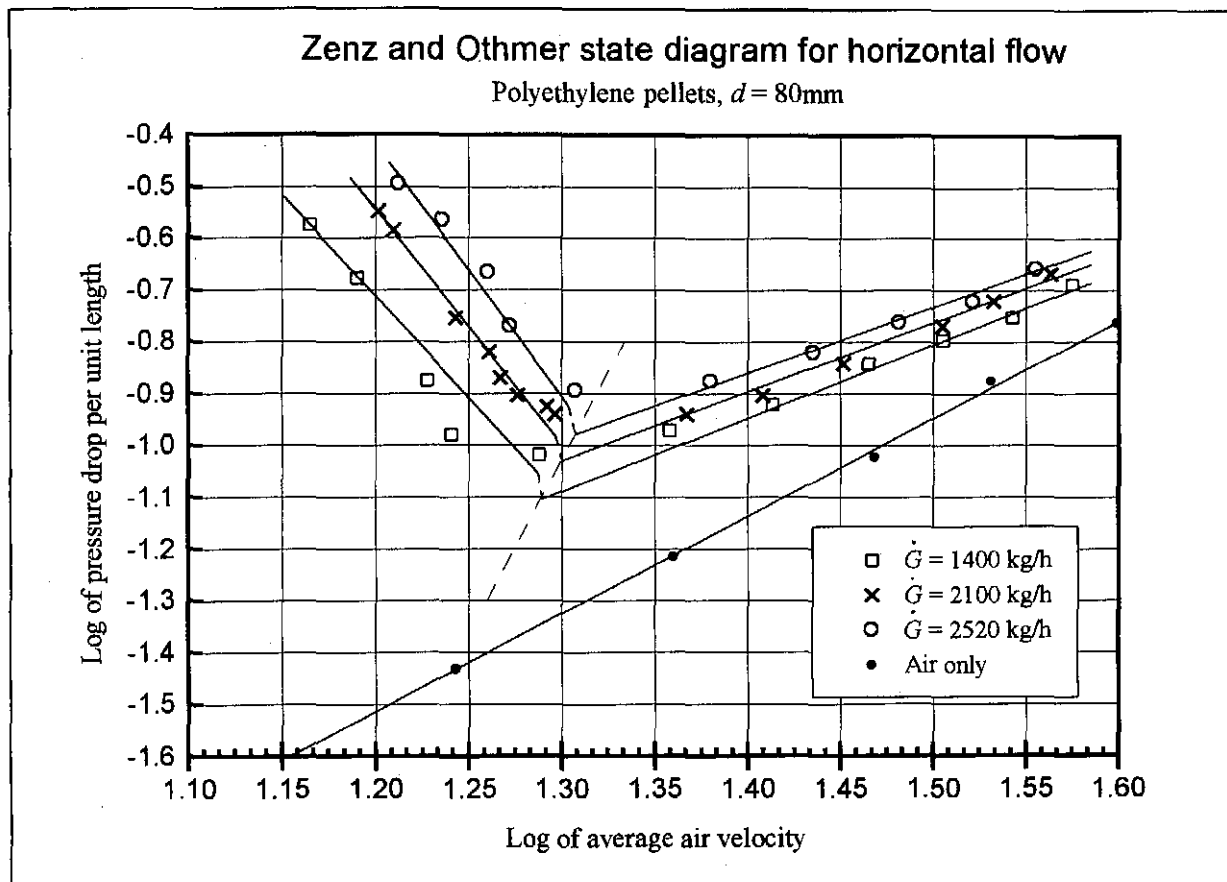


Fig. 1.5 Zenz and Othmer state diagram for polyethylene pellets [92OT1]

for two different pipe configurations he finds that the data of the two diagrams do not overlap if plotted on a mutual set of axes. To rectify this Möhlmann [85MÖ1] proposes the use of the dynamic pressure as the abscissa of the general state diagram. This diagram is called the normalised state diagram by Marcus et al. [90MA1] and is representative of the conveying conditions and independent of the position of the measuring section it was obtained from.

The dimensionless state diagram is a useful tool in determining the validity of experimental data. The logarithm of the solids loading is plotted versus the logarithm of the Froude number for constant solids mass flows. The resultant spacing of the lines should be directly proportional to the difference in solids mass flow. A typical dimensionless state diagram is given in figure 1.6.

Meyers et al. [85ME1] propose a dimensionless pressure minimum curve for coarse solids first presented by Rizk [73RI1, 82RI1] as:

$$\mu = 10^{-\delta} Fr^{\frac{x}{2}} \quad (1.3.1)$$

where: $\delta = 1.44d_s + 1.96$

and $x = 1.1d_s + 2.5$

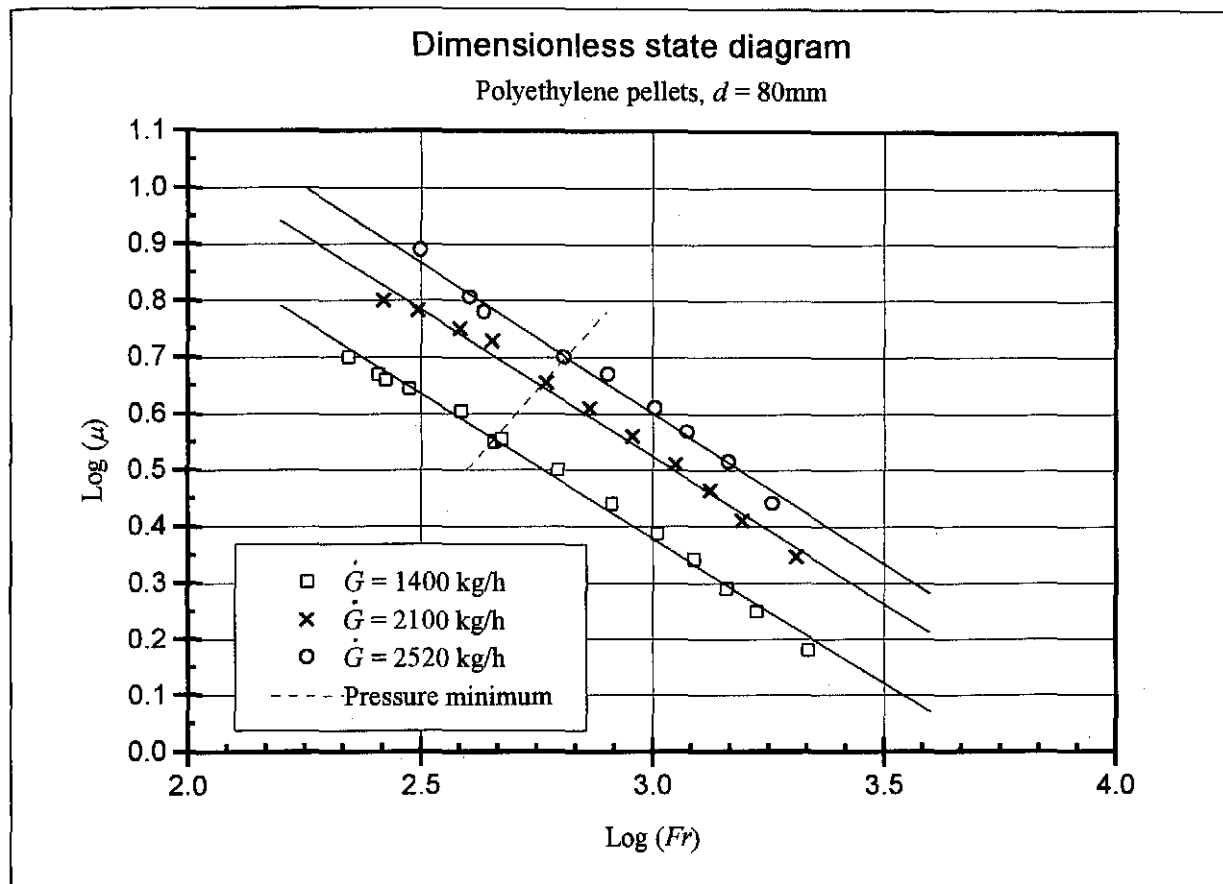


Fig. 1.6 Dimensionless state diagram for polyethylene pellets [92OT1]

Ottermann [92OT1] finds an acceptable correlation with respect to coarse sand ($d_s = 1.778\text{ mm}$; 6.2% difference between actual and calculated Froude number) while the correlations with respect to polyethylene pellets ($d_s = 3.658\text{ mm}$; 35% difference) and fine sand ($d_s = 0.970\text{ mm}$; 39% difference) show that equation 1.3.1 should only be used as an estimate of the dimensionless pressure minimum line.

Sheer [91SH1] finds that the pressure minimum curve does not accurately reflect the pressure minimum conditions for large diameter ice particles due to the size of the exponents and proposes a pressure minimum curve originally used by Barth [58BA1] in the form of:

$$\mu = K Fr^a \quad (1.3.2)$$

where constants K and a are determined by correlation of the minimum points from experimental data.

ii.) The Mills representation of conveying characteristics

An alternative representation of the salient characteristics of a pneumatic conveyor are the conveying characteristics presented by Mills [90MI1]. The conveying line pressure drop, mass

flow ratio, and material and air mass flow rates pertaining to the complete conveyor are represented on one graph as depicted in figure 1.7.

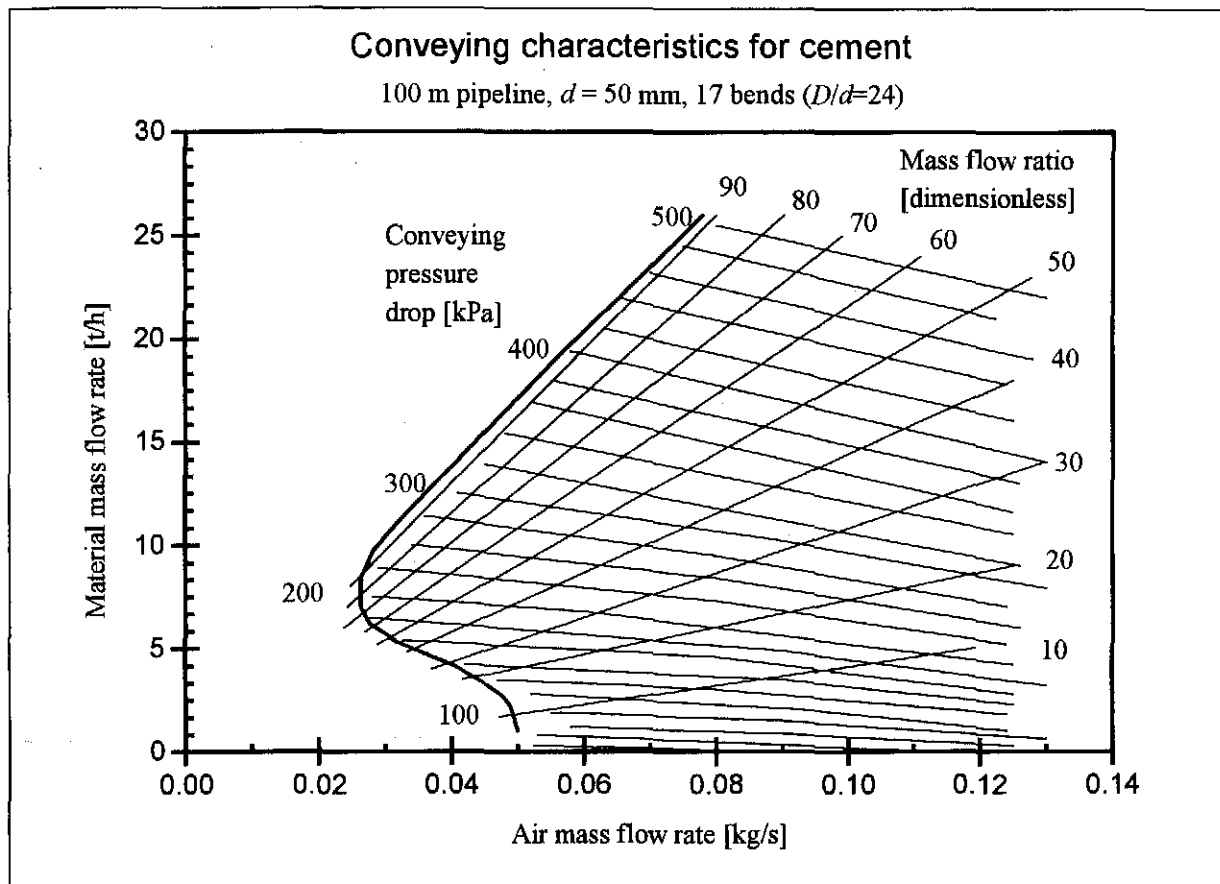


Fig. 1.7 Conveying characteristics for cement [90MI1]

The method for plotting these characteristics is to determine the line pressure drop for a range of material and air flow rates. These are plotted on the graph with the decimal point of the pressure value representing the exact position on the graph. Once this is done curves are fitted through points of constant pressure. Lines of constant mass flow ratio are added to the graph to complete the characteristics. Mills cautions that the extrapolation along lines of constant pressure drop towards the higher mass flow ratios on the left is not recommended as one may move into the dense phase conveying region where pipe blockage may occur. This limitation can be represented by the solid line running down the left hand side of the conveying characteristics. A further limit on the right hand side of the graph is governed by economic and practical considerations. Here high air flow rates correspond to high air velocities at a low line pressure drop. This causes increased erosion and product degradation. Furthermore the prime air mover is limited in the air flow rate it can supply. The upper part of the graph is limited by



the air mover characteristics at high pressures. The most important region of the conveying characteristics is in the area just to the right of the solid line on the left where the most efficient conveying can be effected. Superposition of lines of constant power onto the conveying characteristics confirms that the least power is required at lower air flow rates. If the performance curves for the prime air mover are available, these can be superimposed on the conveying characteristics to determine possible operating point at maximum air mover efficiency.

1.3.2 Differential equations governing two phase flow

The pressure drop equation, the motion equation and the solids and air continuity equations in conjunction with the gas equation of state have been used to simulate both dilute phase and dense phase pneumatic conveying [66WE1, 74WE1, 83FE1, 88WE1, 90MA1]. Saccani [93SA1] presents the results of a computer programme based on these five differential equations. The programme makes use of a step by step calculation method to determine the values of pressure loss, density, solids and air velocity and the voidage at discrete intervals along the pipeline. The continuity equations and gas equation of state are common to both dilute and dense phase conveying while equations of differing complexity are derived for the equations of motion and pressure drop. A detailed derivation of the equations is given in chapter three as these are fundamental to the work presented in this thesis.

1.3.3 Acceleration pressure drop

When the material is fed into the conveying pipeline or when decelerated material exits a bend it is accelerated to a steady state conveying velocity. The determination of the pressure loss and the length of pipe required to effect this acceleration is of importance to the designer of the conveying system. It is generally recommended to have a straight section of pipe of sufficient length to allow for complete acceleration of the solids after the material feeder and after bends [85MA1].

In the dimensional analysis by Rose and Duckworth [69RO1] the acceleration length is represented as:

$$\frac{L_a}{d} = 5.7 \left(\frac{\dot{G}}{\rho_g g^{\frac{1}{2}} d^{\frac{5}{2}}} \right)^{0.36} \left(\frac{d_s}{d} \right)^{-0.16} \left(\frac{\rho_s}{\rho_g} \right)^{0.18} \quad (1.3.3)$$

Marcus, Hilbert and Klinzing [85MA1] find that equation 1.3.3 correctly predicts the trend with respect to the influence of the solids mass flow rate for fly ash and the particle diameter in the transport of rock particles with a diameter varying in size bands from 10 mm to 15 mm and 35 mm to 40 mm. In contrast the influence of the solid mass flow rate for cement is not as significant as predicted by equation 1.3.3. Equation 1.3.3 tends to underpredict the values of the acceleration length determined by experiment by up to 38%.

An alternative representation to determine the acceleration length is given by Enick and Klinzing [85EN1] and also presented in Marcus et al. [90MA1]:

$$\frac{L_a}{d} = 0.527 \left(\frac{d}{d_s} \right)^{-1.26} (1 - \mu) Re_d \quad (1.3.4)$$

Marcus et al. [90MA1] provide a simplified integral equation of motion for the particle for the determination of the acceleration length as:

$$\int_{c_1}^{c_2} dl = \int_{c_1}^{c_2} cdc \left(\frac{3 C_d}{4 e^{4.7}} \frac{\rho_g}{\rho_s - \rho_g} \frac{(v_e - c)^2}{d_s} - g - \lambda_s^* \frac{c^2}{2d} \right)^{-1} \quad (1.3.5)$$

The effects of the air phase are taken into account through the drag term. Note the modification of the drag coefficient by means of the term $e^{4.7}$. This compensates the drag coefficient for the effects of voidage which is discussed in detail in section 1.3.10. A more comprehensive expression for the equation of motion is developed in chapter three.

1.3.4 Bend pressure drop

Ito [59IT1] suggests a pressure drop equation for single phase flow of the following format:

$$\Delta P = \left(\frac{0.029 + 0.304 De^{-0.25}}{\left(\frac{2}{d} r_b \right)} \right) \frac{L_b \rho_g v^2}{2d} \quad (1.3.6)$$

where L_b is the bend length. Equation 1.3.6 is valid in the following range:

$$300 > De > 0.034 \quad \text{where the Dean number is defined as } De = Re_d \left(\frac{d}{2r_b} \right)^2$$

If the Dean number is smaller than 0.034 the bend is of such large radius that it can be considered as a straight length of pipe.

In addition to the single phase pressure loss the pressure loss due to the influence of the solids has to be added to obtain the total bend pressure drop.

The simplest method of pressure drop determination is the assumption that all material flowing into a bend moves against the outer bend wall due to centrifugal forces. The material is then modelled as a cohesive mass sliding along the wall. The dynamic sliding friction coefficient of one solid sliding over another is used to determine friction losses. This treatment of the bend pressure loss is first described by Weidner [55WE1]. Weidner gives the following equation for the bend pressure loss:

$$\Delta P = \mu \rho_g e v (c_a - c_o) \quad (1.3.7)$$

where c_a is the solids velocity after re-acceleration behind the bend and c_o is the solids velocity at the outlet of the bend. Graphs are given to determine the bend outlet solids velocity with respect to the bend inlet solids velocity for differing orientation and radius of the bend.

The use of this equation is recommended by Weber and Stegmeier [83WE1]. Sheer [91SH1] notes that in the light of more recent work the assumptions used by Weidner are not sufficiently realistic.

In a simplified approach to pneumatic conveyor design Fischer [58FI1] also makes use of the assumption that the material is thrown against the outer wall of the pipe and derives the bend pressure loss equation as:

$$\Delta P = \mu \frac{L_b f \rho_g v^2}{r_o} \quad (1.3.8)$$

where L_b is the bend length and f is the dynamic sliding friction coefficient.

Ferretti [83FE1] equates the force term using the Darcy-Weisbach or Fanning friction equation with the force required to drag the material along the wall and thus derives a solids friction coefficient in terms of the sliding friction coefficient and the orientation of the section of the bend pipeline under consideration. The friction coefficient for a bend in the vertical plane is given as:

$$\lambda_s = 2f \left(1 - \frac{\rho_g}{\rho_s} \right) \frac{d}{c^2} \left(\frac{c^2}{r_o} - g \sin \alpha \sin \beta \right) \quad (1.3.9)$$

and as:

$$\lambda_s = 2f \left(1 - \frac{\rho_g}{\rho_s} \right) \frac{d}{r_o} \quad (1.3.10)$$

for a bend in the horizontal plane where r_o is the radius of the bend to the outer bend wall. The definitions of angles α and β are given in figure 1.8.

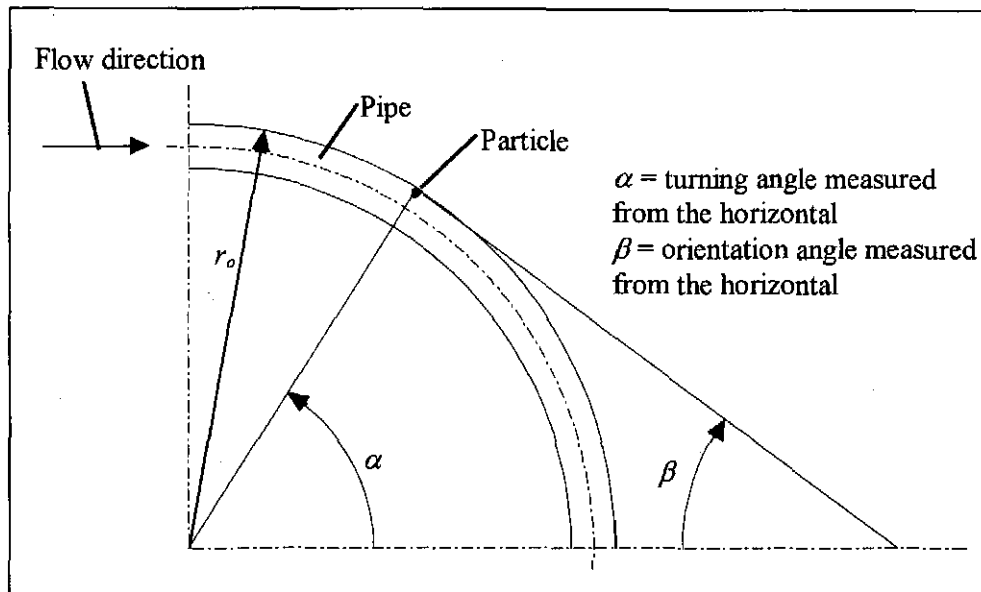


Fig. 1.8 Definition of bend geometry angles for a bend in the vertical plane [83FE1]

After detailed derivation of the equation 1.3.9 it is shown in section 3.5 that the angle β is not required for the definition of the friction coefficient for bend flow in the vertical plane. Ferretti [83FE1] confirms that the bend pressure loss is not only caused in the bend itself and that half of the total bend pressure loss can be attributed to the reacceleration of the solids after the bend. He also points out that the use of the given bend pressure loss model tends to overestimate the pressure drop encountered in experiments.

Ito [59IT1] and Bradley and Reed [88BR1] demonstrate that most of the pressure drop caused by a bend can be attributed to the reacceleration of the material after a bend and Marcus, Hilbert and Klinzing [85MA1] confirm that material deposition often occurs at the exit of the bend and that designers must allow for a length of straight pipe after a bend to allow for reacceleration.

Although the bend pressure loss equation by Schuchart [68SC1] is based on detailed experimental work, it is of limited use due to the limited particle size range that it can be applied to. Furthermore bend orientation is not taken into account. Both the equations by Schuchart [68SC1] and that of Morikawa et al. [78MO1] have been shown to under- or overpredict bend pressure losses when compared to experimental data [90MA1].

Bradley and Reed [90BR1] present a method of determining the bend pressure drop in an experimental setup by extrapolating the constant gradient pressure drop after the bend acceleration zone back to the apex of the bend. Figure 1.9 depicts the method applied to experimental data. The same method of determining the bend pressure drop is used by Schuchart [68SC1] for his experimental work.

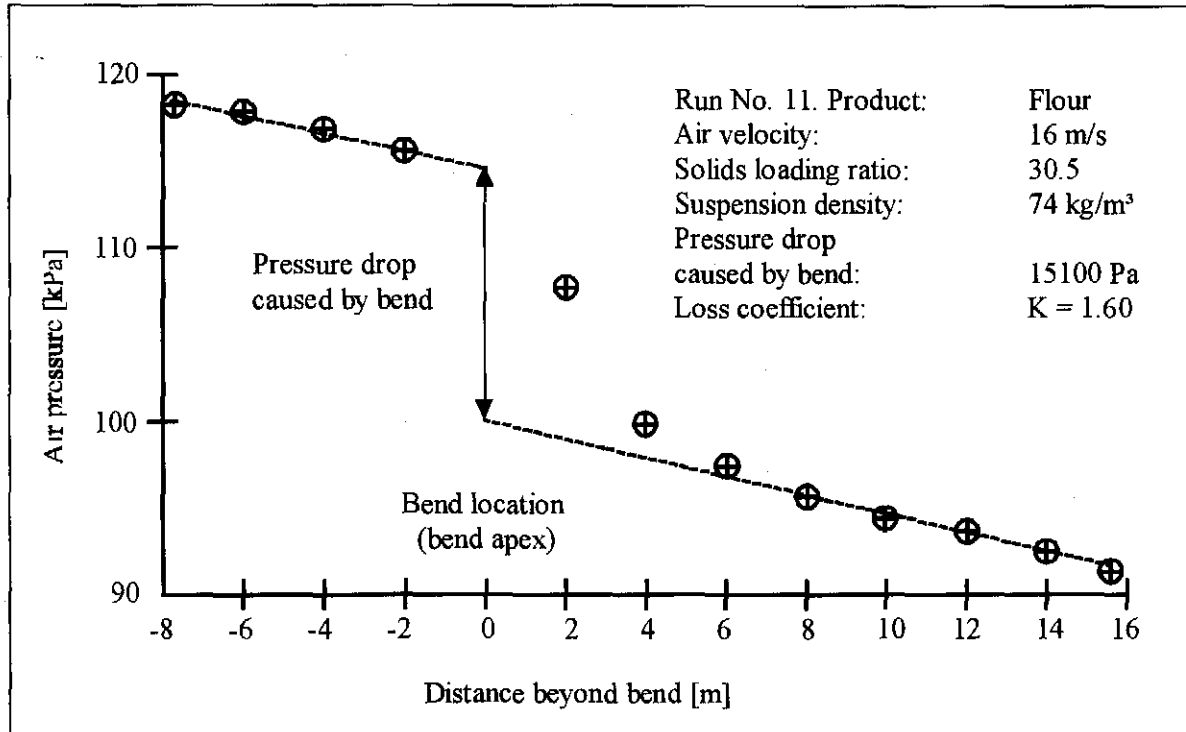


Fig. 1.9 Bend pressure drop determination [90BR1, 91RE1]

Bradley and Reed [90BR1, 91RE1] present equation 1.3.11 to determine the bend pressure drop:

$$\Delta P = K \frac{1}{2} \rho_{susp} v^2 \quad (1.3.11)$$

where K is determined as a function of the suspension density from experimental data for a specific bend type and conveying material. The suspension density ρ_{susp} is defined as the material mass flow rate divided by the air volume flow rate at the pressure in the pipe.

1.3.5 Air alone pressure drop

The pressure drop equations used for single phase flows in pipelines are well documented in the literature [88WH1]. The Darcy-Weisbach equation for the pressure drop in pipe flows can be written in the following form:

$$\Delta P = \lambda_g \frac{\rho_g v^2 L}{2d} \quad (1.3.12)$$

The exact solution for the pipe friction coefficient in the laminar flow region for smooth pipes is given as:

$$\lambda_g = \frac{64}{Re_d} \quad Re_d < 2300 \quad (1.3.13)$$

while Blasius gives the solution for the turbulent flow region as:

$$\lambda_g = \frac{0.316}{Re_d^{0.25}} \quad 4000 < Re_d < 10^5 \quad (1.3.14)$$

The effects of surface roughness were first determined by Nikuradse [33NI1]. He points out that in laminar flow the surface roughness has no effect on the friction coefficient and that equation 1.3.13 is also valid for pipes with surface roughness. For turbulent flow, integration of the modified logarithm law for roughness yields an equation for the friction coefficient in terms of the pipe roughness:

$$\lambda_g = \left(-2.0 \log \frac{(\varepsilon/d)}{3.7} \right)^{-2} \quad Re_d > 4000 \quad (1.3.15)$$

Colebrook [38CO1] presents an interpolation equation that combines both the smooth and rough wall pipe flows which is modified to an explicit form by Haaland [83HA1] to yield:

$$\lambda_g = \left(-1.8 \log \left[\frac{6.9}{Re_d} + \left(\frac{\varepsilon/d}{3.7} \right)^{1.11} \right] \right)^{-2} \quad Re_d > 4000 \quad (1.3.16)$$

The original Colebrook equation is used by Moody [44MO1] to plot the famous Moody chart for pipe friction.

Marcus [78MA1] notes that fine material such as Portland cement tends to form a thin deposit on the conveying pipe wall that in effect reduces pipe roughness so that the smooth pipe friction coefficient data can be used for determining air alone pressure losses. The same

phenomenon was noted when conveying hydrated lime in a full scale test rig at the University of Stellenbosch [94WO1].

1.3.6 Combined friction pressure loss for air and solid particles

The classical method of the solids friction coefficient representation is to assume that the same relation based on the Darcy-Weisbach equation used for gas flows holds for the solids phase. Based on publications by Vogt and White [48VO1] and Hariu and Molstad [49HA1], Pinkus [52PI1] gives this as:

$$\Delta P = \lambda_s^* \frac{\rho_g c^2 L}{2d} \quad (1.3.17)$$

Equation 1.3.17 represents the solids impact and friction component alone. By deriving a term for the energy required to keep particles suspended in horizontal flow and adding this to equation 1.3.17, Barth [58BA1] presents the equation for horizontal flow in a modified form as:

$$\Delta P_s = \mu \frac{\rho_g v^2 L}{2d} \left(\lambda_s^* \left(\frac{c}{v} \right) + \frac{2 \left(\frac{w_s}{v} \right)}{\left(\frac{c}{v} \right) Fr} \right) \quad (1.3.18)$$

A detailed derivation of this equation is presented in section 3.3.3. The combined solids friction coefficient incorporating the pressure drop coefficient due to impact and friction λ_s^* and the lifting term can thus be written as:

$$\lambda_s = \lambda_s^* \left(\frac{c}{v} \right) + \frac{2 \left(\frac{w_s}{v} \right)}{\left(\frac{c}{v} \right) Fr} \quad (1.3.19)$$

Barth [58BA1] notes that the term w_s/v in equation 1.3.19 becomes unity in vertical conveying if the effect of lifting the solid particles vertically is included in the definition of the combined solids friction coefficient. The pressure drop due to the influence of solids can now be written as:

$$\Delta P_s = \lambda_s \mu \frac{\rho_g v^2 L}{2d} \quad (1.3.20)$$

which is currently the form used most frequently [90MA1].

The classical calculation method in dilute phase conveying [63BA1, 88WE1, 90MA1, 91SH1] using the above is to add the pressure drop caused by the solids to that caused by the conveying gas alone where the frictional pressure drop can then be represented by:

$$\Delta P = (\lambda_g + \mu\lambda_s) \frac{\rho_g v^2 L}{2d} \quad (1.3.21)$$

Care must be taken when comparing solids friction coefficients published in the literature as the definition may either relate to the combined solids friction coefficient λ_s or the friction coefficient due to impact and friction λ_s^* (see equation 1.3.19).

While comparing the results of a single material overlapping friction coefficient correlation for fine solids [78ST1] and coarse solids [87SZ1] based on the classical representation, Weber [88WE1] found that the correlations could be improved significantly by defining a total friction coefficient embracing both the air and solids effects on the pressure drop. Marcus [78MA1] notes that viscous sublayer thickening is thought to occur as a result of fine particles added to the conveying gas stream which may reduce the skin friction. It is thus clear that the gas velocity profile is no longer the same as that on which the gas alone frictional losses presented in section 1.3.5 are based. It is thus difficult to separate the two pressure drop components when using experimental data to determine the solids friction factors by subtracting the theoretical air alone pressure drop or even the experimentally determined air alone pressure drop from the total pressure drop.

In a later paper Weber [91WE1] points out that the use of the classical representation may erroneously yield a negative value for the solids friction factor when using it to calculate the friction factor from experimental data as a result of subtracting the air alone pressure losses from the experimentally determined friction pressure drop. This is in agreement with the findings of Marcus [78MA1]. Weber notes that this is particularly evident with smaller solids loading. Three alternative approaches are presented. The first is a modification to the Blasius air friction coefficient for smooth pipes in turbulent flow. A constant α is used to account for the effect of the particle interaction. The friction pressure drop equation takes the form:

$$\Delta P = \left(\frac{0.3164}{Re_d^{0.25\alpha}} + \mu\lambda_s \right) \frac{\rho_g v^2 L}{2d} \quad (1.3.22)$$

Another approach is to make use of a gas friction factor that is a function of the loading ratio so that the pressure drop equation can be written as:

$$\Delta P = (\lambda_g(\mu) + \mu\lambda_s) \frac{\rho_g v^2 L}{2d} \quad (1.3.23)$$

where:

$$\lambda_g(\mu) = \frac{a}{Re_d^b} \frac{1}{1 - \mu^c} \quad (1.3.24)$$

and a, b and c are constants.

The most useful approach is the combination of separate solids and gas friction factors to determine a total friction coefficient. The pressure drop due to friction can then be written as:

$$\Delta P = \lambda_{tot} \frac{\rho_g v^2 L}{2d} \quad (1.3.25)$$

where:

$$\lambda_{tot} = f(\mu, Fr, Re_d, \frac{d_s}{d}, \dots) \quad (1.3.26)$$

This approach is particularly suited for determination from experimental results as the pressure drop measured is a combination of the influences of the solids and the air alone which are difficult to separate in practice. A single correlation is often used for both vertical and horizontal conveying without taking into account that the definition of friction coefficients is not the same for horizontal and vertical flow. A detailed discussion of the merits of this simplification is presented in chapter three and in appendix B.

1.3.7 Friction coefficient correlations for horizontal flow

Numerous correlations for the solids friction coefficient can be found in the literature and in recent years attempts have been made with reasonable success to define material overlapping correlations using a large volume of experimental data [87SZ1, 88WE1, 91WE1]. These can be classified as correlations for fine and coarse materials. The importance of the review of the correlations is to gain an insight into the non-dimensional groups used and to determine which are important in defining the friction coefficient. Sheer [91SH1] presents a table of friction coefficients for granular material. At this stage it must be cautioned that the definition of the Froude number may differ from author to author and it has been found that friction coefficient

correlations have been used in publications without modifying the constants to correspond to the definition of the Froude number in that publication.

Tab. 1.1 Expressions for solids and total friction coefficients for horizontal dilute phase flows

Friction coefficient λ_s or λ_{tot}	Reference	Notes
$\lambda_s = \frac{3}{2} C_d \frac{\rho_g d (v-c)^2}{\rho_s d_s v c}$	[53HI1, 78SC1, 81MO1, 91SH1] equation 1.3.27	Granular particles $d_s = 0.36 - 8.4$ mm, $d = 50$ mm and 75 mm glass pipes.
$\lambda_s = 0.0116 \mu^{-0.12} Fr^{-0.45} \left(\frac{d_s}{d}\right)^{-0.88}$	[58HI1, 91SH1] equation 1.3.28	Spherical peas, pills and glass balls $d_s = 2-7$ mm. $d = 50$ mm, and 75 mm steel pipes.
$\lambda_s = 0.005 \left(\frac{1 - 1/Fr}{1 + 0.00125 Fr_t^2} \right)$	[58BA1, 91SH1] equation 1.3.29	Average constants for a range of materials.
$\lambda_s = 2.1 \mu^{-0.3} Fr^{-1} Fr_t^{0.25} \left(\frac{d_s}{d}\right)^{-0.1}$	[78ST1, 83WE1, 88WE1] equation 1.3.30	Fine solids $d_s < 0.15$ mm. Mean deviation $\pm 64\%$.
$\lambda_s = 0.082 \mu^{-0.3} Fr^{-0.86} Fr_t^{0.25} \left(\frac{d_s}{d}\right)^{-0.1}$	[82WE1, 91SH1] equation 1.3.31	Polystyrene, glass and steel spheres $d_s = 1.1 - 2.7$ mm. $d = 32 - 400$ mm
$\lambda_s = 2.7 \left(\mu + \frac{\rho_s}{\rho_g} \right) - 1 \frac{d}{d_s} \frac{v}{c} \left(1 - \frac{c}{v} \right)^2 \frac{\xi}{K^2}$ $\xi = 24 Re_s^{-1} + 4 Re_s^{-2} + 0.4$ $Re_s = \frac{d_s (v-c)}{v}$ $K = \frac{w_{s,ns}}{w_s} \text{ (shape factor)}$	[83WE1] equation 1.3.32	Granular material $d_s = 0 - 40$ mm Derived from [68SC1]
$\lambda_s = 0.072 Fr^{-0.5}$	[87MI1] equation 1.3.33	Average for 10 coarse materials in steel pipes
$\lambda_{tot} = 0.02 \mu^{-0.343} Fr^{-0.8} Fr_t^{0.225} \left(\frac{d_s}{d}\right)^{-0.194} \cdot \left(\frac{\rho_s}{\rho_g}\right)^{0.1865}$	[88WE1] equation 1.3.34	Fine solids $d_s < 0.15$ mm. Mean deviation $\pm 37.1\%$. Derived using data from [78ST1].

Tab. 1 1 continued

Friction coefficient λ_s or λ_{tot}	Reference	Notes
$\lambda_s = 0.0223 \mu^{0.741} Fr^{-0.872} Fr_t^{0.288} \left(\frac{d_s}{d}\right)^{-0.259}$ $\cdot \left(\frac{\rho_s}{\rho_g}\right)^{0.081}$ in conjunction with $\lambda_g = 0.3164 Re_d^{-0.325}$	[88WE1] equation 1.3.35	Fine solids $d_s < 0.15$ mm. Mean deviation $\pm 29.93\%$. Derived using data from [78ST1].
$\lambda_{tot} = \mu^{-0.921} Fr^{-0.208} \left(\frac{d_s}{d}\right)^{-0.03} \left(\frac{\rho_s}{\rho_g}\right)^{0.353}$ $\cdot (Sz f)^{0.0504}$	[87SZ1, 88SZ1 88WE1] equation 1.3.36	Coarse solids $d_s = 0.1 - 3$ mm. Mean deviation $\pm 13.74\%$
$\lambda_{tot} = \mu^{-0.921} Fr^{-0.208} \left(\frac{d_s}{d}\right)^{-0.03} \left(\frac{\rho_s}{\rho_g}\right)^{0.353}$ $\cdot (Sz f)^{0.0504} Re_d^{0.2085}$	[88WE1] equation 1.3.37	Coarse solids $d_s = 0.1 - 3$ mm. Mean deviation $\pm 11.66\%$. Derived using data from [87SZ1]
$\lambda_{tot} = \mu^{0.0453} Fr^{-0.1516} \left(\frac{d_s}{d}\right)^{0.0126} \left(\frac{\rho_s}{\rho_g}\right)^{-0.00482}$ $\cdot (Sz f)^{-0.0505} Re_d^{-0.2085}$ in conjunction with $\lambda_g = 0.3164 Re_d^{-1}$	[88WE1, 91WE1] equation 1.3.38	Coarse solids $d_s = 0.1 - 3$ mm. Mean deviation $\pm 11.66\%$. Derived using data from [87SZ1]
$\lambda_s = 0.407 \mu^{-0.525} Fr^{-0.385} Fr_t^{0.11} Re_d^{-0.084}$ $\left(\frac{w_s}{v}\right)^{-0.084} \left(\frac{d_s}{d}\right)^{0.138} \left(\frac{\rho_s}{\rho_g}\right)^{0.283} Sz^{0.133} f^{0.195}$ with $\lambda_g = 0.1 Re_d^{-0.151} \frac{1}{1 + \mu^{0.7}}$	[91WE1] equation 1.3.39	Coarse solids $d_s = 0.1 - 3$ mm. Mean deviation $\pm 6.15\%$. Derived using data from [87SZ1]

In a detailed dimensional analysis Rose and Duckworth [69RO1] conclude that the friction coefficient for suspensions is a function of the following non-dimensional groups:

$$\lambda_{tot} = f_1 \left(Re_d, \frac{\varepsilon}{d} \right) + f_2 \left(Re_d, Fr, \mu, \frac{\rho_s}{\rho_g}, \gamma, \frac{d_s}{d}, \frac{\varepsilon}{d}, Z, \phi, \beta \right) \quad (1.3.40)$$

where γ is defined as a coefficient of restitution, ϕ is a parameter defining the spread in particle size distribution and Z is the shape factor defined in equation 1.3.42. Rose and Duckworth [69RO1] conclude that the solids friction coefficient is not dependent on the Reynolds number. Furthermore the roughness term has a relatively small influence on the solids friction factor and that its effects are taken into account in the correlation for the air flow friction coefficient. The size distribution effects were not studied and the influence of particle shape is considered of minor importance. The suspension friction coefficient can thus be written as a function of the following non-dimensional groups:

$$\lambda_{tot} = f_1\left(Re_d, \frac{\varepsilon}{d}\right) + f_2(Fr) \cdot f_3(\mu) \cdot f_4\left(\frac{d_s}{d}\right) \cdot f_5\left(\frac{\rho_s}{\rho_g}\right) \cdot f_6(\beta) \cdot f_7(\gamma) \quad (1.3.41)$$

Correlations are presented in form of figures to determine the required relationships $f_2 - f_7$ that the non-dimensional groups must be multiplied with.

1.3.8 Particle shape definition

The particle shape definition is important in pneumatic conveying as most particles that are pneumatically conveyed cannot be modelled as perfect spheres. The most important influence of particle shape is the effect on the particle drag coefficient which is required to determine particle air resistance. It is thus appropriate to discuss the definitions of particle shape before proceeding to the influences on the drag coefficient. Wadell [34WA1] introduces a definition of the particle dimension based on measuring the drag coefficients of a particle while Heywood [38HE1] proposes the use of the projected diameter of a particle. This projected diameter is defined as the diameter of a circle having the same area as the projected area of a particle in its most stable position. Heywood defines a volume shape factor Z as:

$$Z = \frac{V_s}{d_s^3} \quad (1.3.42)$$

where V_s is particle volume and d_s is defined as the projected diameter. Zenz and Othmer [60ZE1] point out that the correlation given by Heywood is not supported by experimental data and that the locations of the curves of C_d versus Re_d for particles with different values of Z with respect to that of a sphere are not plausible.

A better means of defining a shape factor for non-spherical solids is given in Govier and Aziz [72GO1] as:

$$\psi = \frac{d_{avg}}{\phi d_s} \quad (1.3.43 \text{ a})$$

where d_{avg} is the average particle diameter obtained from a mesh screen analysis, ϕ is the ratio of the surface area per unit mass of the particles to that of sphere with a diameter of d_s . Boothroyd [71BO1] defines the sphericity as the surface area of a sphere of equivalent volume divided by the particle surface area. This can be written as:

$$\psi = \frac{\pi \left(\frac{6V_s}{\pi} \right)^{\frac{2}{3}}}{A_{s,ns}} \quad (1.3.43 \text{ b})$$

Table 1.2 presents values for the sphericity for different materials.

Tab. 1.2 Sphericity data [84CH1, 90MA1, 72GO1]

Material	Sphericity ψ	Shape of material	Sphericity ψ
Sand	0.534-0.861	Octahedron	0.847
Silica	0.554-0.628	Cube	0.806
Pulverised coal	0.696	Prisms	
		$a \times a \times 2a$	0.767
		$a \times 2a \times 2a$	0.761
		$a \times 2a \times 3a$	0.725
Bituminous coal	0.625	Cylinders	
		$h = 3r$	0.860
		$h = 10r$	0.691
		$h = 20r$	0.580
Celite cylinders	0.861	Discs	
		$h = r$	0.827
		$h = r/3$	0.594
		$h = r/10$	0.323
		$h = r/15$	0.254
Iron catalyst	0.578	$a = \text{length}; h = \text{height}; r = \text{radius}$	
Broken solids	0.63		

1.3.9 The influence of particle shape on the drag coefficient

The drag coefficient for spherical particles in an infinite dilution is well documented in the literature [33SC1, 66WE2] with a summary of equations and the appropriate references given by Boothroyd [71BO1]. Marcus et al. [90MA1] recommends the use of a modification of the

Schiller and Naumann equation [33SC1] by Clift and Gauvin [70CL1] with a maximum deviation of 4%. This is given as:

$$C_{d,s} = \frac{24}{Re_{ds}} (1 + 0.15 Re_{ds}^{0.687}) + \frac{0.42}{1 + 4.25 \cdot 10^4 Re_{ds}^{-1.16}} \quad Re_{ds} < 100000 \quad (1.3.44)$$

In pneumatic conveying the drag coefficient must be modified to take account of the particle shape and the effect of particle interaction in a cloud of particles. Both effects significantly alter the particle drag coefficient.

In an experiment using isometric particles in the form of cubes, cube octahedrons, octahedrons and tetrahedrons Pettyjohn and Christiansen [48PE1] conclude that the sphericity is a satisfactory criterion to determine the effect of particle shape on the drag coefficient. For Stokes flow they suggest a correction factor. The drag coefficient for single non-spherical particles can then be written as:

$$C_{d,ns} = 0.843 \log \frac{\psi}{0.065} C_{d,s} \quad Re_{ws} < 0.05 \quad (1.3.45 a)$$

with an accuracy of 2% while the drag coefficient in the turbulent region can be determined to an accuracy of 4% by:

$$C_{d,ns} = 5.31 - 4.88 \psi \quad 2000 < Re_{ws} < 200000 \quad (1.3.45 b)$$

For the Reynolds numbers between Stokes and turbulent flow Pettyjohn and Christansen [48PE1] suggest using graphical data (fig. 8 in [48PE1]).

The use of this modification for non-spherical particles is recommended by Yang [73YA1]. Marcus et al. [90MA1] also recommends the sphericity as a means of correcting the drag coefficient of spherical particles but notes that the relationship between sphericity and the drag coefficient is only an approximate one as particles with the same sphericity may have different shapes and as a result of that may not have the same drag coefficient. A correlation for the ratio of the free fall velocity of a single non-spherical particle to that of a single spherical particle given by Marcus et al. [90MA1] can be rewritten in terms of the definition of the free fall velocity as given in equation 1.3.48 to yield a useful expression to determine the drag coefficient of a single non-spherical particle as:

$$C_{d,ns} = \left(\frac{1}{0.843 \log \frac{\psi}{0.065}} \right)^2 C_{d,s} \quad (1.3.46)$$

1.3.10 The influence of voidage on the drag coefficient

Particle interaction is significant in pneumatic conveying as drag coefficient correlations for a particle in an infinite fluid must be modified to account for particle-particle interaction at higher solids concentrations (or lower values of voidage). Wen and Yu [66WE2] found that the drag coefficient of spherical particles is influenced by an increase in particle concentration and can be related to the voidage as follows:

$$C_{d,c} = C_{d,s} e^{-4.7} \quad (1.3.47)$$

While Wen and Yu suggest this relationship to hold for $Re_p < 1000$ as a result of the use of the Schiller and Naumann equation for the drag coefficient [33SC1], Marcus et al. [90MA1] points out that the range of applicability of equation 1.3.47 can be extended by using equation 1.3.44.

1.3.11 Free fall velocity of particles

The free fall velocity of a single particle in still air can be derived by equating the particle buoyancy and gravitational forces to the drag force. Terminal velocity is reached when these forces are in equilibrium. For spherical particles this can be derived as [73YA1, 84CH1, 90MA1]:

$$w_{s,s} = \sqrt{\frac{4d_s g(\rho_s - \rho_g)}{3\rho_g C_{d,s}}} \quad (1.3.48)$$

Determination of the free fall velocity for a non-spherical particle is important for determining the energy that is required to keep particles in suspension during horizontal conveying and requires the modification of the drag coefficient as discussed in the previous section. The effect of the drag coefficient modified for shape can be expressed by plotting the ratio of free fall velocity of a particle of shape factor ψ to that of a spherical particle. This ratio can be represented as a function of the particle Reynolds number as depicted by Govier and Aziz (fig. 1.5 in [72GO1]).

Barth [60BA1] points out that the relative velocity between the carrier gas and the particles increases as a result of the volume of the pipe section occupied by the particles. Furthermore in a simplification of equation 1.3.48 Barth [60BA1] does not take the buoyancy effect into account as the gas density is small compared with that of the particle in pneumatic conveying.

1.3.12 Methods of pneumatic conveyor design

i.) Empirical design models

The simplest pneumatic conveyor design guidelines make use of the assumption that the conveying gas is incompressible. One of these methods with a high degree of simplification in the derivation of the equations is presented by Fischer [58FI1]. The total pressure loss in the conveying system, excluding filter units and feeding mechanisms can be written as a sum of individual pressure losses:

$$\Delta P_{tot} = \Delta P_g + \Delta P_a + \Delta P_{grav} + \Delta P_{horiz} + \Delta P_b \quad (1.3.49)$$

where the separate terms can be represented by:

$$\Delta P_g = \lambda_g \frac{\rho_g v^2 L_{tot}}{2d} \quad (1.3.49 a)$$

$$\Delta P_a = \mu \frac{\rho_g v^2}{2} \quad (1.3.49 b)$$

$$\Delta P_{grav} = \mu \rho_g g L_{vert} \quad (1.3.49 c)$$

$$\Delta P_{horiz} = \mu \rho_g g f L_{horiz} \quad (1.3.49 d)$$

$$\Delta P_b = \mu \frac{L_b f \rho_g v^2}{r_o} \quad (1.3.49 e)$$

where: $\Delta P_{tot} =$	Total pressure drop
$\Delta P_g =$	Pressure drop due to air alone
$\Delta P_a =$	Pressure drop due to material acceleration at the feed point
$\Delta P_{grav} =$	Pressure drop due to gravity for the vertical lift only
$\Delta P_{horiz} =$	Pressure drop due to horizontal conveying of material
$\Delta P_b =$	Pressure drop due to bends

Among the simplifying assumptions made in the derivation of these equations are:

- i.) The friction coefficient for the material in horizontal, vertical and bend flow is equivalent to the dynamic sliding friction coefficient. Thus the assumption is that the material slides along the wall of the pipeline at all times.
- ii.) The solids velocity equals the air velocity.

These assumptions result in an underprediction by up to 39% in a model study when conveying hydrated lime in a 90.12 mm diameter pipeline with a total length of 24 m and a material

friction coefficient of 0.9 [94WO1]. It is thus clear that such a simplified model cannot be used to predict the system pressure loss accurately.

A more advanced design equations [90MA1] include the use of the material friction coefficient as defined by Barth [58BA1]. The total system pressure drop is once again assumed to be a sum of individual pressure losses as given in equation 1.3.50.

$$\Delta P_{tot} = \Delta P_g + \Delta P_a + \Delta P_s + \Delta P_{grav} + \Delta P_b + \Delta P_{sep} \quad (1.3.50)$$

The separate terms can thus be defined as:

$$\Delta P_g = \lambda_g \frac{\rho_g v^2 L_{tot}}{2d} \quad (1.3.50 \text{ a})$$

$$\Delta P_a = \mu v \rho_g c \quad (1.3.50 \text{ b})$$

$$\Delta P_s = \mu \lambda_{s2} \frac{\rho_g v^2 L_{tot}}{2d} \quad (1.3.50 \text{ c})$$

$$\Delta P_{grav} = (1-e) \rho_p g L_{vert} = \mu \frac{\rho_g}{CV^{-1}} g L_{vert} \quad (1.3.50 \text{ d})$$

$$\Delta P_b = \frac{0.029 + 0.304 De^{-0.25} L_b \rho_g v^2}{\left(\frac{2}{d} r_b\right)} + 210 \left(\frac{2r_b}{d}\right)^{-1.15} \Delta P_s \quad (1.3.50 \text{ e})$$

where: $\Delta P_s =$ Additional pressure drop due to solids in both horizontal and vertical sections under the assumption that λ_{s2} is identical for both

$\Delta P_{sep} =$ Pressure drop to the solids and air separation equipment

For the bend pressure drop equation 1.3.50 e, the first term is that for the air alone (equation 1.3.6) while the second term is the bend pressure loss due to solids as given by Schuchart [68SC1] valid for particle sizes from 1-2 mm and a voidage higher than 0.95. Note that this term includes the pressure drop due to solids which must be determined before applying equation 1.3.50 e. The total length of pipe in equations 1.3.50 a and 1.3.50 c thus excludes the bend pipe length. Using the above combination of equations the definition of λ_{s2} contains a lifting term in horizontal conveying which is not present in vertical conveying (refer to appendix B for the definition details). The assumption made for practical purposes that the definitions are the same for vertical and horizontal conveying cause the vertical pressure drop due to friction to be overestimated. This results in a conservative estimate of the pressure drop.

Compressibility is not taken into account as the initial conveying pressure and thus density and conveying velocity are unknown. The simplest method is to use atmospheric conditions to determine the density. Limited account of compressibility effects can be included by breaking up the pipeline into successive components. As the pressure drops are calculated for the successive components the pressure and hence the density can be adjusted. This requires a more complex iteration procedure. The initial pipe diameter estimation is done using the Froude number at the pressure minimum from the Zenz and Othmer state diagram.

It is clear that the calculation method presented above requires the determination of the solids friction coefficient and the velocity ratio of air velocity to solids velocity for a given material by means of experimental data. The velocity ratio can be determined from correlations where necessary.

A more accurate approach is to use a system of differential equations and to integrate these numerically. Ferretti [83FE1] and Weber [88WE1] show that this method can be used to accurately predict the sonic velocity of a mixture. This is in effect the limiting condition for pneumatic conveying. Higher mass flow rates cannot be achieved once this limiting condition has been reached. Weber [88WE1] comments that the step by step numerical integration procedure produces the most accurate results when compared to experimental data. Saccani [93SA1] describes the results of a computer programme based on the step by step solution of the differential equations for pneumatic conveying simulation but does not provide the details of the differential equations used or the solution method. One inherent advantage in using the basic differential equations is that the effects of voidage, acceleration and compressibility can be fully accounted for.

It is also clear that the empirical models for pneumatic conveying cannot be used without reliable experimental data for friction coefficient, solids velocity and freefall velocity correlations.

ii.) Using experimental results for conveyor design

A further approach to pneumatic conveyor design is to use an experimental facility and scale the results to reproduce the final conveying system. This method is described by Kraus [80KR1] and is also used by Mills [90MI1] in conjunction with the performance curves discussed in section 1.3.1.

1.4 Discussion and conclusion

For a successful design of a pneumatic conveying system it is clearly an advantage to have an indication of the values of the most important parameters such as the pressure and air and solids velocity at any point in a conveying pipeline. This allows for an exact determination at what point in the pipeline blockages may occur due to reduced particle velocities. Furthermore a trace of these parameters along the complete length of the pipeline also allows for the determination of the exact point where stepped pipelines can be introduced to reduce particle and air velocities and hence reduce wear by abrasion in very long pipelines. The model used for the design programme developed for this thesis should incorporate effects of acceleration and density to allow for an accurate representation of two-phase flow. The effects of compressibility are often ignored in the global design approach where average values between the start and the end of the pipe are used to determine pressure drops and air velocities. Compressibility effects cannot be ignored when long conveying distances are involved. From the differential equations for two-phase flow it becomes clear that such a model requires the accurate determination of for example particle free fall velocities for which the drag coefficient for spherical or non-spherical particles is required. Furthermore a model for bend flow is required and it seems most appropriate to modify the solids friction coefficient to account for the deceleration of the solids in a bend.

1.5 Objectives of this thesis

The objective of this thesis is to develop a computer programme that can be used for the design of a dilute phase pneumatic conveyor. This should at least include the selection of the prime air mover and a complete model of the two-phase flow which represents the conveying of solid material in an air stream in a pneumatic conveyor

This requires the derivation of a suitable mathematical model for two-phase flow from first principles incorporating effects such as acceleration and density and to find a method to solve the mathematical model in an efficient manner.

Furthermore a user friendly interface is to be developed to simplify the definition of for example the pipeline geometry and the analysis of the results.

The results of the computer simulations using the mathematical model are to be compared with experimental conveying data to identify areas which require further refinement and verify the usefulness of the model. As a result of the required user friendly implementation, the final computer programme should allow easy comparison of the output with experimental data.

To allow for useful implementation of such a computer programme the friction coefficients for the type of material that is to be conveyed must be available. For the sake of simplicity an attempt will be made to determine a method for correlating a total friction coefficient incorporating both the effects of air friction and solids friction coefficient. By redefining the friction coefficient it should be possible to use the same correlation for both horizontal and vertical flow pneumatic conveying.

The criteria set for the pneumatic conveyor design programme can be stated as follows:

- The design programme is to be broken up into separate modules such as a pipeline geometry definition module, a simulation module and a output data visualisation module. In addition a separate module for the prime air mover or Roots blower selection should be created with an option to add feeding mechanism and air and solids separation equipment selection modules at a later stage.
- An efficient and user friendly interface for each of the modules must be implemented.
- The two-phase flow simulation programme should be able to implement the following
 - single and two-phase flows in vertical and horizontal pipelines, bends and expansions.
 - use a complete mathematical model so that the output from the programme includes traces of the following variables: the pressure, air density, air average and interstitial velocity, the average particle velocity and the voidage.
 - model vacuum and positive pressure conveying systems
 - allow for a switch from single to two-phase flow for simulation of a complete pipeline system including the air supply pipe to the feeding point.
 - incorporate a bend flow model
 - allow for the incorporation of stepped pipelines
 - make provision for air leakage at the material feeding point

CONVEYING PIPE LAYOUT

2.1 Introduction

The first task for a designer of a pneumatic conveying system is to determine the layout of the conveying pipeline. The routing of the pipeline is often determined by the structures surrounding the conveying plant. It is thus essential that a fast and efficient means be presented to create the data file containing all relevant data on the pipeline layout. This includes bend coordinates and radii, horizontal and vertical pipe section positions, feeding point positions and pipeline expansions which are coupled to a change in pipe diameter. This data file serves as the basis for the conveyor simulation programme. To improve the user interface it was decided to use the programming language DELPHI which is based on PASCAL and makes use of object orientated programming and a visual interface. Computer graphics techniques are used to implement the generation of the pipeline coordinates and a visual on-screen representation of the pipe layout as it is being created. This includes the development of a transformation technique so that the mathematical manipulation of adding a line segment in line with another in three-dimensional space is simplified to a single operation on the x-axis of a Cartesian coordinate system. Examples of the screen output are given in the pneumatic conveyor design programme user manual in appendix E.

2.2 Chapter contents

Section 2.3 of this chapter defines the criteria which must be met by the pipe layout data file generation programme while the theory of working with the basic pipe element, the straight line in three dimensional space, is presented in section 2.4. The three dimensional graphics representation on the computer screen is also included in this section. Section 2.5 describes the output data file and section 2.6 briefly discusses the data interchange file format (DXF) implementation. Concluding remarks are presented in section 2.7.

2.3 Programme requirements

For an analysis of two-phase flow in a pipeline, the exact pipeline geometry has to be defined by the user. To simplify this task the following requirements and criteria can be identified for

the user-friendly implementation of a geometry definition programme that will also generate a data file for use by the two-phase flow analysis programme.

- Break-up of the pipeline geometry into components that are used in the industry to build up a pneumatic conveying pipeline. These include:
 - straight, horizontal and vertical pipe sections
 - bend sections with standard and custom defined bend angles
 - material feeding points
 - expansions in pipe diameter
- Subdivision of the bend components according to their orientation
 - a bend connecting a horizontal pipe with a pipe running vertically upwards
 - a bend connecting a horizontal pipe with a pipe running vertically downwards
 - a bend to the right viewed in direction of the flow connecting two horizontal pipe sections
 - a bend to the left viewed in direction of the flow connecting two horizontal pipe sections
 - a bend connecting a vertical and horizontal pipeline (with flow in an upward direction in the vertical pipe) and an arbitrary rotation around the vertical axis
 - a bend connecting a vertical and horizontal pipeline (with flow in a downward direction in the vertical pipe) and an arbitrary rotation around the vertical axis
- Three dimensional visual representation of the pipeline layout with the definition of the axis system used
- Possibility of undoing a component selection if an error has been made during the selection
- Generation of a geometry data file that can be imported into a standard computer aided design programme such as for example AutoCAD
- User selection of preferred dimension units
- Automatic generation of a geometry data file to be used in the two-phase flow analysis

2.4 Theory and programme implementation

2.4.1 Introduction

The definition of the pipeline geometry requires the definition of the coordinates of the selected components in three-dimensional space. Single components have to be connected to each other following a compatible sequence and alignment to create a continuous conveying pipe layout. The addition of components is broken down into the addition of sequences of straight lines. The bend component for example is divided into a finite number of connected straight sections

to define the bend geometry. Determining the required coordinates in a general three-dimensional space is work intensive as all three coordinates of both the start and end points of a line have to be calculated. A method presented in section 2.4.2 is developed to simplify the coordinate definition by translating and rotating an arbitrary line segment in space so that it is aligned with the x-axis of the coordinate system. This is effectively achieved by coordinate transformation routines which are well known in computer graphics applications. Once this is done the addition of a straight line section requires the determination of a single endpoint coordinate while the addition of a bend requires the definition of two endpoint coordinates for each line segment used to make up a complete bend. Retransformation of the coordinates back into three dimensional space is done using the inverse of the rotation angles and translation distances determined during the alignment of the original line segment with the x-axis. This ensures the correct final component coordinates.

2.4.2 Aligning a line in three dimensional space with a coordinate axis

Figure 2.1 (a) shows a line segment lying in a three dimensional space with the definition of the axis system used. The apostrophe after the coordinate variables indicates the successive matrix operations performed on the coordinate vector. The dummy variable a is used to obtain the correct matrix size for multiplication.

The following operations are executed to align the line segment with the x-axis:

- i.) Translation of the start and end coordinates of the line segment so that the start point of the line segment is moved to the origin of the axis system. This matrix operation on the coordinates of the start and end point of the line segment can be represented as follows:

$$\begin{bmatrix} x_1' \\ y_1' \\ z_1' \\ a_1' \end{bmatrix} = \begin{bmatrix} 1 & 0 & 0 & -x_0 \\ 0 & 1 & 0 & -y_0 \\ 0 & 0 & 1 & -z_0 \\ 0 & 0 & 0 & 1 \end{bmatrix} \begin{bmatrix} x_1 \\ y_1 \\ z_1 \\ 1 \end{bmatrix} \quad (2.4.1)$$

The result of this operation is shown in figure 2.1 (b).

- ii.) Determination of the angle of rotation around the z-axis to move the line segment into the x-z plane. A subroutine is used to determine the angle θ_1 that the projection of the line segment on the x-y plane makes with the x-axis. The definition of angle θ_1 is given in figure 2.1 (b).
- iii.) Rotation the line segment into the x-z plane around the y-axis. This is done by means of a second matrix operation on the translated coordinates represented in equation 2.4.2.

$$\begin{bmatrix} x_1'' \\ y_1'' \\ z_1'' \\ a_1'' \end{bmatrix} = \begin{bmatrix} \cos \theta_1 & \sin \theta_1 & 0 & 1 \\ -\sin \theta_1 & \cos \theta_1 & 0 & 1 \\ 0 & 0 & 1 & 1 \\ 0 & 0 & 0 & 1 \end{bmatrix} \begin{bmatrix} x_1' \\ y_1' \\ z_1' \\ a_1' \end{bmatrix} \quad (2.4.2)$$

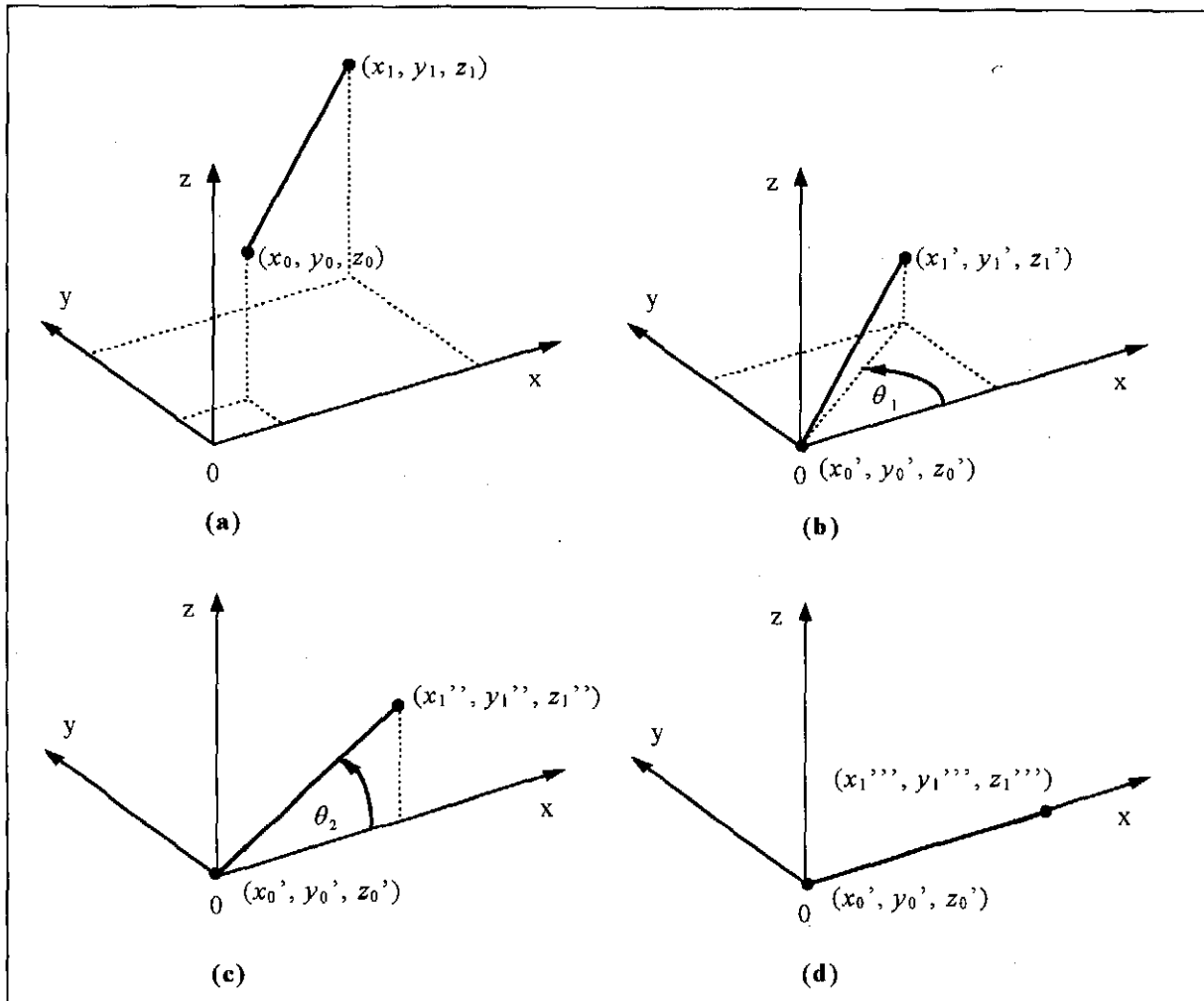


Fig. 2.1 Line segment end coordinate transformation

- iv.) Determination of the angle θ_2 between the line segment and the x-axis. This angle is the effective inclination angle β of the line segment representing the pipe as defined in figure 3.1. This is required during the two-phase flow analysis described in chapter 3. The effects of rotation around the z-axis and the definition of angle θ_2 is depicted in figure 2.1 (c).
- v.) Rotation of the line segment onto the x-axis is done by means of a third matrix operation given in equation 2.4.3. The results of this operation are depicted in figure 2.1 (d).

$$\begin{bmatrix} x_1''' \\ y_1''' \\ z_1''' \\ a_1''' \end{bmatrix} = \begin{bmatrix} \cos \theta_2 & 0 & -\sin \theta_2 & 1 \\ 0 & 1 & 0 & 1 \\ \sin \theta_2 & 0 & \cos \theta_2 & 1 \\ 0 & 0 & 0 & 1 \end{bmatrix} \begin{bmatrix} x_1'' \\ y_1'' \\ z_1'' \\ a_1'' \end{bmatrix} \quad (2.4.3)$$

2.4.3 Adding components

Both the vertical and horizontal line segments are added by letting the start coordinates of the new line segment be equal to the end coordinates of the preceding segment. The coordinates of the end point of the new segment are determined by adding the length of the line segment to the x-coordinate of the end point of the previous line segment.

Bend segments are added by first determining the bend identification points which are the bend start coordinates, bend apex coordinates, bend end coordinates and the centerpoint coordinates. Depending on the type of bend these will lie in the x-y or in the x-z plane. The bend is then subdivided into n subsections and each arc segment treated as a straight line segment. The exact start and end coordinates of the line segments are determined using the parametric circle equation. Once all relevant coordinates have been determined they are transformed back into three dimensional space to yield the required three dimensional component coordinates used for graphics and data file generation.

The bend apex coordinates and the bend end coordinates are transformed back onto the x-axis as described in section 2.4.2 to form the basis on which to add the following component. This ensures correct alignment.

Following is an example of the generation of the coordinate points for a bend connecting a vertical pipe with flow in an upward direction to a horizontal pipeline. The user may specify the rotation of the component around the vertical z-axis.

Figure 2.2 depicts the bend segment as it is added to the end of a line segment that has been transformed onto the x-axis by rotating the segment 90° in a clockwise direction around the y-axis as described in section 2.4.2.

The bend identification coordinates with the numbered subscripts referring to the identification points defined in figure 2.2 are determined as follows:

Coordinate 1: $x_1 = x_p$

$$y_1 = y_p$$

$$z_1 = z_p$$

Coordinate 2: $x_2 = x_p + r$

$$y_2 = y_p$$

$$z_2 = z_p$$

Coordinate 3: $x_3 = x_p + r$

$$y_3 = y_p$$

$$z_3 = z_p - r$$

Coordinate 4: $x_4 = x_p$

$$y_4 = y_p$$

$$z_4 = z_p - r$$

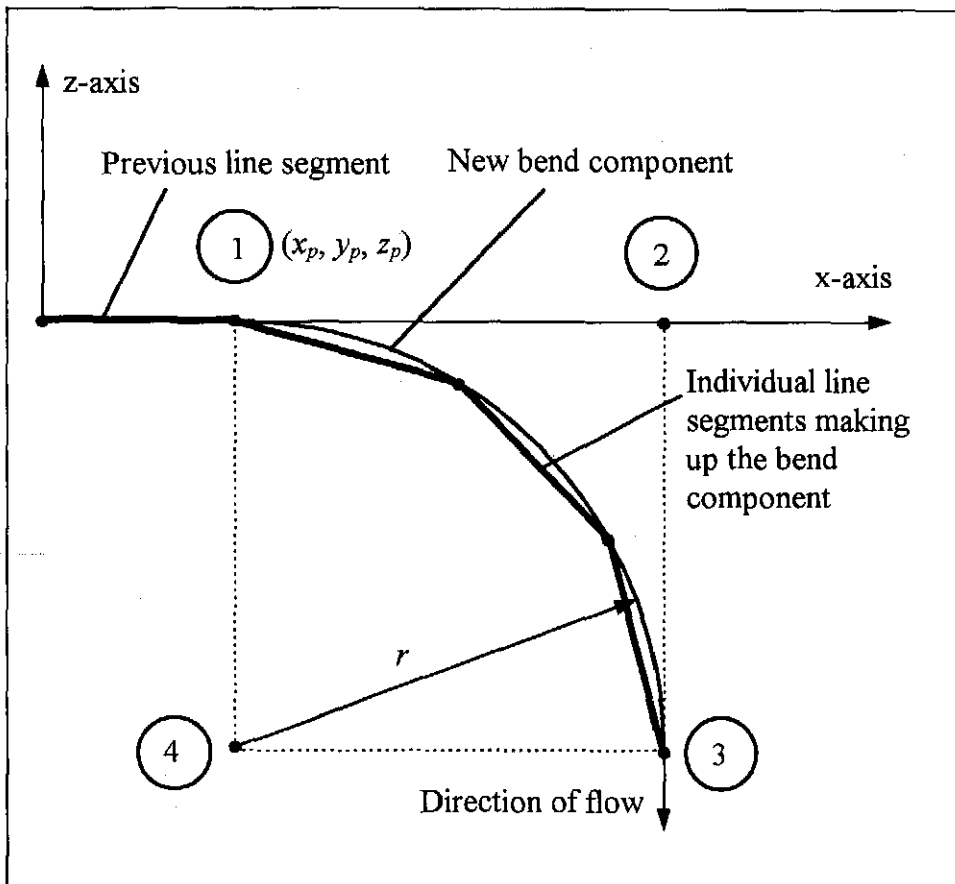


Fig. 2.2 Adding a bend segment

The parametric circle equation used for the generation of the bend segment start and end coordinates is given as:

$$\begin{aligned} x &= r \cos(2\pi t) + x_4 \\ z &= r \sin(2\pi t) + z_4 \end{aligned} \quad (2.4.4)$$

where x_4 and z_4 represent the centerpoint coordinates of the bend in the x-z plane and t is the independent parameter that is chosen to run from 0 to 1 to generate a circle in the anti-clockwise direction. For the quarter circle segment that is generated to represent the bend section in figure 2.2, t runs from 0.25 to 0. The bend segment coordinates are generated by

dividing the distance that t runs by the required number of segments and determining the coordinates for each step in t from equation 2.4.4.

The user defined angle of rotation of the bend around the z -axis is added to the inverse of the angle of rotation θ_1 around the z -axis determined in section 2.4.2.

A feeding point component is identified by an additional entry in the component data file and a component identifier code. Additional data required are the feeding tee pipeline diameter.

2.4.4 Transforming a line segment from the x -axis back into 3-D space

The sequence of translations and rotations described in section 2.4.2 are used in the opposite order of execution to transform line segment start and end coordinates back into three dimensional space. The coordinate transformation can be performed as a series of matrix operations as follows without the need for determining angles or translation distances between operations as in section 2.4.2. The angle θ_3 represents the rotation angle around the y -axis and the angle θ_4 the rotation angle around the z -axis. These angles are equivalent to the inverse of θ_2 and θ_1 respectively.

$$\begin{bmatrix} x_1 \\ y_1 \\ z_1 \\ a \end{bmatrix} = \begin{bmatrix} \cos\theta_3 & 0 & -\sin\theta_3 & 1 \\ 0 & 1 & 0 & 1 \\ \sin\theta_3 & 0 & \cos\theta_3 & 1 \\ 0 & 0 & 0 & 1 \end{bmatrix} \begin{bmatrix} \cos\theta_4 & \sin\theta_4 & 0 & 1 \\ -\sin\theta_4 & \cos\theta_4 & 0 & 1 \\ 0 & 0 & 1 & 1 \\ 0 & 0 & 0 & 1 \end{bmatrix} \begin{bmatrix} 1 & 0 & 0 & x_0 \\ 0 & 1 & 0 & y_0 \\ 0 & 0 & 1 & z_0 \\ 0 & 0 & 0 & 1 \end{bmatrix} \begin{bmatrix} x_1''' \\ y_1''' \\ z_1''' \\ 1 \end{bmatrix} \quad (2.4.5)$$

2.4.5 Three-dimensional graphics representation

The pipe layout is represented in three-dimensional space. To visualise this on a graphics screen, the three-dimensional coordinates have to be transformed into a two-dimensional world coordinate system to create an impression of three-dimensional space. The term world coordinate system is used for a two-dimensional full scale representation of three-dimensional space. These two-dimensional world coordinates have to be transformed to viewing coordinates so that the complete pipe layout is always visible within the boundaries of the graphics window on the screen. This is done by means of a scaling and a translation operation [94HE1]. Finally the viewing coordinates have to be transformed to device coordinates. This operation is necessary as the direction of the coordinate system used to address the graphics window on the computer monitor is different to the convention used for the viewing coordinate system.

Figure 2.3 shows the derivation required for the three-dimensional to two-dimensional world coordinate transformation. The isometric angle of 30° is chosen for angles α_w and β_w .

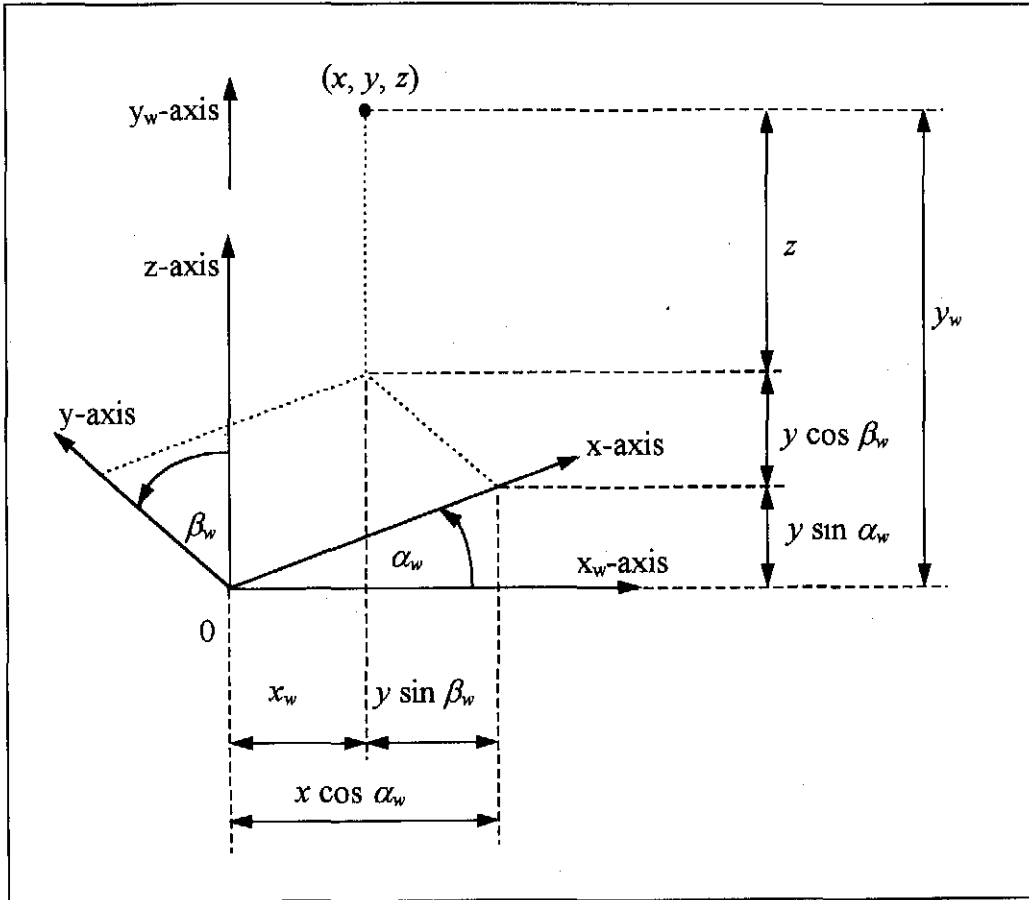


Fig. 2.3 Coordinate system transformation

The world coordinates can be calculated as follows:

$$\begin{aligned} x_w &= x \cos \alpha_w - y \sin \beta_w \\ y_w &= x \sin \alpha_w + y \cos \beta_w + z \end{aligned} \quad (2.4.6)$$

where the subscript w refers to the world coordinate system.

The scaling and transformation factors are determined by finding the maximum and minimum values of the x - and y -coordinates calculated in equation 2.4.6 where w_t and w_b represents the maximum and minimum y -coordinates and w_r and w_l represents the maximum and minimum x -coordinates respectively. Figure 2.4 depicts the notation used for the world and viewing coordinate system boundaries.

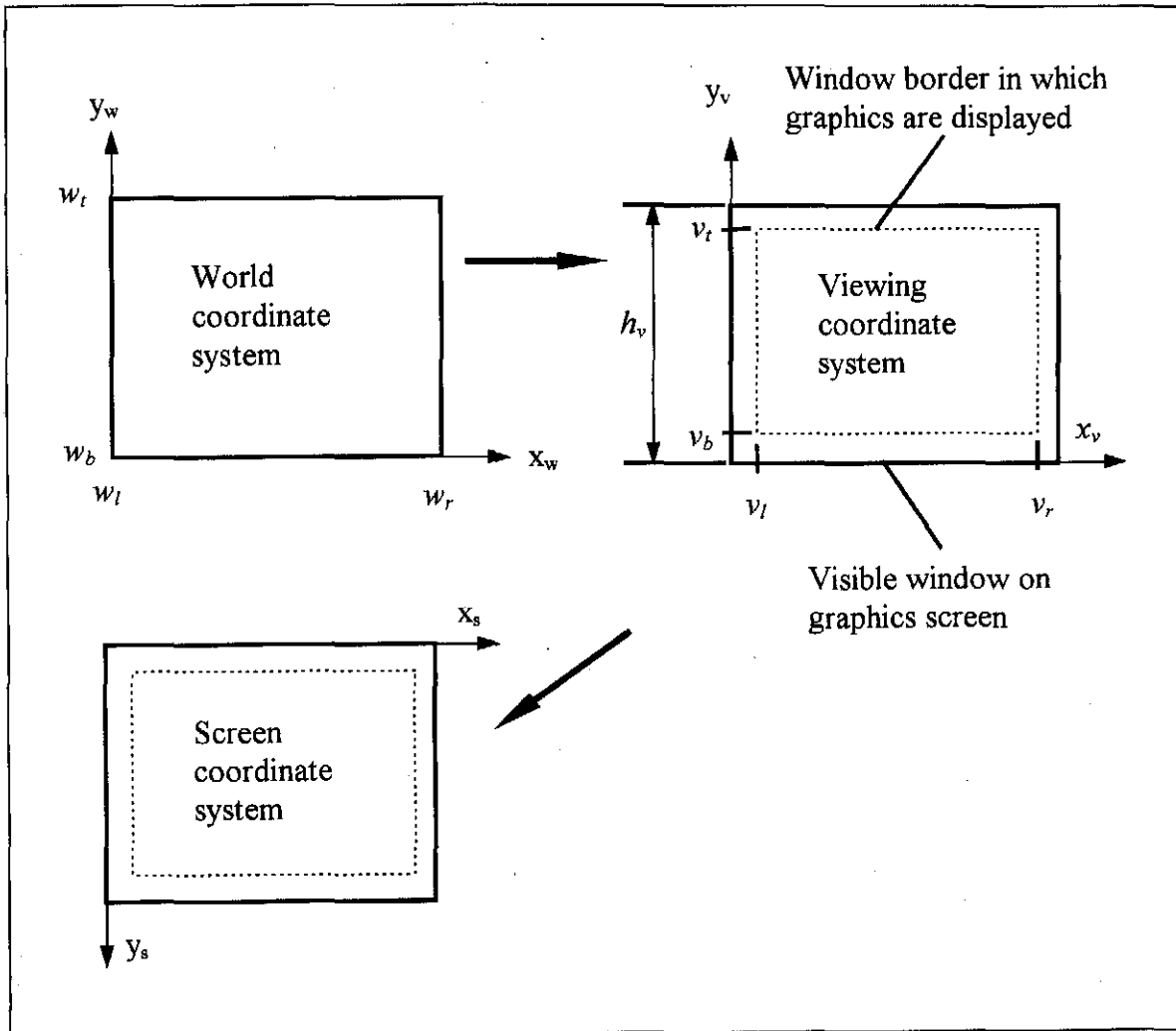


Fig. 2.4 Coordinate system notation

The scaling factors and translation distances are determined respectively as follows [90HI1]:

$$s_x = \frac{v_r - v_l}{w_r - w_l} \tag{2.4.7}$$

$$s_y = \frac{v_t - v_b}{w_t - w_b}$$

$$t_x = \frac{v_l w_r - w_l v_r}{w_r - w_l} \tag{2.4.8}$$

$$t_y = \frac{v_b w_t - w_b v_t}{w_t - w_b}$$

The viewing window coordinates with subscript v are then calculated as:

$$\begin{aligned} x_v &= x_w s_x + t_x \\ y_v &= y_w s_y + t_y \end{aligned} \tag{2.4.9}$$

Transformation to the required screen coordinate system is done as follows:

$$\begin{aligned}x_s &= x_v \\y_s &= h_v - y_v\end{aligned}\tag{2.4.10}$$

where h_v is the viewing window height and subscript s refers to the screen coordinates.

After each addition or deletion of a component by the user, the graphics window is regenerated by first determining the maximum and minimum x -and y -coordinates from the complete component data file using equation 2.4.6. One by one the screen coordinates for the start and end point of each line segments making up a component are calculated using equations 2.4.6, 2.4.9 and 2.4.10. A line is drawn on the graphics screen by connecting these start and end coordinates with a line.

Further manipulations such as perspective views or hidden line identification are not included in the graphics representation as the above is believed to give a satisfactory visual representation of the pipeline geometry. Figure 2.5 depicts the results of the pipeline geometry visualisation during generation of the pipeline layout.

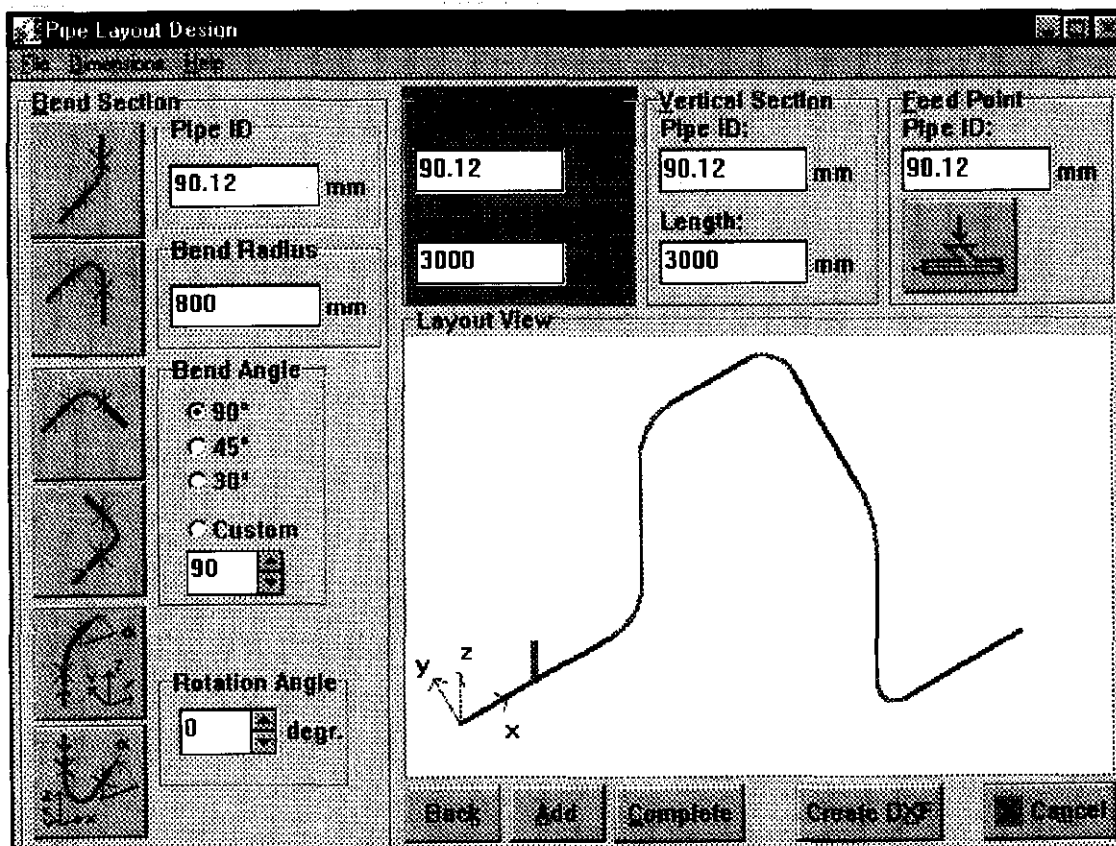


Fig. 2.5 Example of the pipeline layout generation interface

2.5 Component data file

A sample component data file generated by the pipe layout generation programme and the definition of each entry is presented in appendix A.

2.6 DXF file format

The DXF or Drawing Interchange File format is used by many computer software vendors as a standard format for the exchange of drawing files. A subroutine in the pipe layout generation programme converts the component data file to the DXF file format [93AN1] so that the programme user can import the geometry of the pipe layout into a draughting programme for further manipulation and creation of pipeline assembly drawings. Figure A.1 in appendix A for example is generated using the DXF output file.

2.7 Discussion and conclusion

The data file generation programme is successfully implemented and allows fast generation of data files for use in the main simulation programme. This is one of the prerequisites to the optimisation of a pneumatic conveying pipeline layout as more than one layout can be created in a short time. These layouts can also be imported into computer aided design packages for further manipulation.

A method for the simple manipulation of line segments representing pipeline segments is developed and implemented.

Visual representation of the bend types and the break up of components into the four main classes, namely feed points, bends, horizontal and vertical pipes allows for logical grouping of the data input windows as shown in figure 2.5. This allows new users to become familiar with the programme without reading instruction manuals. Built in checks ensure that components are not added in incorrect sequences and an option to undo a selection improves the user friendliness. The units of the dimensions can also be selected according to user preference.

The theory and implementation of the graphics manipulation presented in this chapter and subsequently implemented in the pipeline geometry definition programme provides an insight into the complexity of computer graphics representation.

A user manual for this part of the pneumatic conveyor design programme can be found in section E.3 in appendix E.

TWO-PHASE FLOW THEORY

3.1 Introduction

The complete set of differential equations governing two-phase flow for a mixture of gas and solids are given by Ferretti [83FE1]. To gain an understanding of the significance and origin of each term in the equations it is deemed essential to present a detailed derivation of each equation and explore the different definitions of the friction coefficients as discussed in the literature study.

3.2 Chapter contents

This chapter contains the derivation of the differential equations that are used as the mathematical two-phase flow model in the pneumatic conveyor simulation programme. Sections 3.3.1 and 3.3.2 deal with the derivation of the gas continuity and the solids continuity equation. Section 3.3.3 presents the derivation of the momentum equation for two-phase flow resulting in an expression for the pressure drop equation while section 3.3.4 makes use of Newton's second law of motion to derive the solids motion equation. The ideal gas equation is used to derive the differential equation of state for the gas in section 3.3.5. Once the derivation of the two-phase flow equations is complete, the clean air or single-phase flow equations are presented in section 3.4

The derivation of an approximation of the friction coefficient for the solids moving through a bend is presented in section 3.5 while section 3.6 presents the theory involved in the definition of the pipe expansions. Concluding remarks are given in section 3.7.

3.3 Derivation of the two-phase flow differential equations

To simplify the understanding and the derivation of the two-phase flow differential equations, the solid phase can be thought of as moving as a coherent block along the pipeline as shown in the two-phase flow model in figure 3.1. This simplifies the definition of the respective solids and gas flow areas and clarifies the interaction of forces with the pipe wall and the solids and gaseous phase.

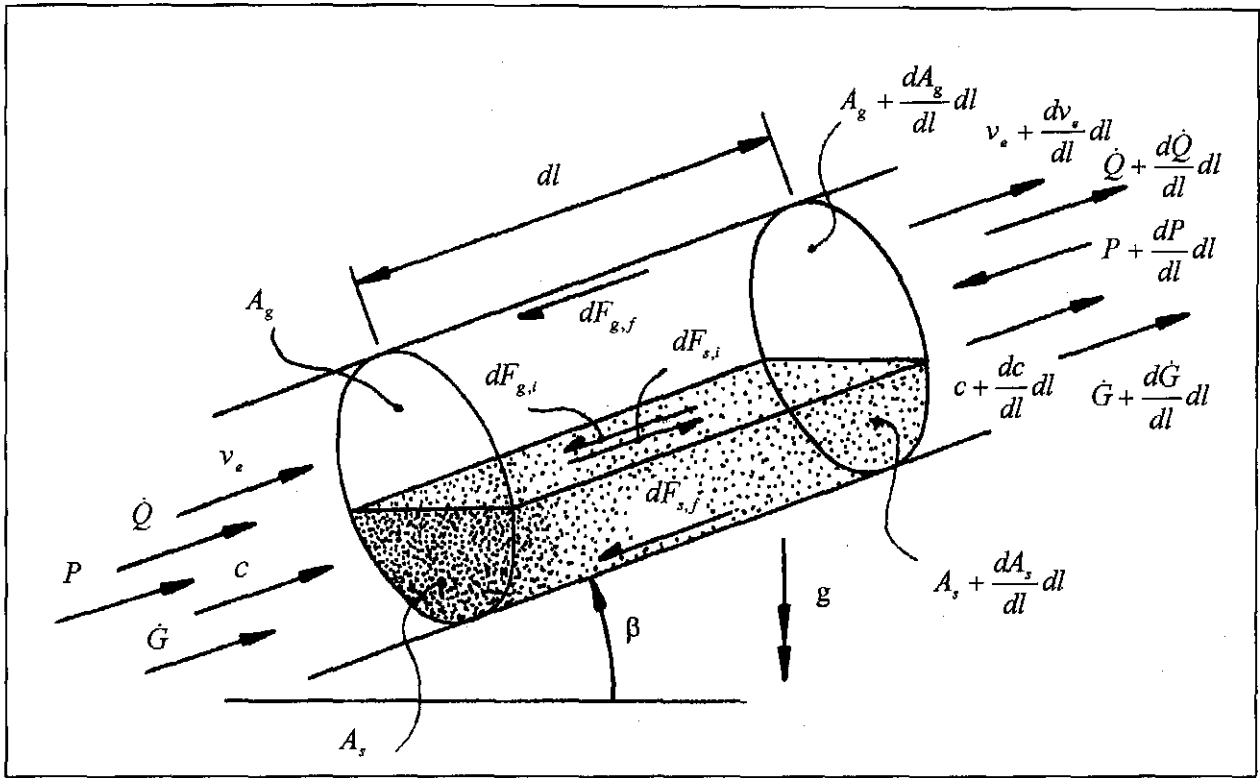


Fig. 3.1 Model of two-phase flow

3.3.1 Continuity equation for the gaseous phase

The mass flow rate for the gas phase can be written as:

$$\dot{Q} = \rho_g A_g v_e \tag{3.3.1}$$

where the interstitial velocity v_e is the air velocity between the particles and can be defined as the average air velocity v divided by the voidage e . The voidage defines the fraction of a section of pipe volume occupied by the gaseous phase. In dilute phase flow the voidage is close to unity. Inspecting the definition of the voidage as given in equation 3.3.2, the length can be cancelled out of the terms defining the volumes of the gaseous and solid phase respectively. The voidage:

$$e = \frac{V - V_s}{V} \tag{3.3.2}$$

can then be written as:

$$e = \frac{A - A_s}{A} \tag{3.3.3}$$

Substituting the total pipe cross sectional area with the sum of the pipe areas through which the solid and the gaseous phase flows, equation 3.3.3 can be rewritten as:

$$e = \frac{A_g}{A} \quad \text{or} \quad 1 - e = \frac{A_s}{A} \quad (3.3.4)$$

The total area in equation 3.3.4 can be replaced with the area formula of a circular cross section:

$$A_g = \frac{e\pi d^2}{4} \quad (3.3.5)$$

Using equation 3.3.4 and the definition of the mass flow ratio:

$$\mu = \frac{\dot{G}}{\dot{Q}} \quad (3.3.6)$$

and substituting this into equation 3.3.1 one can solve for the interstitial air velocity as:

$$v_e = \frac{\dot{G}}{\rho_g e \mu A} \quad (3.3.7)$$

Differentiating equation 3.3.7 with respect to the pipe length and assuming that the solids mass flow rate and mass flow ratio remain constant while the pipe cross sectional area may vary yields the following :

$$\begin{aligned} \frac{d}{dl}(Av_e e \rho_g) &= Ae\rho_g \frac{dv_e}{dl} + Av_e e \frac{d\rho_g}{dl} + Av_e \rho_g \frac{de}{dl} + v_e e \rho_g \frac{dA}{dl} \\ &= 0 \end{aligned} \quad (3.3.8)$$

Rewritten in terms of the interstitial air velocity gradient equation 3.3.8 yields:

$$\frac{dv_e}{dl} = -\frac{v_e}{\rho_g} \frac{d\rho_g}{dl} - \frac{v_e}{e} \frac{de}{dl} - \frac{v_e}{A} \frac{dA}{dl} \quad (3.3.9)$$

3.3.2 Continuity equation for the solid phase

Introducing the cross sectional area from equation 3.3.4, the flow area for the solid phase can be rewritten as:

$$A_s = (1 - e)A \quad (3.3.10)$$

Setting equation 3.3.10 into the solids continuity equation:

$$\dot{G} = \rho_s A_s c \quad (3.3.11)$$

and rewriting in terms of the solid particle velocity:

$$c = \frac{\dot{G}}{\rho_s (1-e) A} \quad (3.3.12)$$

Differentiating with respect to the pipe length once again under the assumption that the solids mass flow rate remains constant and that the pipe cross sectional area may vary yields:

$$\begin{aligned} \frac{d}{dl}(Ac(1-e)) &= A(1-e) \frac{dc}{dl} - Ac \frac{de}{dl} + c(1-e) \frac{dA}{dl} \\ &= 0 \end{aligned} \quad (3.3.13)$$

Rewriting equation 3.3.13 in terms of the voidage gradient yields:

$$\frac{de}{dl} = \frac{(1-e)}{c} \frac{dc}{dl} + \frac{(1-e)}{A} \frac{dA}{dl} \quad (3.3.14)$$

3.3.3 Pressure drop equation

The pressure drop equation is derived for a pipeline with an arbitrary angle of inclination β measured from the horizontal. Referring to figure 3.1 and equating the resultant force to the rate of change of momentum for the gaseous phase in the axial pipe direction yields:

$$\begin{aligned} PA_g - \left(P + \frac{dP}{dl} dl \right) \left(A_g + \frac{dA_g}{dl} dl \right) - dF_{g,f} - dF_{g,i} - \rho_g A_g g \sin \beta dl = \\ \left(\dot{Q} + \frac{d\dot{Q}}{dl} dl \right) \left(v_e + \frac{dv_e}{dl} dl \right) - \dot{Q} v_e \end{aligned} \quad (3.3.15)$$

where dF_{g} and $dF_{g,i}$ are the wall shear and interface shear forces respectively.

In a similar manner equating the resultant force to the rate of change of momentum for the solid phase in the axial pipe direction yields:

$$\begin{aligned} PA_s - \left(P + \frac{dP}{dl} dl \right) \left(A_s + \frac{dA_s}{dl} dl \right) - dF_{s,f} + dF_{s,i} - \rho_s A_s g \sin \beta dl - dF_{s,i} = \\ \left(\dot{G} + \frac{d\dot{G}}{dl} dl \right) \left(c + \frac{dc}{dl} dl \right) - \dot{G} c \end{aligned} \quad (3.3.16)$$

The term $dF_{s,l}$ represents the lifting force required to keep solid particles in suspension during horizontal conveying.

Referring to figure 3.1 the two interfacial forces must balance yielding:

$$dF_{g,i} - dF_{s,i} = 0 \quad (3.3.17)$$

Both the wall friction terms for the gaseous phase and solid phase can be represented in the conventional manner yielding:

$$dF_{g,f} = A_g \lambda_g \frac{\rho_g v_e^2}{2d} dl \quad (3.3.18)$$

and:

$$dF_{s,f} = A_s \lambda_s^* \frac{\rho_s c^2}{2d} dl \quad (3.3.19)$$

The derivation of the term $dF_{s,l}$ requires elucidation. The energy required to move a particle a distance of Δz under the influence of a force F_s can be expressed as :

$$\Delta W_{s,l} = F_s \Delta z \quad (3.3.20)$$

The distance Δz that a particle falls during the time it traverses a distance Δl at a pipe inclination angle β can be coupled to the particle terminal falling velocity w_s and the particle axial velocity c by inspecting the vector triangles in figure 3.2. Using the triangle geometry the following relation holds:

$$\Delta z = \frac{\Delta l w_s \cos \beta}{c} \quad (3.3.21)$$

Neglecting particle acceleration, a balance of forces according to figure 3.3 yields:

$$F_s = (\rho_s - \rho_g) V_s g \cos \beta \quad (3.3.22)$$

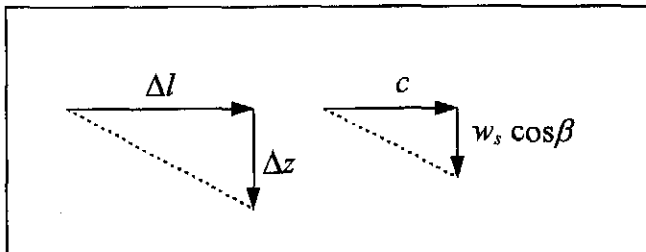


Fig. 3.2 Particle velocity and distance relationship

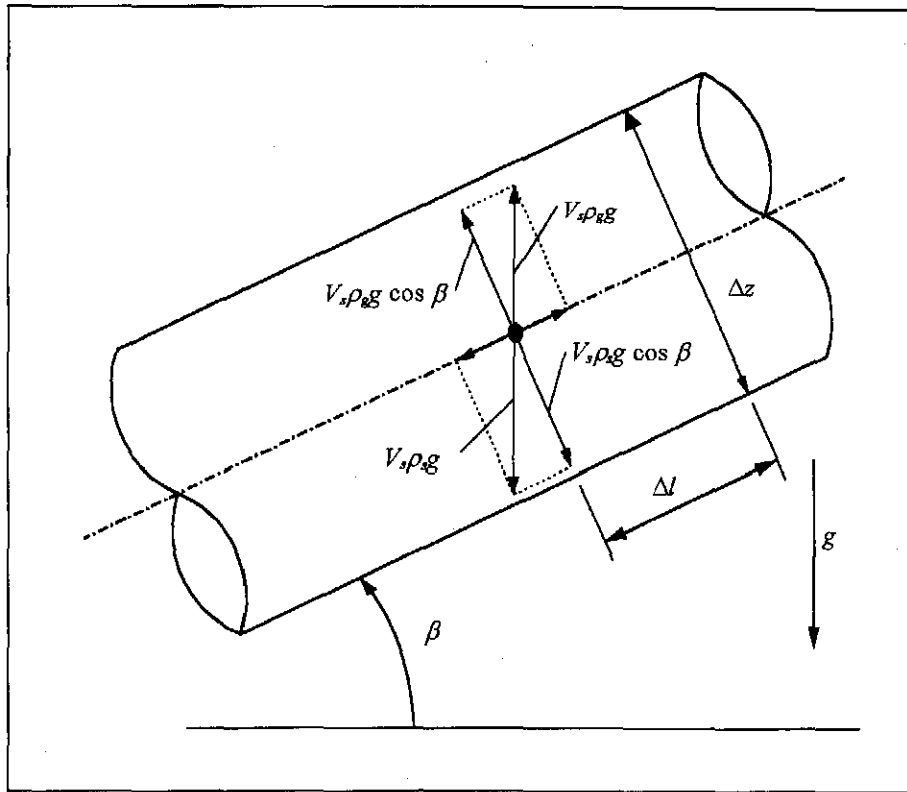


Fig. 3.3 Buoyancy and gravity forces on a single particle

Setting equations 3.3.21 and 3.3.22 into equation 3.3.20 and multiplying by the number of particles present in a volume element to obtain the total energy required:

$$\Delta W_{s,l} = A_s \Delta l (\rho_s - \rho_g) g \cos^2 \beta \frac{w_s}{c} \Delta l \quad (3.3.23)$$

Here the solids area $A_s \Delta l$ equals the total number of particles in a pipe volume element of length Δl multiplied with the volume of a single particle V_s . Substituting the solids flow area with the definition of the voidage, dividing by the traversed length and rewriting equation 3.3.23 in differential form results in the required expression:

$$dF_{s,l} = (1 - e) A (\rho_s - \rho_g) g \cos^2 \beta \frac{w_s}{c} dl \quad (3.3.24)$$

Ferretti [83FE1] uses the interstitial air velocity instead of the particle velocity as the denominator in the velocity ratio term w_s/c in equation 3.3.24. Barth [58BA1] uses the same derivation given above to determine the relationship presented in equation 3.3.21 but nevertheless recommends the use of the ratio of the terminal velocity to the interstitial air velocity instead of the ratio of the terminal velocity to the solids velocity to determine the lifting energy required. No satisfactory explanation is given to substantiate this recommendation. According to the derivation presented above it is believed correct to use the

particle velocity as denominator in the velocity ratio term w_s/c in equation 3.3.24 instead of the interstitial air velocity.

Equations 3.3.15 and 3.3.16 are added, multiplied out and second order terms discarded to yield the overall pressure balance equation. Substituting equations 3.3.17, 3.3.18, 3.3.19 and 3.3.24 into the resultant equation yields:

$$\begin{aligned} \dot{Q} \frac{dv}{dl} dl + v_e \frac{d\dot{Q}}{dl} dl + \dot{G} \frac{dc}{dl} dl + c \frac{d\dot{G}}{dl} dl = & -A_g \frac{dP}{dl} dl - P \frac{dA_g}{dl} dl - A_s \frac{dP}{dl} dl - P \frac{dA_s}{dl} dl \\ & -A_g \lambda_g \frac{\rho_g v_e^2}{2d} dl - A_s \lambda_s^* \frac{\rho_s c^2}{2d} dl \\ & -A_g \rho_g g \sin \beta dl - A_s \rho_s g \sin \beta dl \\ & -(1-e)A(\rho_s - \rho_g)g \cos^2 \beta \frac{w_s}{c} dl \quad (3.3.25) \end{aligned}$$

The separate phase areas in the pressure terms can be added into a single term containing the total pipe area and the solid and gas mass flows replaced with the definitions given in equations 3.3.1 and 3.3.12. Equation 3.3.25 can then be divided by the pipe area throughout and the resulting area ratio terms substituted with the voidage as defined in equation 3.3.4.

Furthermore the differential mass flow terms are zero as the respective mass flows are constant. Collecting terms and simplifying, equation 3.3.25 can be written as:

$$\begin{aligned} -\frac{dP}{dl} = & e \left(\rho_g v_e \frac{dv_e}{dl} + \lambda_g \frac{\rho_g v_e^2}{2d} + \rho_g g \sin \beta \right) \\ & + (1-e) \left(\rho_s c \frac{dc}{dl} + \lambda_s^* \frac{\rho_s c^2}{2d} + \rho_s g \sin \beta + (\rho_s - \rho_g)g \cos^2 \beta \frac{w_s}{c} \right) \quad (3.3.26) \end{aligned}$$

The following two terms in equation 3.3.26:

$$e \lambda_g \frac{\rho_g v_e^2}{2d} + (1-e) \lambda_s^* \frac{\rho_s c^2}{2d} \quad (3.3.27)$$

can be modified by rewriting $(1-e)$ in terms of the solids continuity equation 3.3.12 and cancelling out the material mass flow rate by using the air continuity equation 3.3.7. The terms in equation 3.3.27 can thus be rewritten as:

$$e \left((\lambda_g + \mu \lambda_{s1}) \frac{\rho_g v_e^2}{2d} \right) \quad (3.3.28)$$

The solids friction coefficient is defined as:

$$\lambda_{s1} = \lambda_s^* \frac{c}{v_e} \quad (3.3.29)$$

Rewriting equation 3.3.26 in this format results in:

$$\begin{aligned} -\frac{dP}{dl} = & e \left(\rho_g v_e \frac{dv_e}{dl} + \rho_g g \sin \beta \right) \\ & + (1-e) \left(\rho_s c \frac{dc}{dl} + \rho_s g \sin \beta + (\rho_s - \rho_g) g \cos^2 \beta \frac{w_s}{c} \right) \\ & + e \left(\lambda_g + \mu \lambda_{s1} \right) \frac{\rho_g v_e^2}{2d} \end{aligned} \quad (3.3.30)$$

The pressure drop equation can also be rewritten in terms of a total friction coefficient and the free fall velocity replaced with the free fall velocity in a cloud of particles:

$$\begin{aligned} -\frac{dP}{dl} = & e \left(\rho_g v_e \frac{dv_e}{dl} + \rho_g g \sin \beta \right) \\ & + (1-e) \left(\rho_s c \frac{dc}{dl} + \rho_s g \sin \beta + (\rho_s - \rho_g) g \cos^2 \beta \frac{w_{s,c}}{c} \right) \\ & + e \lambda_{tot} \frac{\rho_g v_e^2}{2d} \end{aligned} \quad (3.3.30 \text{ a})$$

allowing the pressure drop equation to be used for the determination of a correlation equation for the total friction coefficient from experimental data.

Note that equation 3.3.29 is presented with the friction coefficient defined in a different form to that given by Barth [58BA1]. This is as a result of excluding the gravitational terms from the friction coefficient. For the development of the friction coefficient as defined by Barth [58BA1] refer to appendix B. A further two possible versions of the pressure drop equation with the respective merits in the definition of the friction coefficient are also given. Equation 3.3.30 ensures that the friction coefficient definition remains the same for horizontal and vertical flow which is not the case for the other two definitions given in appendix B. For future references to the friction coefficients it is imperative at this point to understand the different definitions of the solids friction coefficient λ_s and that of the solids impact and friction coefficient λ_s^* by referring to the definitions given in appendix B.

3.3.4 Derivation of the equation of motion

Newton's second law of motion can be used to derive the motion equation for the solid particles as follows:

$$V_s \rho_s c \frac{dc}{dl} = F_{s,d} - F_{s,g} - F_{s,wd} + F_{s,p} \quad (3.3.31)$$

with the force terms defined as:

$$F_{s,d} = \frac{3}{4} V_s C_d \frac{\rho_g (v_e - c)^2}{d_s e} \quad (3.3.32)$$

$$F_{s,g} = V_s \rho_s g \sin \beta \quad (3.3.33)$$

$$F_{s,wd} = V_s \rho_s \lambda_s^* \frac{c^2}{2d} \quad (3.3.34)$$

The pressure force on a particle is a result of the pressure gradient across the particle and can be written as:

$$\begin{aligned} F_{s,p} &= PA_s - (P + \frac{dP}{dl} dl) (A_s + \frac{dA_s}{dl} dl) \\ &= -P \frac{dA_s}{dl} dl - A_s \frac{dP}{dl} dl \end{aligned} \quad (3.3.35)$$

Replacing the pressure gradient term with the pressure drop equation 3.3.30 and combining equations 3.3.31 to 3.3.35 the resultant term yields the general particle motion equation.

$$\begin{aligned} \frac{dc}{dl} &= \frac{3}{4} C_d \frac{\rho_g}{\rho_s d_s} \frac{(v_e - c)^2}{ce} - \frac{1}{c} g \sin \beta + \frac{\rho_g}{\rho_s c} \left(v_e \frac{dv_e}{dl} + g \sin \beta \right) \\ &\quad - \frac{1}{ce} \lambda_s^* \frac{c^2}{2d} + \frac{\rho_g}{\rho_s c} (\lambda_g + \mu \lambda_{s1}) \frac{v_e^2}{2d} \\ &\quad + \frac{(1-e)(\rho_s - \rho_g)}{e c \rho_s} g \cos^2 \beta \frac{w_s}{c} - \frac{P}{\rho_s ce} \left(\frac{1}{A_s} \frac{dA_s}{dl} \right) \end{aligned} \quad (3.3.36)$$

Assuming that the particle frontal area is constant, the last term in equation 3.3.36 can be neglected. Rewriting the particle impact and friction coefficient in terms of the definition given in equation 3.3.29, the equation of motion can be written as:

$$\begin{aligned} \frac{dc}{dl} = & \frac{3}{4} C_d \frac{\rho_g}{\rho_s d_s} \frac{(v_e - c)^2}{ce} - \frac{1}{c} g \sin \beta + \frac{\rho_g}{\rho_s c} \left(v_e \frac{dv_e}{dl} + g \sin \beta \right) \\ & - \frac{1}{ce} \lambda_{s1} \frac{cv_e}{2d} + \frac{\rho_g}{\rho_s c} (\lambda_g + \mu \lambda_{s1}) \frac{v_e^2}{2d} \\ & + \frac{(1-e)(\rho_s - \rho_g)}{e c \rho_s} g \cos^2 \beta \frac{w_s}{c} \end{aligned} \quad (3.3.37)$$

As in the pressure drop equation 3.3.30 the friction coefficients in the fifth term in equation 3.3.37 can be replaced with the total friction coefficient:

$$\begin{aligned} \frac{dc}{dl} = & \frac{3}{4} C_{d,c} \frac{\rho_g}{\rho_s d_s} \frac{(v_e - c)^2}{ce} - \frac{1}{c} g \sin \beta + \frac{\rho_g}{\rho_s c} \left(v_e \frac{dv_e}{dl} + g \sin \beta \right) \\ & - \frac{1}{ce} \lambda_{s1} \frac{cv_e}{2d} + \frac{\rho_g}{\rho_s c} \lambda_{tot} \frac{v_e^2}{2d} \\ & + \frac{(1-e)(\rho_s - \rho_g)}{e c \rho_s} g \cos^2 \beta \frac{w_{s,c}}{c} \end{aligned} \quad (3.3.37 \text{ a})$$

The particle free fall velocity and the drag coefficient are replaced with the respective terms relating to a particle in a cloud of other particles. It can be seen that the motion equation cannot be rewritten entirely in terms of the total friction coefficient as the solids friction coefficient λ_{s1} remains in term four of equation 3.3.37 a. The determination of the friction coefficients for the simulation programme is discussed in detail in chapter five.

3.3.5 Equation of state

For the gas flow in the pipe the gas equation of state can be approximated by the ideal gas equation:

$$P = \frac{\rho_g}{RT} \quad (3.3.38)$$

For pneumatic conveying the flow conditions are assumed to be at a constant temperature.

Rearranging equation 3.3.38 and differentiating, the fifth differential equation becomes:

$$\frac{d\rho_g}{dl} = \frac{dP}{dl} \frac{1}{RT} \quad (3.3.39)$$

3.4 Derivation of single-phase flow equations

The single phase flow equations can easily be derived by simplifying equations 3.3.9, 3.3.14, 3.3.30 and 3.3.37. As the solids velocity is zero, the voidage becomes unity. The gas continuity equation simplifies to:

$$\frac{dv_e}{dl} = -\frac{v_e}{\rho_g} \frac{d\rho_g}{dl} - \frac{v_e}{A} \frac{dA}{dl} \quad (3.4.1)$$

where it must be noted that the interstitial air velocity is synonymous with the average air velocity in this case so that $v_e = v$. The definition of the interstitial air velocity is retained in the single-phase flow equations to keep the definition of the variables uniform in the simulation programme.

The solids continuity equation is no longer required as all terms become zero. The pressure drop equation simplifies as follows:

$$\begin{aligned} -\frac{dP}{dl} &= \rho_g v_e \frac{dv_e}{dl} + \rho_g g \sin \beta \\ &+ \lambda_s \frac{\rho_g v_e^2}{2d} \end{aligned} \quad (3.4.2)$$

The solids motion equation is no longer applicable and the equation of state remains:

$$\frac{d\rho_g}{dl} = \frac{dP}{dl} \frac{1}{RT} \quad (3.3.39)$$

3.5 Derivation of the bend friction coefficient

For the derivation of the friction coefficient for the solid phase in bend flow it is assumed that the solids stream is displaced towards the outer wall of the pipe and that a solids friction coefficient equivalent to the dynamic friction coefficients used for two solids sliding across each other. In a bend in the horizontal plane the gravitational effects are negligible while they must be taken into account in bends in a vertical plane.

Using Newton's second law of motion in a cylindrical coordinate system for particles dragging along the pipe wall at a radius r_o and referring to figure 3.4 one can write for the positive r-axis direction:

$$-(V_s \rho_s - V_s \rho_g) \alpha_r = -V_s \rho_s g \sin \alpha + V_s \rho_g g \sin \alpha - F_n \quad (3.5.1)$$

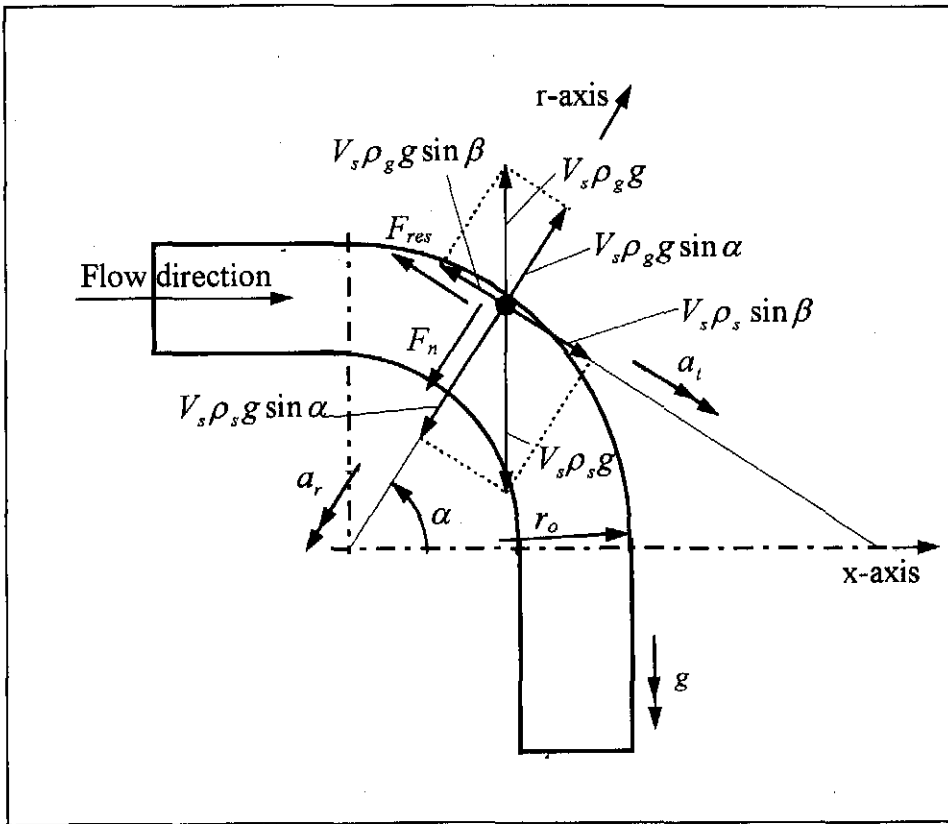


Fig. 3.4 Particle flow in a bend in the vertical plane

where F_n is the resulting normal force on the particle. For a detailed derivation of equation 3.5.1 refer to section B.2 in appendix B. Rearranging equation 3.5.1 results in:

$$F_n = V_s (\rho_s - \rho_g) \left(\frac{c^2}{r_o} - g \sin \alpha \right) \quad (3.5.2)$$

The resultant friction force on the particle is given by:

$$F_{res} = f F_n \quad (3.5.3)$$

Inserting equation 3.5.2 into equation 3.5.3 yields:

$$F_{res} = V_s g (\rho_s - \rho_g) f \sin \alpha - f V_s (\rho_s - \rho_g) \frac{c^2}{r_o} \quad (3.5.4)$$

In terms of the mass flow rate of the solid phase equation 3.3.4 can be rewritten using the solids continuity equation 3.3.11 and letting:

$$V_s = A_s l \quad (3.5.5)$$

This results in:

$$F_{res} = \frac{\dot{G}l}{c} \left(1 - \frac{\rho_g}{\rho_s} \right) \left(f \frac{c^2}{r_o} - fg \sin \alpha \right) \tag{3.5.6}$$

The term in equation 3.5.6 can now be equated to the standard friction coefficient which in terms of the force is:

$$F_{res} = \frac{\dot{G} \lambda_s^* c^2 l}{2cd} \tag{3.5.7}$$

Rearranging this results in a definition of the bend friction coefficient. For a bend in the vertical plane this becomes:

$$\lambda_s^* = \frac{2d}{c^2} f \left(1 - \frac{\rho_g}{\rho_s} \right) \left(\frac{c^2}{r_o} - g \sin \alpha \right) \tag{3.5.8}$$

For the bend in the horizontal plane where the turning angle α as defined in figure 3.5 is zero, equation 3.5.8 simplifies to:

$$\lambda_s^* = f \left(1 - \frac{\rho_g}{\rho_s} \right) \frac{2d}{r_o} \tag{3.5.9}$$

For an arbitrary bend orientation in the vertical plane the angle α is defined in figure 3.5.

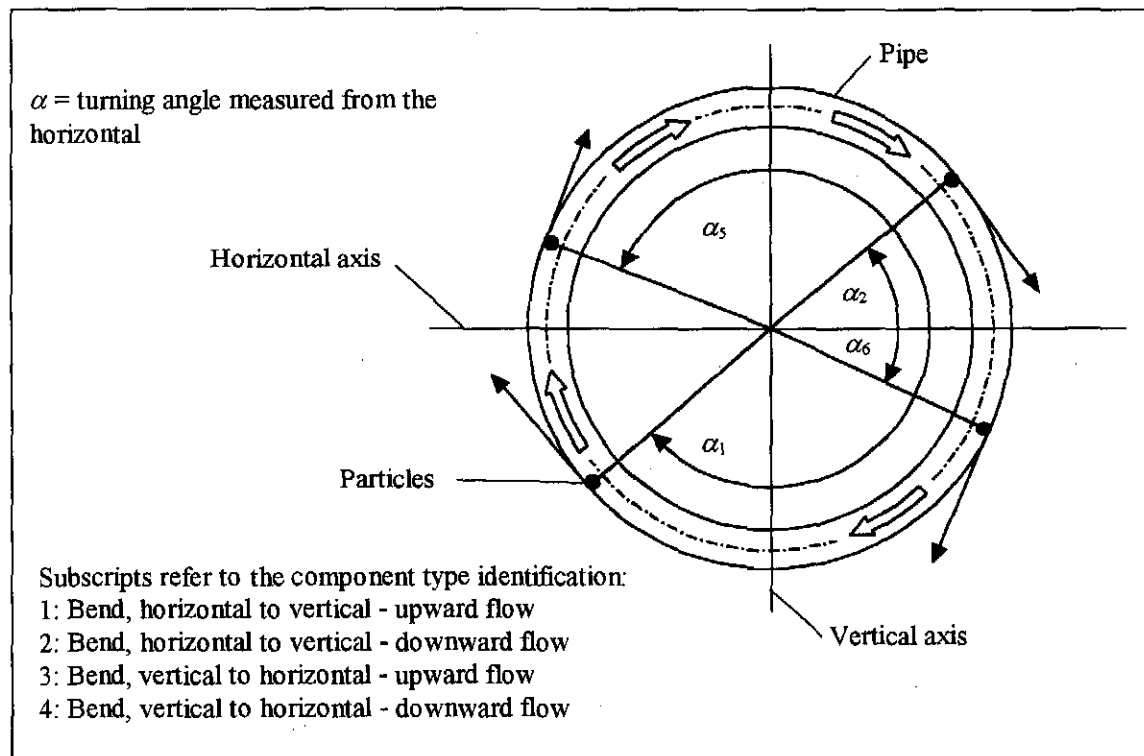


Fig. 3.5 Definition of bend angles for bends in a vertical plane

3.6 Model for expansions

The model for the expansion is based on a sine-profile expansion connecting the smaller to the larger diameter pipe. During initial checking of the model, a mass flow check is instituted to ensure that the continuity equations are satisfied at all times. Equation 3.6.1 is used to calculate the mass flow of the gas at the data output points in the pipeline which includes ten stations along the expansion.

$$\dot{Q} = \epsilon \rho_g v_g A \quad (3.6.1)$$

The gas mass flow must be the same at all points along the pipeline. It was found that a conical expansion resulted in the loss of mass flow which can be traced to the sudden change in pipe wall profile at the transition from the pipe to the cone and at the point where the cone connects to the larger diameter pipe. The use of the sine-profile ensures that the transition to the larger pipe diameter is a smooth one and results in a consistency in mass flow is maintained to within the sixth decimal place of the required gas mass flow rate. Furthermore commercially available expansion pieces closely resemble sine profiles. The diameter of the pipe at any point l along the expansion can be derived as:

$$d(l) = \frac{d_2 - d_1}{2} \sin \left[\frac{\pi(l - l_o)}{l_1 - l_o} - \frac{\pi}{2} \right] + \frac{d_2 + d_1}{2} \quad (3.6.2)$$

where d_1 and d_2 are the smaller pipe diameter and the larger pipe diameter respectively, l_o and l_1 are the distances from the start of the conveying pipeline to the entry and exit of the expansion respectively and l is the distance from the start of the conveying pipeline. Equation 3.6.2 is valid only for the expansion section. The cross sectional area at point l in the expansion is calculated as:

$$A(l) = \frac{\pi}{4} \left(\frac{d_2 - d_1}{2} \sin \left[\frac{\pi(l - l_o)}{l_1 - l_o} - \frac{\pi}{2} \right] + \frac{d_2 + d_1}{2} \right)^2 \quad (3.6.3)$$

The slope dA/dl required for the continuity equations is determined by differentiation and simplification of equation 3.6.3 resulting in equation 3.6.4.

$$\begin{aligned} \frac{dA}{dl} = & \frac{\pi^2}{2(l_1 - l_o)} \left(\frac{d_2 - d_1}{2} \right) \left(\frac{d_2 + d_1}{2} \right) \sin \left(\frac{\pi(l - l_o)}{l_1 - l_o} \right) \\ & - \frac{\pi^2}{2(l_1 - l_o)} \left(\frac{d_2 - d_1}{2} \right)^2 \cos \left(\frac{\pi(l - l_o)}{l_1 - l_o} \right) \sin \left(\frac{\pi(l - l_o)}{l_1 - l_o} \right) \end{aligned} \quad (3.6.4)$$

3.7 Conclusion

The derivation of the two-phase flow differential equations from first principles is presented. These can be simplified to yield the clean air or single phase differential equations. The equations are successfully rearranged to a format suitable for the implementation of a total friction coefficient. A solids friction coefficient in the motion equation cannot be written in terms of the total friction coefficient and must be retained. Three alternative representations of the differential equations according to the definition of the friction coefficient can be derived from the basic equations as given in appendix B. Only the first set of equations (equations B.1.1 to B.1.5) is useful if a single definition of the friction coefficients is to be used for both horizontal and vertical flow. This generalised set of equations is thus best suited for implementation in a two-phase flow simulation programme and is chosen for the subsequent implementation.

The derivation of the differential equations thus provides an insight into the different definitions that are possible for the friction coefficients and highlights the importance of providing a detailed account on the type of differential equation used to determine a friction coefficient. This is particularly important when publishing friction coefficient information and it is found that these details are lacking in many papers.

By understanding the origin of each of the separate terms in the differential equations a path is opened for future work to be done on the improvement of the mathematical model. The effects of each of the terms on the accuracy of the simulation results when compared with experimental data can be determined.

The bend flow model is based on the assumption that the sliding friction coefficient can be used to derive an expression for the solids friction coefficient. The validity of this model is discussed in detail in chapter 5.

A sine-profile formulation for a pipe expansion which is aimed at modelling stepped pipelines in long distance conveying is required to allow for a smooth transition from the smaller diameter pipe to the larger diameter pipe. Such a sine-profile is also found to be closer to the shape of the expansion pieces that are available from pipe manufacturers as standard stock.

SOLUTION METHOD FOR DIFFERENTIAL EQUATIONS

4.1 Introduction

An analytical solution for the single and two-phase flow differential equations presented in chapter three is not possible so that a numerical integration method must be used. It was decided to attempt the implementation of the Runge-Kutta-Fehlberg integration method which is then applied by successively expanding the complexity of the problem and checking the results after each new implementation. This method of solution is used successfully in the simulation programme as is demonstrated in the following sections and in chapter five where the simulation results are discussed.

4.2 Chapter contents

Section 4.3 describes the computer routine used to solve the differential equations governing two-phase flow and presents the equations in rearranged form which are better suited for solving. Section 4.4 contains details of the verification process used to determine that the integration programme routine functions correctly. Section 4.5 discusses the initial conditions that require definition before the integration process can be started. A method is proposed for determining the initial solids velocity for the simulation programme. The method of switching over from single-phase flows to two-phase flows at the feeding point in the case of a complete system simulation is presented in section 4.6 while an overview of the difference in the implementation of the integration routine with respect to pressure and vacuum conveying is given in section 4.7. A discussion of the work presented in this chapter follows in section 4.8.

4.3 Runge-Kutta-Fehlberg algorithm for solving differential equations

The differential equations for two-phase flow are a set of five first order, ordinary differential equations that are suited for the use of a Runge-Kutta-Fehlberg (RKF) numerical integration routine. The equations are coupled to one another by the differential terms. This requires the estimation of the slopes each time the system of equations is solved in the RKF routine. On first inspection it was believed that a Gauss solver [89GE1] may have to be incorporated to solve for the slopes in the five differential equations before each integration step. They

represent five simultaneous equations. Closer inspection of the equations, however, reveals that by rearranging the equations in the correct order and by substitution, only the spatial gradient of the interstitial velocity requires an estimation using the values of the variables as determined at the previous point of integration along the pipeline or from the initial values at the start of the pipeline.

In the simplest form the equations can be rewritten as follows:

$$\begin{aligned}\frac{dv_e}{dl} &= c_1 \\ \frac{dc}{dl} &= c_2 + c_3 \frac{dv_e}{dl} \\ \frac{dP}{dl} &= c_4 + c_5 \frac{dv_e}{dl} + c_6 \frac{dc}{dl} \\ \frac{d\rho_s}{dl} &= c_7 \frac{dP}{dl} \\ \frac{de}{dl} &= c_8 \frac{dc}{dl} + c_9\end{aligned}\tag{4.4.1}$$

where c_1 to c_7 are constants during a single integration step. These contain the dependent variables determined at a previous step and variables such as friction coefficients that are recalculated and adjusted after each integration step. These equations simplify substantially for the single-phase flow case where the solids velocity is zero and the voidage fixed at unity.

Simple RKF routines are available with a user-defined integration step length [91WH1]. The accuracy of the solution is dependent on the step length so that it is preferable to use a routine that adjusts this step size automatically. This improves the speed of the programme as longer step lengths can be used in areas where the slopes are essentially constant. An example is in long stretches of straight horizontal and vertical flow. Furthermore it is possible to define the points along the pipeline at predefined intervals where one requires output of the dependent variable results.

It was decided to use an algorithm originally developed by Watts and Shampine at Sandia Laboratories in New Mexico. The programme listing is presented in FORTRAN as RKF45 in Forsythe, Malcolm and Moler [77FO1]. The programme utilises fourth and fifth order Runge-Kutta formulas that allow for an error estimate which is used to determine the required step size during integration. The FORTRAN code required translation into PASCAL for implementation in the conveyor simulation programme. This code represents the core of the

differential equation solver. The core programme RKF45PAS used for initial testing is presented in appendix G for reference as it proves to be a useful tool in solving other ordinary differential equation problems.

4.4 Integration programme verification

The Runge-Kutta-Fehlberg routine is a complex one and as a result of the translation from FORTRAN to PASCAL, a satisfactory method had to be found to verify the correct functioning of the code before implementing it to solve the two-phase flow differential equations. It was decided to use the differential equations developed as the similarity solutions for steady two-dimensional flow for the Blasius flat-plate flow [91WH1] and Falkner-Skan wedge flows [91WH1]. The numerical results for these two problems are given by White [91WH1] utilising a simple Runge-Kutta routine in which the step size must be defined manually. Table 4.1 at the end of this chapter presents a comparison of the results obtained by White [91WH1] and those from the programme RKF45PAS. The results are the solution to the differential equation representing the non-linear Blasius equation for flat-plate flow:

$$f'''(\eta) + f(\eta)f''(\eta) = 0 \quad (4.4.2)$$

with the initial conditions:

$$f'(0) = f(0) = 0, \quad f'(\infty) = 1, \quad f''(0) = 0.469600$$

The results from RKF45PAS are found to be the same as those given by White [91WH1] except for the last term in columns four and seven in table 4.1. This can be attributed to an improved accuracy in RKF45AS. The same testing procedure is implemented for the more complex Falkner-Skan wedge flows [91WH1]. The results are in agreement with those given in by White [91WH1] and are not shown here.

The functioning of the core code used for the two-phase flow simulation is thus verified. After verification, the core integration programme is expanded for the single and two-phase flow differential equations used to simulate the pneumatic conveyor.

4.5 Initial conditions and the influence on the final solution

An important aspect of using the Runge-Kutta-Fehlberg solver is that the initial conditions must be specified to commence integration. These can either be supplied in form of the slopes of the dependent variables or as values of the dependent variables. In this case the dependent variables used are the pressure, the air density, the interstitial air velocity, the solids velocity

and the voidage. For positive pressure conveyors the absolute inlet pressure of the conveyor can be estimated. For vacuum conveyors, the inlet pressure is usually at ambient conditions. The density can be calculated utilising the ideal gas equation 4.4.3 below using the inlet pressure and a constant conveying temperature. The air mass flow rate is determined from the required material mass flow through the definition of the mass flow ratio. With the known density and pipe cross-sectional area, the average air velocity can be determined. Two variables remain, the voidage and the initial solids velocity. During implementation of an user-estimated voidage, the simulation programme was found to be unstable during initialisation. This is as a result of the sensitivity of the calculated initial solids velocity using the voidage in equation 3.3.12. A better solution is to use an estimate of the initial solids velocity. The initial voidage is calculated by rearranging equation 3.3.12 to yield equation 4.4.4. The interstitial air velocity can then be determined using equation 4.4.5. The simulation programme was found to be more stable using this approach and it is easier to implement as the designer has a better feel for a velocity than the voidage. The initial conditions can thus be calculated as follows:

$$\rho_g = \frac{P}{RT} \quad (4.4.3)$$

$$e = 1 - \frac{4\dot{G}}{\pi d^2 \rho_g c} \quad (4.4.4)$$

$$v_e = \frac{4\dot{G}}{\rho_g e \mu \pi d^2} \quad (4.4.5)$$

For determining the optimum initial solids velocity, a graph of the initial solids Froude number versus the pressure ratio of the pneumatic conveyor system can be determined. Such a graph shows a distinct maximum which is essentially independent of the mass flow rate and mass flow ratio. The initial solids velocity corresponding to the maximum pressure ratio at a constant mass flow rate is used as the initial solids velocity for further simulations. Examples of the graphs obtained are presented in section 5.4.2 and 5.6.3 in chapter five.

The initial solids velocity estimate is found to have little influence on the downstream solution of the two-phase flow differential equations. During tests it can be seen that the solution converges to a single solution within less than 10% of the total length of the pipeline after the feed point. Figure 4.1 depicts an example of the results for the average air velocity at varying initial solids velocities and a constant mass flow rate and mass flow ratio. Only the first 10 m of the 195 m long conveying pipeline is shown.

Equation 4.4.4 yields a useful criterion to check the chosen initial solids velocity. As the voidage cannot be less than zero:

$$c > \frac{4\dot{G}}{\pi d^2 \rho_s} \quad (4.4.6)$$

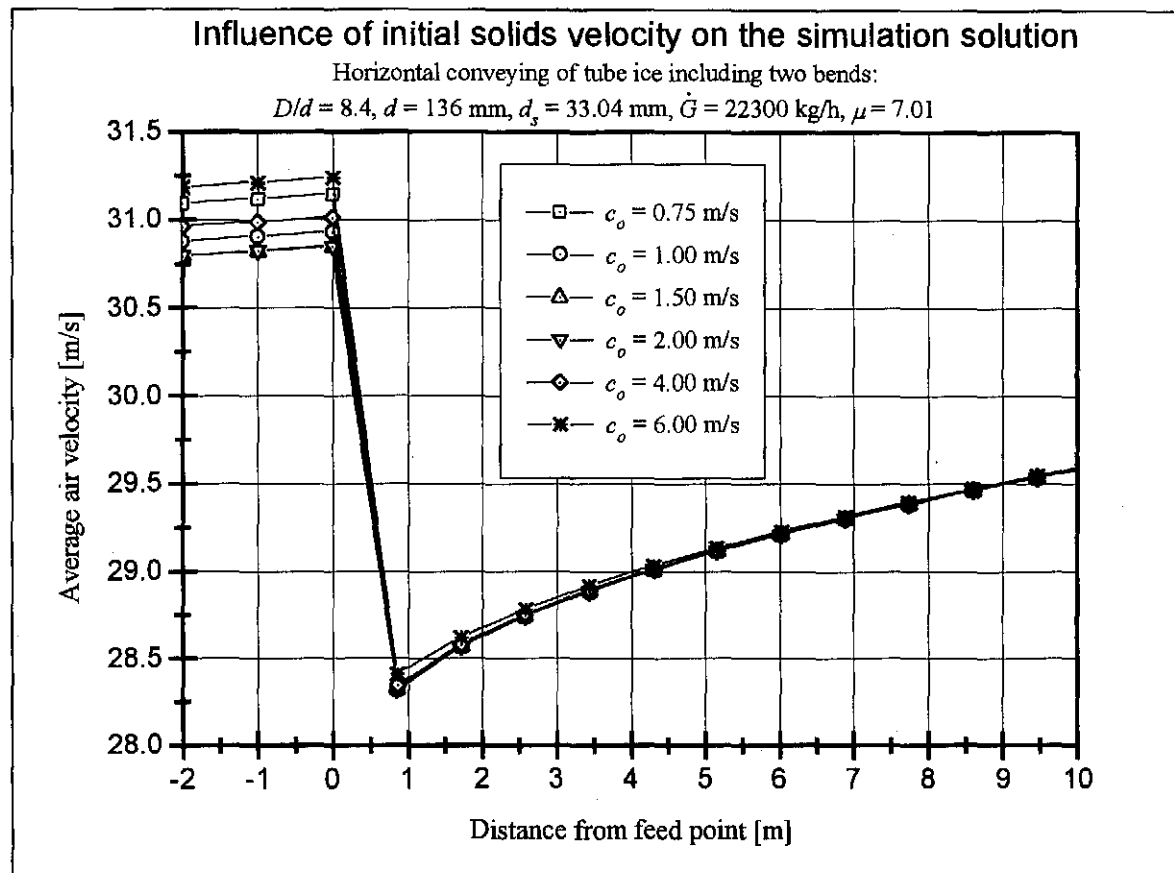


Fig. 4.1 Influence of the initial solids velocity on the simulation solution

4.6 Single to two-phase flow switchover

The switch from single to two-phase flow at the feed point is implemented by reinitialising the integration procedure and supplying new initial values at the point when material is injected into the pipeline. Furthermore a switch is undertaken from using the simplified single-phase flow equations presented in section 3.4 of chapter three to the two-phase flow equations given in section 3.3. The initial conditions for single-phase flow are the pipe inlet pressure, the air density and the inlet air velocity. Because the voidage is unity in single-phase flow the average air velocity equals the interstitial air velocity in pipe section with air flow alone. The initial conditions used to initiate the two-phase flow consist of the absolute pressure and density determined at the end of the clean air flow section. The initial solids velocity is estimated by the programme user utilising the method given in section 4.5 from which the voidage and

consequently the initial interstitial air velocity can be calculated as presented in equations 4.4.4 and 4.4.5.

It must be noted that the method implemented during the switchover assumes that the feeding tee consists of a pipe with the same diameter throughout corresponding to the pipe inlet and outlet diameter. The material is fed directly into the pipe at a specific point. Provision for air leakage out of the pipe as a result of leakage through the feeding mechanism is also made. Feeding tee pressure losses cannot be modelled and a safety factor with regard to the determined pressure drop must be added to make provision for this. In reality expansion of the air occurs at the inlet to the feeding as a result of an increase of the flow cross sectional area due to the physical space required under the feeding mechanism, the material is fed into the feeding tee over a finite length of the feeding tee and the solids and air mixture then flows through a contraction in cross sectional area down to the pipe cross sectional area of the conveying pipeline at the outlet of the feeding tee.

4.7 The difference in pressure and vacuum conveying

In vacuum conveying the conveying pipe inlet pressure is known and is usually taken at atmospheric pressure. As the integration proceeds downstream, only a single complete calculation for the complete pipe length is required. The main variable that is determined by the simulation programme in this type of conveying is the pipe outlet pressure.

In positive pressure conveying the situation is reversed. The outlet pressure of the pipe is known and the inlet pressure has to be determined in an iterative process. The designer supplies an estimated inlet pressure to the simulation programme and the simulation then runs, checking whether the outlet pressure corresponding to the supplied inlet pressure is higher or lower than the required outlet pressure. By means of the Golden Section Search Routine [96ER1] the inlet pressure is successively adjusted until the required outlet pressure is attained to a specified error percentage of the required outlet pressure. A flow chart embodying the core of the computer routine performing this iteration procedure, the implementation of the switch from clean air to two-phase flow and the selection of the expansions is presented in appendix F.

4.8 Discussion and conclusion

The integration procedure is found to be applicable to the problem and presents a simple and efficient method of solving the two-phase flow differential equations. The main advantage of the specific Runge-Kutta-Fehlberg routine used is that the step size is self adjusting and as a

result the point at which output data are to be written to the data file can be specified. This is not the case where a fixed, user defined step size is used as the step size determines the points where the output is generated.

It will be seen in chapter five that the graphs of the simulation results may at points seem to be jagged from a visual point of view. This is as a result of the intervals chosen for the data output. These are ten intervals for each straight pipe section, ten intervals for each bend and ten intervals for each expansion. If more data are output to the data file the curves can be generated with a smoother profile. It is believed that a good balance has been achieved between the size of the data output file and the visual appearance of the resultant graph in this case.

The problem of the selection of the initial conditions has been resolved while the switchover from single-phase to two phase flow is successfully implemented at the feed point. The iteration routine for pressure conveying is used with success to determine the comparison between experimental and simulated data which is presented in the following chapter.

Tab. 4.1 Comparison of the solutions to the Blasius flat-plate flow differential equations

η	[91WH1] $f(\eta)$	[91WH1] $f''(\eta)$	[91WH1] $f'''(\eta)$	RKF45PAS $f'(\eta)$	RKF45PAS $f''(\eta)$	RKF45PAS $f'''(\eta)$
---	---	---	---	---	---	---
0	0.00000	0.00000	0.46960	0.00000	0.00000	0.46960
0.2	0.00939	0.09391	0.46931	0.00939	0.93910	0.46931
0.4	0.03755	0.18761	0.46725	0.03755	0.18761	0.46725
0.6	0.08439	0.28058	0.46173	0.08439	0.28058	0.46173
0.8	0.14967	0.37196	0.45119	0.14967	0.37196	0.45119
1	0.23299	0.46063	0.43438	0.23299	0.46063	0.43438
1.2	0.33366	0.54525	0.41057	0.33366	0.54525	0.41057
1.4	0.45072	0.62439	0.37969	0.45072	0.62439	0.37969
1.6	0.58296	0.69670	0.34249	0.58296	0.69670	0.34249
1.8	0.72887	0.76106	0.30045	0.72887	0.76106	0.30045
2	0.88680	0.81669	0.25567	0.88680	0.81669	0.25567
2.2	1.05495	0.86330	0.21058	1.05495	0.86330	0.21058
2.4	1.23153	0.90107	0.16756	1.23153	0.90107	0.16756
2.6	1.41482	0.93060	0.12861	1.41482	0.93060	0.12861
2.8	1.60328	0.95288	0.09511	1.60328	0.95288	0.09511
3	1.79557	0.96905	0.06771	1.79557	0.96905	0.06771

Tab.4.1 continued

η	[91WH1] $f(\eta)$	[91WH1] $f''(\eta)$	[91WH1] $f'''(\eta)$	RKF45PAS $f'(\eta)$	RKF45PAS $f''(\eta)$	RKF45PAS $f'''(\eta)$
---	---	---	---	---	---	---
3.2	1.99058	0.98037	0.04637	1.99058	0.98037	0.04637
3.4	2.18747	0.98797	0.03054	2.18747	0.98797	0.03054
3.6	2.38559	0.99289	0.01933	2.35590	0.99289	0.01933
3.8	2.58450	0.99594	0.01176	2.58450	0.99594	0.01176
4	2.78389	0.99777	0.00687	2.78388	0.99777	0.00687
4.2	2.98356	0.99882	0.00386	2.98355	0.99882	0.00368
4.4	3.18338	0.99940	0.00208	3.18338	0.99940	0.00208
4.6	3.38330	0.99970	0.00108	3.38329	0.99970	0.00108
4.8	3.58325	0.99986	0.00054	3.58325	0.99986	0.00054
5	3.78323	0.99994	0.00026	3.78323	0.99994	0.00026
5.2	3.983226	0.999972	0.000119	3.983220	0.999971	0.000119
5.4	4.183222	0.999988	0.000052	4.183220	0.999988	0.000052
5.6	4.383221	0.999995	0.000022	4.383220	0.999995	0.000022
5.8	4.583220	0.999998	0.000009	4.583220	0.999998	0.000009
6	4.783220	0.999999	0.000004	4.783220	0.999999	0.000003

SIMULATION RESULTS

5.1 Introduction

To evaluate the simulation programme results for two-phase flows it was decided to use existing conveying data for cement by Lange [89LA1] and van Straaten [94VS1] and data for tube ice by Sheer [91SH1]. These data represent both the fine powdered material and coarse particles that can be conveyed pneumatically. It was found that the above data contains all the required information for determining friction coefficient data correlations. This includes measurements or correlations for the solids velocity. Data by other workers was found to lack important information such as the exact dimensions of the conveying pipe layout or solids velocity correlations or measurements over the test sections which are important for the evaluation of simulation programme. Most of these data are for horizontal flow and detailed data regarding vertical flow are lacking. This is most likely due to the impracticality of setting up test facilities with large vertical pipe sections. The data by Sheer [91SH1] contain numerous experiments with vertical conveying down a mine shaft. However, due to practical limitations the solids velocities along the vertical pipeline could only be measured after the bend transition from vertical to horizontal at the bottom of the mine shaft and no data are available for evaluating the solids velocity profile along the vertical pipe.

5.2 Chapter contents

The following section discusses the two friction coefficient representations used for the validation of the simulation programme. The results for simulations using cement are compared with experimental results in section 5.4 and the non-dimensional and normalised simulated state diagrams presented in section 5.5. The results for the ice conveying are given in section 5.6 with the non-dimensional and normalised simulated state diagrams for tube ice presented in section 5.7. A discussion of the overall results follows in section 5.8 and a summary of the goals achieved in this section are presented in section 5.9. Recommendations are given in section 5.10.

5.3 Differential equations and friction coefficients

5.3.1 Introduction

Two representations of the friction coefficients are used in the simulation programme. The first involves the use of a correlation for the total friction coefficient λ_{tot} and the solids impact and friction coefficient λ_s^* . The total friction coefficient can be written as a combined friction coefficient of the solids impact and friction coefficient and the air alone friction coefficient λ_g as in equation 5.3.1.

$$\lambda_{tot} = \lambda_g + \mu\lambda_s^* \frac{c}{v_e} \quad (5.3.1)$$

The total friction and solids impact and friction coefficients are determined by rearranging the integrated pressure drop equation 5.3.5 and using experimental data to determine the friction coefficient correlations. Details and sample calculations for these are presented in appendix C sections C.2.5 (total friction coefficient) and C.2.6 (solids impact and friction coefficient) for cement. During the determination of the values of the solids impact and friction coefficient for tube ice, 90% of the values were found to be negative. This friction coefficient representation can thus not be used for tube ice. The possible reasons for these negative values are discussed below.

The failure to determine the solids impact and friction coefficient for tube ice and the fact that the solids velocity is not accurately represented in the simulation for cement as shown in figures 5.4 to 5.7 in section 5.4.3 using the above representation requires the development of an alternative method for determining the friction coefficients. The inherent problem is that the differential equations cannot be rewritten entirely in terms of the total friction coefficient. The motion equation still contains the solids impact and friction coefficient which is usually determined by the somewhat artificial method of separating the air alone from the total friction coefficient as represented in equation 5.3.1. Researchers [66WE1, 78MA1, 89LA1] have pointed out that the air velocity profile is modified as a result of the influence of particles in two-phase flow. Lange [89LA1] notes that the separate analysis of the air alone and particle effects is unacceptable for fine particles. The two influences cannot be separated correctly by using classical single-phase air flow theory [44MO1, 83HA1] which is based on the single-phase velocity profile to determine the air alone friction component.

This problem can be resolved if both the pressure drop equation 5.3.5 and the solids motion equation 5.3.6 are integrated. Instead of determining both the total friction coefficient and the solids impact and friction coefficient from the integrated pressure drop equation alone,

the solids impact and friction coefficient can be determined from the solids motion equation. To avoid confusion as to which method is used to determine the solids impact and friction coefficient, the solids impact and friction coefficient λ_s^* is renamed the alternative solids impact and friction coefficient λ_s' when determined directly from the solids motion equation.

A detailed account of the method and a sample calculation with a summary of the equations used is given in sections C.1 and C.2 for cement. This includes the sphericity determination. The same methods applied in sections C.2 are used for tube ice. The resultant friction coefficient correlations which are used to determine the results presented in the following sections are given in equations C.2.16 to C.2.18 in section C.2.8 for cement and in equations C.4.1 and C.4.2 in section C.4 for tube ice.

Note the improvement in correlation that is achieved by using the motion equation to determine the alternative solids impact and friction coefficient for cement in comparison with the traditional method of determining the solids impact and friction coefficient from the pressure drop equation. This is clearly demonstrated by comparing figures C.2 and C.3 in appendix C where an improvement of the correlation coefficient from 62% to 95% is achieved. The correlation for tube ice shows the same trend with the correlation coefficient determined at 99% as shown in figure C.5 in appendix C.

5.3.2 Friction coefficient representation for bend flow

The bend flow model is discussed in detail in section 3.5. It is used to determine an equivalent solids impact and friction coefficient as given in equation 3.5.8 for bends in the vertical plane and equation 3.5.9 for bends in the horizontal plane. This replaces the correlation for the solids impact and friction coefficient in the succession of straight pipe sections that are used to model the bend. The total friction coefficient for bend flow is determined using equation 5.3.1 where the solids impact and friction coefficient is replaced by equations 3.5.8 or 3.5.9 and the gas flow friction coefficient determined from the Haaland [83HA1] equation 1.3.16. Equation 3.5.8 and 3.5.9 replace the solids impact and friction coefficient in the motion equation when using the first representation of the friction coefficients. It also replaces the alternative friction coefficient when utilising the second representation of the friction coefficients discussed in the previous section.

5.3.3 Summary of the differential equations used

The following differential equations are used in the simulation programme evaluation. When utilising the first of the friction coefficient representations discussed above, these become the

following:

The solids continuity equation:

$$\frac{de}{dl} = \frac{(1-e)}{c} \frac{dc}{dl} + \frac{(1-e)}{A} \frac{dA}{dl} \quad (5.3.2)$$

the gas continuity equation:

$$\frac{dv_e}{dl} = -\frac{v_e}{\rho_g} \frac{d\rho_g}{dl} - \frac{v_e}{e} \frac{de}{dl} - \frac{v_e}{A} \frac{dA}{dl} \quad (5.3.3)$$

the ideal gas equation:

$$\frac{d\rho_g}{dl} = \frac{dP}{dl} \frac{1}{RT} \quad (5.3.4)$$

the pressure drop equation:

$$\begin{aligned} -\frac{dP}{dl} = & e \left(\rho_g v_e \frac{dv_e}{dl} + \rho_g g \sin \beta \right) \\ & + (1-e) \left(\rho_s c \frac{dc}{dl} + \rho_s g \sin \beta + (\rho_s - \rho_g) g \cos^2 \beta \frac{w_{s,c}}{c} \right) \\ & + e \lambda_{tot} \frac{\rho_g v_e^2}{2d} \end{aligned} \quad (5.3.5)$$

and the equation of motion:

$$\begin{aligned} \frac{dc}{dl} = & \frac{3}{4} C_{d,c} \frac{\rho_g}{\rho_s d_s} \frac{(v_e - c)^2}{ce} - \frac{1}{c} g \sin \beta + \frac{\rho_g}{\rho_s c} \left(v_e \frac{dv_e}{dl} + g \sin \beta \right) \\ & - \frac{1}{ce} \lambda_s^* \frac{c^2}{2d} + \frac{\rho_g}{\rho_s c} \lambda_{tot} \frac{v^2}{2d} + \frac{(1-e)}{e} \frac{(\rho_s - \rho_g)}{c \rho_s} g \cos^2 \beta \frac{w_{s,c}}{c} \end{aligned} \quad (5.3.6)$$

where the solids impact and friction coefficient is either determined from:

$$\lambda_s^* = \left(\lambda_{tot} - \lambda_g \right) \frac{v_e}{c\mu} \quad (5.3.7)$$

or by integrating the solids motion equation 5.3.6 and rearranging for what will be called the alternative solids impact and friction coefficient so as to distinguish between the two methods used to determine the coefficient. For the method of representation of the alternative solids impact and friction coefficient, equations 5.3.2 to 5.3.5 remain the same with equation 5.3.6 becoming:

$$\begin{aligned} \frac{dc}{dl} = & \frac{3}{4} C_{d,c} \frac{\rho_g (v_e - c)^2}{\rho_s d_s c e} - \frac{1}{c} g \sin \beta + \frac{\rho_g}{\rho_s c} \left(v_e \frac{dv_e}{dl} + g \sin \beta \right) \\ & - \frac{1}{ce} \lambda_s' \frac{c^2}{2d} + \frac{\rho_g}{\rho_s c} \lambda_{tot} \frac{v^2}{2d} + \frac{(1-e)(\rho_s - \rho_g)}{e c \rho_s} g \cos^2 \beta \frac{w_{s,c}}{c} \end{aligned} \quad (5.3.8)$$

where the solids impact and friction coefficient is replaced with the alternative solids impact and friction coefficient.

5.4 Comparison of experimental and simulation results for cement

5.4.1 Introduction

The experimental data used for comparison with simulated results was previously determined by Lange [89LA1] and van Straaten [94VS1]. The data are first utilised to determine a suitable correlation for the total friction coefficient and the solids impact and friction coefficient and alternative solids impact and friction coefficient respectively in terms of the non-dimensional parameters the mass flow ratio, the Froude number, the Reynolds number based on pipe diameter and the diameter ratio of particle to pipe diameter. Details of the correlation method and the resulting correlation equations are presented in appendix C, section C.2.8. Care is taken to ensure that only valid data are used. The mathematical model for the two-phase flow simulation is only valid under the assumption that all particles are evenly distributed in the pipe cross-section. Experimental data in the region of the onset of deposition of material at the

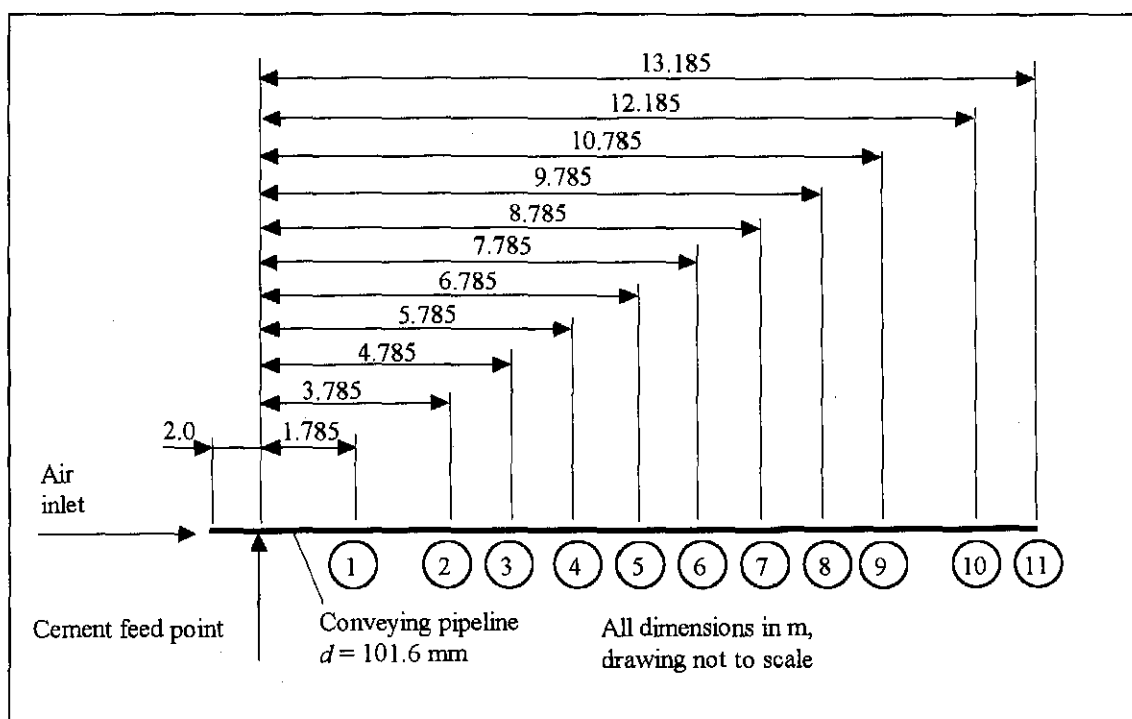


Fig. 5.1 Pipe layout used for cement conveying experiments[89LA1] and simulation

bottom of the pipeline can thus not be utilised in the determination of the friction coefficient correlations.

The friction coefficient correlations are then used to simulate conveying cases for varying mass flow rates and mass flow ratios and compared with experimental data by Lange [89LA1]. The horizontal pipe layout for the 101.6 mm diameter pipe is presented in figure 5.1. The material feeding arrangement consists of a drop-through rotary vane feeder feeding into a blow through rotary vane feeder. In this configuration air leakage is considered negligible.

5.4.2 Initial conditions

As discussed in chapter four the Runge-Kutta-Fehlberg integration routine requires initial conditions to start the integration process. The initial solids velocity is unknown and must be determined by plotting a graph of the initial solids Froude number versus the pressure ratio for a constant mass flow rate. The characteristic curve shows a maximum pressure ratio corresponding to a specific initial solids Froude number. This is essentially independent of varying material mass flow rate as can be seen in figures 5.2 and 5.3. The pressure ratio maximum is used to determine the initial solids velocity on the basis of reasoning that it results in the most conservative estimate of the conveying line pressure drop. The initial solids velocity

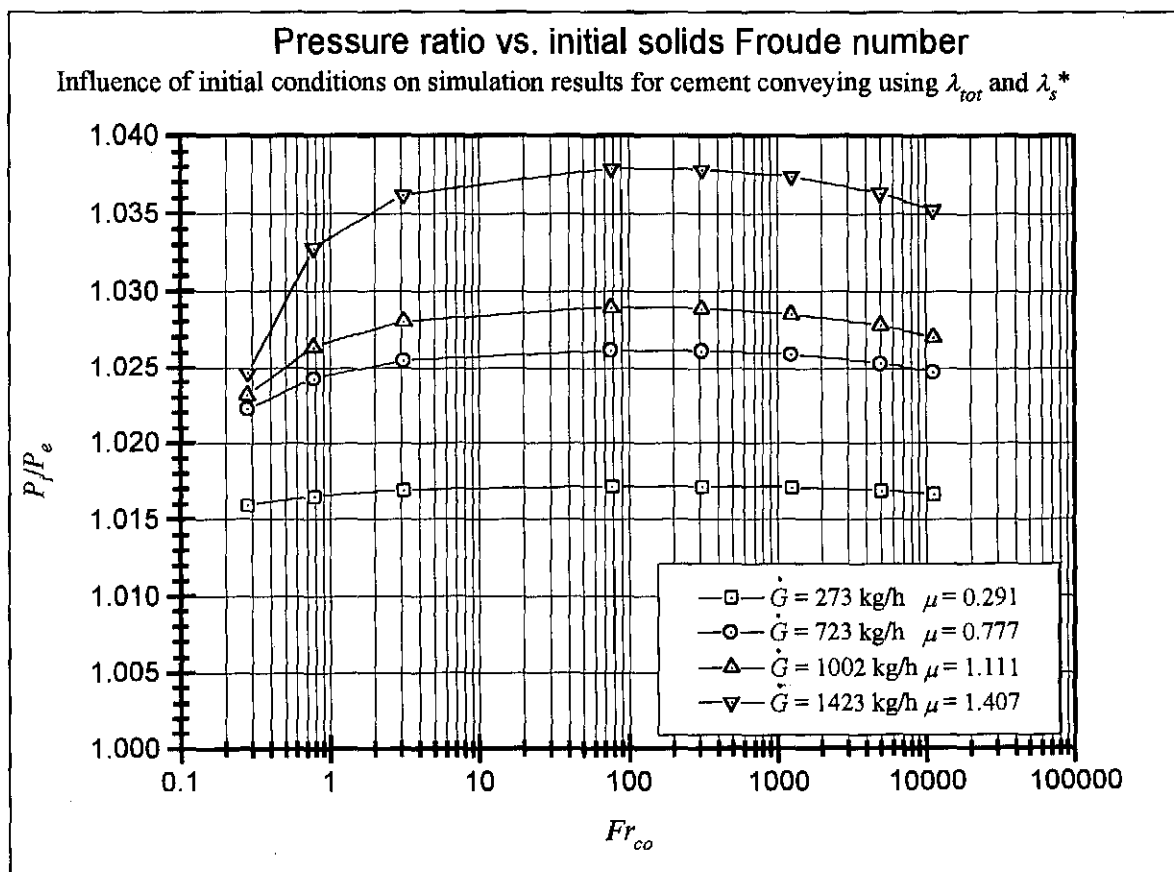


Fig. 5.2 Pressure ratio vs. initial solids Froude number for cement using λ_{tot} and λ_s^*

for cement is chosen at $Fr_{co} = 80$ corresponding to an initial velocity of $c_o = 0.5$ m/s. The data used to create figures 5.2 and 5.3 are found in section D.1 in appendix D.

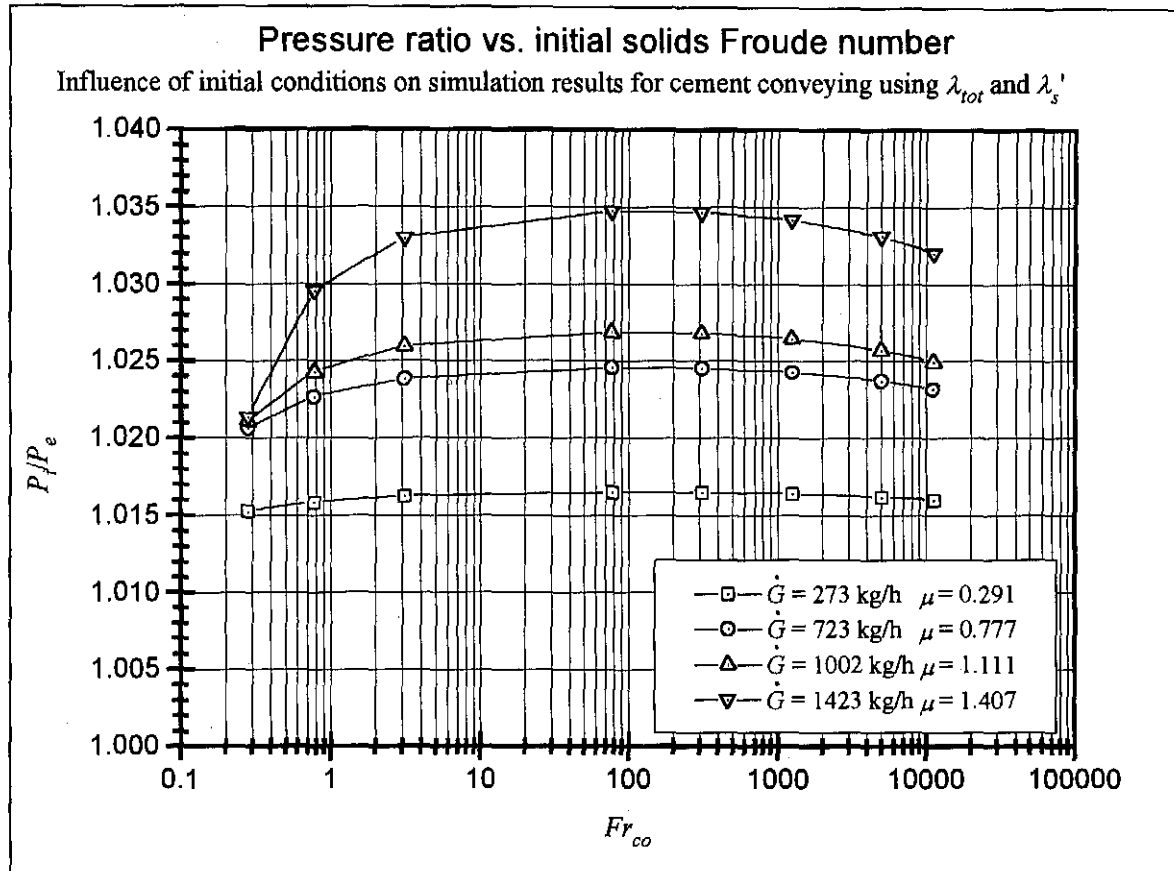


Fig. 5.3 Pressure ratio vs. initial solids Froude number for cement using λ_{tot} and λ_s'

5.4.3 Results for cement using λ_{tot} and λ_s^*

Figures 5.4 to 5.7 show the results for horizontal conveying of cement at different material mass flow rates and mass flow ratios utilising the total friction and solids impact and friction coefficient. A section of 2 m is added upstream of the feeding point so that the values of pressure drop and air and solids velocity are easier to identify. The analysis is thus single-phase flow to the feed point and then continues as two-phase flow. The corresponding data of the results are given in tabular form in section D.2 in appendix D. Note that all pressure data presented in figures 5.4 to 5.7 are relative to the exit point 11 shown in figure 5.1.

5.4.4 Results for cement using λ_{tot} and λ_s'

Figures 5.8 to 5.11 depict the simulation results utilising the same simulation parameters used previously but implementing the alternative solids impact and friction coefficient in the place of the solids impact and friction coefficient. The corresponding data of the results are given in tabular form in section D.3 in appendix D.

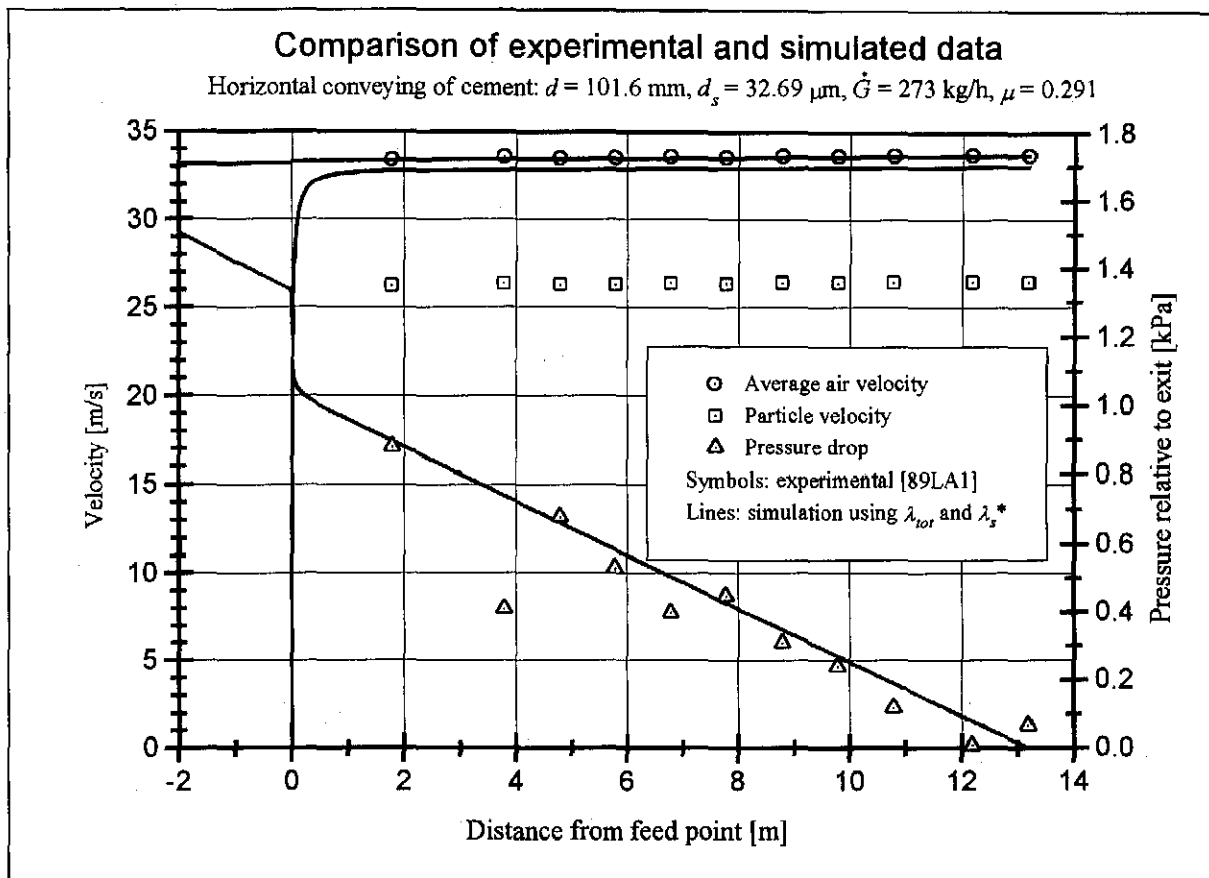


Fig. 5.4 Comparison of experimental and simulated data for cement at $\dot{G} = 273 \text{ kg/h}$

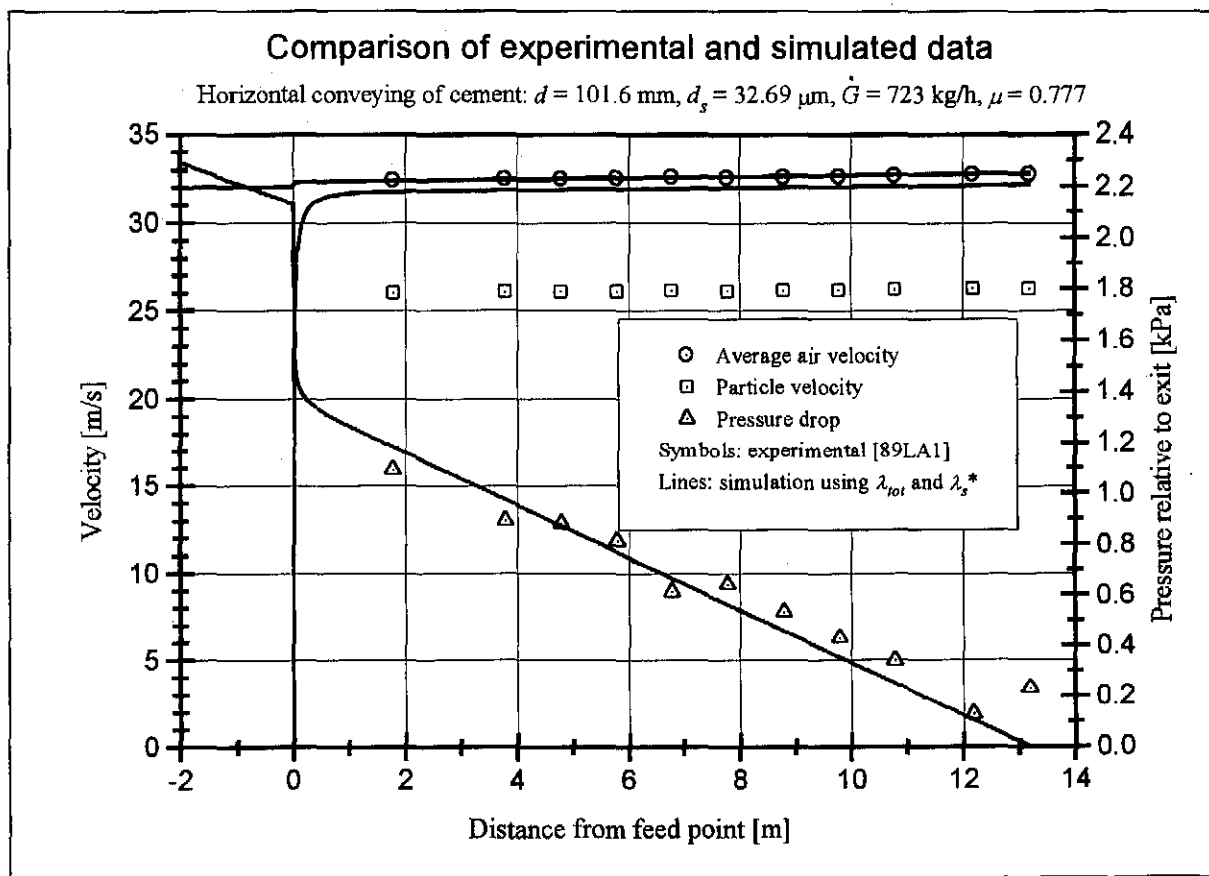


Fig. 5.5 Comparison of experimental and simulated data for cement at $\dot{G} = 723 \text{ kg/h}$

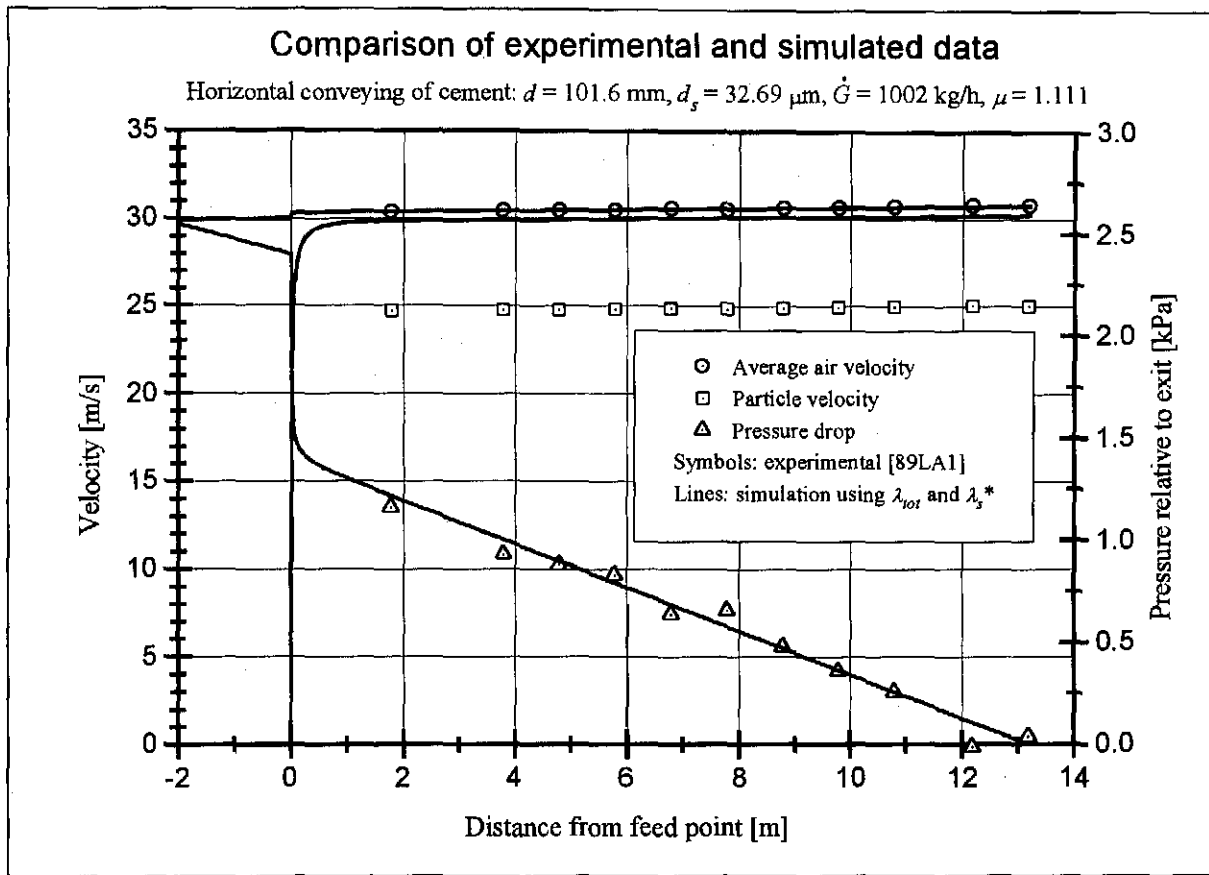


Fig. 5.6 Comparison of experimental and simulated data for cement at $\dot{G} = 1002 \text{ kg/h}$

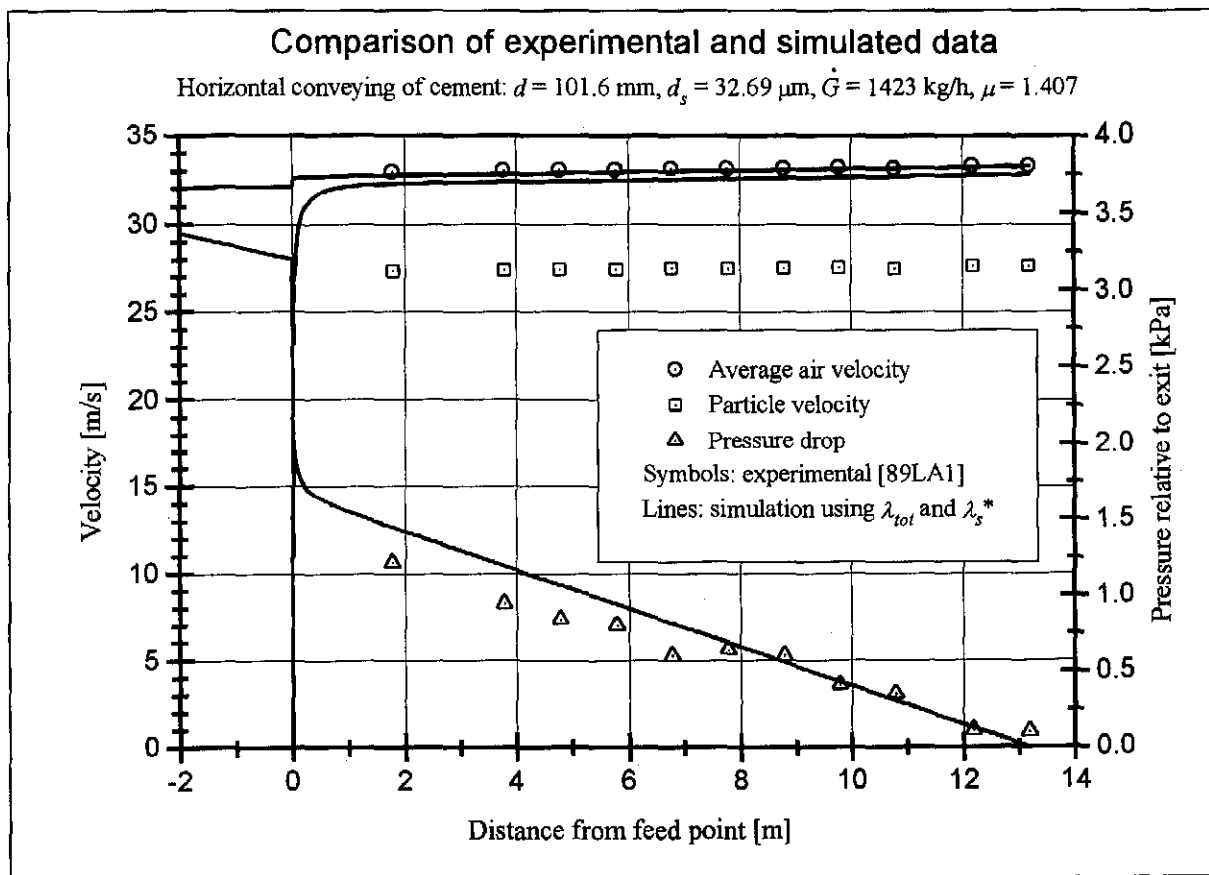


Fig. 5.7 Comparison of experimental and simulated data for cement at $\dot{G} = 1423 \text{ kg/h}$

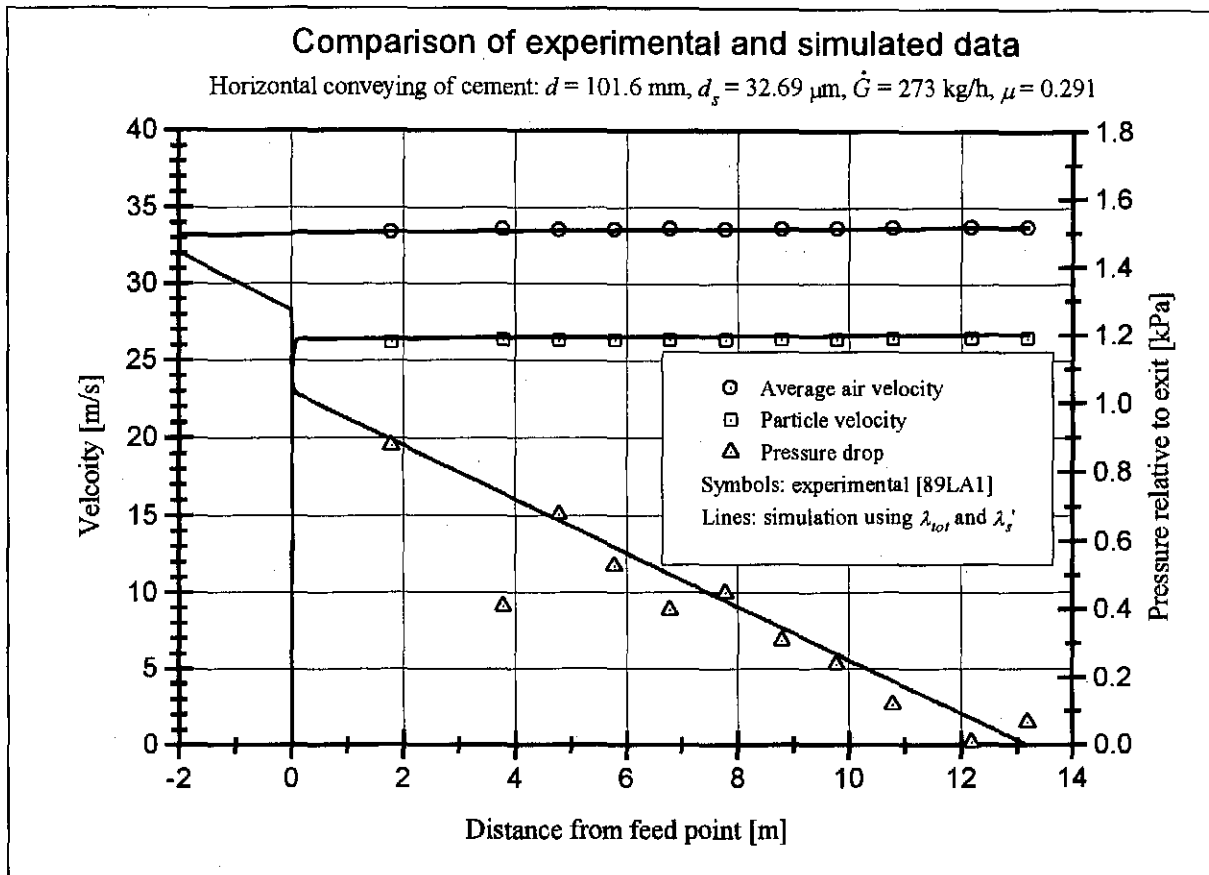


Fig. 5.8 Comparison of experimental and simulated data for cement $\dot{G} = 273 \text{ kg/h}$

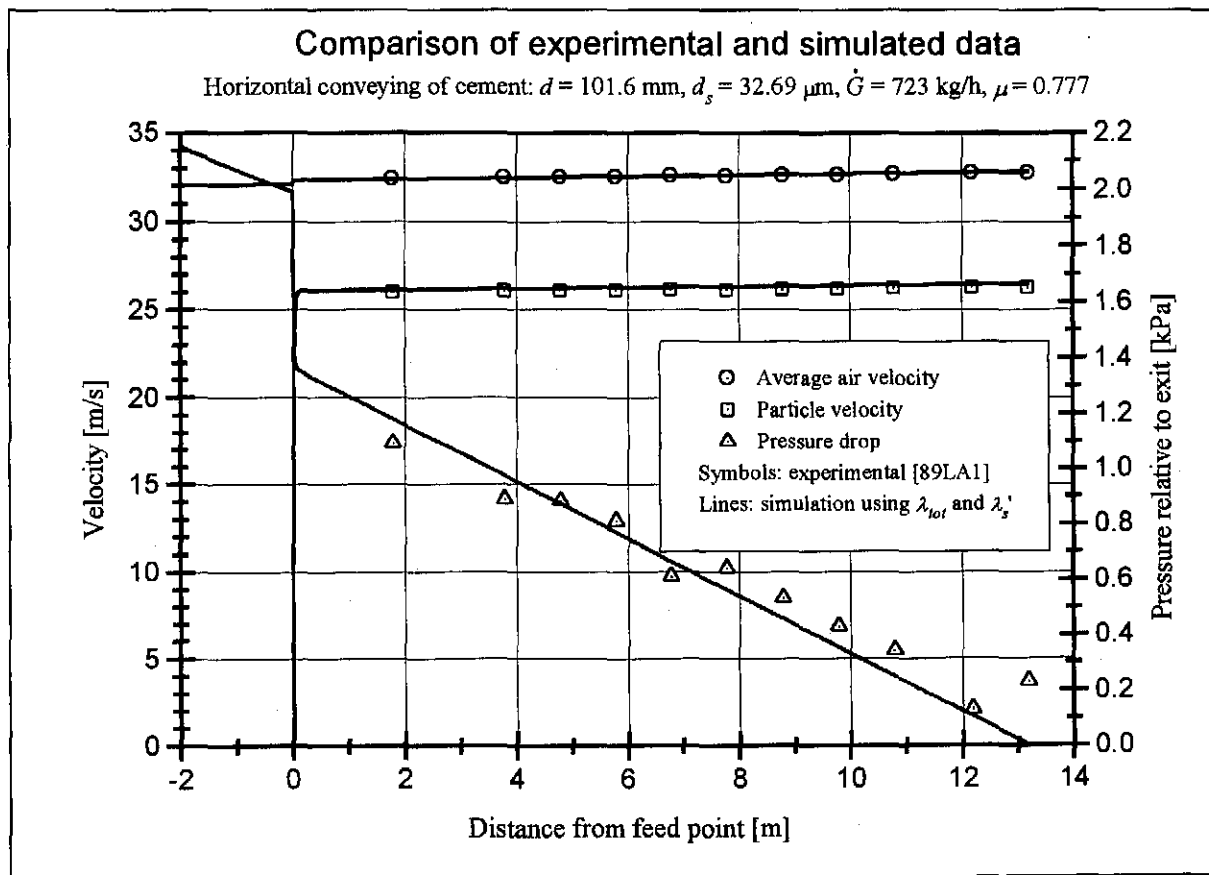


Fig. 5.9 Comparison of experimental and simulated data for cement $\dot{G} = 723 \text{ kg/h}$

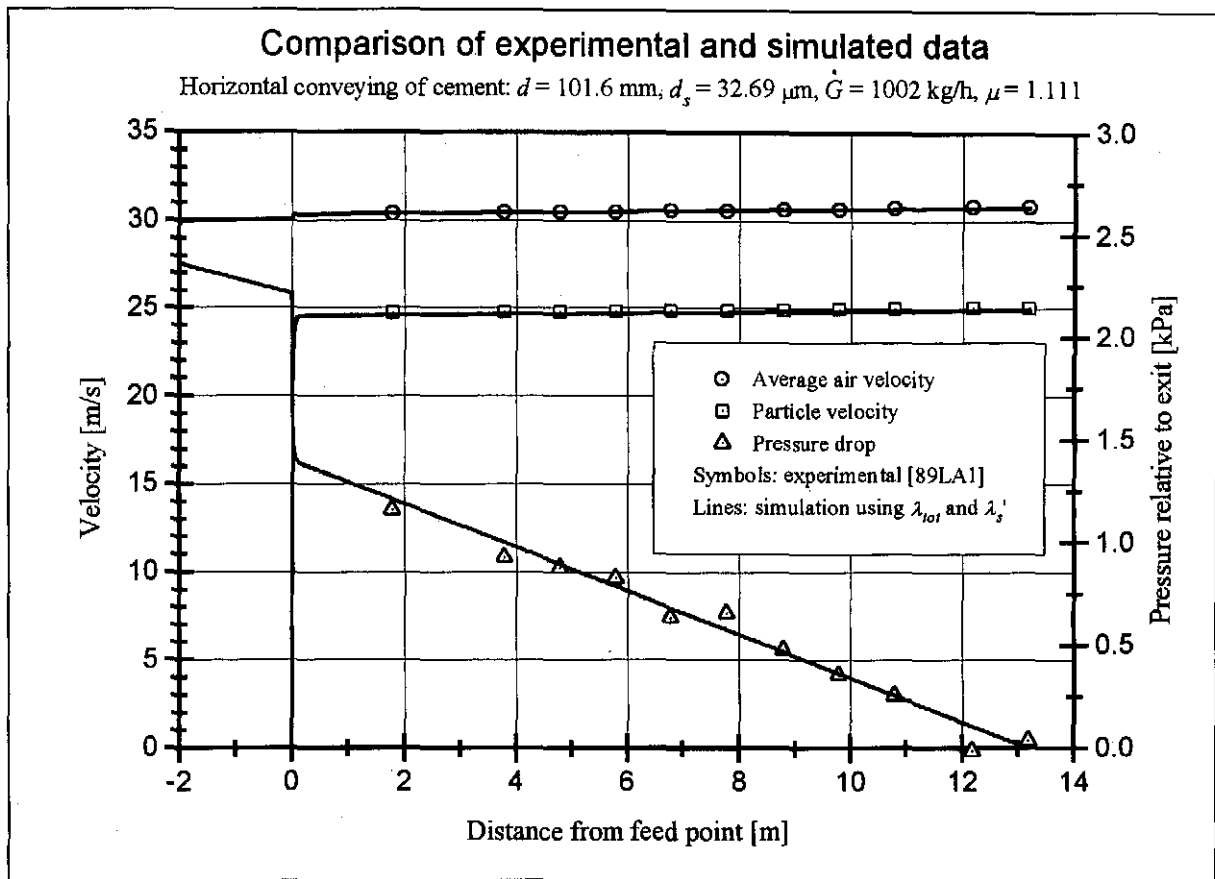


Fig. 5.10 Comparison of experimental and simulated data for cement $\dot{G} = 1002 \text{ kg/h}$

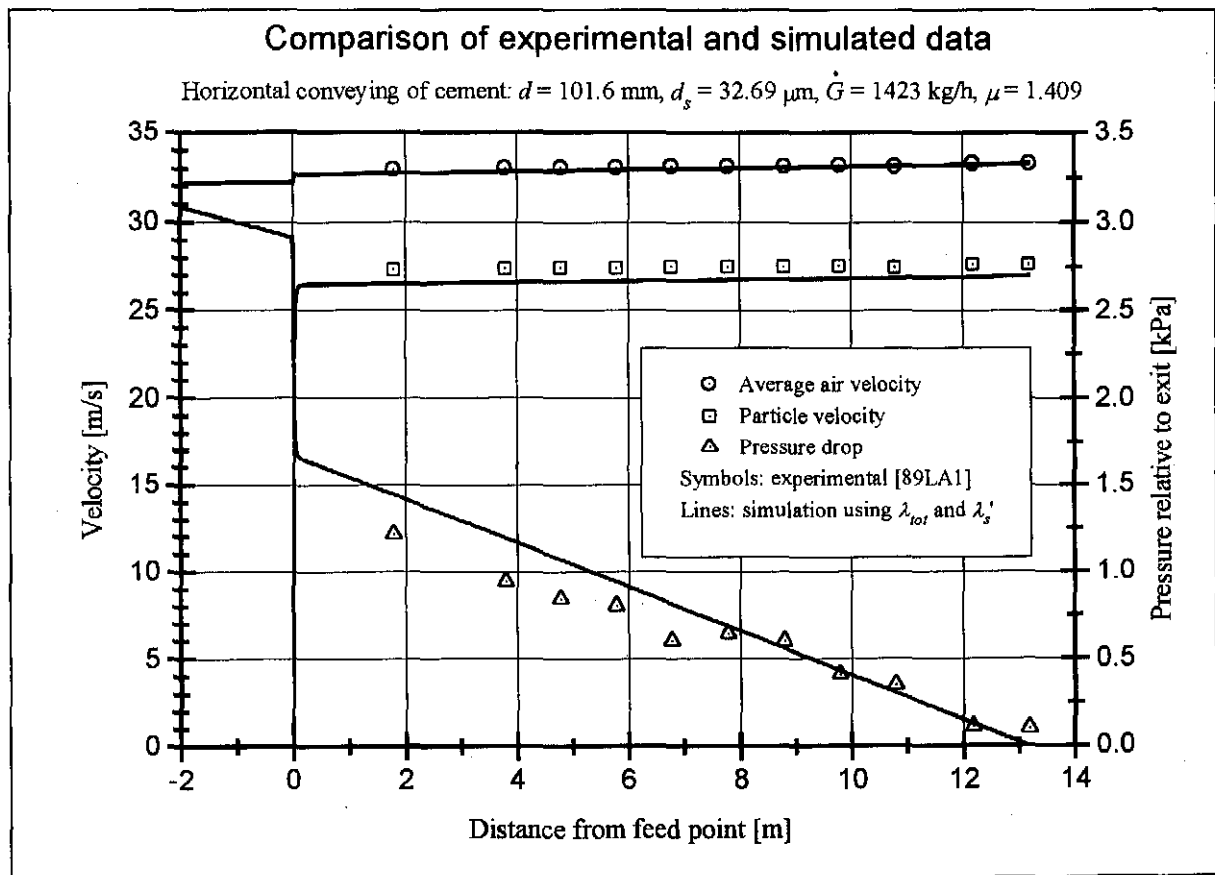


Fig. 5.11 Comparison of experimental and simulated data for cement $\dot{G} = 1423 \text{ kg/h}$

5.4.5 Discussion

The results in figures 5.4 to 5.7 utilising the total friction coefficient and the solids impact and friction coefficient show that the pressure is predicted to within 35% of the experimental value. Some experimental points deviate from the predicted by up to 45% as a result of the scatter in experimental data. The average air velocity is predicted to within 1% of the experimental data. Note that the pressure with respect to point 11 in the pipeline shown in figure 5.1 is used to plot the data so that the maximum possible error is indicated. The solids velocity is overpredicted by up to 20% for the lowest material mass flow rate. Figures D.2.1 to D.2.3 in appendix D show the detailed error plots for the three parameters.

Two other important features that can be seen on the graphs are the acceleration length and the rise in average air velocity after the feeding point. The acceleration length is defined as the length of pipeline required for the particles to be accelerated from rest to a constant conveying velocity. In the above cases the acceleration length lies in the order of 1 m to 1.5 m. The increase in air velocity is as a result of a decrease in density associated with the acceleration pressure drop and will only be evident if there is no air leakage through the rotary vane feeder at the feed point.

Comparing the results in figures 5.8 to 5.11 to the previous results from figures 5.4 to 5.7, an improvement in the prediction of the solids velocity is evident as a result of using the alternative solids impact and friction coefficient. The predictions for the solids velocity improve by 17% to within 3% of the experimental values while the pressure and air velocity shows no notable change to the previous results. For complete error plots for the results refer to figures D.3.1 to D.3.3 in appendix D. These results indicate that the effects of the motion equation on the solution of the remaining differential equations is small. The effect of the alternative solids impact and friction coefficient also reduces the acceleration length of the particles after the feeding tee when compared with the previous results. These now lie in the region of 0.25 m to 0.5 m. This affects the total system pressure drop which is reduced by between 3.3% and 7.6% compared with previous data as a result of the decreased acceleration length.

5.5 The simulated non-dimensional and normalised state diagram for cement

The simulation programme can be used to simulate both the non-dimensional and the normalised state diagrams that are discussed in section 1.3.1 in chapter one. The non-dimensional state diagram using the solids impact and friction coefficient is shown in figure 5.12 for a mass flow range between 257 kg/h and 1300 kg/h. For all practical purposes the

non-dimensional state diagram using the alternative solids impact and friction coefficient is identical to figure 5.12 and is thus not repeated here. This confirms that the influence of changing the friction coefficient representation on the average air velocity used in the Froude number is minimal in the conveying section downstream of the material feed point. This is consistent with the results obtained during the simulation of the experimental data.

Figure 5.13 depicts the normalised state diagram for cement conveying using the solids impact and friction coefficient. This is similar to the normalised state diagram using the alternative solids impact and friction coefficient for the same reasons discussed above. Section D.4 presents the tabulated data used to generate figures 5.12 and 5.13.

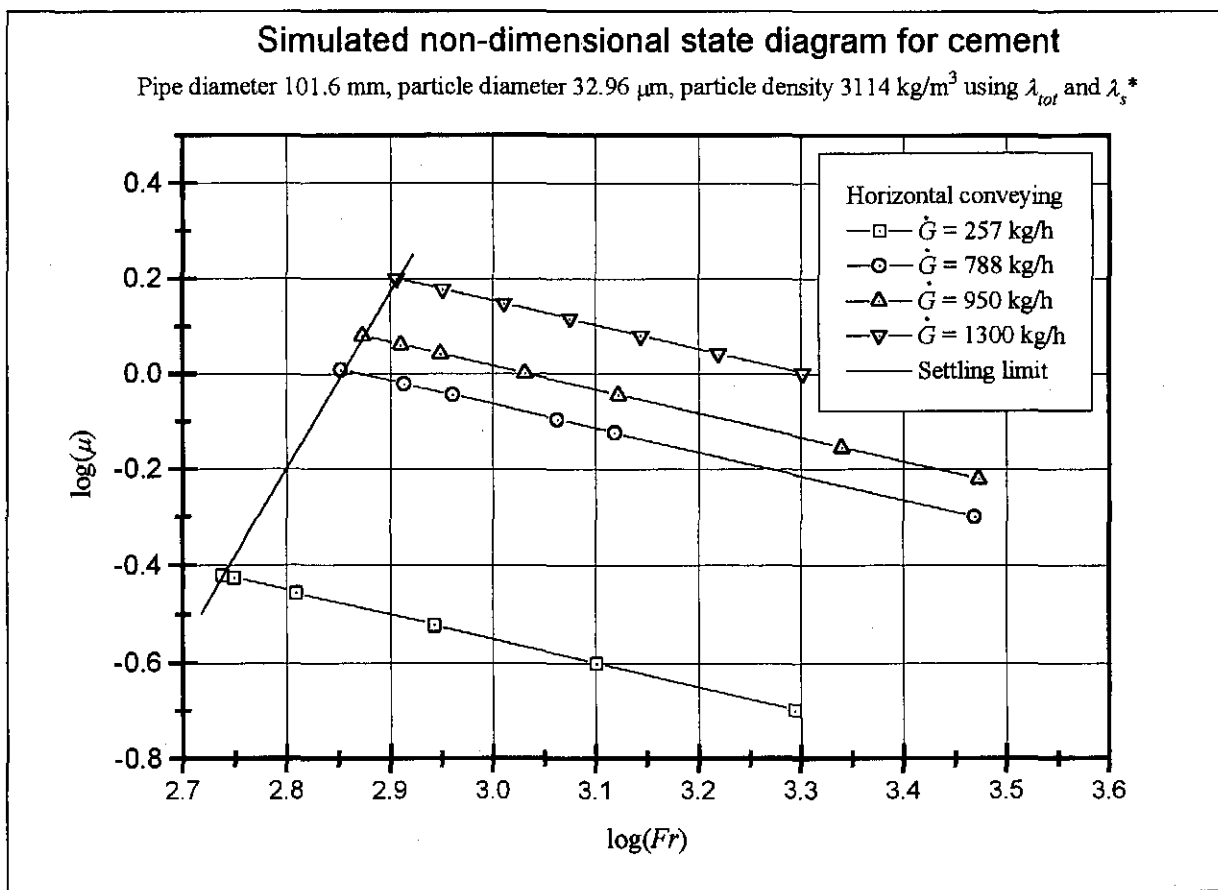


Fig. 5.12 Simulated non-dimensional state diagram for cement

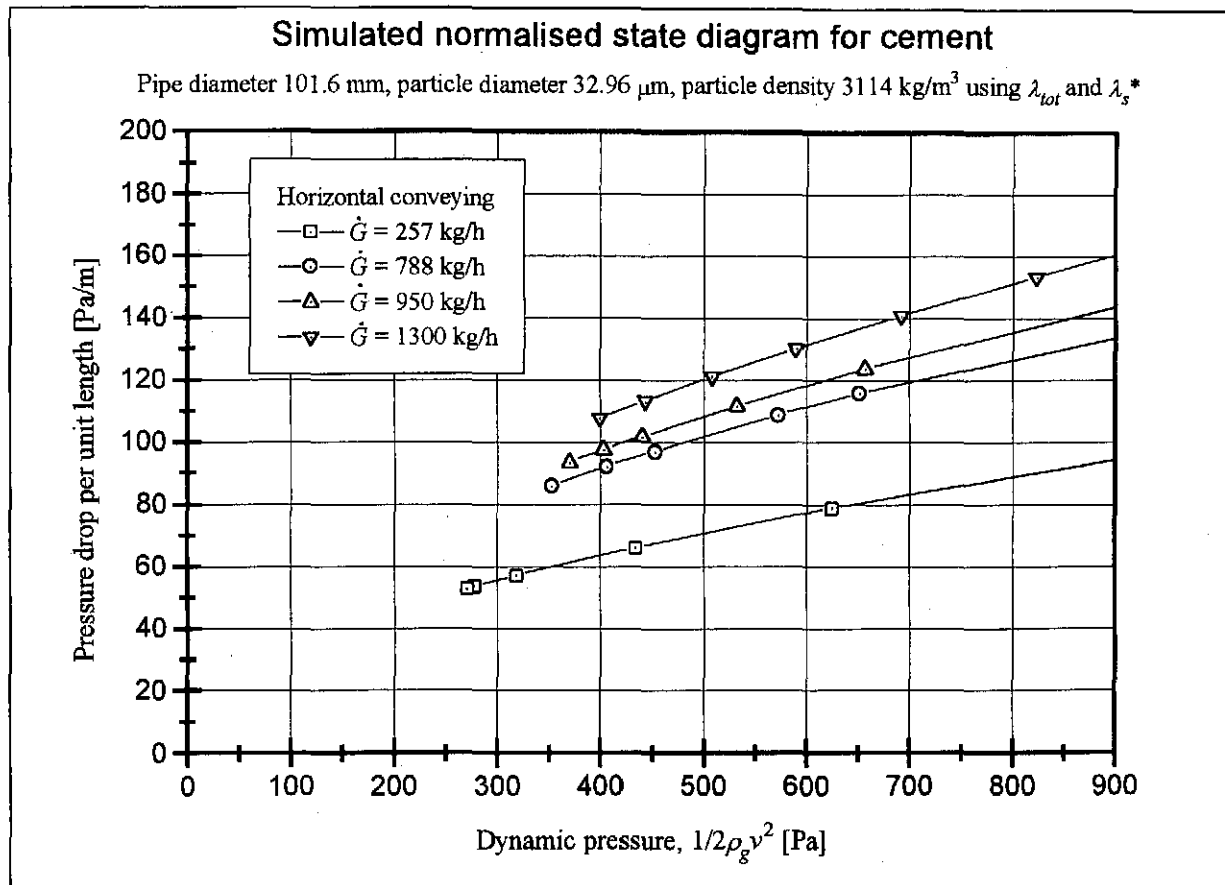


Fig. 5.13 Simulated normalised state diagram for cement

5.6 Comparison of experimental and simulation results for tube ice

5.6.1 Introduction

The solids impact and friction coefficient could not be determined for the ice particles using equation 5.3.7. The Haaland [83HA1] equation 1.3.16 is used with a surface roughness of 0.1 mm as suggested by Sheer [91SH1] to determine the air alone friction coefficient. Subtracting this from the total friction coefficient results in negative coefficients for 90% of the experimental data. This may be a verification that the separation of the solids pressure drop from the total pressure drop by subtracting the air alone pressure drop is indeed artificial and an unacceptable practice. During the calculation of the friction coefficients it was found that the lifting term equation 3.3.24 introduced in the pressure drop equation has a large influence for the case of the large particles such as tube ice and may be a contributing factor to the resultant negative coefficients. Standard practice is to include the lifting term in the friction coefficient as shown in the differential equations (Version 2) in appendix B. This, however, precludes a generalisation of the equations for horizontal and vertical flow and it is for this reason that equations 5.3.2 to 5.3.8 (Version 1 in appendix B) are used for the simulation programme. The merits of doing so are discussed in the final conclusion in chapter seven. It is

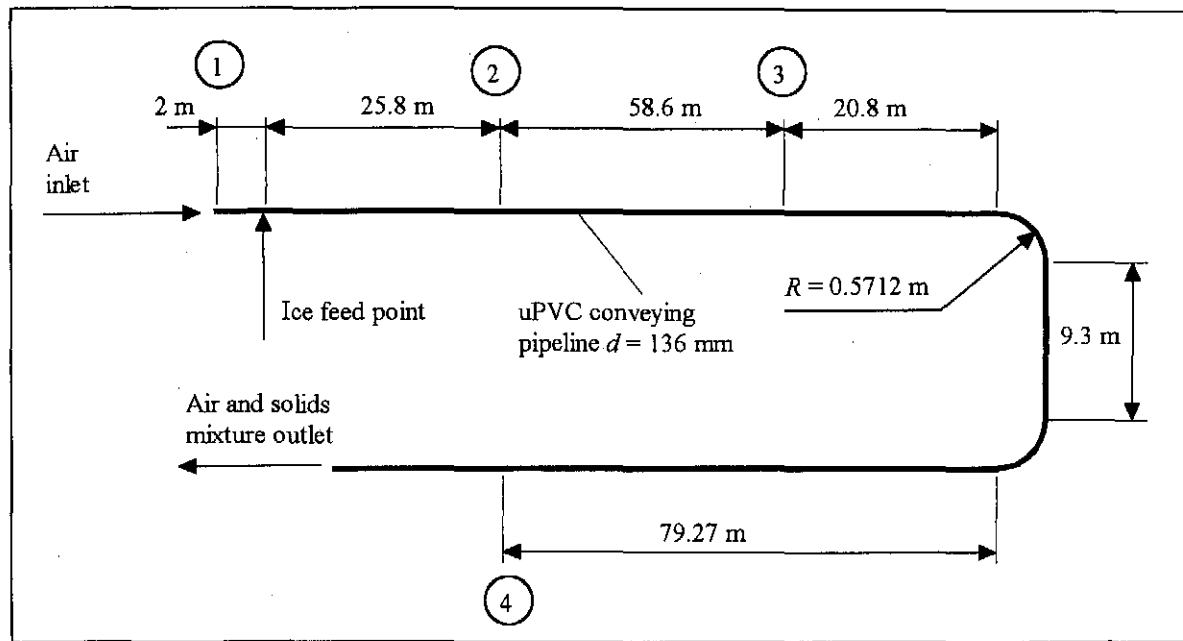


Fig. 5.14 Pipe layout used for ice conveying experiments [91SH1] and simulation

thus only possible to determine the alternative solids impact and friction coefficient for tube ice and use this with the total friction coefficient for the simulation. The conveying facility used by Sheer [91SH1] for horizontal flow contains two bends as shown in figure 5.14. This allows for an evaluation of the bend flow model. The sliding friction coefficient which is used in the bend flow model as presented in equations 3.5.8 and 3.5.9 is found to underpredict the pressure drops associated with the bends during ice conveying and requires adjustment. From the simulations for ice flow it can be shown that the sliding friction coefficient used in the bend flow model varies linearly with the ice mass flow rate. A detailed account is presented in section 5.6.4.

5.6.2 Air leakage at the feed point

The simulation programme makes provision for air leakage at the feed point in terms of a percentage of conveyor inlet air mass flow rate that is lost through the feeding mechanism. For the ice conveying experiments a rotary vane feeder is used to feed the tube ice into the pipeline. The average air mass flow leakage rate for the experimental setup lies in the order of 10%. Sheer [91SH1] gives the inlet air and the conveying air mass flow rates for each experimental test run so that the exact percentage can be calculated from equation 5.3.9 as:

$$\text{Air leakage percentage} = 100 \cdot \left(1 - \frac{\text{Conveying air mass flow rate}}{\text{Inlet air mass flow rate}} \right) \quad (5.3.9)$$

This value is used during the simulation of the corresponding experimental results.

5.6.3 Initial conditions for tube ice

The characteristic curve with respect to varying initial solids velocities determined for tube ice conveying shows a similar trend to that determined for cement where the initial solids Froude number is essentially independent of varying material mass flow rate as shown in figures 5.15.

For tube ice the initial solids Froude number is chosen between $Fr_{co} = 3$ and $Fr_{co} = 8$ corresponding to an initial solids velocity of $c_o = 1$ m/s to $c_o = 1.5$ m/s. The data used for figure 5.15 can be found in section D.5 in appendix D.

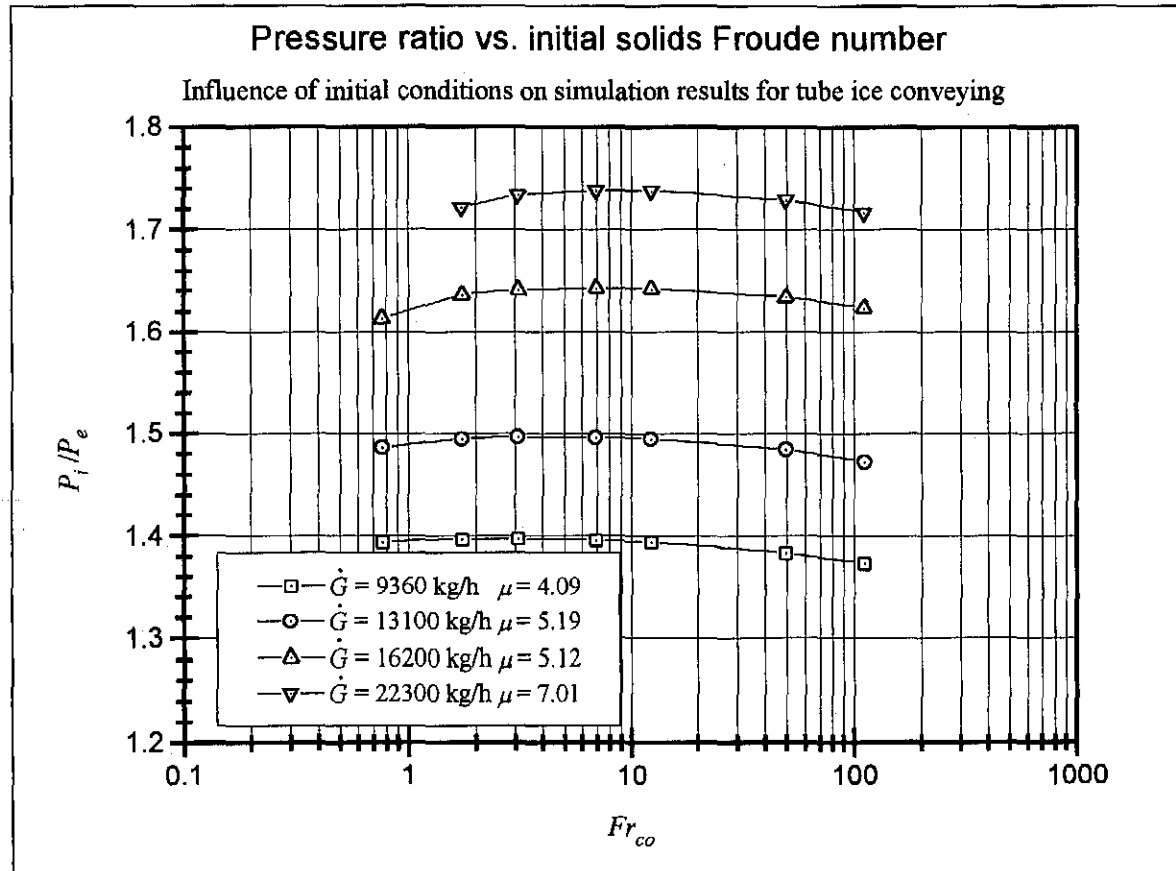


Fig. 5.15 Pressure ratio vs. initial solids Froude number for tube ice using λ_{tot} and λ_s'

5.6.4 Bend friction coefficient

The sliding friction coefficient used for the first simulations is the value $f = 0.018$ determined by Sheer [91SH1]. The results show that this value is too low to be used to model the pressure drop in the bend section correctly. Consequently the required sliding friction coefficient is determined by the following method: the simulations for the ice flow are first run for the horizontal section using the absolute pressure at point 3 in figure 5.14 as the pipe outlet pressure. This is done to verify that the pressure and velocity traces along the pipeline are correctly predicted. Once this is completed the simulation is run with the two bends in place and the sliding friction coefficient adjusted for the different material mass flow rates so that the

pressure at point 3 and point 4 at the outlet are correctly predicted. The tests without the bends show an accurate simulation of the experimental conditions and it can thus be assumed that for the case where the complete pipe layout is used with the bends in place, the pressure drop in the remaining straight sections is also correctly predicted. The resulting sliding friction coefficients are shown to be linearly dependent on the mass flow rate of the tube ice in the following equation:

$$f = 0.4345\dot{G} - 0.0614 \quad r^2 = 0.93 \quad 2.56 \text{ kg/s} < \dot{G} < 6.19 \text{ kg/h} \quad (5.3.10)$$

The sliding friction coefficient varies between 0.075 and 0.3 with a lower sliding friction coefficient at higher mass flow rates. A table of the sliding friction coefficient for bend flow of tube ice in a 136 mm diameter uPVC pipe is given in section D.6 in appendix D. The bend friction coefficient thus reduces the higher the mass flow rate. A detailed discussion of the merits of the bend flow model are presented in section 5.8

5.6.5 Results for tube ice conveying using λ_{tot} and λ_s'

The results for the tube ice conveying are shown in figures 5.16 to 5.19 utilising the total friction coefficient and alternative solids impact and friction coefficient. For the corresponding table of results refer to section D.7 in appendix D. Once again a section of 2 m is added upstream of the feeding point so that the values of pressure drop and air and solids velocity are easier to identify. Pressure data are relative to point 4 shown in figure 5.14. Sheer [91SH1] does not present details of the exact positioning of the pressure tap point 1 upstream of the feeding point. It is thus assumed that this tap point lies 2 m upstream of the feed tee. The influence of the exact positioning of this tap point can be assumed negligible as the pressure drop associated with the shift in position of the tap point is small compared with the total system pressure drop. As in the cement conveying condition the analysis is for single-phase flow upstream of the feed point and then continues as two-phase flow downstream of the feed point.

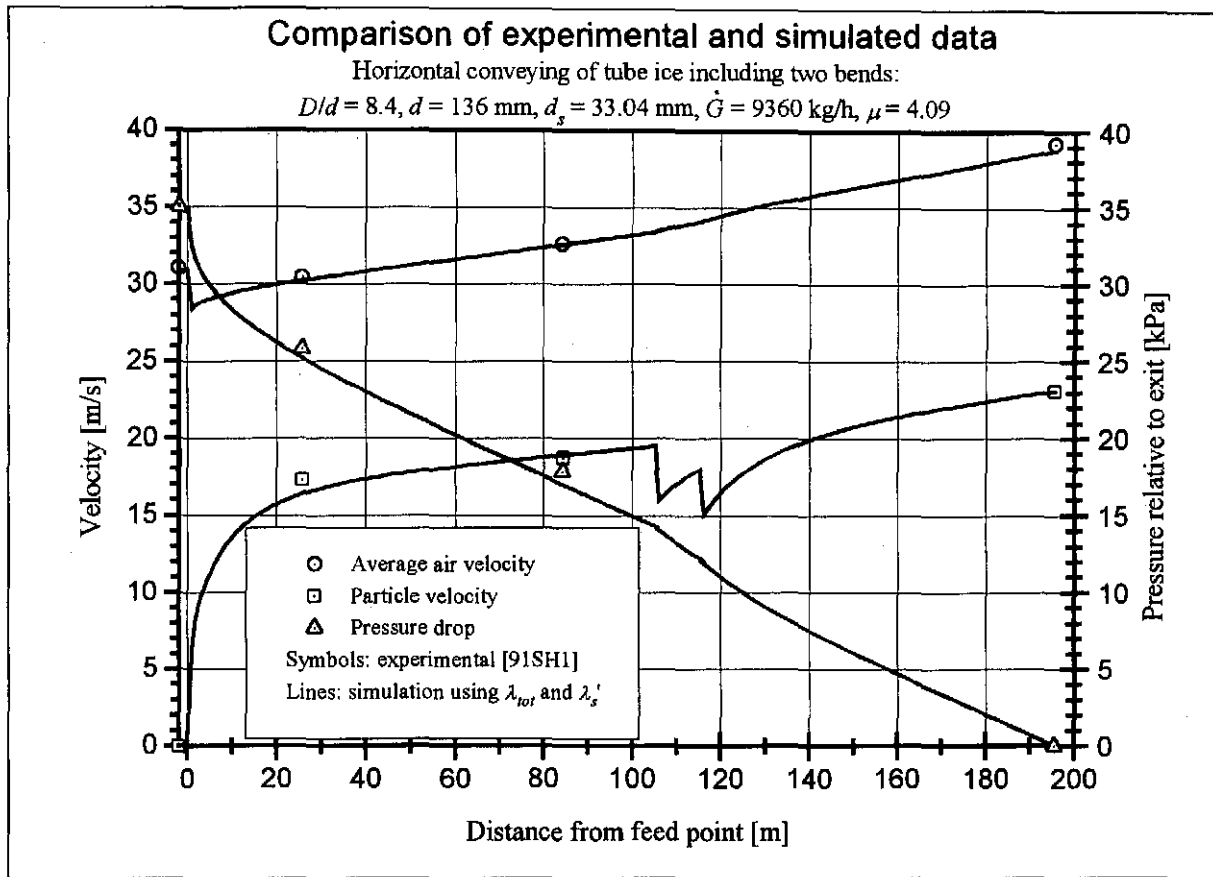


Fig. 5.16 Comparison of experimental and simulated data for tube ice $\dot{G} = 9360 \text{ kg/h}$

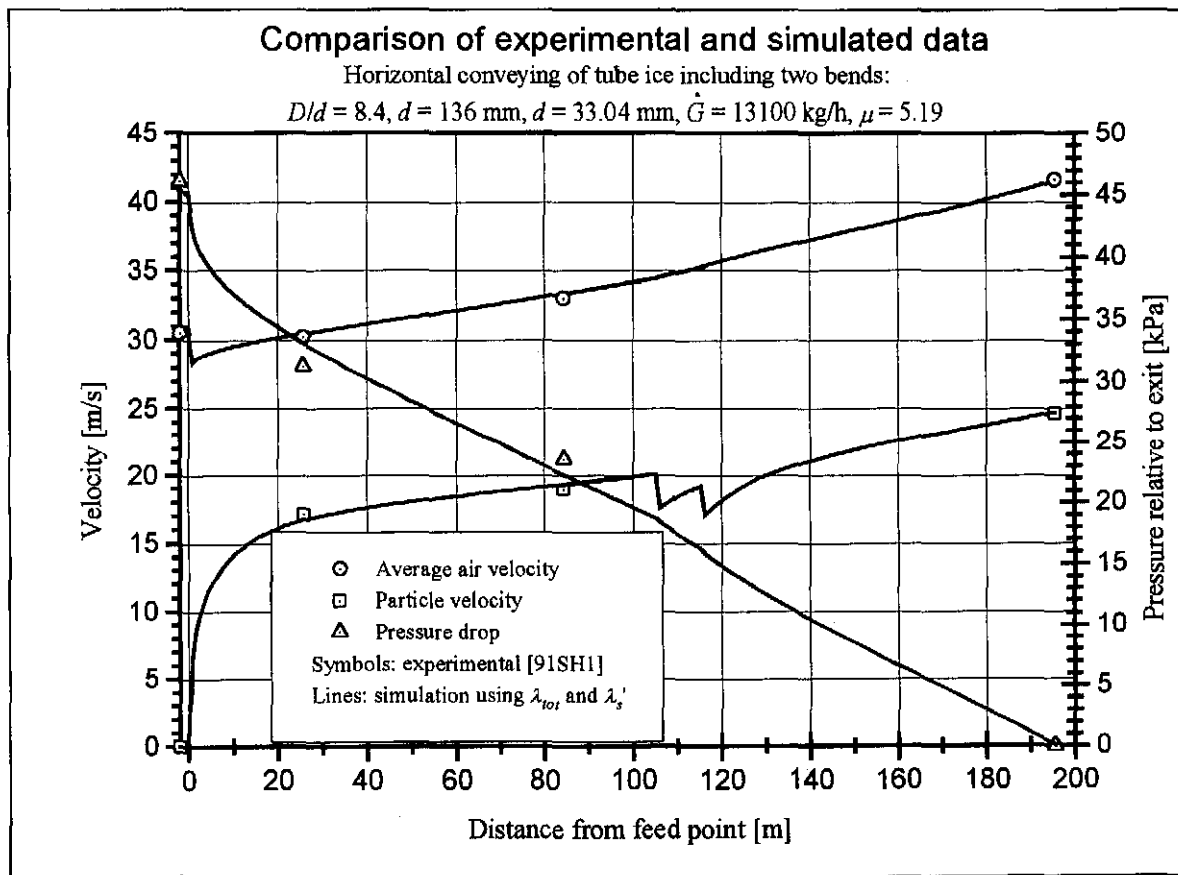


Fig. 5.17 Comparison of experimental and simulated data for tube ice $\dot{G} = 13100 \text{ kg/h}$

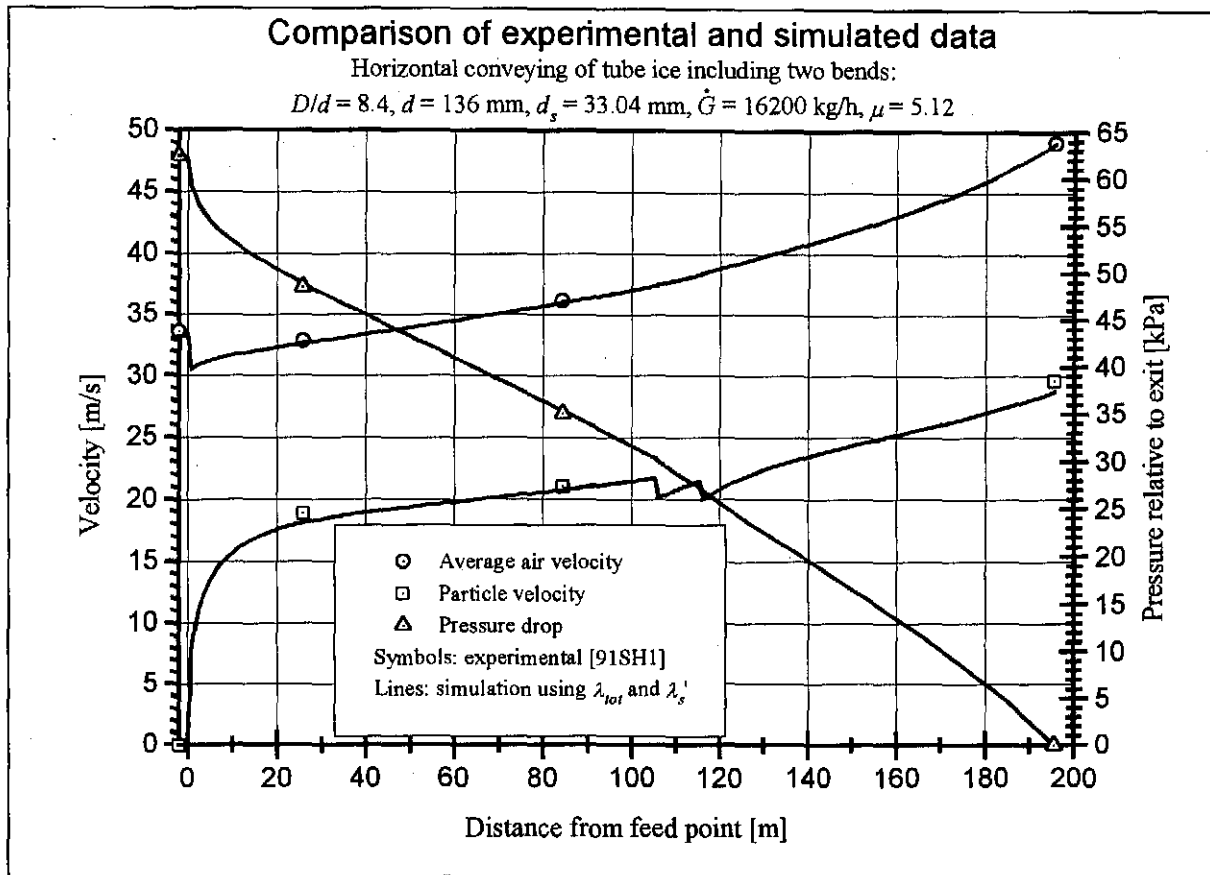


Fig. 5.18 Comparison of experimental and simulated data for tube ice $\dot{G} = 16200 \text{ kg/h}$

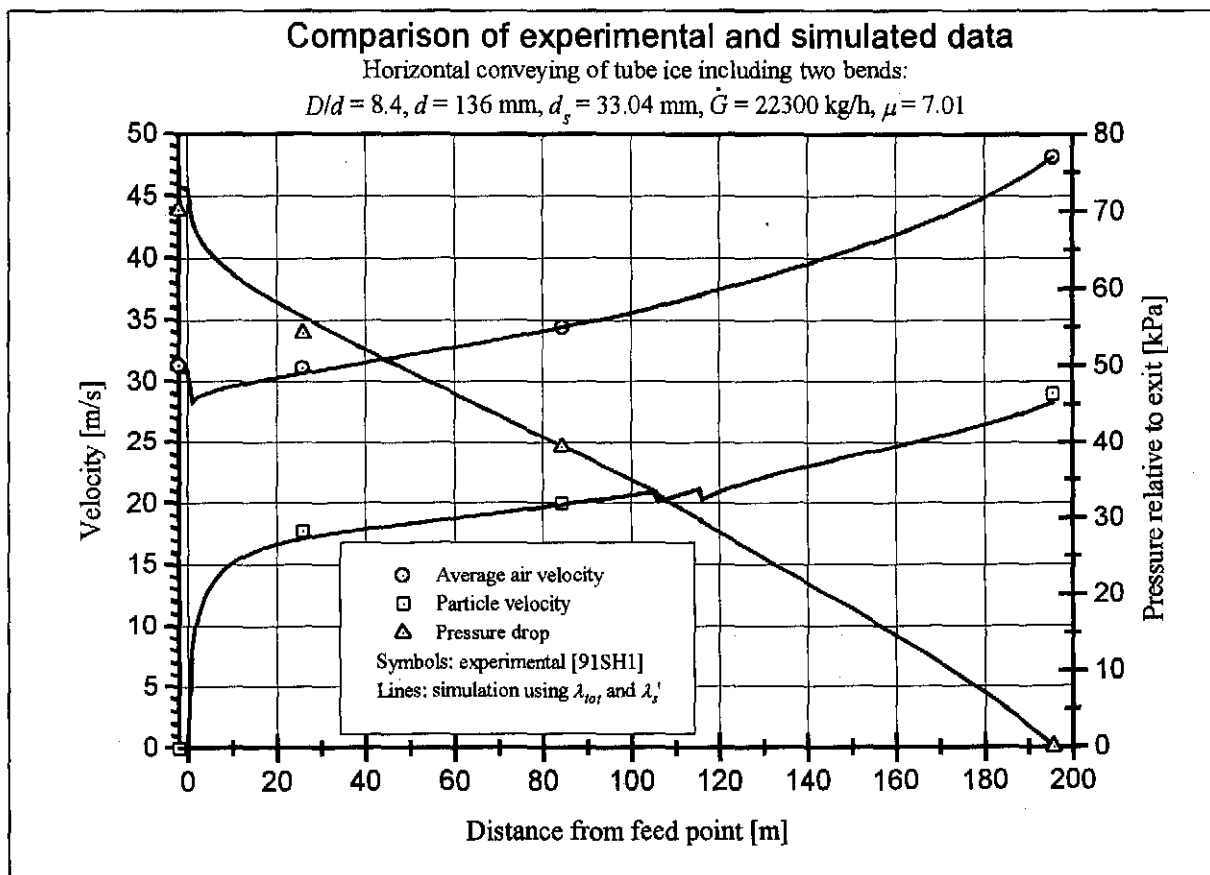


Fig. 5.19 Comparison of experimental and simulated data for tube ice $\dot{G} = 22300 \text{ kg/h}$

5.6.6 Discussion

The simulation results presented in figures 5.16 to 5.19 show good agreement with the experimental data. The individual experimental pressure points are predicted to within 6% of the experimental value while the average air velocities show a maximum error of 2% and the solids velocities lie within 6% of those calculated from the experimental values. For complete error plots refer to figures D.7.1 to D.7.3 in appendix D.

Of interest in the simulation results is the acceleration length of around 180 pipe diameters required for large particles such as tube ice to reach a constant conveying velocity. For this reason Sheer [91SH1] suggests that bends only be set into place at a minimum distance of 200 pipe diameters downstream of the feed point for the 136 mm diameter uPVC pipe. The simulations also show that the acceleration length decreases the higher the initial average air velocity at the feed point. This is to be expected and also illustrates the importance of a sufficiently high initial average air velocity to effect safe acceleration of the particles. It can also be seen that the air leakage of around 10% of the inlet air mass flow rate has the effect of reducing the initial air velocity by the order of 8%. The complete reduction is not equal to the percentage of air lost as a small percentage of velocity recovery can be attributed to the decrease in density as a result of the acceleration pressure drop after the feeding point which in turn increases the air velocity. The velocity recovery effect is clearly illustrated in the case of the cement conveying where air leakage is neglected.

The bend flow effects are clearly visible as a distinct deceleration of the particles in the bends with subsequent reacceleration after the bends. It is of practical interest to note the effects of placing the two bends only 9.3 m apart (68 pipe diameters) in the experimental facility. The particle flow exiting the first bend does not have sufficient time to reaccelerate after the bend before reaching the second bend. The result is that the particle velocity is reduced below the minimum particle velocity attained in the first bend. It is at the exit of the second bend where the first signs of pipe blockage can be expected. This illustrates clearly the merits of good pneumatic conveyor design practice already recommended by Marcus, Hilbert & Klinzing [85MA1] by placing bends following each other as far apart as possible to allow the particles to re-accelerate after the initial bend. The use of the bend flow model itself requires caution as it has been shown that the use of the sliding friction coefficient in the bend flow model cannot be used to predict the bend pressure loss for tube ice. Given the fact that ice is an unusual material to work with, the influences of wall wetting through the melting of some of the ice can have a large influence on the friction coefficients in the bends. It is thus

imperative that more experimental data for different kinds of material be analysed and compared with the simulation model for bend flow before it can be applied universally.

A further effect clearly illustrated is the constant increase in air velocity as a result of the decrease in air density due to the pressure drop along the conveying pipeline. This may cause excessively high air velocities towards the end of the pipeline in long lines with an associated increase in wear due to the increase in particle velocity. If one for example sets an upper average air velocity limit of 40 m/s for the ice conveying case it would be necessary to increase the pipe diameter at a point 180 m downstream of the feed point for the cases shown in figures 5.17 and 5.19 to reduce the air velocity. For this to be implemented in the simulation programme one requires friction coefficient correlations that are applicable to required range of pipeline diameters and also have an indication of the values of the sliding friction coefficient for the bends at different bend radii and a range of pipe diameters. As the data to determine such a friction coefficient correlation are lacking such an example cannot be presented at this time.

5.7 The simulated non-dimensional and normalised state diagram for tube ice

The non-dimensional state diagram using the alternative solids impact and friction coefficient is

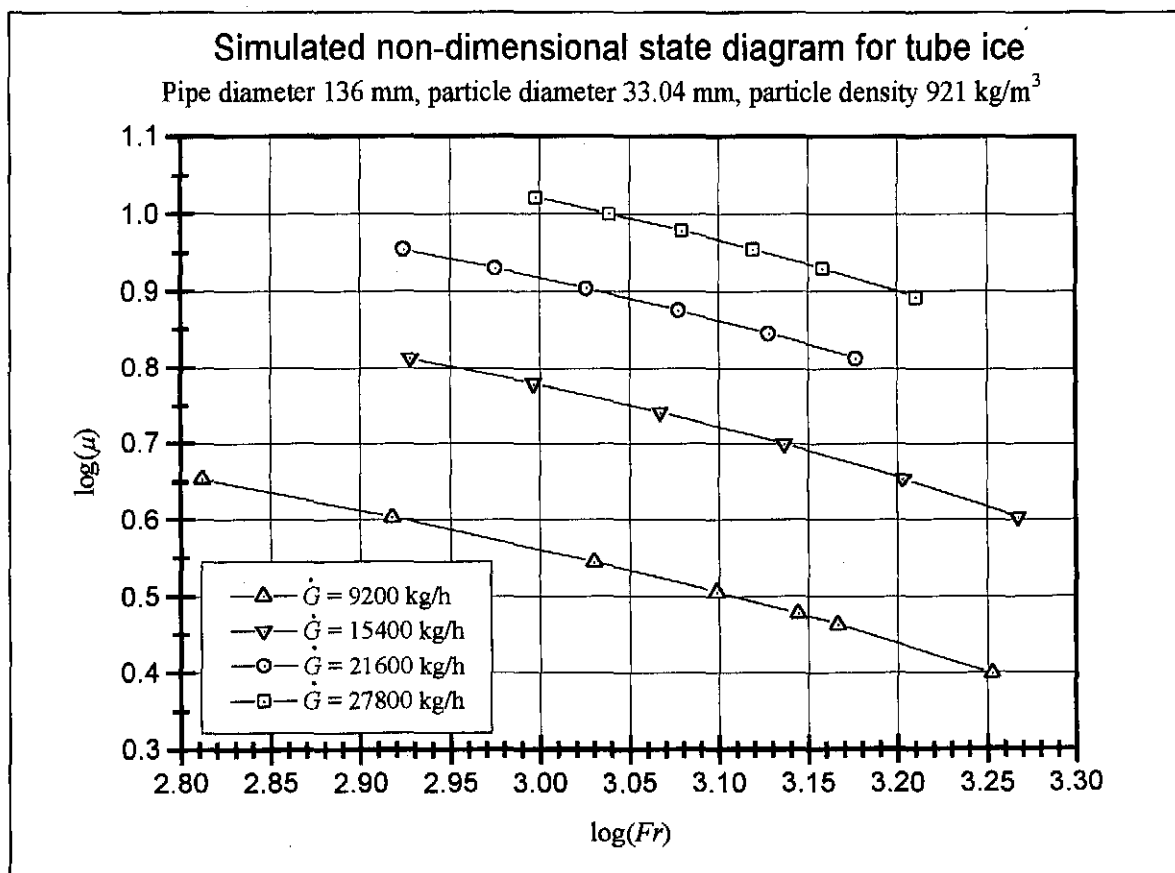


Fig. 5.20 Simulated non-dimensional state diagram for tube ice

shown in figure 5.20 for a mass flow range between 9200 kg/h and 27800 kg/h. Figure 5.21 depicts the normalised state diagram for tube ice conveying using the solids impact and friction

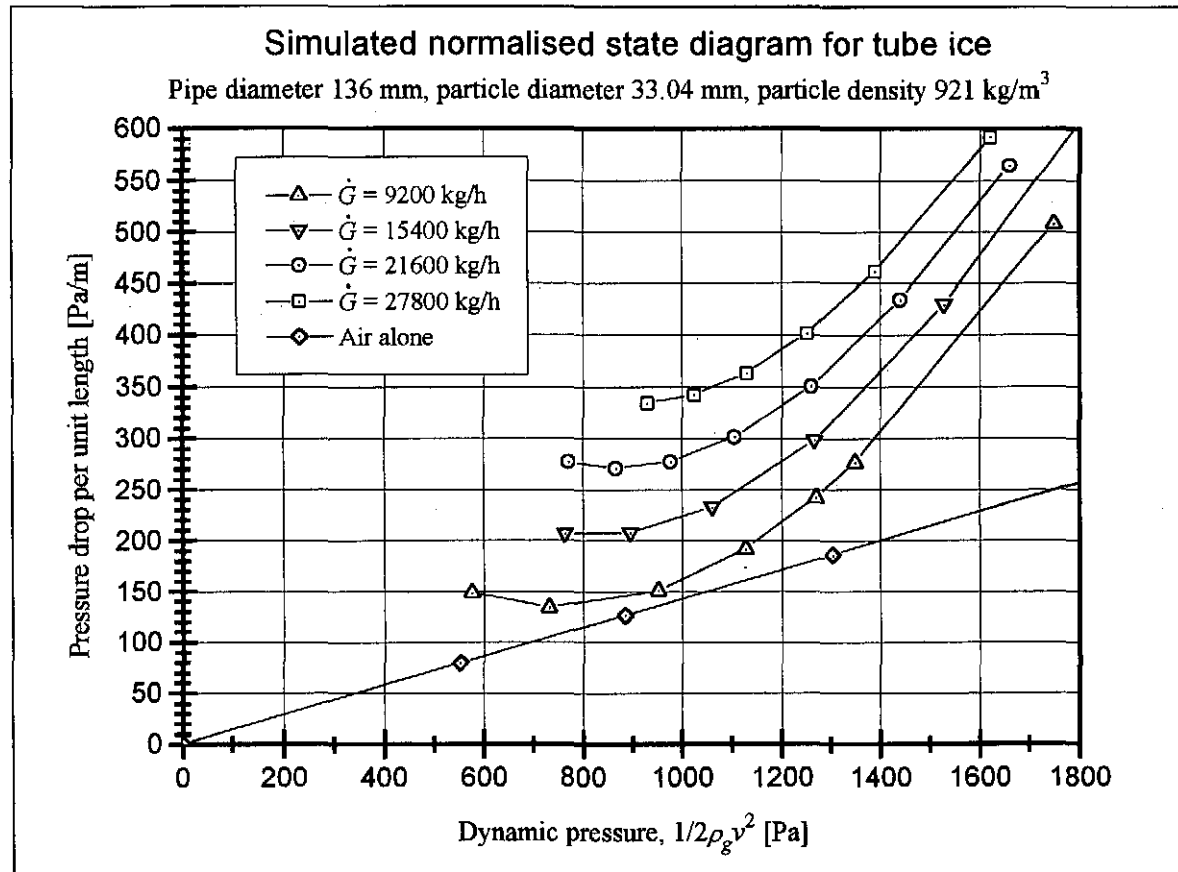


Fig. 5.21 Simulated normalised state diagram for tube ice

coefficient. The data for figures 5.20 and 5.21 are presented in tabular form in section D.8 in appendix D.

5.8 Discussion of the overall results

The results presented in sections 5.4 to 5.7 confirm the validity of the mathematical model used for horizontal two-phase flow and prove the correct implementation of the model in the simulation programme. The use of the alternative solids impact and friction coefficient results in a better prediction of the solids velocity in the conveying pipeline when compared to the results of the use of the solids impact and friction coefficient. It also proves to have a minimal effect on the determination of the average air velocity and the pressure drop which indicates that the main effect on these two variables is the total friction coefficient in the pressure drop equation. The main design parameters required from the simulation programme are the total pressure drop and the air volume or mass flow rate. The air volume flow rate is coupled to the density which in turn is dependent on the pressure through the gas state equation. Thus the pressure drop equation has a primary influence on the important design parameters.

Furthermore the correlation for the alternative solids impact and friction coefficient for both the cement and the tube ice shows a marked improvement in the correlation coefficient compared with that of the total friction coefficient and the solids impact and friction coefficient as can be seen in figures C.3 and C.5 in appendix C.

The method for the estimate of the initial solids velocity presented in section 5.4.2 has proven to yield good results for the conveyor inlet pressure and velocity for the case of the ice conveying and can be recommended as standard procedure for the simulation programme. In view of the fact that the curves of initial solids Froude number vs. pressure ratio show the same trend for cement conveying as for ice conveying it is reasonable to assume that the same procedure can also be applied to other particles.

The most important result from the experimentation with the different friction coefficient representations is an improved method for determining the solids velocity by making use of the alternative solids impact and friction coefficient. This is of practical importance as an improved estimate of the solids velocity can be used to determine the onset of blockages in the pipeline where the solids velocity falls below a predetermined limit and is considered a prime design variable. Saccani [96SA1] emphasises the importance of determining the solids velocity and utilising it for design purposes. The determination of the solids velocity is particularly important after bends in cases where these must be positioned close to the feeding point and where bends follow closely after each other. The recommendation by Sheer [91SH1] for the placing of the bends 200 pipe diameters downstream of the feed point is verified by the simulation results with the tube ice. The main aim of this recommendation is to prevent blockages as a result of low solids velocities after particle deceleration through the bend. Enough time must also be allowed for particles to reaccelerate after a bend before placing the following bend in the flow. If this is not done the pipe may start to block up after the second bend as a result of low solids velocities.

It is also important to realise that the minimum conveying air velocity recommended in the literature can only be used to ensure that the initial air velocity is high enough in terms of a minimum Froude number to affect acceleration of the particles directly after the feeding tee. In the remaining pipeline it is the minimum solids velocity that is of importance in determining whether a blockage will occur or not.

The simulations clearly show the effects of the increasing velocity as a result of the decreasing density as the pressure drops along the conveying pipeline. The simulation programme can thus also be used to determine the optimum position for an increase in pipeline diameter to reduce the average air velocity and in turn also reduce the solids velocity. Where

suitable friction coefficient correlations have been determined for the same material for a range of different pipe diameters the two-phase flow simulation can be run with pipe expansions in place.

5.9 Conclusion

In summary the following results have been attained from the simulations and the comparison to experimental data:

- The differential equations governing two-phase flow have been successfully rearranged for implementation of the total friction coefficient and the alternative solids impact and friction coefficient.
- An improved method of determining the alternative solids impact and friction coefficient from the integrated motion equation has been presented, implemented and verified for use in horizontal conveying. The accuracy of the correlations for the alternative solids impact and friction coefficient as determined from the motion equation in comparison to the solids impact and friction coefficient determined from the pressure drop equation is improved substantially.
- The use of the alternative solids impact and friction coefficient has been shown to yield better results in terms of the solids velocity predictions than with the use of the solids impact and friction coefficient.
- The bend flow model has been shown to be inadequate for simulating bend flow without a modification of the sliding friction coefficient used in the model.
- The simulation programme can be used to determine the main variables, the system pressure drop and air flow rate, which are required for the prime air mover selection.
- Vertical flow could not be verified for a lack of sufficient data.

5.10 Recommendation

The following recommendations can be made on the basis of the results described in this chapter:

- The bend flow model requires further refinement. One possibility is to determine an equivalent solids impact and friction coefficient correlation and total friction coefficient correlation for bend flow from experimental data.
- The applicability of the friction coefficients determined for horizontal flow to vertical flow requires verification.

- An improvement of the correlation equations for the total friction coefficient. This may require a modification of the differential equations to incorporate terms such as the particle free fall velocity and drag coefficient into the definition of the friction coefficients and thus reduce the uncertainty in determining these properties by calculation. As the total friction correlation is required in the determination of the alternative solids impact and friction coefficient this is likely to further improve the correlations of the alternative solids impact and friction coefficient.

POSITIVE DISPLACEMENT BLOWERS

6.1 Introduction to Roots blowers

Roots blowers are medium pressure positive displacement machines. In the standard configuration two figure of eight shaped rotors run at 90° to each other with one lobe of the rotor sweeping into the hollow at the side of the second rotor during rotation as shown in figure 6.1. The two rotors run in a figure of eight shaped housing bore and during rotation a fixed volume of gas is moved along the cavity formed at the outer perimeter of the rotors from the inlet side to the outlet side of the blower. Three lobed blowers with the same principle of operation as the two lobed blowers are being used to decrease the peaks in pressure pulses characteristic of roots blowers. Together with an increase in pressure pulse frequency this allows for more effective sound proofing.

Running clearances between the two rotors and between the rotor and housing wall are responsible for return air leakage which takes place from the blower outlet to the blower inlet side as a result of a pressure gradient across the blower.

6.2 Chapter contents

Section 6.3 discusses the application of Roots blowers in the field of pneumatic conveying. The theoretical calculation of blower performance is discussed in section 6.4. A method for determining the operating characteristic parameters such as the blower volume and leakage coefficient from performance curves is presented in section 6.5. Dimensional analysis is applied for transforming performance curves from standard to non-standard operating conditions in section 6.6. This is used to verify of the theory presented in section 6.4.1. The application of the theory in the blower selection programme, which is an integral part of the pneumatic conveyor design programme, is discussed in section 6.7. The chapter ends with the discussion and conclusions in section 6.8.

6.3 Application to pneumatic conveying

Roots blowers are used extensively as prime air movers for dilute phase pneumatic conveying systems primarily for their ability to supply high volumes of air at medium pressures. The

maximum pressure differential across the positive pressure blowers lies in the region of 90 to 110 kPa at sea level conditions. When used as exhausters the pressure differentials are reduced to between 45 to 50 kPa. At altitude these pressure differentials are reduced as they are primarily governed by a maximum permissible pressure ratio for a specific roots blower. The implications are discussed in section 6.4.1.

Blowers are used as exhausters for vacuum conveying systems or as positive pressure blowers for positive pressure pneumatic conveying systems. They can also be used for combined vacuum and positive pressure systems.

Due to the fine machining clearances between rotors and housing, air filters have to be installed at the suction side of blowers to prevent the ingress of dust. This is especially important when using blowers for vacuum conveying systems. Non-return valves should be installed on the delivery side of blowers to prevent conveying material and dust from reaching the rotors in positive pressure conveying applications.

6.4 Theory

The final equations of the analytical model presented in section 6.4.1 for the analysis of positive displacement blowers are used extensively in the industry [96AE1] and it is deemed essential at this point to present the derivation of these equations and highlight the assumptions made in the process in order to gain a better understanding of the processes involved. To compare the results of the theoretical model to published performance curves at non-standard blower inlet conditions, a dimensional analysis is performed to determine the laws required to transform standard performance curves (usually at an inlet pressure of 101300 Pa and 20°C) to differing inlet conditions in section 6.6.

6.4.1 Blower performance calculation

The mathematical model for calculating blower performance is based on assuming a perfectly sealing positive displacement pump in parallel with a pipe that allows for the characteristic air leakage or slip through the working clearances of the blower as depicted in figure 6.1.

Analysing the mixing region I, where one assumes steady state, steady flow under adiabatic conditions:

$$\dot{Q}_i \left(h_i + \frac{v_i^2}{2} + gz_i \right) + \dot{Q}_l \left(h_4 + \frac{v_4^2}{2} + gz_4 \right) = \dot{Q}_{th} \left(h_2 + \frac{v_2^2}{2} + gz_2 \right) \quad (6.4.1)$$

Where $\dot{Q}_4 = \dot{Q}_l$ and $\dot{Q}_3 = \dot{Q}_{th}$. Assuming that $z_1 = z_4 = z_2$ and that the kinetic energy changes are negligible, equation 6.4.1 can be simplified to:

$$\dot{Q}_i h_i + \dot{Q}_l h_4 = \dot{Q}_{th} h_2 \tag{6.4.2}$$

Furthermore the leakage flow through the by-pass pipe is assumed adiabatic so that $h_4 = h_3$.

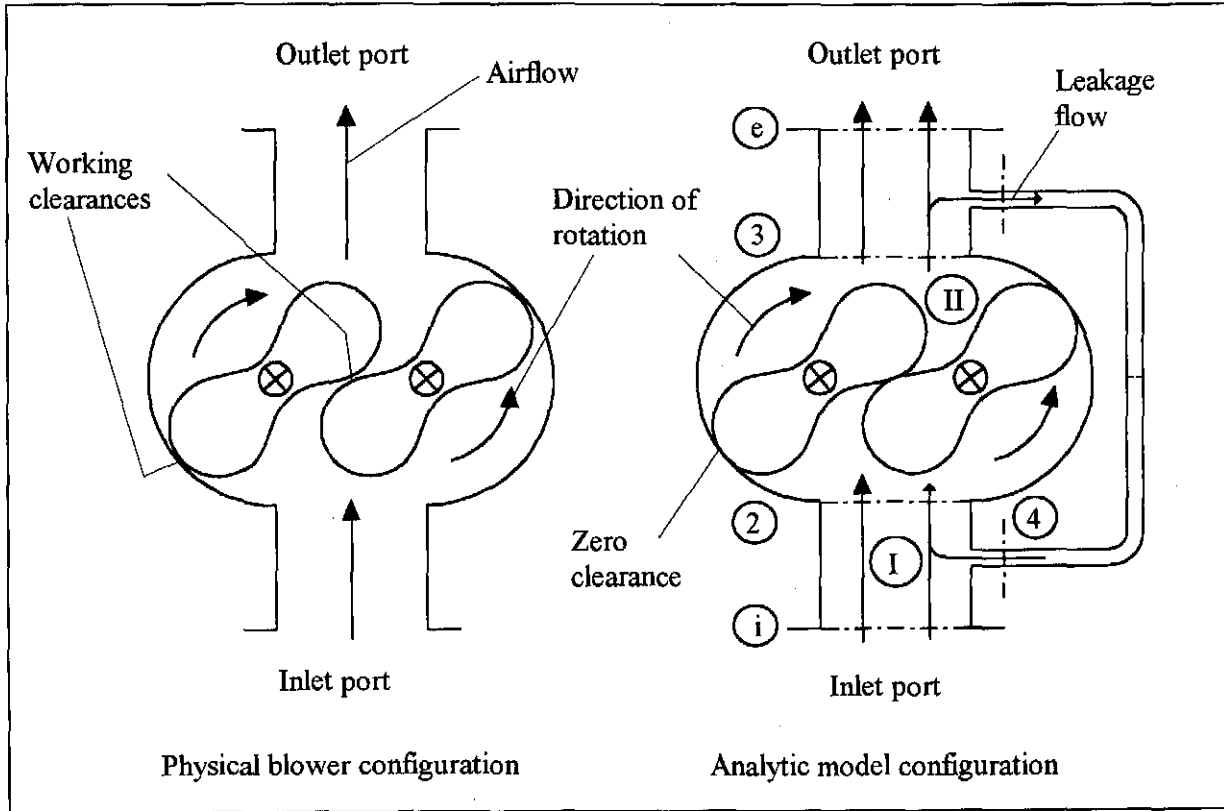


Fig. 6.1 Physical and analytic Roots blower configuration

Introducing the conservation of mass and assuming the specific heat of the gas to be constant within the working temperature range up to a blower outlet temperature 140°C allows the integration of the definition of the specific heat:

$$C_p = \left(\frac{\partial h}{\partial T} \right)_p \tag{6.4.3}$$

to yield:

$$h_i - h_2 = C_p (T_i - T_2) \text{ and } h_2 - h_3 = C_p (T_2 - T_3) \tag{6.4.4}$$

Equation 6.4.1 can thus be rewritten as:

$$T_2 = \frac{\dot{Q}_i T_i + \dot{Q}_l T_3}{\dot{Q}_i + \dot{Q}_l} \tag{6.4.5}$$

Note that the assumptions made in deriving this equation essentially revert to incompressible flow in the mixing region. By setting the mass flow rates in terms of the product of volume flow rate times the density and rewriting the temperatures in terms of the density, pressure and gas constant according to the ideal gas equation, equation 6.4.5 can be shown to reduce to:

$$Q_{th} = Q_i + Q_l \quad (6.4.6)$$

thus implying $\rho_i \approx \rho_2 \approx \rho_4$. The volumetric efficiency across the leakage free blower and the bypass pipe is defined as:

$$\eta_{vol} = \frac{Q_i}{Q_{th}} = \frac{\dot{Q}_i \rho_2}{\dot{Q}_{th} \rho_i} \quad (6.4.7)$$

Setting equation 6.4.7 into equation 6.4.5 yields the blower inlet temperature after the mixing region in terms of the true blower inlet and exit temperature. Noting that $T_3 = T_e$ one obtains:

$$T_2 = \frac{T_e}{1 - \eta_{vol} \left(1 - \frac{T_e}{T_i}\right)} \quad (6.4.8)$$

For the flow through the leakage free blower (region II) under the assumption of isentropic flow or reversible and adiabatic flow, the temperature rise can be written in terms of the pressure ratio:

$$T_e = T_2 \left(\frac{P_e}{P_i}\right)^{\frac{\gamma-1}{\gamma}} \quad (6.4.9)$$

Combining equations 6.4.8 and 6.4.9 to eliminate T_2 yields an estimate of the blower outlet temperature in terms of the true blower inlet temperature and the volumetric efficiency:

$$T_e = \frac{T_i}{\eta_{vol}} \left[\left(\frac{P_e}{P_i}\right)^{\frac{\gamma-1}{\gamma}} - 1 \right] + T_i \quad (6.4.10)$$

The shaft power requirements are derived assuming steady state isentropic flow across the blower:

$$\dot{W}_{cv} + \dot{H}_{cv} + \dot{Q}_2 \left(h_2 + \frac{v_2^2}{2} + gz_2 \right) = \frac{dE_{cv}}{dt} + \dot{Q}_3 \left(h_3 + \frac{v_3^2}{2} + gz_3 \right) \quad (6.4.11)$$

Assuming the following:

- 1.) No heat transfer takes place during the compression process i.e. $\dot{H}_{cv} = 0$.
- 2.) Steady state flow conditions exist so that $\frac{dE_{cv}}{dt} = 0$.
- 3.) The gas mass flow into the blower equals the gas mass flow out of the blower i.e. $\dot{Q}_2 = \dot{Q}_3 = \dot{Q}_{th}$.
- 4.) The blower inlet and outlet planes are at the same elevation i.e. $z_2 = z_3$.
- 5.) The kinetic energy changes are negligible.
- 6.) The specific heat of the gas is constant,

equation 6.4.11 simplifies to:

$$\dot{W}_{cv} = \dot{Q}_{th} C_p T_2 \left[\left(\frac{P_e}{P_i} \right)^{\frac{\gamma-1}{\gamma}} - 1 \right] \quad (6.4.12)$$

Introducing the volumetric efficiency into equation 6.4.12 yields:

$$\dot{W}_{cv} = \frac{\dot{Q}_i C_p \rho_i T_i}{\eta_{vol}} \left[\left(\frac{P_e}{P_i} \right)^{\frac{\gamma-1}{\gamma}} - 1 \right] \quad (6.4.13)$$

A further equation for the shaft power can be derived from equation 6.4.12 by replacing the theoretical mass flow rate with the product of the density at point 2 in figure 6.1 and the theoretical volume flow rate:

$$\dot{W}_{cv} = \dot{Q}_{th} C_p \frac{P_i}{R} \left[\left(\frac{P_e}{P_i} \right)^{\frac{\gamma-1}{\gamma}} - 1 \right] \quad (6.4.14)$$

The air leakage through the by-pass pipe is defined as [90MA1]:

$$\dot{Q}_l = k \left(\frac{\Delta P}{\rho_i} \right)^{\frac{1}{2}} \quad (6.4.15)$$

where the leakage coefficient k is defined as an area which is constant depending on the blower size and configuration. Note that the leakage flows are given in terms of a volume flow rate.

The theoretical volume flow through the blower is the sum of the air leakage and the required volume flow at inlet conditions as given in equation 6.4.6. The required blower rotational

speed can be calculated if the swept volume or blower displacement volume per revolution of the rotor is known:

$$n = \frac{60Q_{th}}{V_p} \quad (6.4.16)$$

Inspecting equations 6.4.10, 6.4.13 and 6.4.14 the pressure ratio term can be rewritten in terms of a binomial expansion and the higher order terms discarded to yield the following three equations:

$$T_e = \frac{\Delta P}{\rho_i \eta_{vol} C_p} + T_i \quad (6.4.17)$$

$$\dot{W}_{cv} = \frac{Q_i \Delta P}{\eta_{vol}} \quad (6.4.18)$$

$$\dot{W}_{cv} = Q_{th} \Delta P \quad (6.4.19)$$

Both variations of the equations are used in blower analysis with equal success, the only prerequisite being that they are used consistently in both the derivation of the leakage coefficient and in the subsequent calculation of the blower performance as the value for the leakage coefficient will vary according to the equation used.

The dimensionless pressure ratio rp for a blower is defined as [90MA1]

$$rp = \frac{P_e}{P_i} \quad (6.4.20)$$

using the absolute inlet and outlet pressures.

The pressure ratio can be determined from the maximum allowable pressure rise at reference conditions. Generally the pressure ratio may not exceed 2 for roots blowers. As a result of the lower atmospheric pressure at a higher altitude at which the blower may be sited, equation 6.4.20 dictates that pressure ratio increases if the absolute pressure decreases. As a result of this the maximum pressure differential a blower can generate is decreased with an increase of altitude. The pressure ratio can thus be used to determine the maximum altitude at which a blower can sustain a given pressure ratio and is also useful for determining the maximum pressure differential that a blower is able to generate at altitude.

6.5 Method for determining leakage coefficient and swept volume of a blower

6.5.1 Introduction

In order to use the calculation method presented in section 6.4.1 the swept volume and the leakage coefficient of the blower must be known. As a company policy most blower manufacturers do not publish this information for general use.

This has resulted in the need to develop a method to determine these characteristics with reasonable accuracy from standard blower performance curves which are generally available. Once the leakage coefficient and blower swept volume are known they can be set into the calculation method as set out in section 6.4.1. This makes the calculation of the performance characteristics of blower-exhauster combinations possible.

Furthermore the integration of the calculation method into a blower selection programme is simplified. There is no need to rely on curve fits and the corresponding use of dimensional analysis to correct for differing operating condition to those given in standard performance curves.

6.5.2 Method

The two unknowns, the leakage coefficient and the swept volume, dictate that two independent equations are required to solve for these two variables. Performance curves supplied by manufacturers are given in a format such that:

$$\begin{aligned} Q &= f(n) \\ T_e &= f(n) \\ \dot{W} &= f(n) \end{aligned}$$

Choosing the first two of these where the volume flow rate and the blower outlet temperature is a function of revolution speed of the rotor one can combine equations 6.4.6 and 6.4.15 and set this into equation 6.4.16 to obtain:

$$V_p = \frac{60(Q_i + k \left(\frac{\Delta P}{\rho_i} \right)^{\frac{1}{2}})}{n} \quad (6.5.1)$$

Combining equations 6.4.5, 6.4.6 and 6.4.7 and setting this into equation 6.4.17 yields the second independent equation as:

$$T_e - T_i = \frac{\Delta P \left(Q_i + k \left(\frac{\Delta P}{\rho_i} \right)^{\frac{1}{2}} \right)}{Q_i \rho_i C_p} \quad (6.5.2)$$

Solving this equation for the leakage coefficient, equation 6.5.2 becomes:

$$k = \left(\frac{(T_e - T_i) Q_i \rho_i C_p}{\Delta P} - Q_i \right) / \left(\frac{\Delta P}{\rho_i} \right)^{\frac{1}{2}} \quad (6.5.3)$$

The procedure to obtain the two unknown variables is as follows: A pressure rise is chosen and at this pressure rise the volume flow rate and the exit temperature at different revolution speeds is determined graphically from performance curves. The inlet density and specific heat are evaluated at the conditions at which the performance curves are valid.

An average value of the leakage coefficient and swept volume can be calculated from the data obtained over a range of revolution speeds.

Alternatively a curve fit is applied to the performance curves to obtain the volume flow rate and exit temperature in terms of the revolution speed thereby simplifying the process of calculation. The second method is preferred as more data points can be evaluated.

To check the results, the equations given in section 6.4.1 can be used to generate the complete set of performance curves at reference conditions and these compared with the published performance curves.

6.5.3 Results

As an example for the implementation of the above method for determining the swept volume and leakage coefficient, calculations are performed for a HIBON XN 4.5 blower. A sample calculation for the determination of the blower swept volume and leakage coefficient is presented in section C.5.1 in appendix C. In the case of the above blower the leakage coefficient was determined to within 0.5% of the value used by the manufacturer. The swept volume can be determined to within 1% of the value determined by the manufacturer. The performance curves are then drawn up using the theoretical calculation method presented in section 6.4.1 and compared with the performance curves given by the manufacturer [96HI1]. Sample calculations and numerical data for this are presented in section C.5.2 in appendix C. Figures 6.2 to 6.4 show the inlet volume flow rate, exhaust temperature and shaft power requirements respectively.

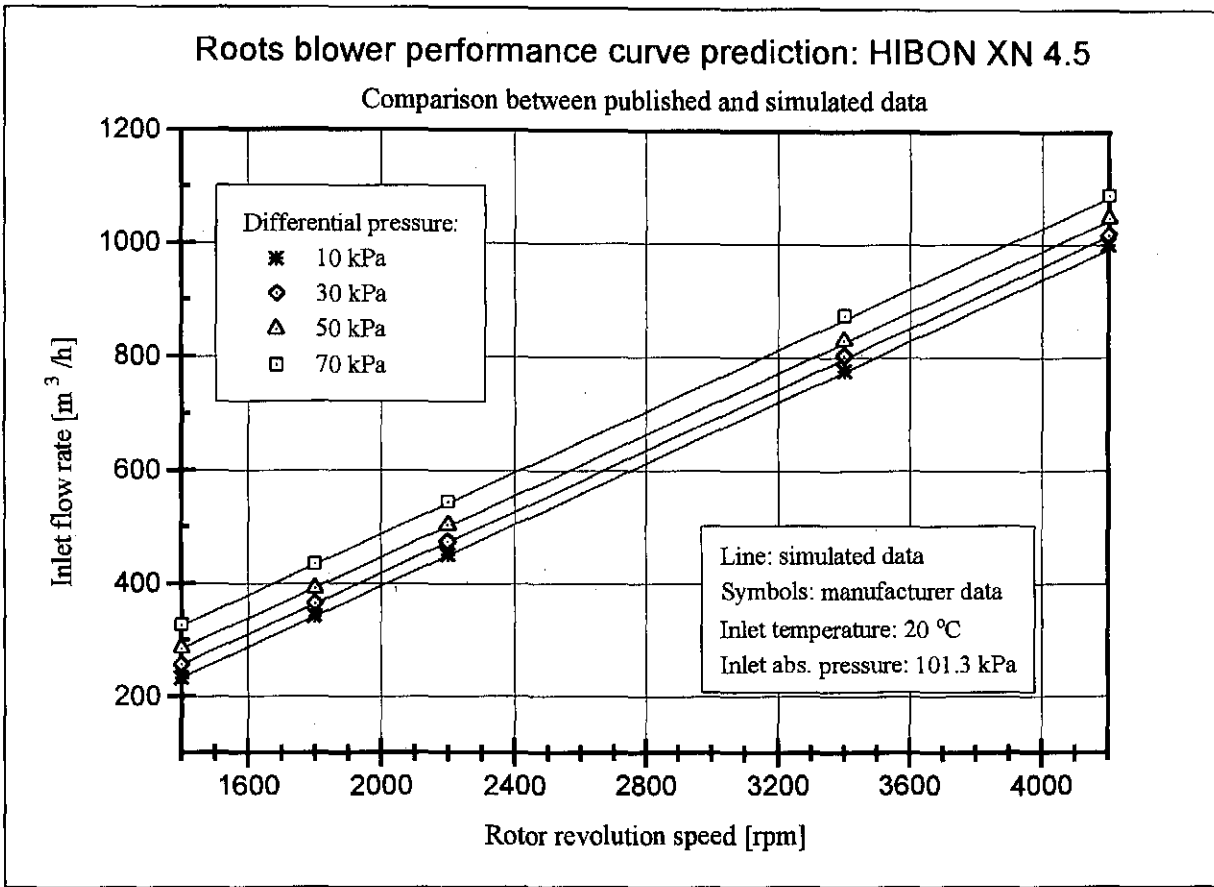


Fig 6.2 Blower performance prediction: inlet volume flow rate

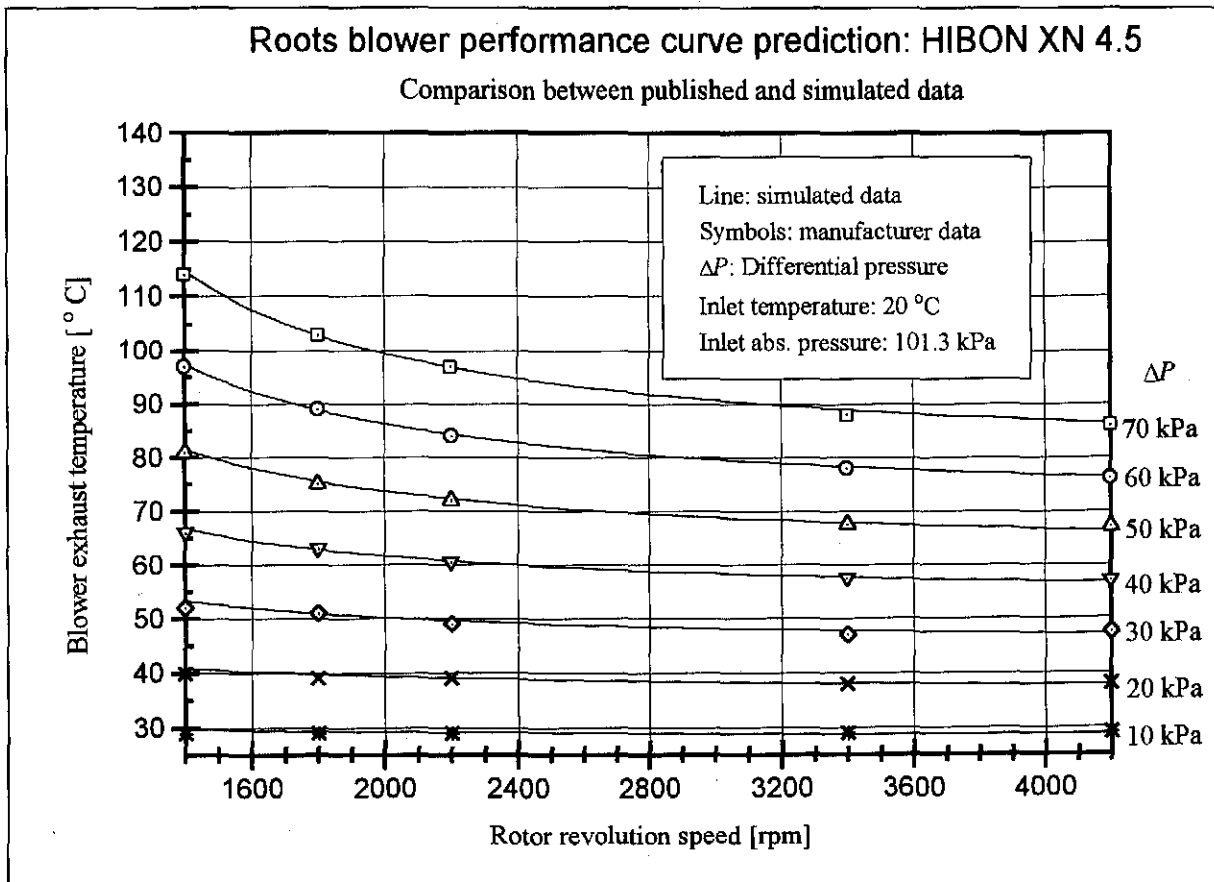


Fig. 6.3 Blower performance prediction: exhaust temperature

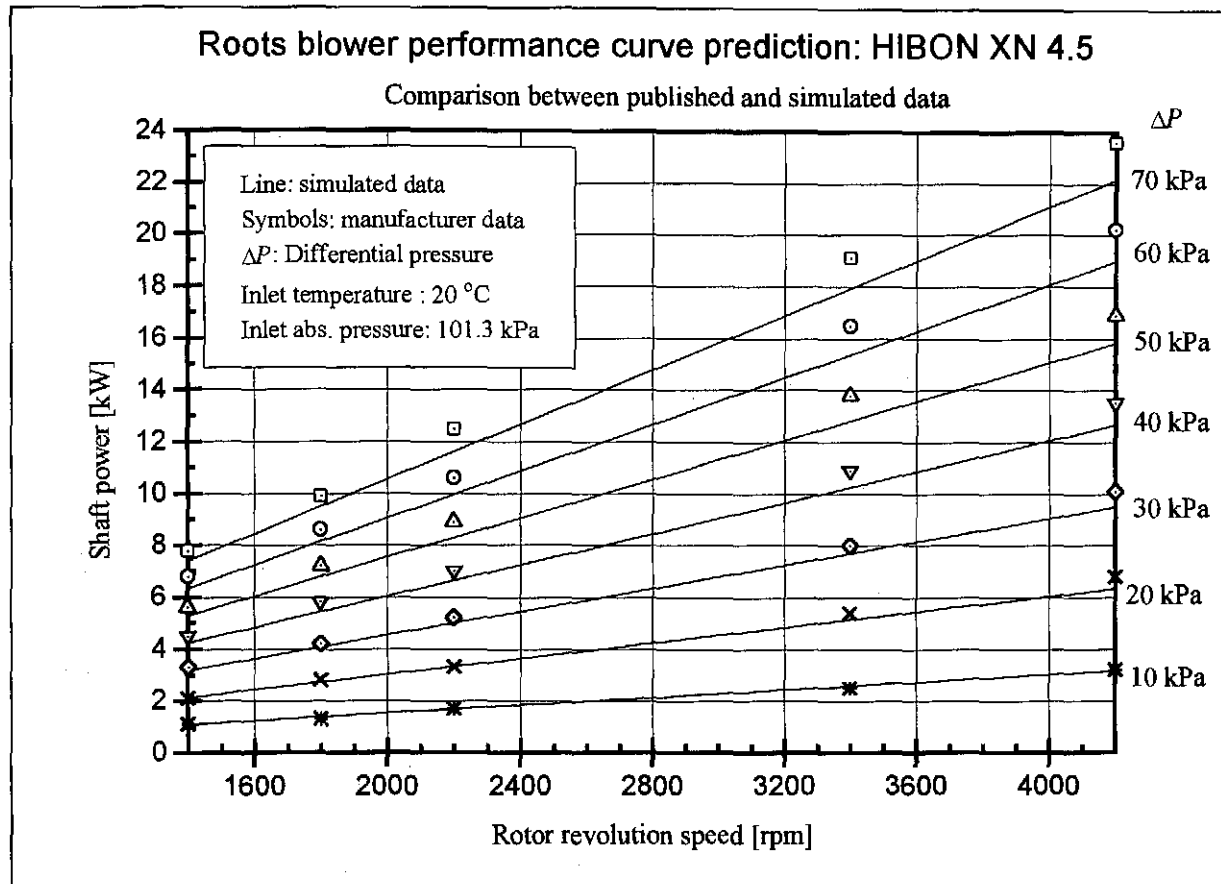


Fig. 6.4 Blower performance prediction: shaft power

The inlet volume flow rate is accurate to within 1% of the values given by the manufacturer while the exhaust temperature is accurate to within 2.5%. The shaft power shows a difference of up to 8% of the value given by the manufacturer. The values of the shaft power given by the manufacturer are higher than those determined by theoretical considerations which indicate the importance of additional mechanical losses in the practical operating environment of the roots blower. This result also underlines the importance of the use of safety factors when specifying a motor to run such a blower when the calculation of the power requirements is based on theory. In general a coupling loss of between 5-10% is added to the shaft power depending on the type of coupling (belt drive or direct coupling) used to connect the motor to the blower. A further 10-15% safety factor is then added to determine the size of the motor. These safety factors should not be reduced in value.

6.6 Manufacturers performance curve transformation

6.6.1 Dimensional analysis and scaling of performance data

In order to verify the theory presented in section 6.4.1 at non-standard inlet conditions, dimensional analysis can be performed so that an alternative method to that presented in

section 6.4.1 is available for determining blower performances at these conditions. This is in effect a transformation method for standard blower performance curves which are usually given at reference conditions. A comparison of the two methods is presented in the following section. From dimensional analysis dimensionless groups can be determined as:

$$\text{Temperature ratio:} \quad \Pi_1 = \frac{T_i}{\Delta T} \quad \text{or:} \quad \Pi_1 = \frac{T_i}{T_e} \quad (6.6.1)$$

$$\text{Pressure ratio:} \quad \Pi_2 = \frac{\Delta P}{P_i} \quad \text{or:} \quad \Pi_2 = \frac{P_e}{P_i} \quad (6.6.2)$$

$$\text{Power coefficient:} \quad \Pi_3 = \frac{\dot{W}}{nV_p P_i} \quad (6.6.3)$$

$$\text{Flow coefficient:} \quad \Pi_4 = \frac{Q_i}{nV_p} \quad (6.6.4)$$

For transforming the performance curves one can assume a constant rotor revolution speed and blower swept volume. This results in the following relations where subscript 1 refers to the reference condition for which performance curves are given and subscript 2 refers to the operating conditions other than at reference condition:

$$Q_{i2} = Q_{i1} \quad (6.6.5)$$

$$\Delta P_2 = \frac{P_{i2}}{P_{i1}} \Delta P_1 \quad (6.6.6)$$

$$T_{e2} = \frac{T_{i2}}{T_{i1}} T_{e1} \quad (6.6.7)$$

$$\dot{W}_2 = \frac{P_{i2}}{P_{i1}} \dot{W}_1 \quad (6.6.8)$$

6.6.2 Comparison of the calculation and transformation method

To verify the theory presented above a comparison between the two methods is performed using a HIBON XN 4.5 roots blower as an example. The performance curves provided by the manufacturer [96HI1] are transformed for the new inlet conditions at an absolute pressure of 81300 Pa and an inlet temperature of 40°C using equations 6.6.5 to 6.6.8. The resultant performance curves for the new inlet conditions are compared with the performance curves calculated using the blower performance calculation method presented in section 6.4.1. The

inlet volume flow rate determined with the two methods is presented in figure 6.5. The difference in inlet volume flow rate between the two methods for this example reaches a maximum of 2.5%.

The roots blower exhaust temperature comparison is given in figure 6.6. The maximum percentage difference between the transformed and simulated data is 2.5%. Figure 6.7 depicts the comparison of the shaft power required for the blower. A maximum difference around 10% is found at low rotor revolution speeds and low differential pressures while most data points lie

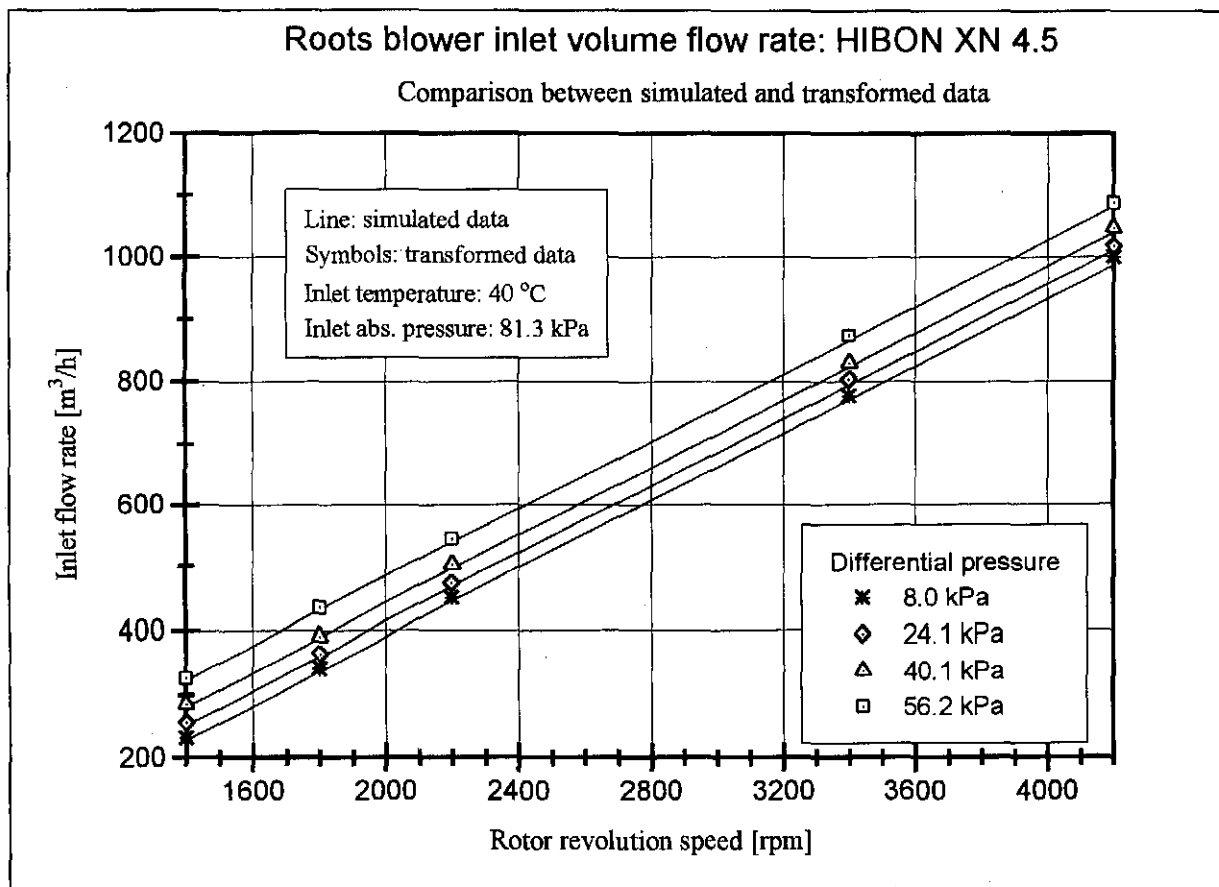


Fig. 6.5 Roots blower performance curve transformation: inlet volume flow rate

within 5% of each other. Sample calculations and numerical data for the transformation method are presented in section C.5.3 in appendix C.

From the above comparison it is clear that both the calculation and transformation method can be applied with equal success. The required shaft power difference of up to 8% is a result of an inaccuracy that is introduced in the theoretical calculation of the shaft power.

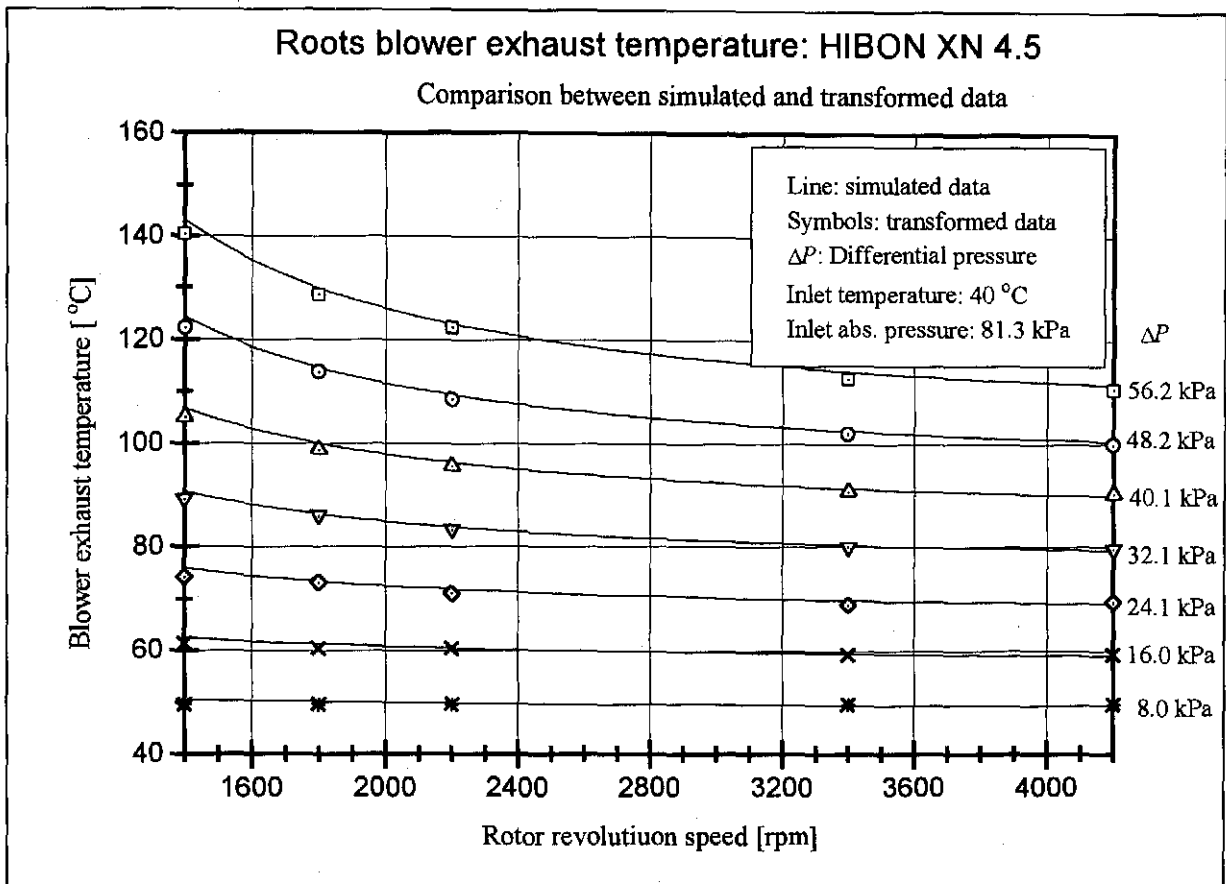


Fig. 6.6 Roots blower performance curve transformation: exhaust temperature

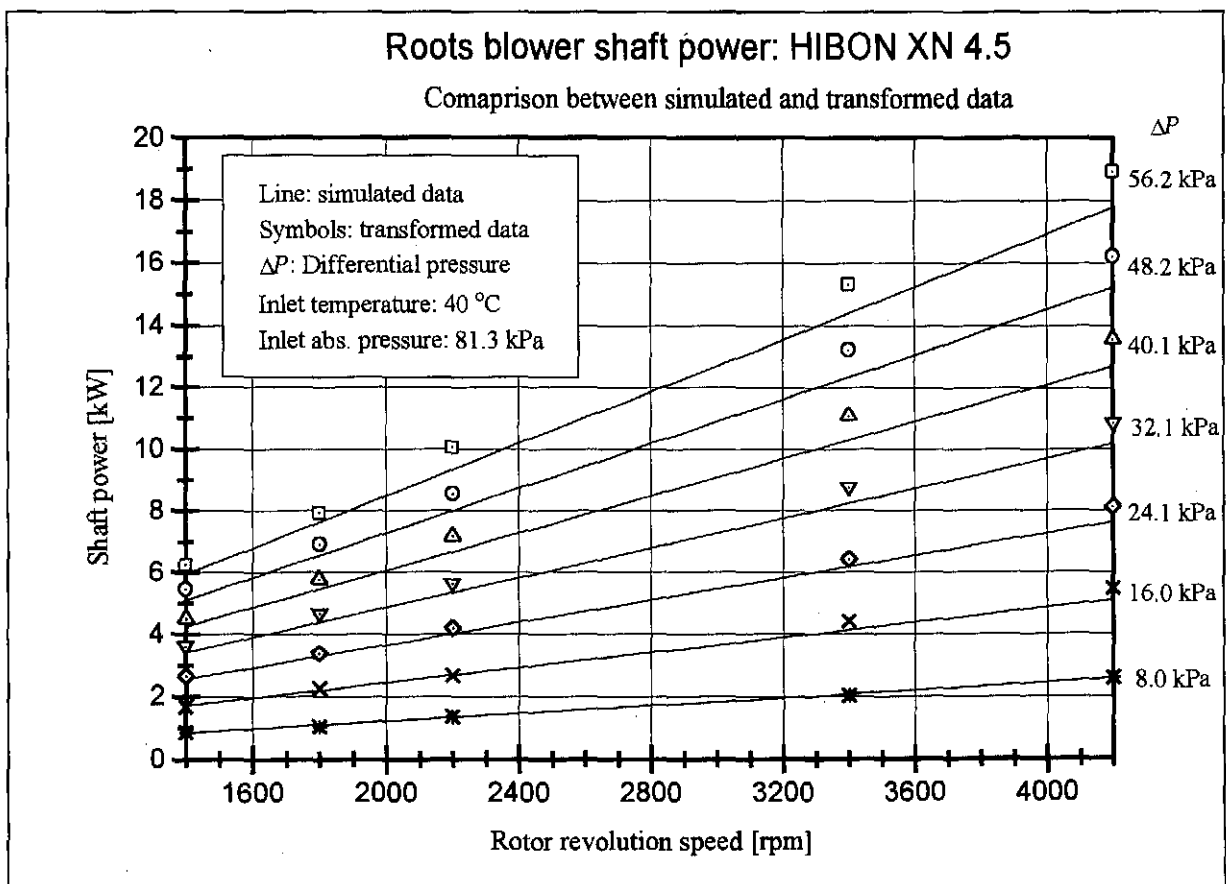


Fig. 6.7 Roots blower performance curve transformation: shaft power

The calculation method does not take into account any mechanical losses that occur as a result of bearing friction or the gear box arrangement that is used to drive and synchronise the running of the rotors. Hence the transformed values for the shaft power determined from experimental performance curves are more accurate.

6.7 Application to the pneumatic conveyor design programme

A selection programme based on the blower performance calculations presented in section 6.4.1 is written in DELPHI for the selection of blowers for vacuum, positive pressure and a combination of vacuum and pressure operation. Data files for specific roots blower vendors are created containing parameters such as the leakage coefficient, blower swept volume, maximum and minimum speed of revolution, maximum differential pressure at reference conditions and exhaust temperature limits. Data input takes place by means of the visual DELPHI interface and allows various options of entering the required pressure, volume or mass flow rate, altitude and temperatures. The use of the air mass flow rate as an input parameter for the blower selection is an important option as the required air mass flow rate can be calculated from the required material mass flow rate and mass flow ratio used as input for the pneumatic conveyor simulation programme. As the blower inlet air flow rate must be specified, the use of the mass flow rate as input parameter ensures that the correct air volume flow rate is available at the exit of the blower for positive pressure conveying.

The user can select the manufacturer from which he wishes to purchase the machine and subsequently calculations are performed with each of the blowers available and checked for the limits in performance. The machines that satisfy the required air flow rates and pressure differential and machine performance limits are listed for closer inspection of the operating characteristics and final selection. Details on the use of the blower selection programme are presented in appendix E. Figures E.9 to E.12 depict the user interface windows for the blower selection programme.

6.8 Discussion and conclusion

The implementation of the analytic blower performance calculations and transformation by means of non-dimensional analysis is successfully demonstrated. In addition a method is presented for determining the leakage coefficient and swept volume of a blower by using published performance curves. This allows for the subsequent implementation of the performance calculation of roots blowers using the equations presented in section 6.4.1. This method is in preference to using curve fitting to the performance curves and subsequently

implementing the scaling laws to adjust the values to operating conditions that are not at reference conditions. The calculation method of the blower performance presented in section 6.4.1 is successfully implemented in a blower selection programme as an integral part of the pneumatic conveyor design programme.

The selection of an appropriate blower becomes a simple task once the required airflow and pressures required for a pneumatic conveyor are known from the conveyor simulation programme.

CONCLUSION

7.1 Introduction

This chapter serves to summarise the conclusions that have been made with respect to the work described in the preceding chapters.

7.2 Chapter contents

Chapter seven is arranged according to the different topics that are addressed during the course of the work done for this thesis. Section 7.3 summarises the implementation method for the friction coefficients while the next two sections are concerned with the application of the friction coefficients to horizontal and vertical conveying. The bend flow model and the expansion model are discussed in sections 7.6 and 7.7 respectively. Section 7.8 concerns itself with the calculation of drag coefficients and particle free fall velocity. The calculations concerning Roots blowers are discussed in section 7.9. The applicability and usefulness of the pneumatic conveyor design programme is highlighted in section 7.10 and a final short summary of the fulfilled objectives of this thesis are presented in section 7.11. The chapter ends with a section on recommendation for future work.

7.3 Friction coefficient implementation

The differential equations for two-phase flow are successfully rearranged to implement the total friction coefficient. This removes the inaccuracy inherent in using a combination of theoretically calculated gas friction coefficient and solids friction coefficient.

A new method of determining the alternative solids impact and friction coefficient directly from the solids motion equation has been demonstrated. This is required as the friction terms in the solids motion equation cannot be written entirely in terms of the total friction coefficient. The resulting correlation has been shown to result in a high degree of accuracy with respect to determining the solids velocity. Two correlations, one for the total friction coefficient and one for the alternative solids impact and friction coefficient are thus required for the simulation programme.

The main design variables of a pneumatic conveyor, the pressure and average air velocity are found to be strongly influenced by the total friction coefficient while the solids velocity is primarily dependent on the alternative solids impact and friction coefficient.

In terms of experimental data, the pressure drop, average or interstitial air velocity and the solids velocity must be measured across a test section on a full scale rig to determine the friction coefficient correlations.

7.4 Application to horizontal flow

The application of the use of the friction coefficients discussed in the previous sections for horizontal flow for a fine powdered material and a coarse material has been proven and it is believed that the design programme can be used successfully for simulating horizontal pneumatic conveyors. As most of the pneumatic conveying applications in the industry make use of primarily long stretches of horizontal pipelines the programme should be useful for the design of such systems.

7.5 Application to vertical flow

The application of the design programme to vertical conveying has not been confirmed as a result of insufficient conveying data for vertical conveying systems. In particular there is a lack of data for systems incorporating both horizontal conveying stretches and long vertical sections. Where such data are available, the exact solids velocity profiles along the vertical stretches have not been determined.

As discussed in section 7.4 most pneumatic conveying plants consist of long horizontal stretches with short vertical parts. It is believed that conveying plants with short vertical risers can be modelled with the simulation programme but it must be borne in mind that the accuracy of these simulations has not been proven.

7.6 Bend flow model

The bend flow model is found to be inaccurate with respect to the use of the dynamic sliding friction coefficient used in the model. Where the sliding friction coefficient is adjusted to fit experimental data, a realistic deceleration of the solid particles in the bends and subsequent reacceleration afterwards is demonstrated. This is particularly useful to illustrate the effects of setting bends close to each other and thereby causing the solids velocity to slow down substantially in the second bend. This is the most likely point for a blockage to occur in a conveying plant. Furthermore the importance of placing bends well away from the acceleration

zone of the particles after the feed point is demonstrated. From the simulations it is thus recommended to keep bends following each other as far apart as possible and allow for ample acceleration length after the feed point before placing a bend in the pipeline.

7.7 Expansion model

The expansion model is included in the simulation programme. It has not been tested with respect to conveying simulation as this requires friction coefficient correlations that are valid for a range of pipe diameters together with experimental data to verify this. Once the friction coefficient correlations are available, the expansion model can be used effectively to model stepped pipelines which are extensively used to reduce the air velocity and subsequently the particle velocity in long distance conveying. This will allow the comparison of system pressure drop for stepped versus single bore pipelines and allow for the determination of the optimum position for increases in pipeline diameter.

7.8 Calculation of particle drag coefficients

An inherent uncertainty in the calculation of the friction coefficients and the subsequent simulation which makes use of the same equations is associated with the determination of the particle drag coefficients. This also influences the particle free fall or terminal velocity. It is believed that the use of the particle sphericity as a means to describe the influence of the shape of the particle on the drag coefficient is a useful tool. However, the correlations available for the determination of the drag coefficients are of limited applicability to truly irregular shaped particles most often encountered in pneumatic conveying. The terms in the differential equations containing the drag coefficient cannot be sunk into the definition of the friction coefficients as this results in differing definitions of the friction coefficients for vertical and horizontal flow. This is undesirable in terms of the implementation of the differential equations in the simulation programme. Furthermore this would mean that separate correlations must be determined for vertical and horizontal flow which consequently would mean more expense in the full scale testing of materials.

7.9 Blower selection calculations

The derivation of the equations routinely used in Roots blower performance calculations are given. A useful method has been presented to determine the Roots blower swept volume and leakage coefficient from the performance curves published by manufacturers. These two parameters are required for the blower performance calculations and are generally kept from

public knowledge by company secrecy clauses. The usefulness of the method is demonstrated by comparing performance curves of published and simulated data. Furthermore dimensional analysis has yielded the scaling parameters that can be used to transform standard performance curves published by manufacturers to the working condition of a blower. The blower selection programme section that is included as part of the pneumatic conveyor design programme can thus be used to select suitable blowers for the pneumatic conveyor once a data file has been generated containing the specific blower performance parameters.

7.10 Design programme implementation

An important requirement in the implementation of the design programme is a user-friendly interface. Computers are currently used to simulate complex processes which require a high volume of calculations to be performed and the result is often a high volume of output data. These data have to be interpreted by the designer and the most effective initial evaluation takes place visually by means of graphical representation of the output data. Hand in hand with this goes the efficient input of for example the pipeline geometry and the required conveying parameters. The use and implementation of the programming language DELPHI has allowed these requirements to be met. The underlying code is based on PASCAL and the core of the programme performing the two-phase flow calculations can easily be modified to implement new and different models for example for the bend flow and thus ensure that the programme is kept up to date.

A further advantage is that simulations and comparison of results with modified differential equations and bend or expansion models can be made efficiently and the results used to determine the advantages or disadvantages of such changes in a short time.

It is believed that a useful framework for further development and refinement has been created in the writing of this computer programme. Once fully verified and tested its usefulness in the industry as a design tool will be invaluable.

7.11 Summary with reference to the objectives of the thesis

The primary objectives of this thesis have been met. A computer programme has been developed for designing and evaluating dilute phase pneumatic conveyors. The two-phase flow simulation programme is able to implement the criteria set for the project. These include:

- the use of a complete mathematical model using all five parameters fundamental to pneumatic conveying. These are the pressure, density, air interstitial and average velocity, particle velocity and voidage.

- modelling of both single- and two-phase flows,
- modelling of vacuum and positive pressure conveyors,
- the incorporation of stepped pipelines,
- incorporation of a bend flow model,
- the provision for air leakage at the feeding point,
- the ability to switch automatically from single to two-phase flows to allow the modelling of complete conveying systems including the air supply pipeline.

The total friction coefficient has been incorporated in the governing differential equations and as a consequence of this a need has arisen to develop an alternative method of determining the solids impact and friction coefficient other than deriving it from the total friction coefficient as has been done in the past. The alternative method is successfully implemented.

Furthermore a Roots blower selection programme has been developed to select an appropriate prime air mover for the pneumatic conveyor.

Although not all of the models implemented could be verified by comparison with experimental data, the development of the models has yielded new insights into the requirements that a testing facility must fulfil for the further refinement and validation of the computer model.

7.12 Recommendation for future work

As discussed in the previous section the work presented in this thesis has resulted in the requirement of additional work before the programme can be used for general purpose pneumatic conveyor design. Some of these points are listed below:

- The applicability of the mathematical model and the definition of the friction coefficients to vertical flow must be verified. Where such testing facilities are not available it may be of benefit to use an existing installation in the industry that can be instrumented accordingly. Included in this verification process should be the possible refinement of the term generally referred to as the lifting term in the horizontal flow differential equation.
- An alternative bend flow model should be investigated and compared to experimental data on a full scale test facility. Suggestions are to use a separate correlation for the friction coefficients determined from experimental data instead of calculating them from a bend flow model as presented in chapter three.
- The upgrading and modification of the full scale test facility available at the University of Stellenbosch with the requirements of measuring both pressure drops and solids velocity is shown to be necessary from the work presented here. The current test facility could not be

used during the time that this thesis was being completed due to the unavailability of the compressor system used to supply the air to the conveying facility.

- Fundamental work is still required with respect to the accurate determination of the drag coefficient of material specific to pneumatic conveying. Although extensive work has been done with clearly defined shapes, little information is available on truly irregular shaped particles. Directly coupled to this research is the determination of the terminal velocity of particles.
- There is also a need to improve the correlations for the friction coefficients, particularly the total friction coefficient. The friction coefficients are ultimately responsible for a successful simulation of a pneumatic conveyor. Further work should be aimed at improving the dimensionless groups used to correlate the data.
- With respect to the pneumatic conveyor design programme additional programme modules for selecting the solids feeding mechanisms and the solids and air separation equipment should be developed.

References are given as follows: the first two digits represent the year of publication, the following two letters represent the first two letters of the principal author's name. If the author has published more than one paper in any given year or there are two authors with the same initial letters, the last digit is used to differentiate between the papers.

- 33NI1 Nikuradse, J., 1933. Strömungsgesetze in rauhen Rohren. *Zeitschrift des Vereines Deutscher Ingenieure* 77(39): 1075-1076
- 33SC1 Schiller, L. & Naumann, A., 1933. Über die grundlegenden Berechnungen bei der Schwerkraftaufbereitung. *Zeitschrift des Vereines Deutscher Ingenieure* 77(12): 318-320
- 34WA1 Wadell, H., 1934. Title unknown. *Journal of the Franklin Institute* 217: 459.
- 38CO1 Colebrook, C.F., 1938-1939. Turbulent flow in pipes, with particular reference to the transition region between smooth and rough pipe laws. *Journal of the Institute of Civil Engineers of London* 11: 133-156.
- 38HE1 Heywood, H., 1938. Title unknown. *Proceedings of the Institute of Mechanical Engineers* 140: 257-308.
- 44MO1 Moody, L.F., 1944. Friction factors for pipe flow. *Transactions of the ASME* 66: 671-648.
- 48PE1 Pettyjohn, E.S. & Christiansen, E.B., 1948. Effect of particle shape on free-settling rates of isometric particles. *Chemical Engineering Progress* 44(2): 157-172.
- 48VO1 Vogt, E.G. & White, R.R., 1948. Friction in the flow of suspensions. *Industrial and Engineering Chemistry* 40(9): 1731.

- 49HA1 Hariu, O.H. & Molstad, O.C., 1949. Pressure drop in vertical tubes in transport of solids by gases. *Industrial and Engineering Chemistry* 41(6): 1148-1160.
- 52PI1 Pinkus, O., 1952. Pressure drops in the pneumatic conveyance of solids. *Journal of Applied Mechanics* 19(4): 425-431.
- 53HI1 Hinkle, B.L., 1953. *Acceleration of particles and pressure drops encountered in horizontal pneumatic conveying*. Ph.D. Dissertation. Georgia Institute of Technology, U.S.A.
- 55WE1 Weidner, G., 1955. Grundsätzliche Untersuchungen über den pneumatischen Fördervorgang, insbesondere über die Verhältnisse bei Beschleunigung und Umlenkung. *Forsch. Ingenieurwes.* 21: 145-155.
- 58BA1 Barth, W., 1958. Strömungsvorgänge beim Transport von Festteilchen und Flüssigkeitsteilchen in Gasen. *Chemie-Ing.-Technik* 30(3): 171-180.
- 58FI1 Fischer, J., 1958. Practical conveyor design. *Chemical Engineering* 66: 114-118.
- 58HI1 Hitchcock, J.A. & Jones, C., 1958. The pneumatic conveying of spheres through straight pipes. *British Journal of Applied Physics* 9(6): 218-222.
- 59IT1 Ito, H., 1959. Pressure losses in smooth pipe bends. *Transactions of the American Society of Mechanical Engineers*. Paper 59.
- 60BA1 Barth, W., 1960. Physikalische und wirtschaftliche Probleme des Transportes von Festteilchen in Flüssigkeiten und Gasen. *Chemie-Ing.-Techn.* 32(3): 164-171.
- 60ZE1 Zenz, F.A. & Othmer, D.F., 1960. *Fluidization and fluid-particle systems*. Reinhold Publishing Co., New York.
- 63BA1 Barth, W., 1963. Absetzung, Transport und Wiederaufwirbelung von staubförmigem Gut im Luftstrom. *Chemie-Ing.-Techn.* 35(3): 209-214.
- 63DO1 Doig, I.D. & Roper, G.H., 1963. Energy requirements in pneumatic conveying. *Australian Chemical Engineering* 4(2): 9-23.
- 66WE1 Weber, M., 1966. Kompressible Rohrströmung von Gas-Feststoffgemischen bei hohen Materialbeladungen. *Aufbereitungs-Technik* 10: 603-613.

- 66WE2 Wen, C.Y. and Yu, Y.H., 1966. Mechanics of fluidization. *Chemical Engineering Progress Symposium Series* 62(62): 100-111.
- 68SC1 Schuchart, P., 1968. Widerstandsgesetze beim pneumatischen Transport in Rohrkrümmern. *Chemie-Ing.-Technik* 40(21/22): 1060-1067.
- 69RO1 Rose, H.E. and Duckworth, R.A., 1969. Transport of solid particles in liquids and gasses. *The Engineer* 227(5903): 392-396; 227(5904): 430-433; 227(5905): 478-483.
- 70CL1 Clift, R. & Gauvin, W.H., 1970. *Proceedings of Chemca 70*, Vol.1. Butterworths, Melbourne.
- 71BO1 Boothroyd, R.G., 1971. *Flowing gas-solids suspensions*. Chapman & Hall Ltd. London.
- 71DA1 Davidson, J.F. & Harrison, D., 1971. *Fluidization*. Academic Press, London.
- 72GO1 Govier, G.W. and Aziz, K., 1972. *The flow of complex mixtures in pipes*. Von Nostand Rheinhold Co., New York.
- 73RI1 Rizk, F., 1973. *Pneumatic conveying of plastic coarse materials in horizontal ducts, taking into consideration the influence of the height in connection with the properties of the solids and pipe materials, specially in the optimal operating zone*. Dissertation. University Karlsruhe, Karlsruhe.
- 73YA1 Yang, W.-C., 1973. Estimating the solid particle velocity in vertical pneumatic conveying lines. *Ind. Eng. Chem. Fundam.* 12(3): 349-352.
- 74WE1 Weber, M., 1974. *Strömungsfördertechnik*. Krausskopf-Verlag, Mainz.
- 77FO1 Forsythe, G.E., Malcolm, G.E. & Moler, C.B., 1977. *Computer Methods for Mathematical Computations*. Prentice Hall, New York.
- 78MA1 Marcus, R.D., 1978. *An investigation into the influence of pressure pulsations on the flow characteristics of solid-gaseous suspensions*. Ph.D. Dissertation. Faculty of Engineering. University of Witwatersrand, Johannesburg.

- 78MO1 Morikawa, Y., Tsuji, Y., Matsui, K.J. & Jittani, Y., 1978. Pressure drop due to pipe bends in air-solids two phase flows; circular and elliptical bends. *International Journal of Multiphase Flow* 4(5/6): 575-583.
- 78SC1 Scott, A.M., 1978. The influence of particle properties on the pressure drop during the pneumatic transport of granular materials. *Proceedings of the fourth International Conference on the pneumatic transport of solids in pipes, Pneumotransport 3*. BHRA, California.
- 78ST1 Stegmaier, W., 1978. Zur Berechnung der horizontalen pneumatischen Förderung feinkörniger Stoffe. *Fördern und Heben* 28(5/6): 363-366.
- 80KR1 Kraus, M.N., 1980. *Pneumatic conveying of bulk materials*, second edn. McGraw-Hill Publications Co., New York.
- 81MO1 Molerus, O., 1981. Prediction of pressure drop with steady state pneumatic conveying of solids in horizontal pipes. *Chemical Engineering Science* 36(12): 1977-1984.
- 81WE1 Weber, M., 1981. Principles of hydraulic and pneumatic conveying in pipes. *Bulk Solids Handling* 1(1): 57-63.
- 82RI1 Rizk, F., 1982. Pneumatic transport in dilute and dense phase. *Bulk Solids Handling* 2(2): 235-241.
- 82WE1 Weber, M., 1982. Correlation analyses in the design of pneumatic transport plants. *Bulk Solids Handling* 2(2): 231-233.
- 83FE1 Ferretti, G., 1983. Calcolo degli impianti per il trasporto pneumatico di materiali sfusi. *Fluid* 231/232: 57-63.
- 83HA1 Haaland, S.E., 1983. Simple and explicit formulas for the friction factor in turbulent pipe flow. *Journal of Fluids Engineering Trans. ASME* 105(1): 89-90.
- 83WE1 Weber, M. & Stegmaier, W., 1983. Solid-Gas Flow in: *Heat Exchanger Design Handbook*. Hemisphere Publishing Corporation, Washington.
- 84CH1 Cheremisinoff, N.P. & Cheremisinoff, P.N., 1984. *Hydrodynamics of gas-solids fluidization*. Gulf Publishing Co., Houston.

- 85EN1 Enick, R. and Klinzing, G.E., 1985. Title unknown. *Proceedings of the Fine Particle Society*, Miami.
- 85MA1 Marcus, R.D., Hilbert, J.D. & Klinzing, G.E., 1985. Flow through bends and acceleration zones in pneumatic conveying systems. *Bulk Solids Handling* 5(4): 769-774.
- 85ME1 Meyers, S., Marcus, R.D. & Rizk, F., 1985. The state diagram for fine-particle gas/solids suspensions. *Bulk Solids Handling* 5(4): 779-782.
- 85MÖ1 Möhlmann, J.D., 1985. *Parameters influencing the pneumatic conveying of large rock particles* (3 volumes). Ph.D. Dissertation. Faculty of Engineering. University of Witwatersrand, Johannesburg.
- 85VA1 Van Wylen, G.J. and Sonntag, R.E., 1985. *Fundamentals of Classical Thermodynamics*, third edn. John Wiley & Sons, New York.
- 86ME1 Meijers, S.J., 1986. *An investigation into the measurement of slip velocity for dilute phase gas/solids suspensions and the progression of the state diagram*. Ph.D. Dissertation. Faculty of Engineering. University of Witwatersrand, Johannesburg.
- 87MI1 Michaelides, E.E., 1987. Motion of particles in gases: average velocity and pressure loss. *Journal of Fluids Engineering Trans. ASME* 109(2): 172-178.
- 87SZ1 Szikszay, G., 1987. *Feststoffreibungsbeiwert bei der pneumatischen Dünnstromförderung*. Ph.D. Dissertation. University of Karlsruhe, Karlsruhe.
- 88BR1 Bradley, M.S.A. & Mills, D., 1988. Approaches to dealing with the problem of energy loss due to bends. *13th Powder and Bulk Conference*. Rosemont. pp. 705-715.
- 88SZ1 Szikszay, G., 1988. Friction factor for dilute phase pneumatic conveying. *Bulk Solids Handling* 8(4): 395-399.
- 88WE1 Weber, M., 1988. Compressible flow of gas-solid mixtures and pressure loss evaluation. *Aufbereitungs-Technik* 29(12): 693-702.
- 88WH1 White, F.M., 1988. *Fluid Mechanics*, second edn. McGraw-Hill Book Co., New York.

- 89GE1 Gerald, C.F. & Wheatley, P.O., 1989. *Applied numerical analysis*, fourth edn. Addison-Wesley Publishing Company, New York.
- 89GI1 Gieck, K., 1989. *Technische Formelsammlung*. Gieck Verlag, Heilbronn.
- 89LA1 Lange, L.M., 1989. *An analysis of fine particle gas/solid suspension flow in the dilute phase as a continuum according to the pipe diameter*. M.Sc. Dissertation. Faculty of Engineering. University of Witwatersrand, Johannesburg.
- 90BR1 Bradley, M.S.A. & Reed, A.R., 1990. An improved method of predicting pressure drop along pneumatic conveying pipelines. *Powder Handling & Processing* 2(3): 223-227.
- 90HI1 Hill, F.S., 1990. *Computer Graphics*. MacMillan Publishing Co., New York.
- 90MA1 Marcus, R.D., Leung, L.S., Klinzing, G.E. and Rizk, F., 1990. *Pneumatic Conveying of Solids*. Chapman and Hall, London.
- 90MI1 Mills, D., 1990. *Pneumatic conveying design guide*. Butterworths, London.
- 91RE1 Reed, A.R. and Bradley, M.S.A., 1991. Advances in the design of pneumatic conveying systems. *Bulk Solids Handling* 11(1): 93-97.
- 91SH1 Sheer, T.J., 1991. *Pneumatic conveying of ice particles through mine-shaft pipelines*. Ph.D. Dissertation. Faculty of Engineering. University of Witwatersrand, Johannesburg
- 91WE1 Weber, M., 1991. Friction of the air and the air/solid mixture in pneumatic conveying. *Bulk Solids Handling* 11(1): 99-102.
- 91WH1 White, F.M., 1991. *Viscous fluid flow*, second edn. McGraw-Hill, New York
- 92OT1 Ottermann, H.H., 1992. *Pressure drop across a pneumatic conveying feeding tee*. M.Sc. Dissertation. Faculty of Engineering. University of Pretoria, Pretoria.
- 93AN1 Anon., 1993. *AutoCAD release 12. Customisation Manual*. Autodesk Inc. U.S.A. pp. 243-277.
- 93SA1 Saccani, C., 1993. A new simulation program for designing pneumatic conveying plants. *Bulk Solids Handling* (13)1: 111-121.

- 94HE1 Hearn, D. and Baker, M.P., 1994. *Computer Graphics*. Prentice Hall Inc. New Jersey. pp.423-425.
- 94VS1 Van Straaten, W.H., 1994. *The operating characteristics of a high efficiency axial cyclone in a dilute phase pneumatic conveyor system*. M.Sc. Dissertation. Faculty of Engineering. University of Pretoria, Pretoria.
- 94WO1 Wodrich, K.H.K., 1994. *An experimental facility for air flow with solid particles*. Undergraduate project. Department of Mechanical Engineering. University of Stellenbosch, Stellenbosch.
- 95KR1 Kröger, D.G., 1995. *Air-cooled heat exchangers and cooling towers*. Lecture notes for the post-graduate course in heat transfer. Department of Mechanical Engineering. University of Stellenbosch, Stellenbosch.
- 96AE1 Anon., 1996. Aerzen Technical Note: *Layout of Roots Blowers*. Aerzener Maschinenfabrik, Germany.
- 96ER1 Ertas, A. and Jones, J.C., 1996. *The Engineering Design Process*. Second edn. John Wiley & Sons, New York.
- 96HI1 Anon., 1996. *HIBON positive displacement blowers performance curves*. Ets G. HIBON S.A., France.
- 96SA1 Saccani, C., 1996. Solid speed and pressure loss in pneumatic conveying plants: simulation and experimental measurements. *Bulk Solids Handling* 16(3): 383-390.

PIPE LAYOUT DATA FILE FORMAT

The data file generated by the pipe layout generation programme is a standard text file in the following format:

Each line in the data file contains 16 numeric entries separated by a single space.

Entry number:

1: Component number

2: Component identifier

- 1 A bend connecting a horizontal pipe with a pipe running vertically upwards
- 2 A bend connecting a horizontal pipe with a pipe running vertically downwards
- 3 A bend to the right viewed in direction of the flow connecting two horizontal pipe sections
- 4 A bend to the left viewed in direction of the flow connecting two horizontal pipe sections
- 5 A bend connecting a vertical and horizontal pipeline (with flow in an upward direction in the vertical pipe) and an arbitrary rotation around the vertical axis
- 6 A bend connecting a vertical and horizontal pipeline (with flow in a downward direction in the vertical pipe) and an arbitrary rotation around the vertical axis
- 7 Horizontal pipe section
- 8 Vertical pipe section
- 9 Feed point

3: Pipeline inner diameter in mm

Subsequent entries are formatted according to the component identifier entries above.

For any bend component (component identifiers 1 through 6) the first line in the data file identifies the bend identification points as follows:

Entry number:

4. Center point x-coordinate of a circular arc defining the bend in mm

5. Center point y-coordinate of a circular arc defining the bend in mm
6. Center point z-coordinate of a circular arc defining the bend in mm
7. 0
8. x-coordinate for the start point of the bend in mm
9. y-coordinate for the start point of the bend in mm
10. z-coordinate for the start point of the bend in mm
11. x-coordinate for the apex of the bend in mm
12. y-coordinate for the apex of the bend in mm
13. z-coordinate for the apex of the bend in mm
14. x-coordinate for the end point of the bend in mm
15. x-coordinate for the end point of the bend in mm
16. x-coordinate for the end point of the bend in mm
17. 0

All subsequent lines with the same component identifier store the information for the line segments making up the bend component and are formatted as follows

Entry number:

4. Center point x-coordinate of a circular arc defining the bend in mm
5. Center point y-coordinate of a circular arc defining the bend in mm
6. Center point z-coordinate of a circular arc defining the bend in mm
7. For bend identifiers 5 and 6 the angle of rotation around the z-axis in the positive direction with respect to the x-axis in radians. For component identifiers 1 to 4 entry is 0.
8. x-coordinate for the start point of the bend in mm
9. y-coordinate for the start point of the bend in mm
10. z-coordinate for the start point of the bend in mm
11. x-coordinate for the start point of the line segment in mm
12. y-coordinate for the start point of the line segment in mm
13. z-coordinate for the start point of the line segment in mm
14. x-coordinate for the end point of the line segment in mm
15. x-coordinate for the end point of the line segment in mm
16. x-coordinate for the end point of the line segment in mm
17. angle of inclination of the line segment in the vertical direction with respect to the x-y plane in radians as defined in figure 2.1.

Component identifier 7 and 8 are used for straight pipeline sections and are formatted as follows:

Entry number:

4. 0
5. 0
6. 0
7. 0
8. 0
9. 0
10. 0
11. x-coordinate for the start point of the line segment in mm
12. y-coordinate for the start point of the line segment in mm
13. z-coordinate for the start point of the line segment in mm
14. x-coordinate for the end point of the line segment in mm
15. x-coordinate for the end point of the line segment in mm
16. x-coordinate for the end point of the line segment in mm
17. angle of inclination of the line segment in the vertical direction with respect to the x-y plane in radians as defined in figure 3.1 in chapter three.

Component identifier 9 is used for the feed point. All entries 4 to 17 are the same values as those of the previous component unless the feed point is the initial component in which case all entries are zero.

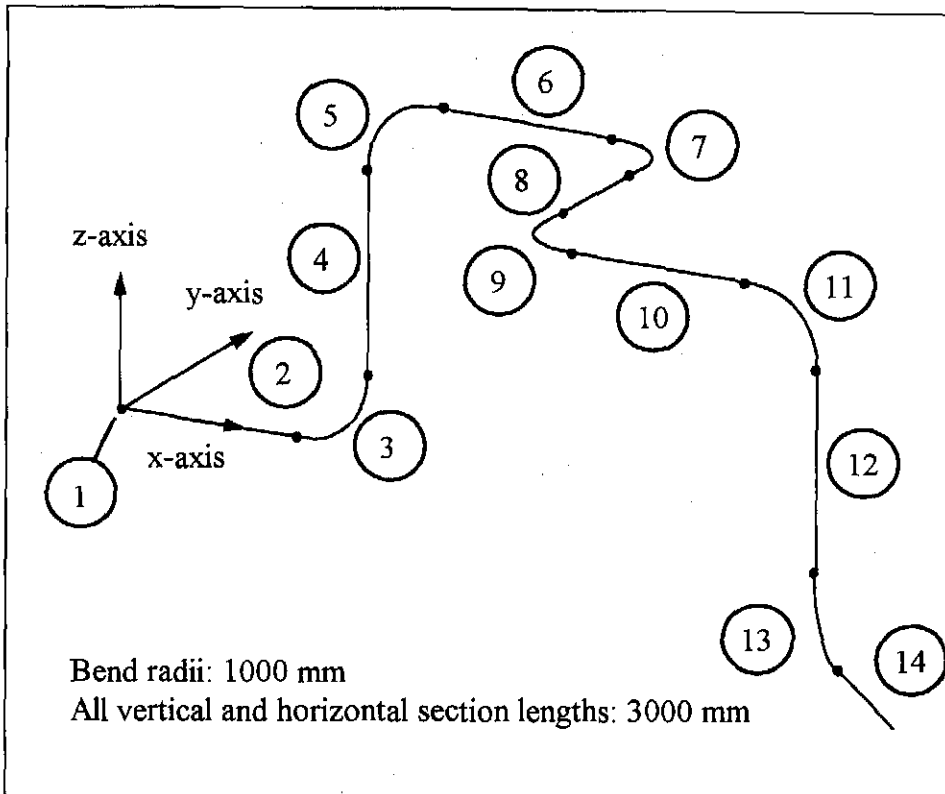


Fig. A.1 Sample pipe layout

Table A.1 is an example of the data file for the pipe layout depicted in figure A1.

Tab. A.1 Sample data file for pipe layout in figure A.1

1	90.12	0.00	0.00	0.00	0.00	0.00	0.00	0.00	0.00	0.00	0.00	0.00	0.00	0.00	0.00	0.00	0.00	0.00	0.00
2	7	90.12	0.00	0.00	0.00	0.00	0.00	0.00	0.00	0.00	0.00	3000.00	0.00	0.00	0.00	0.00	0.00	0.00	0.00
3	1	90.12	3000.00	0.00	1000.00	0.00	3000.00	0.00	0.00	4000.00	0.00	0.00	4000.00	0.00	1000.00	0.00	0.00	0.00	0.00
3	1	90.12	3000.00	0.00	1000.00	0.00	3000.00	0.00	0.00	4000.00	0.00	0.00	3156.43	0.00	12.31	0.08	0.00	0.00	0.00
3	1	90.12	3000.00	0.00	1000.00	0.00	3156.43	0.00	12.31	4000.00	0.00	0.00	3309.02	0.00	48.94	0.24	0.00	0.00	0.00
3	1	90.12	3000.00	0.00	1000.00	0.00	3309.02	0.00	48.94	4000.00	0.00	0.00	3453.99	0.00	108.99	0.39	0.00	0.00	0.00
3	1	90.12	3000.00	0.00	1000.00	0.00	3453.99	0.00	108.99	4000.00	0.00	0.00	3587.79	0.00	190.98	0.55	0.00	0.00	0.00
3	1	90.12	3000.00	0.00	1000.00	0.00	3587.79	0.00	190.98	4000.00	0.00	0.00	3707.11	0.00	292.89	0.71	0.00	0.00	0.00
3	1	90.12	3000.00	0.00	1000.00	0.00	3707.11	0.00	292.89	4000.00	0.00	0.00	3809.02	0.00	412.21	0.86	0.00	0.00	0.00
3	1	90.12	3000.00	0.00	1000.00	0.00	3809.02	0.00	412.21	4000.00	0.00	0.00	3891.01	0.00	546.01	1.02	0.00	0.00	0.00
3	1	90.12	3000.00	0.00	1000.00	0.00	3891.01	0.00	546.01	4000.00	0.00	0.00	3951.06	0.00	690.98	1.18	0.00	0.00	0.00
3	1	90.12	3000.00	0.00	1000.00	0.00	3951.06	0.00	690.98	4000.00	0.00	0.00	3987.69	0.00	843.57	1.34	0.00	0.00	0.00
3	1	90.12	3000.00	0.00	1000.00	0.00	3987.69	0.00	843.57	4000.00	0.00	0.00	4000.00	0.00	1000.00	1.49	0.00	0.00	0.00
4	8	90.12	0.00	0.00	0.00	0.00	0.00	0.00	4000.00	0.00	1000.00	4000.00	0.00	4000.00	1.57	0.00	0.00	0.00	0.00
5	5	90.12	5000.00	0.00	4000.00	0.00	4000.00	0.00	4000.00	0.00	4000.00	0.00	5000.00	5000.00	0.00	5000.00	0.00	0.00	0.00
5	5	90.12	5000.00	0.00	4000.00	0.00	4000.00	0.00	4000.00	4000.00	0.00	5000.00	4012.31	0.00	4156.43	1.49	0.00	0.00	0.00
5	5	90.12	5000.00	0.00	4000.00	0.00	4012.31	0.00	4156.43	4000.00	0.00	5000.00	4048.94	0.00	4309.02	1.34	0.00	0.00	0.00
5	5	90.12	5000.00	0.00	4000.00	0.00	4048.94	0.00	4309.02	4000.00	0.00	5000.00	4108.99	0.00	4453.99	1.18	0.00	0.00	0.00
5	5	90.12	5000.00	0.00	4000.00	0.00	4108.99	0.00	4453.99	4000.00	0.00	5000.00	4190.98	0.00	4587.79	1.02	0.00	0.00	0.00
5	5	90.12	5000.00	0.00	4000.00	0.00	4190.98	0.00	4587.79	4000.00	0.00	5000.00	4292.89	0.00	4707.11	0.86	0.00	0.00	0.00
5	5	90.12	5000.00	0.00	4000.00	0.00	4292.89	0.00	4707.11	4000.00	0.00	5000.00	4412.21	0.00	4809.02	0.71	0.00	0.00	0.00
5	5	90.12	5000.00	0.00	4000.00	0.00	4412.21	0.00	4809.02	4000.00	0.00	5000.00	4546.01	0.00	4891.01	0.55	0.00	0.00	0.00
5	5	90.12	5000.00	0.00	4000.00	0.00	4546.01	0.00	4891.01	4000.00	0.00	5000.00	4690.98	0.00	4951.06	0.39	0.00	0.00	0.00
5	5	90.12	5000.00	0.00	4000.00	0.00	4690.98	0.00	4951.06	4000.00	0.00	5000.00	4843.57	0.00	4987.69	0.24	0.00	0.00	0.00
5	5	90.12	5000.00	0.00	4000.00	0.00	4843.57	0.00	4987.69	4000.00	0.00	5000.00	5000.00	0.00	5000.00	0.08	0.00	0.00	0.00
6	7	90.12	0.00	0.00	0.00	0.00	0.00	0.00	5000.00	0.00	5000.00	8000.00	0.00	5000.00	0.00	0.00	0.00	0.00	0.00
7	4	90.12	8000.00	-1000.00	5000.00	0.00	8000.00	0.00	5000.00	9000.00	0.00	5000.00	9000.00	-1000.00	5000.00	0.00	0.00	0.00	0.00
7	4	90.12	8000.00	-1000.00	5000.00	0.00	8000.00	0.00	5000.00	9000.00	0.00	5000.00	8156.43	-12.31	5000.00	0.00	0.00	0.00	0.00
7	4	90.12	8000.00	-1000.00	5000.00	0.00	8156.43	-12.31	5000.00	9000.00	0.00	5000.00	8309.02	-48.94	5000.00	0.00	0.00	0.00	0.00
7	4	90.12	8000.00	-1000.00	5000.00	0.00	8309.02	-48.94	5000.00	9000.00	0.00	5000.00	8453.99	-108.99	5000.00	0.00	0.00	0.00	0.00
7	4	90.12	8000.00	-1000.00	5000.00	0.00	8453.99	-108.99	5000.00	9000.00	0.00	5000.00	8587.79	-190.98	5000.00	0.00	0.00	0.00	0.00
7	4	90.12	8000.00	-1000.00	5000.00	0.00	8587.79	-190.98	5000.00	9000.00	0.00	5000.00	8707.11	-292.89	5000.00	0.00	0.00	0.00	0.00
7	4	90.12	8000.00	-1000.00	5000.00	0.00	8707.11	-292.89	5000.00	9000.00	0.00	5000.00	8809.02	-412.21	5000.00	0.00	0.00	0.00	0.00
7	4	90.12	8000.00	-1000.00	5000.00	0.00	8809.02	-412.21	5000.00	9000.00	0.00	5000.00	8891.01	-546.01	5000.00	0.00	0.00	0.00	0.00
7	4	90.12	8000.00	-1000.00	5000.00	0.00	8891.01	-546.01	5000.00	9000.00	0.00	5000.00	8951.06	-690.98	5000.00	0.00	0.00	0.00	0.00

Tab. A.1 continued

7 4 90.12	8000.00	-1000.00	5000.00	0.00	8951.06	-690.98	5000.00	9000.00	0.00	5000.00	8987.69	-843.57	5000.00	0.00
7 4 90.12	8000.00	-1000.00	5000.00	0.00	8987.69	-843.57	5000.00	9000.00	0.00	5000.00	9000.00	-1000.00	5000.00	0.00
8 7 90.12	0.00	0.00	0.00	0.00	0.00	0.00	9000.00	-1000.00	5000.00	9000.00	-4000.00	5000.00	0.00	
9 3 90.12	10000.00	-4000.00	5000.00	0.00	9000.00	-4000.00	5000.00	9000.00	-5000.00	5000.00	10000.00	-5000.00	5000.00	0.00
9 3 90.12	10000.00	-4000.00	5000.00	0.00	9000.00	-4000.00	5000.00	9000.00	-5000.00	5000.00	9012.31	-4156.43	5000.00	0.00
9 3 90.12	10000.00	-4000.00	5000.00	0.00	9012.31	-4156.43	5000.00	9000.00	-5000.00	5000.00	9048.94	-4309.02	5000.00	0.00
9 3 90.12	10000.00	-4000.00	5000.00	0.00	9048.94	-4309.02	5000.00	9000.00	-5000.00	5000.00	9108.99	-4453.99	5000.00	0.00
9 3 90.12	10000.00	-4000.00	5000.00	0.00	9108.99	-4453.99	5000.00	9000.00	-5000.00	5000.00	9190.98	-4587.79	5000.00	0.00
9 3 90.12	10000.00	-4000.00	5000.00	0.00	9190.98	-4587.79	5000.00	9000.00	-5000.00	5000.00	9292.89	-4707.11	5000.00	0.00
9 3 90.12	10000.00	-4000.00	5000.00	0.00	9292.89	-4707.11	5000.00	9000.00	-5000.00	5000.00	9412.21	-4809.02	5000.00	0.00
9 3 90.12	10000.00	-4000.00	5000.00	0.00	9412.21	-4809.02	5000.00	9000.00	-5000.00	5000.00	9546.01	-4891.01	5000.00	0.00
9 3 90.12	10000.00	-4000.00	5000.00	0.00	9546.01	-4891.01	5000.00	9000.00	-5000.00	5000.00	9690.98	-4951.06	5000.00	0.00
9 3 90.12	10000.00	-4000.00	5000.00	0.00	9690.98	-4951.06	5000.00	9000.00	-5000.00	5000.00	9843.57	-4987.69	5000.00	0.00
9 3 90.12	10000.00	-4000.00	5000.00	0.00	9843.57	-4987.69	5000.00	9000.00	-5000.00	5000.00	10000.00	-5000.00	5000.00	0.00
10 7 90.12	0.00	0.00	0.00	0.00	0.00	0.00	10000.00	-5000.00	5000.00	13000.00	-5000.00	5000.00	0.00	
11 2 90.12	13000.00	-5000.00	4000.00	0.00	13000.00	-5000.00	5000.00	14000.00	-5000.00	5000.00	14000.00	-5000.00	4000.00	0.00
11 2 90.12	13000.00	-5000.00	4000.00	0.00	13000.00	-5000.00	5000.00	14000.00	-5000.00	5000.00	13156.43	-5000.00	4987.69	-0.08
11 2 90.12	13000.00	-5000.00	4000.00	0.00	13156.43	-5000.00	4987.69	14000.00	-5000.00	5000.00	13309.02	-5000.00	4951.06	-0.24
11 2 90.12	13000.00	-5000.00	4000.00	0.00	13309.02	-5000.00	4951.06	14000.00	-5000.00	5000.00	13453.99	-5000.00	4891.01	-0.39
11 2 90.12	13000.00	-5000.00	4000.00	0.00	13453.99	-5000.00	4891.01	14000.00	-5000.00	5000.00	13587.79	-5000.00	4809.02	-0.55
11 2 90.12	13000.00	-5000.00	4000.00	0.00	13587.79	-5000.00	4809.02	14000.00	-5000.00	5000.00	13707.11	-5000.00	4707.11	-0.71
11 2 90.12	13000.00	-5000.00	4000.00	0.00	13707.11	-5000.00	4707.11	14000.00	-5000.00	5000.00	13809.02	-5000.00	4587.79	-0.86
11 2 90.12	13000.00	-5000.00	4000.00	0.00	13809.02	-5000.00	4587.79	14000.00	-5000.00	5000.00	13891.01	-5000.00	4453.99	-1.02
11 2 90.12	13000.00	-5000.00	4000.00	0.00	13891.01	-5000.00	4453.99	14000.00	-5000.00	5000.00	13951.06	-5000.00	4309.02	-1.18
11 2 90.12	13000.00	-5000.00	4000.00	0.00	13951.06	-5000.00	4309.02	14000.00	-5000.00	5000.00	13987.69	-5000.00	4156.43	-1.34
11 2 90.12	13000.00	-5000.00	4000.00	0.00	13987.69	-5000.00	4156.43	14000.00	-5000.00	5000.00	14000.00	-5000.00	4000.00	-1.49
12 8 90.12	0.00	0.00	0.00	0.00	0.00	0.00	14000.00	-5000.00	4000.00	14000.00	-5000.00	1000.00	-1.57	
13 6 90.12	14707.11	-5707.11	1000.00	0.00	14000.00	-5000.00	1000.00	14000.00	-5000.00	0.00	14707.11	-5707.11	0.00	0.00
13 6 90.12	14707.11	-5707.11	1000.00	-0.79	14000.00	-5000.00	1000.00	14000.00	-5000.00	0.00	14008.71	-5008.71	843.57	-1.49
13 6 90.12	14707.11	-5707.11	1000.00	-0.79	14008.71	-5008.71	843.57	14000.00	-5000.00	0.00	14034.61	-5034.61	690.98	-1.34
13 6 90.12	14707.11	-5707.11	1000.00	-0.79	14034.61	-5034.61	690.98	14000.00	-5000.00	0.00	14077.07	-5077.07	546.01	-1.18
13 6 90.12	14707.11	-5707.11	1000.00	-0.79	14077.07	-5077.07	546.01	14000.00	-5000.00	0.00	14135.05	-5135.05	412.21	-1.02
13 6 90.12	14707.11	-5707.11	1000.00	-0.79	14135.05	-5135.05	412.21	14000.00	-5000.00	0.00	14207.11	-5207.11	292.89	-0.86
13 6 90.12	14707.11	-5707.11	1000.00	-0.79	14207.11	-5207.11	292.89	14000.00	-5000.00	0.00	14291.48	-5291.48	190.98	-0.71
13 6 90.12	14707.11	-5707.11	1000.00	-0.79	14291.48	-5291.48	190.98	14000.00	-5000.00	0.00	14386.09	-5386.09	108.99	-0.55
13 6 90.12	14707.11	-5707.11	1000.00	-0.79	14386.09	-5386.09	108.99	14000.00	-5000.00	0.00	14488.60	-5488.60	48.94	-0.39
13 6 90.12	14707.11	-5707.11	1000.00	-0.79	14488.60	-5488.60	48.94	14000.00	-5000.00	0.00	14596.49	-5596.49	12.31	-0.24
13 6 90.12	14707.11	-5707.11	1000.00	-0.79	14596.49	-5596.49	12.31	14000.00	-5000.00	0.00	14707.11	-5707.11	0.00	-0.08
14 7 90.12	0.00	0.00	0.00	0.00	0.00	0.00	14707.11	-5707.11	0.00	16828.43	-7828.43	0.00	0.00	

ADDITIONAL EQUATION DERIVATION**B.1 ALTERNATIVE REPRESENTATIONS OF THE GOVERNING EQUATIONS FOR TWO-PHASE FLOW**

The pressure drop equation and consequently the equation of motion for two-phase flow can be represented in different ways according to the definition of the friction coefficient. The gas state equation and the two continuity equations remain the same for all three versions of the pressure drop and motion equations given below.

VERSION 1 (Gravity effects excluded from the friction coefficient)

The solids continuity equation in differential form can be written as:

$$\frac{de}{dl} = \frac{(1-e)}{c} \frac{dc}{dl} + \frac{(1-e)}{A} \frac{dA}{dl} \quad (\text{B.1.1})$$

The gas continuity equation in differential form yields:

$$\frac{dv_e}{dl} = -\frac{v_e}{\rho_g} \frac{d\rho_g}{dl} - \frac{v_e}{e} \frac{de}{dl} - \frac{v_e}{A} \frac{dA}{dl} \quad (\text{B.1.2})$$

The ideal gas equation can be differentiated to give:

$$\frac{d\rho_g}{dl} = \frac{dP}{dl} \frac{1}{RT} \quad (\text{B.1.3})$$

Pressure drop equation:

$$\begin{aligned} -\frac{dP}{dl} = & e \left(\rho_g v_e \frac{dv_e}{dl} + \rho_g g \sin \beta \right) \\ & + (1-e) \left(\rho_s c \frac{dc}{dl} + \rho_s g \sin \beta + (\rho_s - \rho_g) g \cos^2 \beta \frac{w_s}{c} \right) \\ & + e \left(\lambda_g + \mu \lambda_{s1} \right) \frac{\rho_g v_e^2}{2d} \end{aligned} \quad (\text{B.1.4})$$

Equation of motion:

$$\begin{aligned} \frac{dc}{dl} = & \frac{3}{4} C_d \frac{\rho_g}{\rho_s d_s} \frac{(v_e - c)^2}{ce} - \frac{1}{c} g \sin \beta + \frac{\rho_g}{\rho_s c} \left(v_e \frac{dv_e}{dl} + g \sin \beta \right) \\ & - \frac{1}{ce} \lambda_s^* \frac{c^2}{2d} + \frac{\rho_g}{\rho_s c} (\lambda_g + \mu \lambda_{s1}) \frac{v^2}{2d} \\ & + \frac{(1-e)(\rho_s - \rho_g)}{e c \rho_s} g \cos^2 \beta \frac{w_s}{c} \end{aligned} \quad (\text{B.1.5})$$

With the general definition of the solids friction coefficient given as:

$$\lambda_{s1} = \lambda_s^* \frac{c}{v_e} \quad (\text{B.1.6})$$

Note that in this form the friction coefficient is independent of gravity effects and the definition remains the same for both horizontal and vertical flow. This representation is highly desirable if the friction coefficient correlation for horizontal flow is to be applied to vertical flow as well.

The pressure drop equation rewritten for steady state **horizontal flow** results in equation B.1.7 which is used to determine the friction coefficient from experimental pressure drop.

$$-\frac{dP}{dl} = (1-e)(\rho_s - \rho_g) g \frac{w_s}{c} + e(\lambda_g + \mu \lambda_s) \frac{\rho_g v_e^2}{2d} \quad (\text{B.1.7})$$

$$\text{with: } \lambda_{s1} = \lambda_s^* \frac{c}{v_e} \quad (\text{B.1.8})$$

In comparison the pressure drop equation for steady state **vertical flow** is given as:

$$-\frac{dP}{dl} = e \rho_g g + (1-e) \rho_s g + e(\lambda_g + \mu \lambda_s) \frac{\rho_g v_e^2}{2d} \quad (\text{B.1.9})$$

$$\text{with: } \lambda_{s1} = \lambda_s^* \frac{c}{v_e} \quad (\text{B.1.8})$$

VERSION 2 (Gravity effects for horizontal flow incorporated in friction coefficient)

As noted earlier equations A.1.1 to A.1.3 are common to all three representations and will not be repeated here.

Pressure drop equation:

$$-\frac{dP}{dl} = e \left(\rho_g v_e \frac{dv_e}{dl} + \rho_g g \sin \beta \right) + (1-e) \left(\rho_s c \frac{dc}{dl} + \rho_s g \sin \beta \right) + e (\lambda_g + \mu \lambda_{s2}) \frac{\rho_g v_e^2}{2d} \quad (\text{B.1.10})$$

Equation of motion:

$$\frac{dc}{dl} = \frac{3}{4} C_d \frac{\rho_g}{\rho_s d_s} \frac{(v_e - c)^2}{ce} - \frac{1}{c} g \sin \beta + \frac{\rho_g}{\rho_s c} \left(v_e \frac{dv_e}{dl} + g \sin \beta \right) - \frac{1}{ce} \lambda_s^* \frac{c^2}{2d} + \frac{\rho_g}{\rho_s c} (\lambda_g + \mu \lambda_{s2}) \frac{v^2}{2d} \quad (\text{B.1.11})$$

with the general definition of the friction coefficient given as:

$$\lambda_{s2} = \lambda_s^* \frac{c}{v_e} + \frac{2}{\left(\frac{c}{v_e} \right) Fr_e} \frac{\rho_s - \rho_g}{\rho_s} \cos^2 \beta \frac{w_s}{c} \quad (\text{B.1.12})$$

The pressure drop equation for steady state **horizontal flow** used for determining the friction coefficient correlation becomes:

$$-\frac{dP}{dl} = e (\lambda_g + \mu \lambda_s) \frac{\rho_g v_e^2}{2d} \quad (\text{B.1.13})$$

The definition of the horizontal flow friction coefficient is:

$$\lambda_{s2} = \lambda_s^* \frac{c}{v_e} + \frac{2}{\left(\frac{c}{v_e} \right) Fr_e} \frac{\rho_s - \rho_g}{\rho_s} \frac{w_s}{c} \quad (\text{B.1.14})$$

For steady state **vertical flow** the pressure equation can be written as:

$$-\frac{dP}{dl} = e \rho_g g + (1-e) \rho_s g + e (\lambda_g + \mu \lambda_{s2}) \frac{\rho_g v_e^2}{2d} \quad (\text{B.1.15})$$

with the definition of the vertical flow friction coefficient becoming:

$$\lambda_{s2} = \lambda_s^* \frac{c}{v_e} \quad (\text{B.1.16})$$

Note that the two definitions for the friction coefficient differ so that it is not possible to define a single total friction coefficient λ_{tot} for vertical and horizontal flow incorporating the air friction coefficient. The alternative is to determine two separate correlations, one for vertical flow, the other for horizontal flow or calculate a value for λ_s^* and determine a suitable correlation for this.

VERSION 3 (Gravity effects for both horizontal and vertical flow incorporated in friction coefficient)

The following definition of the pressure equation and motion equation is that most often quoted in the literature. It is convenient in a sense that all gravitational terms are included in the friction coefficient which makes the equations much simpler to use but once again results in a friction coefficient that is defined differently for horizontal and vertical flow. Except for minor differences in definition this is the generalised version of the equation for the friction coefficient first proposed by Barth [58BA1]. This becomes clear when rewriting the pressure drop equation for horizontal and vertical flow as in equations B.1.20 to B.1.23.

Pressure drop equation:

$$-\frac{dP}{dl} = e \left(\rho_g v_e \frac{dv_e}{dl} + \rho_g g \sin \beta \right) + (1-e) \rho_s c \frac{dc}{dl} + e (\lambda_g + \mu \lambda_{s3}) \frac{\rho_g v_e^2}{2d} \quad (\text{B.1.17})$$

Equation of motion:

$$\frac{dc}{dl} = \frac{3}{4} C_d \frac{\rho_g}{\rho_s d_s} \frac{(v_e - c)^2}{ce} - \frac{1}{ec} g \sin \beta + \frac{\rho_g}{\rho_s c} \left(v_e \frac{dv_e}{dl} + g \sin \beta \right) - \frac{1}{ce} \lambda_s^* \frac{c^2}{2d} + \frac{\rho_g}{\rho_s c} (\lambda_g + \mu \lambda_{s3}) \frac{v_e^2}{2d} \quad (\text{B.1.18})$$

with the general definition of the friction coefficient as:

$$\lambda_{s3} = \lambda_s^* \frac{c}{v_e} + \frac{2}{\left(\frac{c}{v_e} \right) Fr_e} \frac{\rho_s - \rho_g}{\rho_s} \cos^2 \beta \frac{w_s}{c} + \frac{2}{\left(\frac{c}{v_e} \right) Fr_e} \sin \beta \quad (\text{B.1.19})$$

The pressure drop equation for steady state **horizontal flow** for the determination of the friction coefficient from experimental data becomes:

$$-\frac{dP}{dl} = e(\lambda_g + \mu\lambda_s) \frac{\rho_g v_e^2}{2d} \quad (\text{B.1.20})$$

$$\text{with: } \lambda_{s3} = \lambda_s^* \frac{c}{v_e} + \frac{2}{\left(\frac{c}{v_e}\right) Fr_e} \frac{\rho_s - \rho_g}{\rho_s} \frac{w_s}{c} \quad (\text{B.1.21})$$

The pressure drop equation for steady state **vertical flow** becomes:

$$-\frac{dP}{dl} = e\rho_g g + e(\lambda_g + \mu\lambda_{s3}) \frac{\rho_g v_e^2}{2d} \quad (\text{B.1.22})$$

$$\text{with: } \lambda_{s3} = \lambda_s^* \frac{c}{v_e} + \frac{2}{\left(\frac{c}{v_e}\right) Fr_e} \quad (\text{B.1.23})$$

Equations B.1.21 and B.1.23 are similar to those presented by Barth [58BA1] and summarised in equations 1.3.18 and 1.3.19 in chapter one. The second term in equation B.1.21 contains the buoyancy effects of a particle in air which are neglected in Barth's representation. Another difference in the representation by Barth [58BA1] is the definition of the velocity ratio w_s/c as explained in section 3.3.3.

B.2 EQUATIONS FOR FLOW OF PARTICLES ALONG A BEND WALL

Using the r-momentum equation of motion in cylindrical coordinates [88WH1] for a fluid, the pressure gradient in a bend section can be derived as follows where r , θ and z refer to the radial, θ and z axes of a cylindrical coordinate system respectively.

$$\begin{aligned} \frac{\partial v_r}{\partial t} + v_r \frac{\partial v_r}{\partial r} + \frac{1}{r} v_\theta \frac{\partial v_r}{\partial \theta} + v_z \frac{\partial v_r}{\partial z} - \frac{1}{r} v_\theta^2 = \\ - \frac{1}{\rho_g} \frac{\partial P}{\partial r} + g_r + \frac{\mu}{\rho_g} \left(\frac{1}{r} \frac{\partial}{\partial r} \left(r \frac{\partial v_r}{\partial r} \right) + \frac{1}{r^2} \frac{\partial^2 v_r}{\partial \theta^2} + \frac{\partial^2 v_r}{\partial z^2} - \frac{v_r}{r^2} - \frac{2}{r^2} \frac{\partial v_r}{\partial \theta} \right) \end{aligned} \quad (\text{B.2.1})$$

Assuming the flow to be in a steady state with no flow in the radial and the z-direction, the pressure a function of r alone and the pressure gradient constant at an average radius r_c defined in figure B.1, equation B.2.1 simplifies to:

$$\frac{dP}{dr} = \rho_g g_r + \rho_g \frac{v_\theta^2}{r_c} \quad (\text{B.2.2})$$

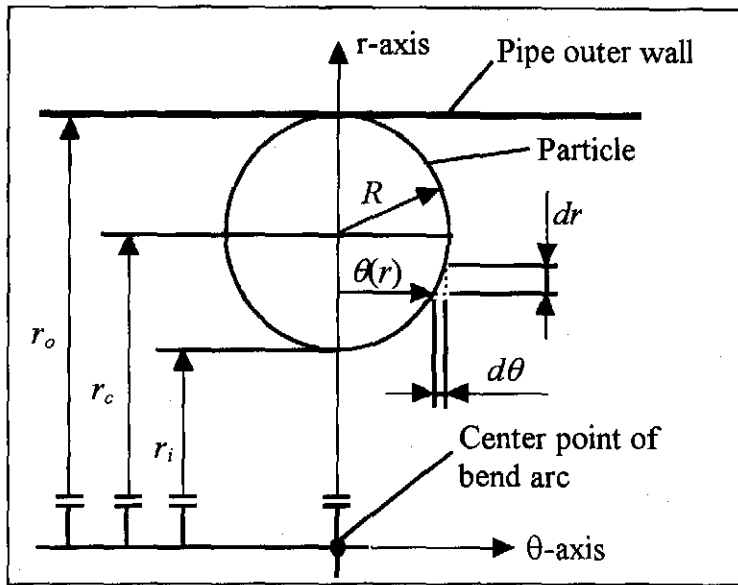


Fig. B.1 Bend geometry variable definition

The gravitation term is replaced with:

$$g_r = -g \sin \alpha \quad (\text{B.2.3})$$

If the circumferential velocity v_θ is replaced with the interstitial fluid velocity and it is assumed that the particle travels at a constant radius r_c from the origin, equation B.2.2 becomes:

$$\frac{dP}{dr} = -\rho_g g \sin \alpha + \rho_g \frac{v^2}{r_c} \quad (\text{B.2.4})$$

The resultant pressure force in the radial direction on a particle as a result of this pressure gradient can be calculated first by integrating equation B.2.4 to obtain the pressure as a function of the radius r :

$$P(r) = \rho_g \left(-g \sin \alpha + \frac{v^2}{r_c} \right) r + c_1 \quad (\text{B.2.5})$$

where c_1 is the integration constant.

To obtain a net pressure force on a particle, the pressure at radius r_i is taken as zero so that equation B.2.5 becomes:

$$P(r) = \rho_g \left(-g \sin \alpha + \frac{v^2}{r_c} \right) (r - r_i) \quad (\text{B.2.6})$$

Assuming the pressure gradient exists across a spherical particle dragging along the outer wall of a pipe bend, the differential area normal to the radial direction as defined in figure B.1 can be approximated as:

$$dA = 2\pi x(r)dx \quad (\text{B.2.7})$$

where $x(r)$ is the equation of a circle centred at $(0, r_c)$. The curvature of the pipe wall in relation to the particle diameter is small so that the curvature of the slice through the particle to determine the differential area is taken as zero.

With this assumption the circle equation can be written as:

$$x(r) = \left(R^2 - (r - r_c)^2 \right)^{\frac{1}{2}} \quad (\text{B.2.8})$$

The net force can be determined as:

$$dF_{s,p} = P(r)dA \quad (\text{B.2.9})$$

Written out, equation B.2.9 becomes:

$$\begin{aligned} F_{s,p} &= \int_{r_i}^{r_o} 2\pi \rho_g \left(-g \sin \alpha + \frac{v^2}{r_c} \right) (r - r_i)(r_c - r) dr \\ &\quad - \int_{r_o}^{r_c} 2\pi \rho_g \left(-g \sin \alpha + \frac{v^2}{r_c} \right) (r - r_i)(r_c - r) dr \\ &= \int_{r_i}^{r_o} 2\pi \rho_g \left(-g \sin \alpha + \frac{v^2}{r_c} \right) (r - r_i)(r_c - r) dr \end{aligned} \quad (\text{B.2.10})$$

Solving equation B.2.10 yields:

$$F_{s,p} = -\frac{\pi d^3}{6} \rho_g \left(-g \sin \alpha + \frac{v^2}{r_c} \right) \quad (\text{B.2.11})$$

The volume of a spherical particle is given by:

$$V_s = \frac{\pi d_s^3}{6} \quad (\text{B.2.12})$$

Combining equations B.2.11 and B.2.12 yields the net pressure force in the radial direction on the particle:

$$F_{s,p} = -V_s \rho_g \left(-g \sin \alpha + \frac{v^2}{r_c} \right) \quad (\text{B.2.13})$$

Newton's second law of motion can now be applied to the particle, taking pressure and gravitational forces into account. Referring to figure 3.4 in chapter three one can write for a particle moving in a circular path of constant radius r_c :

$$-(V_s \rho_s) \frac{c^2}{r_c} = -V_s \rho_s g \sin \alpha + F_{s,p} - F_n \quad (\text{B.2.14})$$

Setting equation B.2.13 into equation B.2.14 results in:

$$F_n = V_s \left(\rho_s \frac{c^2}{r_c} - \rho_g \frac{v^2}{r_c} \right) - V_s (\rho_s - \rho_g) g \sin \alpha \quad (\text{B.2.15})$$

A further simplification can be made by assuming that $v \approx c$ and that the particles are small in relation to the pipe diameter that one can assume $r_c \approx r_o$. This yields equation 3.5.2 given in chapter three:

$$F_n = V_s (\rho_s - \rho_g) \left(\frac{c^2}{r_o} - g \sin \alpha \right) \quad (\text{3.5.2})$$

CALCULATION METHODS AND SAMPLE CALCULATION

C.1 SPHERICITY DETERMINATION FOR CEMENT

The determination of the sphericity of cement is required for the subsequent calculation of the drag coefficient and free fall velocity of the cement particles. Following is the method used to approximate the sphericity of cement. The particle diameter d_s is assumed to be the equivalent volume diameter, i.e. the diameter of a spherical particle with the same volume as the non-spherical particle. If the total specific surface area or total surface area of the particles per unit mass is known, an estimate of the sphericity can be made.

The volume that a single particle of diameter d_s occupies is calculated as:

$$V_s = \frac{1}{6} \pi d_s^3 \quad (\text{C.1.1})$$

$$V_s = \frac{1}{6} \pi \cdot (32.69 \cdot 10^{-6})^3 = 1.8291 \cdot 10^{-14} \text{ m}^3$$

The inverse of the density of the material yields the volume that the particles will occupy per unit mass. The number of spherical particles occupying a unit mass of material can be calculated as:

$$n_s = \frac{1}{\rho_s V_s} \quad (\text{C.1.2})$$

$$n_s = \frac{1}{3114.23 \cdot 1.8291 \cdot 10^{-14}} = 1.75552 \cdot 10^{10} \text{ particles/kg}$$

An estimate of the true surface area of a single particle can be made by using the specific surface area of the particles. Note that for this to be correct the volume of a single particle must be the same as that of a non-spherical particle. For cement the value of the specific surface area can be taken as $300 \text{ m}^2/\text{kg}$ [78MA1].

$$A_{s,ns} = \frac{A_{ss}}{n_s} \quad (C.1.3)$$

$$A_{s,ns} = \frac{300}{1.75552 \cdot 10^{10}} = 1.7089 \cdot 10^{-8} \text{ m}^2$$

The sphericity can now be calculated according to the definition given in section 1.3.8:

$$\psi = \frac{A_{sv}}{A_{s,ns}} = \frac{\pi d_s^2}{A_{s,ns}} \quad (C.1.4)$$

$$\psi = \frac{\pi \cdot (32.69 \cdot 10^{-6})^2}{1.7089 \cdot 10^{-8}} = 0.1965$$

This value is used for the data correlation of the cement friction coefficients for both the data of Lange [89LA1] and van Straaten [94VS1].

C.2 CEMENT FRICTION COEFFICIENT CORRELATION METHOD

The total friction coefficient, solids impact and friction coefficient and alternative solids impact and friction coefficient as presented in the two phase flow differential equations 5.3.2 to 5.3.8 in chapter five are calculated utilising experimental data from Lange [89LA1] and van Straaten [94VS1] for cement and Sheer [91SH1] for tube ice particles.

Following is the method and sample calculation for cement using data point 3 in table C.1 at the end of section C.4 for a solids mass flow rate of 761 kg/h and a mass flow ratio of 0.741.

C.2.1 Determination of the particle velocity

In the case of the data from Lange [89LA1] the solids velocity is given in the table of results. This is determined by means of a slip velocity correlation utilising a radio active tracer method described by Meijers [86ME1]. Lange [89LA1] presents the slip ratio equation for cement as:

$$\frac{c}{v} = 0.774144 + 0.000039\dot{G} \quad (C.2.1)$$

where the solids mass flow rate is given in the units kg/h. Equation C.2.1 is also used to determine the solids velocity for the data presented by van Staaten [94VS1].

C.2.2 Determination of the voidage

The voidage is determined by rearranging the solids continuity equation 3.3.12 as:

$$e = 1 - \frac{4\dot{G}}{\pi d^2 \rho_s c} \quad (\text{C.2.2})$$

$$e = 1 - \frac{4 \cdot 0.211}{\pi \cdot 0.1016^2 \cdot 3114.23 \cdot 28.70} = 0.9997$$

C.2.3 Determination of the particle drag coefficient

The drag coefficient of a single spherical particle is determined using equation 1.3.44. The particle Reynolds number is first calculated as:

$$Re_{ds} = \frac{\rho_g v d_s}{\mu'} \quad (\text{C.2.3})$$

$$Re_{ds} = \frac{0.993 \cdot 35.43 \cdot 32.69 \cdot 10^{-6}}{1.8938 \cdot 10^{-5}} = 60.73$$

where the air dynamic viscosity is calculated at a temperature of 37.1°C using the correlation for dry air properties valid between 220K and 380K at 101325 Pa presented by Kröger [95KR1]. The dynamic viscosity is primarily temperature dependent. White [88WH1] notes that the viscosity varies with only a few percent up to 100 atm (9810 kPa) so that equation C.2.4 can be used within the pressure range of dilute phase pneumatic conveying where:

$$\begin{aligned} \mu' = & 2.287973 \cdot 10^{-6} + 6.259793 \cdot 10^{-8} T \\ & - 3.131956 \cdot 10^{-11} T^2 + 8.15038 \cdot 10^{-15} T^3 \end{aligned} \quad (\text{C.2.4})$$

with the temperature T in Kelvin. The drag coefficient for a spherical particle with a diameter d_s can be calculated as:

$$C_{d,s} = \frac{24}{Re_{ds}} (1 + 0.15 Re_{ds}^{0.687}) + \frac{0.42}{1 + 4.25 \cdot 10^4 Re_{ds}^{-1.16}} \quad (\text{1.3.44})$$

$$C_{d,s} = \frac{24}{60.73} (1 + 0.15 \cdot 60.73^{0.687}) + \frac{0.42}{1 + 4.25 \cdot 10^4 \cdot 60.73^{-1.16}} = 1.392$$

This drag coefficient is now modified to yield the drag coefficient of a single non-spherical particle by using equation 1.3.46:

$$C_{d,ns} = \left(\frac{1}{0.843 \log \frac{\psi}{0.065}} \right)^2 C_{d,s} \quad (1.3.46)$$

where the sphericity of cement is taken as 0.1965. This yields the drag coefficient for the non-spherical particle as:

$$C_{d,ns} = \left(\frac{1}{0.843 \log \frac{0.1965}{0.065}} \right)^2 1.392 = 8.489$$

The drag coefficient of a particle in a cloud can be determined from equation 1.3.47 as:

$$C_{d,c} = C_{d,ns} e^{-4.7} \quad (1.3.47)$$

$$C_{d,c} = 8.489 \cdot 0.9997^{-4.7} = 8.501$$

where the spherical particle drag coefficient in equation 1.3.47 is replaced by the non-spherical drag coefficient. It is assumed that the effects associated with a cloud of spherical particles are equally applicable to non-spherical particles.

C.2.4 Determination of the particle free fall or terminal velocity

The free fall velocity can be estimated by determining the constant falling velocity once the drag and gravitational forces on the particle are in balance using equation 1.3.48.

$$w_{s,c} = \sqrt{\frac{4d_s g (\rho_s - \rho_g)}{3\rho_g C_{d,c}}} \quad (1.3.48)$$

$$w_{s,c} = \sqrt{\frac{4 \cdot 32.69 \cdot 10^{-6} \cdot 9.81 \cdot (3114.23 - 0.993)}{3 \cdot 0.993 \cdot 8.501}} = 0.397 \text{ m/s}$$

C.2.5 Determination of the total friction coefficient

Equation 5.3.5 can be integrated under the assumptions that the total friction coefficient is constant over the length of the test section and that the pressure, density, solids velocity, air velocity and voidage vary linearly along the test section so that one can assume constant average values along the test section.

Equation 5.3.5 then becomes:

$$\begin{aligned}\lambda_{tot} &= (\lambda_g + \mu\lambda_s) \\ &= \left(-\frac{\Delta P}{\Delta L} - (1-e)(\rho_s - \rho_g)g \frac{w_{s,c}}{c} - e\rho_g v_e \frac{\Delta v_e}{\Delta L} - (1-e)\rho_s c \frac{\Delta c}{\Delta L} \right) \frac{2d}{e\rho_g v_e^2}\end{aligned}\quad (C.2.5)$$

Note that the terms $\Delta v_e/\Delta L$ and $\Delta c/\Delta L$ are retained in the differential equation. These two terms are usually neglected during the determination of the friction coefficient but it was found that the simulation results are more accurate in terms of the pressure drop slope if these terms are retained.

Rewriting the interstitial air velocity in terms of the voidage and the average velocity as can be derived from equation 3.3.7:

$$v_e = \frac{v}{e} \quad (3.3.7 \text{ a})$$

and hence rewrite equation C.2.5 as:

$$\begin{aligned}\lambda_{tot} &= (\lambda_g + \mu\lambda_s) \\ &= \left(-\frac{\Delta P}{\Delta L} - (1-e)(\rho_s - \rho_g)g \frac{w_{s,c}}{c} - \rho_g v \frac{\Delta\left(\frac{v}{e}\right)}{\Delta L} - (1-e)\rho_s c \frac{\Delta c}{\Delta L} \right) \frac{2de}{\rho_g v^2}\end{aligned}\quad (C.2.6)$$

Using an average value of the density, superficial air velocity, voidage and solids velocity equation C.2.6 can be solved for the total friction coefficient as:

$$\begin{aligned}\lambda_{tot} &= \left(106.93 - (1 - 0.9997)(3114.23 - 0.993)9.81 \frac{0.397}{28.7} - 0.993 \cdot 35.43 \cdot 0.0283 \right. \\ &\quad \left. - (1 - 0.9997)3114.23 \cdot 28.70.0228 \right) \frac{2 \cdot 0.1016 \cdot 0.9997}{0.993 \cdot 35.43^2} = 0.01715\end{aligned}$$

The total friction coefficient is determined for 48 data points. These exclude data points which lie beyond the settling limit where particles show bed formation at the bottom of the pipe due to a low conveying air velocity. It must be borne in mind that the mathematical model is valid only under the assumption that all particles are equally dispersed in the pipeline. This is not the case during bed formation and hence these data points have to be discarded.

C.2.6 Determination of the solids impact and friction coefficient

Not all of the two-phase flow differential equations can be rewritten in a form containing only the total friction coefficient. The equation of motion for the particles (equation 5.3.6 and 5.3.8) still contains the solids impact and friction coefficient λ_s^* as described in detail in section 5.3 for which a separate correlation is required. As a result of the definition of the total friction coefficient, this requires the subtraction of the air alone friction coefficient from the total friction coefficient by rearranging equation 5.3.1 in chapter five as follows:

$$\lambda_s^* = (\lambda_{tot} - \lambda_g) \frac{v}{\mu ce} \quad (C.2.7)$$

In an attempt to make the subsequent simulation programme for two-phase flow as useful as possible it was decided to use the Haaland equation [83HA1] to determine the air alone friction coefficient. This allows the programme to be used for the simulation of air flow alone for the pipe line leading to the pneumatic conveyor and then switching to two-phase flow at the material feed point for positive pressure systems. It is also used for the determination of the total friction coefficient in bend flow. Implementation of the Haaland [83HA1] equation 1.3.16 first requires the determination of the pipe Reynolds number :

$$Re_d = \frac{\rho_g v d}{\mu'} \quad (C.2.8)$$

$$Re_d = \frac{0.993 \cdot 35.43 \cdot 0.1016}{18938 \cdot 10^{-5}} = 188750$$

The air alone friction coefficient can then be calculated from equation 1.3.16:

$$\lambda_g = \left(-1.81 \log \left[\frac{6.9}{Re_d} + \left(\frac{\varepsilon/d}{3.7} \right)^{1.11} \right] \right)^{-2} \quad (1.3.16)$$

$$\lambda_g = \left(-1.81 \log \left[\frac{6.9}{188750} + \left(\frac{0}{3.7} \right)^{1.11} \right] \right)^{-2} = 0.0157$$

with the solids impact and friction coefficient determined from equation C.2.7 as:

$$\lambda_s^* = (0.01715 - 0.0157) \frac{35.43}{0.741 \cdot 28.70 \cdot 0.9997} = 0.0024057$$

C.2.7 Determination of the alternative solids impact and friction coefficient

As a result of the poor prediction of the solids velocity from the simulations using the alternative solids impact and friction coefficient, a method was developed to correlate the solids friction and impact coefficient directly from the solids motion equation. Integrating the motion equation under the same assumptions as those made for equation C.2.5, equation 5.3.8 becomes:

$$\lambda_s' = \frac{2de}{c} \left[\frac{3}{4} C_{d,c} \frac{\rho_g}{\rho_s d_s} \frac{(v_e - c)^2}{ce} + \lambda_{tot} \frac{\rho_g v_e^2}{\rho_s c 2d} + \frac{(1-e)(\rho_s - \rho_g)}{e c \rho_s} g \frac{w_{s,c}}{c} + \frac{\rho_g}{\rho_s c} v_e \frac{\Delta v_e}{\Delta L} - \frac{\Delta c}{\Delta L} \right] \quad (C.2.9)$$

Equation C.2.9 can be modified by introducing equation C.2.6 and solved to yield:

$$\lambda_s' = 0.694$$

The difference to the data in table C.1 at the end of section C.4 is due to round off errors in the sample calculations.

C.2.8 Correlation method for friction coefficients

On the basis of previously published correlations for friction coefficients as discussed in section 1.3.7 it was decided to use the following non-dimensional numbers in the friction coefficient correlation: solids mass flow ratio μ , the Froude number Fr , the pipe diameter Reynolds number Re_d and the ratio of the particle diameter to the pipe diameter d_s/d .

The form of the correlation equation can be written as:

$$\lambda = \exp(\alpha) \mu^\beta Fr^\gamma Re_d^\delta \left(\frac{d_s}{d} \right)^\varepsilon \quad (C.2.10)$$

where the coefficients α , β , γ , δ and ε have to be determined from experimental data by means of a least squares approximation.

The method is based on taking the logarithm of equation C.2.10 and utilising the basic properties for logarithms and exponents, rewriting this as:

$$\ln \lambda = \alpha \ln \exp(1) + \beta \ln \mu + \gamma \ln Fr + \delta \ln Re_d + \varepsilon \ln \left(\frac{d_s}{d} \right) \quad (C.2.11)$$

The error function which is the difference between the experimentally determined friction coefficient and the proposed correlation equation can then be written as:

$$Error_i = \ln \lambda_i - \left(\alpha \ln e + \beta \ln \mu_i + \gamma \ln Fr_i + \delta \ln Re_{di} + \varepsilon \ln \left(\frac{d_s}{d} \right)_i \right) \quad (C.2.12)$$

and the sum of the squares of the error with N the number of experimental data points:

$$S = \sum_{i=1}^N [Error_i]^2 \quad (C.2.13)$$

$$= \sum_{i=1}^N \left[\ln \lambda_i - \alpha \ln e - \beta \ln \mu_i - \gamma \ln Fr_i - \delta \ln Re_{di} - \varepsilon \ln \left(\frac{d_s}{d} \right)_i \right]^2$$

To obtain the values of the coefficients the sum of the squares of the error can be minimised by successively differentiating equation C.2.13 with respect to each of the non-dimensional groups and setting the result equals to zero. The resulting set of five simultaneous equations can be written in a matrix form as follows:

$\mathbf{A} =$

$$\begin{bmatrix} N & \sum_{i=1}^N \ln \mu_i & \sum_{i=1}^N \ln Fr_i & \sum_{i=1}^N \ln Re_{di} & \sum_{i=1}^N \ln \left(\frac{d_s}{d} \right)_i \\ \sum_{i=1}^N \ln \mu_i & \sum_{i=1}^N (\ln \mu_i)^2 & \sum_{i=1}^N \ln \mu_i \ln Fr_i & \sum_{i=1}^N \ln \mu_i \ln Re_{di} & \sum_{i=1}^N \ln \mu_i \ln \left(\frac{d_s}{d} \right)_i \\ \sum_{i=1}^N \ln Fr_i & \sum_{i=1}^N \ln \mu_i \ln Fr_i & \sum_{i=1}^N (\ln Fr_i)^2 & \sum_{i=1}^N \ln Fr_i \ln Re_{di} & \sum_{i=1}^N \ln Fr_i \ln \left(\frac{d_s}{d} \right)_i \\ \sum_{i=1}^N \ln Re_{di} & \sum_{i=1}^N \ln \mu_i \ln Re_{di} & \sum_{i=1}^N \ln Fr_i \ln Re_{di} & \sum_{i=1}^N (\ln Re_{di})^2 & \sum_{i=1}^N \ln Re_{di} \ln \left(\frac{d_s}{d} \right)_i \\ \sum_{i=1}^N \ln \left(\frac{d_s}{d} \right)_i & \sum_{i=1}^N \ln \mu_i \ln \left(\frac{d_s}{d} \right)_i & \sum_{i=1}^N \ln Fr_i \ln \left(\frac{d_s}{d} \right)_i & \sum_{i=1}^N \ln Re_{di} \ln \left(\frac{d_s}{d} \right)_i & \sum_{i=1}^N \left(\ln \left(\frac{d_s}{d} \right)_i \right)^2 \end{bmatrix}$$

$$\mathbf{x} = \begin{bmatrix} \alpha \\ \beta \\ \gamma \\ \delta \\ \varepsilon \end{bmatrix} \quad \mathbf{B} = \begin{bmatrix} \sum_{i=1}^N \ln \lambda_i \\ \sum_{i=1}^N \ln \lambda_i \ln \mu_i \\ \sum_{i=1}^N \ln \lambda_i \ln Fr_i \\ \sum_{i=1}^N \ln \lambda_i \ln Re_{di} \\ \sum_{i=1}^N \ln \lambda_i \ln \left(\frac{d_s}{d} \right)_i \end{bmatrix} \quad \text{where } \mathbf{Ax} = \mathbf{B} \quad (C.2.14)$$

Equation C.2.14 is solved in a spreadsheet programme Lotus 1-2-3 by using matrix inversion and multiplication functions as follows:

$$\mathbf{x} = \mathbf{A}^{-1}\mathbf{B} \quad (\text{C.2.15})$$

It must be noted that the accuracy of the coefficients depends on the form of the matrix equation C.2.14. Gerald and Wheatly [89GE1] note that the number of coefficients to be determined with this method should be limited to 5 to minimise the effect of ill-conditioning of the matrix equation C.2.14 when using standard methods for solving matrix equation C.2.15.

Utilising this method for 48 experimental data points for cement results in the coefficients for

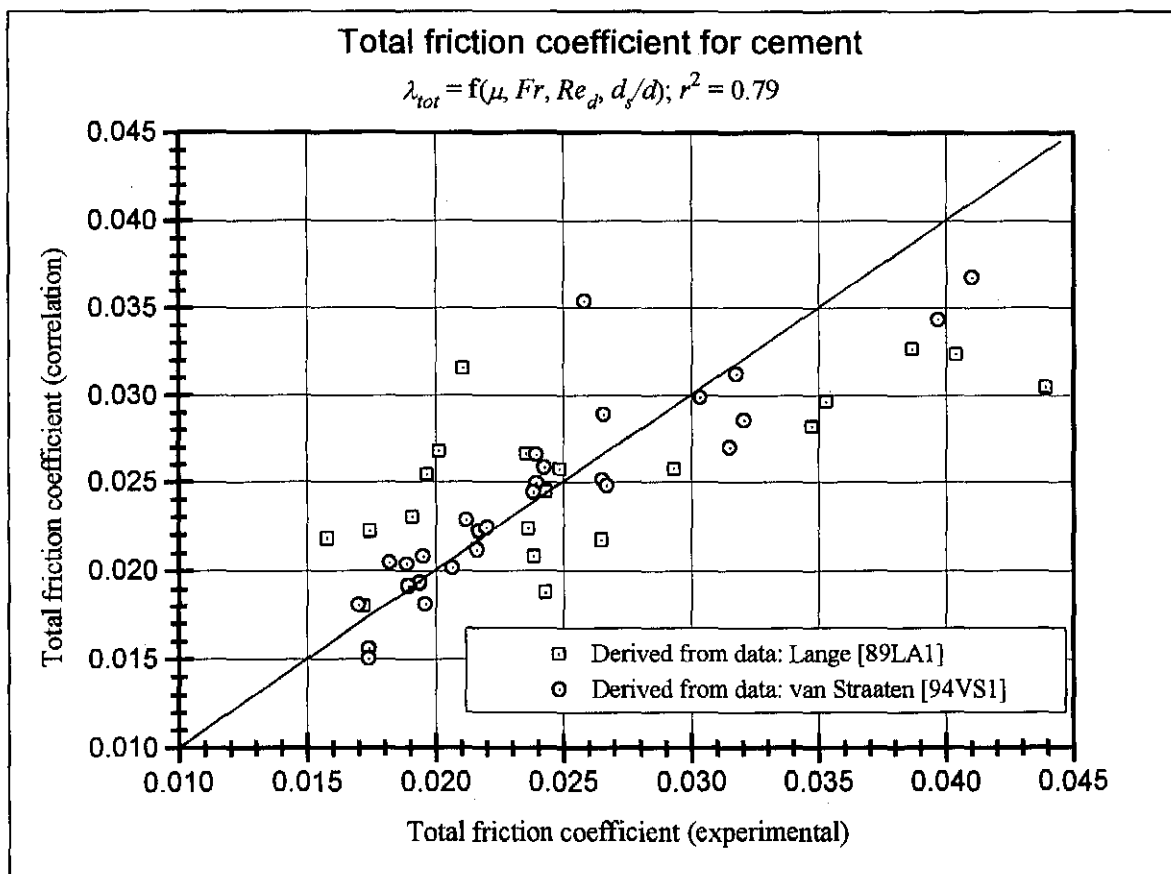


Fig. C.1 Correlation of the total friction coefficient for cement

the total friction coefficient in equation C.2.16. Figure C.1 depicts the correlation results compared to the experimental values graphically.

$$\lambda_{tot} = \exp(\alpha)\mu^\beta Fr^\gamma Re_d^\delta \left(\frac{d_s}{d}\right)^\epsilon \quad (\text{C.2.16})$$

$$\alpha = -0.082$$

$$\beta = 0.3171$$

$$\gamma = 0.0019$$

$$\delta = -0.7420$$

$$\varepsilon = -0.6418$$

$$\text{Correlation coefficient } r^2 = 0.79$$

The solids impact and friction coefficient is given in equation C.2.17. Figure C.2 depicts the correlation results compared to the experimental values graphically.

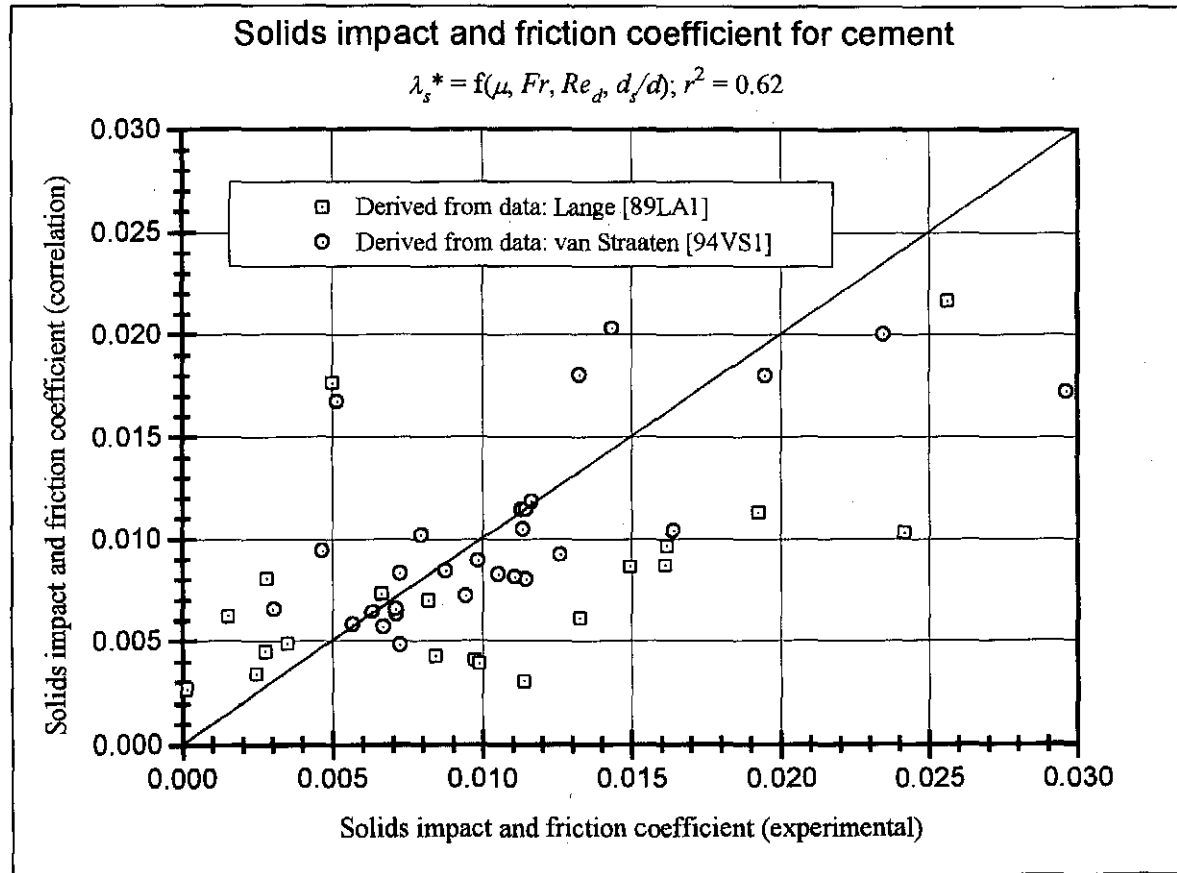


Fig. C.2 Correlation of the solids impact and friction coefficient for cement

$$\lambda_s^* = \exp(\alpha)\mu^\beta Fr^\gamma Re_d^\delta \left(\frac{d_s}{d}\right)^\varepsilon \tag{C.2.17}$$

$$\alpha = 17.1178$$

$$\beta = 0.1778$$

$$\gamma = 1.8984$$

$$\delta = -6.0728$$

$$\varepsilon = -4.6598$$

$$\text{Correlation coefficient } r^2 = 0.62$$

The alternative solids impact and friction coefficient can be determined as:

$$\lambda_s' = \exp(\alpha) \mu^\beta Fr^\gamma Re_d^\delta \left(\frac{d_s}{d}\right)^\epsilon \quad (\text{C.2.18})$$

$$\alpha = -23.8983$$

$$\beta = -0.2059$$

$$\gamma = -0.6818$$

$$\delta = 0.8306$$

$$\epsilon = -2.2785$$

$$\text{Correlation coefficient } r^2 = 0.95$$

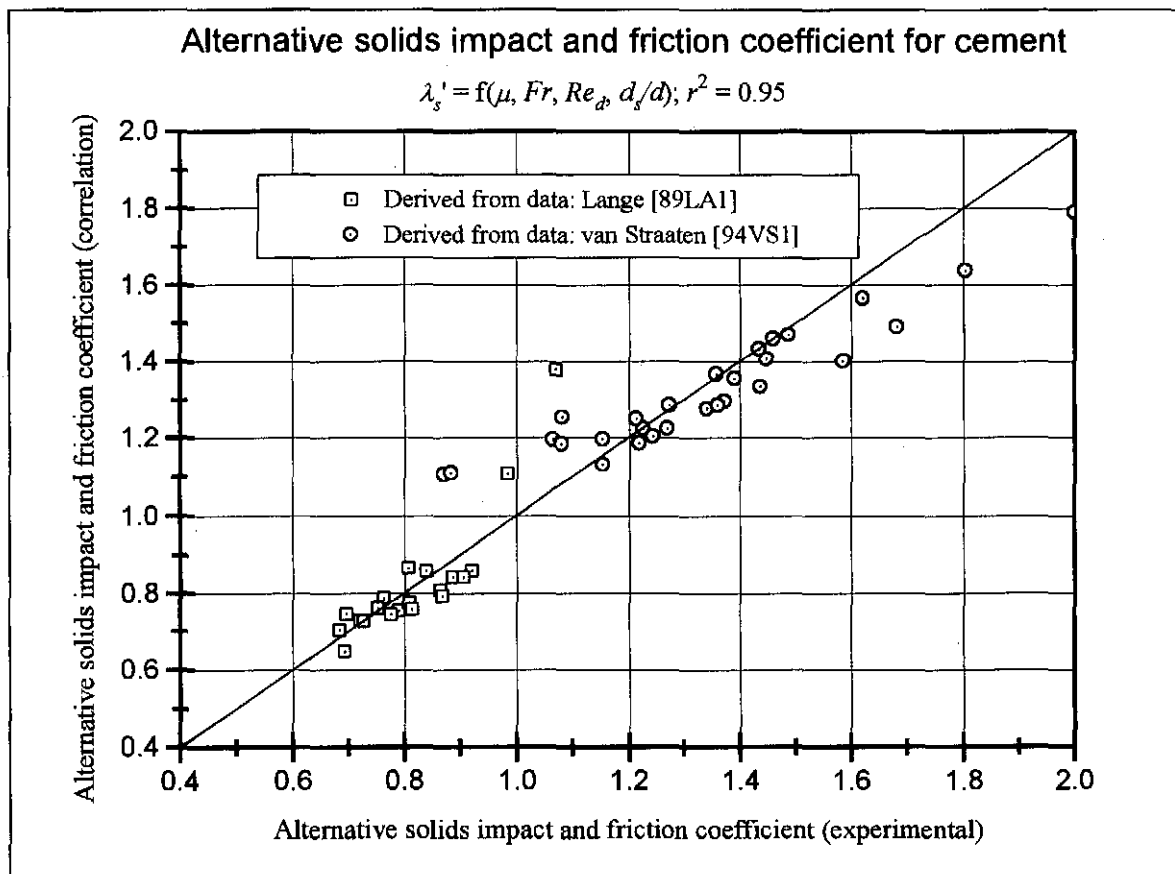


Fig. C.3 Correlation of the alternative solids impact and friction coefficient for cement

Figure C.3 depicts the correlation results compared to the experimental values graphically.

C.3 SPHERICITY DETERMINATION FOR TUBE ICE

The tube ice used by Sheer [91SH1] is shaped like a thick walled cylinder with an average outer diameter of 34 mm and an average length of 30 mm and a hollow central core. Based on

an average mass of a single ice particle determined by Sheer [91SH1], the volume of the particle can be calculated at the following temperature and particle density:

$$T = 0^{\circ}\text{C} \quad \rho_s = 921 \text{ kg/m}^3 \quad [89GI1]$$

$$V_s = \frac{\bar{m}}{\rho_s} = \frac{0.0174}{921} = 1.88925 \cdot 10^{-5} \text{ m}^3 \quad (\text{C.3.1})$$

The equivalent spherical diameter with this volume becomes:

$$d_s = \left(\frac{6V_s}{\pi} \right)^{\frac{1}{3}} = \left(\frac{6 \cdot 1.88925 \cdot 10^{-5}}{\pi} \right)^{\frac{1}{3}} = 0.03304 \text{ mm} \quad (\text{C.3.2})$$

Neglecting the centre hole in the ice particle, the outer surface area of the tube becomes:

$$A_{s,ns} = \pi d \left(\frac{d}{2} + L \right) = \pi 0.034 \left(\frac{0.034}{2} + 0.030 \right) = 5.02 \cdot 10^{-3} \text{ m}^2 \quad (\text{C.3.3})$$

Thus the sphericity becomes according to equation 1.3.43 b:

$$\psi = \frac{\pi \left(\frac{6 \cdot 1.88925 \cdot 10^{-5}}{\pi} \right)^{\frac{2}{3}}}{5.02 \cdot 10^{-3}} = 0.683$$

C.4 ICE FRICTION COEFFICIENT CORRELATION METHOD

The same equations and correlation method presented in section C.2 are used to determine the total friction coefficient and alternative solids impact and friction coefficient for tube ice. The friction coefficient correlations obtained in this manner are:

The total friction coefficient:

$$\lambda_{tot} = \exp(\alpha) \mu^{\beta} Fr^{\gamma} Re_d^{\delta} \left(\frac{d_s}{d} \right)^{\varepsilon} \quad (\text{C.4.1})$$

$$\alpha = -45.8383$$

$$\beta = 0.1032$$

$$\gamma = 1.6706$$

$$\delta = 1.8366$$

$$\varepsilon = -3.9847$$

$$\text{Correlation coefficient } r^2 = 0.68$$

Figure C.4 depicts the comparison of the correlated and experimental data.

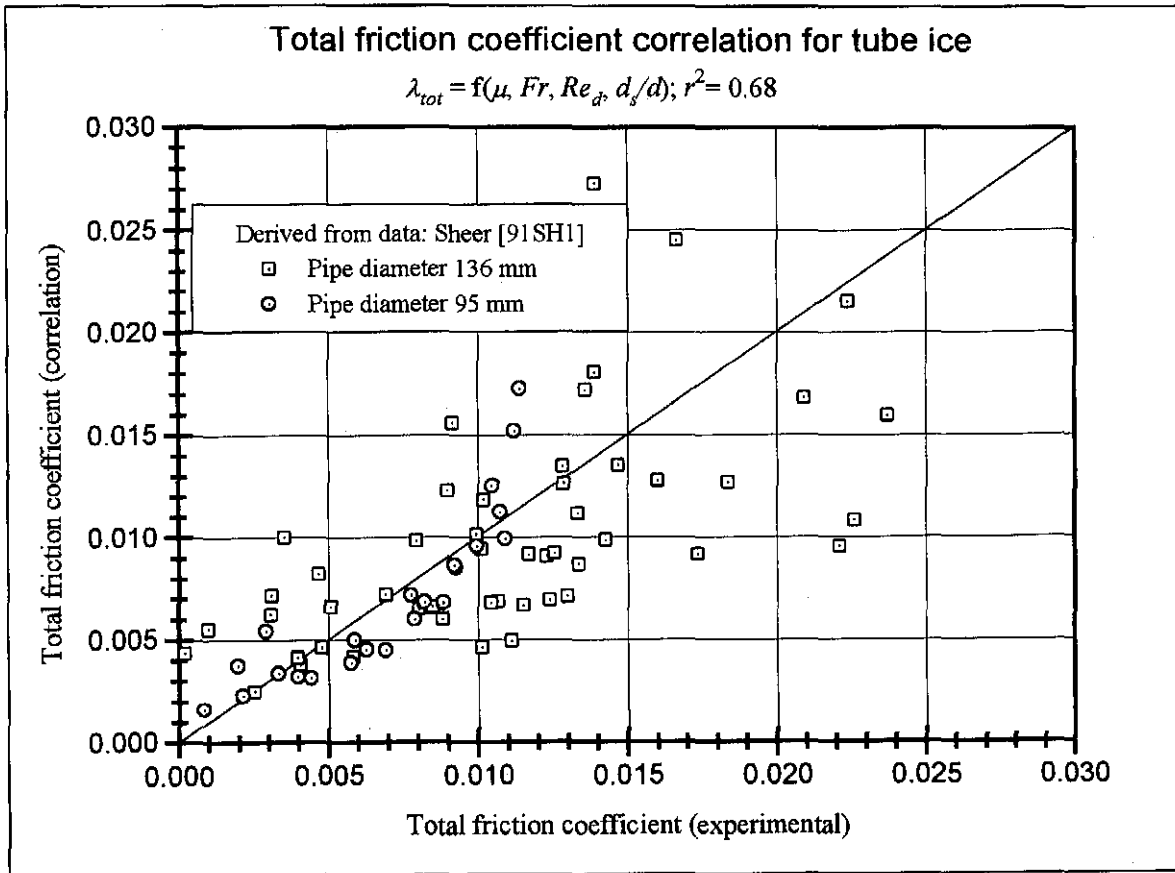


Fig. C.4 Correlation of the total friction coefficient for tube ice

The alternative solids impact and friction coefficient:

$$\lambda_s' = \exp(\alpha) \mu^\beta Fr^\gamma Re_d^\delta \left(\frac{d_s}{d}\right)^\varepsilon \tag{C.4.2}$$

$$\alpha = -22.4667$$

$$\beta = 0.0260$$

$$\gamma = -1.1838$$

$$\delta = 1.6545$$

$$\varepsilon = -2.4511$$

Correlation coefficient $r^2 = 0.99$

Figure C.5 on the following page depicts the correlation results compared to the experimental values graphically.

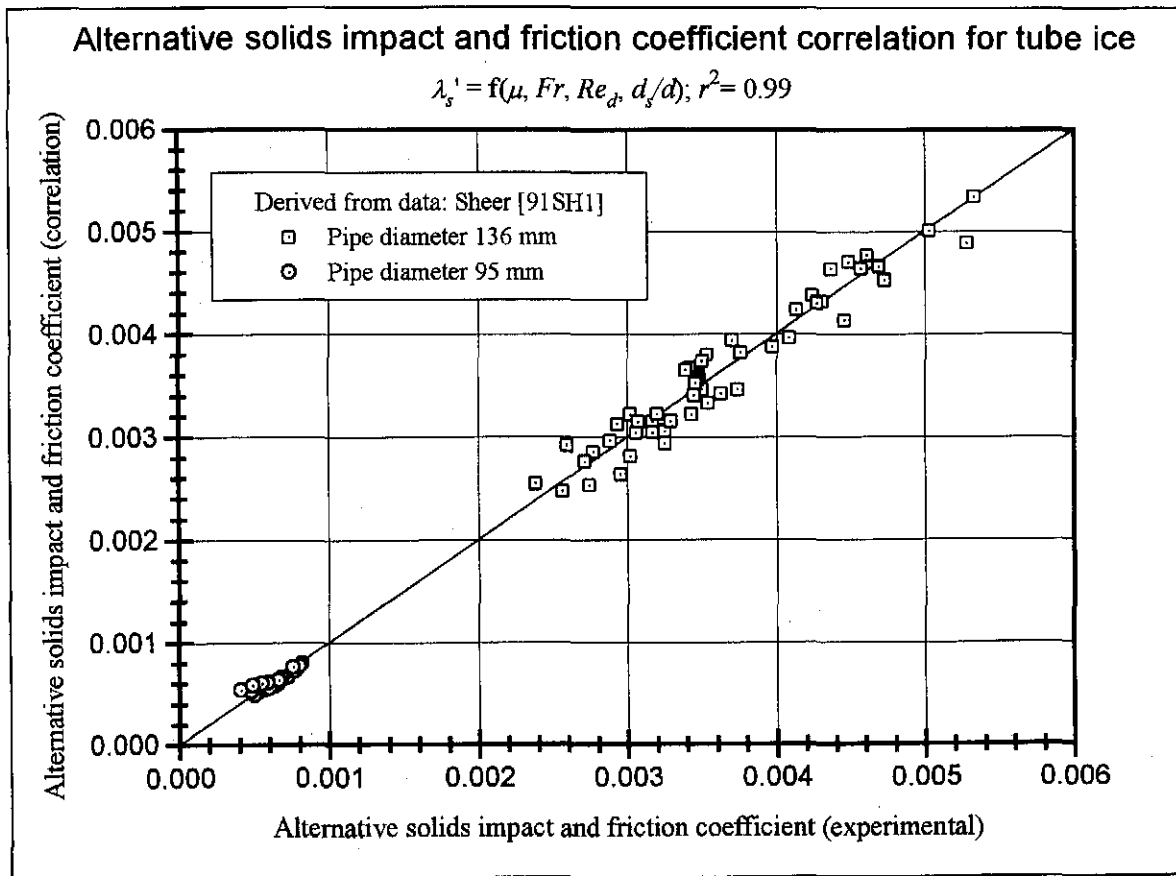


Fig. C.5 Correlation of the alternative solids impact and friction coefficient for tube ice

Tab. C.1 Data used for the friction coefficient correlation for cement
(Data points 1-20 [89LA1]; data points 21-48 [94VS1])

Data point	ρ_s kg/m ³	T °C	μ' kg/ms	d_s/d ---	μ ---	\dot{G} kg/s	$\Delta P/\Delta L$ Pa/m	v m/s	Fr ---	ρ_g kg/m ³
1	3114.23	38.10	0.0000190	3.22E-04	0.518	0.074	31.03	18.40	339.7	0.9600
2	3114.23	36.40	0.0000189	3.22E-04	0.274	0.034	28.74	15.74	248.6	0.9620
3	3114.23	37.10	0.0000189	3.22E-04	0.741	0.211	106.93	35.43	1259.4	0.9930
4	3114.23	39.40	0.0000190	3.22E-04	0.867	0.201	73.10	29.22	856.6	0.9760
5	3114.23	26.10	0.0000184	3.22E-04	0.938	0.207	69.32	26.70	715.3	1.0200
6	3114.23	36.20	0.0000189	3.22E-04	0.952	0.186	86.17	24.51	602.7	0.9820
7	3114.23	35.20	0.0000189	3.22E-04	0.951	0.284	166.43	36.73	1353.6	1.0010
8	3114.23	36.30	0.0000189	3.22E-04	1.013	0.270	131.08	33.09	1098.6	0.9960
9	3114.23	31.80	0.0000187	3.22E-04	1.111	0.278	112.72	30.64	941.9	1.0090
10	3114.23	38.70	0.0000190	3.22E-04	1.264	0.281	94.55	27.80	775.4	0.9850
11	3114.23	36.20	0.0000189	3.22E-04	1.299	0.277	82.63	26.60	709.9	0.9890
12	3114.23	37.60	0.0000190	3.22E-04	1.396	0.266	98.65	23.79	567.8	0.9900
13	3114.23	34.90	0.0000188	3.22E-04	1.368	0.248	110.02	22.50	507.9	0.9930
14	3114.23	34.20	0.0000188	3.22E-04	1.479	0.255	91.28	21.30	455.2	0.9990
15	3114.23	40.50	0.0000191	3.22E-04	1.352	0.390	172.37	36.01	1301.0	0.9900
16	3114.23	24.30	0.0000184	3.22E-04	1.406	0.395	90.30	33.17	1103.9	1.0450
17	3114.23	28.70	0.0000186	3.22E-04	1.555	0.374	84.97	29.00	843.8	1.0240
18	3114.23	31.00	0.0000187	3.22E-04	1.692	0.368	124.59	26.55	707.2	1.0140
19	3114.23	30.90	0.0000187	3.22E-04	1.844	0.359	60.15	23.66	561.7	1.0140
20	3114.23	28.40	0.0000185	3.22E-04	1.781	0.323	95.27	21.92	482.1	1.0240
21	2700.00	23.00	0.0000183	2.697E-04	0.624	0.100	58.00	18.48	342.5	1.0674
22	2700.00	24.00	0.0000183	2.697E-04	0.582	0.127	72.60	24.91	622.6	1.0836
23	2700.00	37.00	0.0000189	2.697E-04	0.444	0.118	87.70	30.95	960.8	1.0576
24	2700.00	38.50	0.0000190	2.697E-04	0.309	0.086	96.60	32.50	1059.9	1.0553
25	2700.00	38.00	0.0000190	2.697E-04	0.316	0.093	108.60	34.26	1177.6	1.0637
26	2700.00	21.00	0.0000182	2.697E-04	1.243	0.189	66.10	17.28	299.6	1.0842
27	2700.00	23.00	0.0000183	2.697E-04	0.926	0.201	78.80	24.34	594.6	1.0997
28	2700.00	31.00	0.0000187	2.697E-04	0.660	0.174	90.80	29.93	898.8	1.0881
29	2700.00	35.00	0.0000188	2.697E-04	0.723	0.195	100.80	31.11	970.9	1.0683
30	2700.00	42.00	0.0000192	2.697E-04	0.649	0.187	116.90	33.81	1147.0	1.0538
31	2700.00	30.00	0.0000186	2.697E-04	1.641	0.357	106.60	24.80	617.2	1.0865
32	2700.00	40.00	0.0000191	2.697E-04	1.503	0.343	113.00	26.37	697.6	1.0691
33	2700.00	42.00	0.0000192	2.697E-04	1.163	0.302	126.70	29.77	889.0	1.0777
34	2700.00	43.00	0.0000192	2.697E-04	1.398	0.398	136.20	32.16	1038.0	1.0929
35	2700.00	34.00	0.0000188	2.697E-04	0.655	0.121	61.30	22.54	509.9	1.0121
36	2700.00	37.00	0.0000189	2.697E-04	0.620	0.142	87.00	28.00	786.6	1.0110
37	2700.00	38.00	0.0000190	2.697E-04	0.567	0.142	85.70	30.52	934.7	1.0108
38	2700.00	39.00	0.0000190	2.697E-04	0.522	0.138	98.30	32.28	1045.5	1.0113
39	2700.00	41.00	0.0000191	2.697E-04	0.515	0.147	120.10	34.78	1213.7	1.0102
40	2700.00	37.00	0.0000189	2.697E-04	0.832	0.153	68.20	22.62	513.4	1.0055
41	2700.00	35.00	0.0000188	2.697E-04	2.121	0.442	84.50	25.22	638.0	1.0193
42	2700.00	36.00	0.0000189	2.697E-04	0.798	0.181	91.90	27.55	761.7	1.0167
43	2700.00	39.00	0.0000190	2.697E-04	0.793	0.198	100.10	30.56	937.3	1.0095
44	2700.00	40.00	0.0000191	2.697E-04	0.721	0.191	115.20	32.47	1057.7	1.0081
45	2700.00	44.00	0.0000193	2.697E-04	0.697	0.197	127.00	34.99	1228.1	0.9988
46	2700.00	28.00	0.0000185	2.697E-04	1.429	0.257	93.90	21.33	456.3	1.0419
47	2700.00	30.00	0.0000186	2.697E-04	1.143	0.260	119.60	26.93	727.6	1.0436
48	2700.00	33.50	0.0000188	2.697E-04	1.040	0.258	121.10	29.54	875.5	1.0340

Tab. C.1 continued

Data point	c m/s	e ---	v_e m/s	Re_{ds} ---	$C_{d,s}$ ---	$C_{d,ns}$ ---	$C_{d,c}$ ---	$w_{s,c}$ m/s	Re_d ---	v_3 m/s
1	14.90	0.9998	18.404	30.418	2.026	12.354	12.365	0.335	94539.49	18.730
2	12.75	0.9999	15.742	26.182	2.213	13.494	13.501	0.320	81372.49	15.700
3	28.70	0.9997	35.440	60.731	1.392	8.489	8.501	0.397	188749.86	35.320
4	23.68	0.9997	29.230	48.958	1.556	9.491	9.506	0.379	152161.54	29.100
5	21.63	0.9996	26.710	48.295	1.567	9.559	9.576	0.369	150100.60	26.620
6	19.86	0.9996	24.519	41.637	1.698	10.353	10.371	0.362	129408.25	24.430
7	29.76	0.9996	36.744	63.758	1.358	8.283	8.298	0.400	198157.75	36.440
8	26.81	0.9996	33.103	57.001	1.438	8.768	8.784	0.390	177157.10	32.920
9	24.82	0.9996	30.654	54.057	1.478	9.011	9.030	0.382	168007.86	30.480
10	22.52	0.9995	27.814	47.087	1.589	9.689	9.711	0.373	146346.28	27.700
11	21.55	0.9995	26.614	45.510	1.618	9.867	9.891	0.369	141444.18	26.520
12	19.27	0.9995	23.803	40.607	1.721	10.496	10.523	0.357	126204.37	23.700
13	18.23	0.9995	22.512	38.773	1.765	10.767	10.794	0.352	120504.48	22.420
14	17.25	0.9994	21.312	36.989	1.812	11.052	11.083	0.347	114961.84	21.200
15	29.18	0.9995	36.029	61.040	1.388	8.467	8.488	0.398	189712.58	35.760
16	26.88	0.9994	33.189	61.747	1.380	8.418	8.441	0.388	191907.31	33.060
17	23.50	0.9994	29.018	52.322	1.503	9.165	9.192	0.376	162615.35	28.910
18	21.51	0.9993	26.568	47.166	1.587	9.680	9.711	0.368	146589.86	26.410
19	19.17	0.9993	23.678	42.042	1.689	10.299	10.335	0.356	130665.45	23.600
20	17.76	0.9993	21.936	39.577	1.746	10.645	10.681	0.349	123006.12	21.830
21	14.56	0.9997	18.483	29.702	2.054	12.526	12.545	0.269	109549.62	18.391
22	19.73	0.9997	24.917	40.650	1.720	10.490	10.504	0.292	149554.73	24.761
23	24.47	0.9998	30.952	49.287	1.551	9.457	9.467	0.311	175623.48	30.763
24	25.55	0.9998	32.508	51.656	1.513	9.227	9.233	0.315	183403.56	32.272
25	26.97	0.9998	34.265	54.882	1.466	8.941	8.947	0.319	195089.88	33.978
26	13.83	0.9994	17.290	28.213	2.117	12.909	12.947	0.263	104587.94	17.190
27	19.53	0.9995	24.355	40.317	1.728	10.537	10.561	0.289	148702.54	24.190
28	23.90	0.9997	29.940	49.045	1.555	9.482	9.497	0.306	177327.86	29.661
29	24.93	0.9996	31.119	50.048	1.538	9.381	9.397	0.310	179197.36	30.913
30	27.06	0.9997	33.823	53.660	1.483	9.045	9.059	0.318	188939.70	33.536
31	20.44	0.9992	24.823	40.584	1.722	10.499	10.539	0.291	147096.87	24.646
32	21.68	0.9993	26.388	42.455	1.680	10.244	10.279	0.297	150198.68	26.172
33	24.31	0.9994	29.784	48.312	1.567	9.558	9.583	0.306	170108.93	29.562
34	26.70	0.9993	32.186	52.938	1.494	9.109	9.139	0.311	185960.16	31.947
35	17.83	0.9997	22.550	34.360	1.889	11.520	11.537	0.288	123326.01	22.434
36	22.24	0.9997	28.008	42.631	1.676	10.221	10.235	0.306	151907.71	27.826
37	24.24	0.9997	30.531	46.464	1.600	9.758	9.770	0.313	165166.01	30.325
38	25.62	0.9998	32.289	49.164	1.553	9.470	9.481	0.318	174347.76	32.004
39	27.64	0.9998	34.789	52.914	1.494	9.112	9.122	0.324	186754.82	34.450
40	18.00	0.9996	22.630	34.254	1.892	11.540	11.561	0.288	122057.51	22.496
41	21.09	0.9990	25.241	38.709	1.767	10.776	10.825	0.296	138599.52	25.034
42	22.03	0.9996	27.563	42.187	1.686	10.279	10.298	0.304	150687.89	27.355
43	24.51	0.9996	30.575	46.466	1.600	9.758	9.775	0.313	164780.54	30.309
44	26.01	0.9997	32.479	49.292	1.551	9.457	9.472	0.318	174386.67	32.167
45	28.05	0.9997	34.997	52.625	1.498	9.138	9.151	0.325	184425.52	34.626
46	17.28	0.9993	21.340	33.461	1.918	11.695	11.733	0.281	121879.87	21.169
47	21.83	0.9995	26.944	42.323	1.683	10.261	10.288	0.300	153399.45	26.673
48	23.94	0.9995	29.555	45.999	1.609	9.811	9.833	0.308	165302.18	29.241

Tab.C.1 continued

Data point	v_{e3} m/s	v_9 m/s	v_{e9} m/s	c_3 m/s	c_9 m/s	$\Delta v_e/\Delta L$ m/sm	$\Delta c/\Delta L$ m/sm	λ_g ---	λ_{tot} ---	λ_s^* ---	λ_s ---
1	18.726	18.410	18.406	14.695	14.444	-0.053	-0.042	0.018	0.020	0.005	0.983
2	15.698	15.750	15.748	12.228	12.267	0.008	0.006	0.019	0.024	0.026	1.070
3	35.310	35.490	35.480	28.391	28.528	0.028	0.023	0.016	0.017	0.002	0.697
4	29.090	29.270	29.260	23.347	23.483	0.028	0.023	0.016	0.017	0.002	0.763
5	26.610	26.730	26.720	21.381	21.470	0.018	0.015	0.016	0.019	0.004	0.806
6	24.421	24.540	24.531	19.549	19.637	0.018	0.015	0.017	0.029	0.016	0.839
7	36.426	36.880	36.866	29.662	30.020	0.073	0.060	0.016	0.024	0.011	0.684
8	32.907	33.210	33.197	26.731	26.967	0.048	0.039	0.016	0.024	0.010	0.721
9	30.466	30.720	30.706	24.787	24.982	0.040	0.033	0.016	0.024	0.008	0.753
10	27.686	27.820	27.806	22.536	22.634	0.020	0.016	0.016	0.025	0.008	0.791
11	26.507	26.650	26.636	21.560	21.666	0.022	0.018	0.017	0.024	0.007	0.808
12	23.687	23.820	23.807	19.234	19.331	0.020	0.016	0.017	0.035	0.016	0.863
13	22.408	22.550	22.538	18.136	18.241	0.022	0.018	0.017	0.044	0.024	0.885
14	21.188	21.310	21.298	17.170	17.259	0.018	0.015	0.017	0.040	0.019	0.919
15	35.741	36.130	36.111	29.643	29.950	0.062	0.051	0.016	0.026	0.010	0.693
16	33.041	33.120	33.101	27.428	27.478	0.010	0.008	0.016	0.016	0.000	0.727
17	28.892	29.030	29.012	23.900	24.000	0.020	0.017	0.016	0.020	0.003	0.777
18	26.392	26.610	26.592	21.810	21.975	0.033	0.028	0.016	0.035	0.013	0.815
19	23.583	23.680	23.662	19.458	19.524	0.013	0.011	0.017	0.021	0.003	0.867
20	21.814	21.960	21.944	17.890	17.996	0.022	0.018	0.017	0.039	0.015	0.905
21	18.385	18.557	18.551	14.495	14.625	0.011	0.009	0.017	0.032	0.030	1.999
22	24.754	25.006	24.999	19.611	19.805	0.017	0.013	0.016	0.022	0.011	1.622
23	30.756	31.763	31.756	24.324	25.114	0.069	0.054	0.016	0.017	0.003	1.448
24	32.267	32.653	32.648	25.372	25.672	0.026	0.021	0.016	0.017	0.007	1.486
25	33.973	34.537	34.532	26.749	27.189	0.038	0.030	0.016	0.017	0.007	1.434
26	17.179	17.356	17.345	13.763	13.896	0.011	0.009	0.018	0.041	0.023	1.804
27	24.179	24.426	24.415	19.409	19.598	0.016	0.013	0.016	0.024	0.011	1.459
28	29.651	29.701	29.691	23.687	23.719	0.003	0.002	0.016	0.019	0.006	1.358
29	30.902	31.294	31.283	24.776	25.082	0.026	0.021	0.016	0.020	0.006	1.273
30	33.525	34.047	34.036	26.843	27.252	0.035	0.028	0.016	0.019	0.007	1.226
31	24.626	25.027	25.007	20.315	20.629	0.026	0.022	0.016	0.032	0.011	1.082
32	26.153	26.542	26.523	21.522	21.827	0.025	0.021	0.016	0.030	0.011	1.065
33	29.545	29.978	29.961	24.140	24.479	0.029	0.023	0.016	0.027	0.011	1.080
34	31.925	32.466	32.444	26.517	26.948	0.036	0.030	0.016	0.024	0.007	0.869
35	22.427	22.652	22.645	17.749	17.921	0.015	0.012	0.017	0.024	0.013	1.681
36	27.818	28.194	28.186	22.097	22.389	0.025	0.020	0.016	0.022	0.011	1.437
37	30.317	30.728	30.720	24.079	24.399	0.028	0.022	0.016	0.018	0.005	1.372
38	31.996	32.027	32.019	25.396	25.414	0.002	0.001	0.016	0.019	0.007	1.340
39	34.442	35.127	35.118	27.379	27.917	0.046	0.037	0.016	0.020	0.009	1.269
40	22.487	22.736	22.727	17.899	18.090	0.016	0.013	0.017	0.027	0.014	1.585
41	25.010	25.373	25.349	20.932	21.216	0.023	0.019	0.017	0.026	0.005	0.883
42	27.345	27.757	27.747	21.872	22.194	0.028	0.022	0.016	0.024	0.012	1.360
43	30.298	30.796	30.785	24.308	24.698	0.033	0.027	0.016	0.021	0.008	1.244
44	32.156	32.745	32.734	25.765	26.228	0.040	0.032	0.016	0.022	0.010	1.218
45	34.615	35.331	35.320	27.764	28.330	0.048	0.039	0.016	0.021	0.009	1.154
46	21.155	21.480	21.465	17.152	17.404	0.021	0.017	0.017	0.040	0.020	1.391
47	26.658	27.190	27.175	21.623	22.043	0.035	0.029	0.016	0.032	0.016	1.213
48	29.227	29.819	29.804	23.694	24.162	0.040	0.032	0.016	0.027	0.013	1.154

C.5 ROOTS BLOWER SAMPLE CALCULATIONS

C.5.1 Determination of the leakage coefficient and swept volume of a blower

The performance curves of the roots blowers which are readily available from the manufacturer can be used to determine the swept volume and leakage coefficient of the blower. These two variables are treated as confidential information by most blower manufacturers. The inlet conditions for the following example of a HIBON XN 4.5 blower are given as:

$$T_i = 20 \text{ }^\circ\text{C} = 293.15 \text{ K}$$

$$P_i = 101300 \text{ Pa}$$

Thus the inlet density can be calculated by means of the ideal gas equation as:

$$\rho_i = \frac{P_i}{RT_i} \quad (\text{C.5.1})$$

$$\rho_i = \frac{101300}{287.07 \cdot 293.15} = 1.2037 \text{ kg/m}^3$$

Choosing a differential pressure of $\Delta P = 20000 \text{ Pa}$ at a rotor revolution speed of $n = 1800 \text{ rpm}$ one can read off an exhaust temperature of $T_e = 39 \text{ }^\circ\text{C}$ or $T_e = 312.15 \text{ K}$ and an air inlet flow rate of $Q_i = 411.76 \text{ m}^3/\text{h}$ or $Q_i = 0.1144 \text{ m}^3/\text{s}$. The average specific heat of the air can be calculated by utilising the inlet and exit temperatures respectively and applying equation C.5.2 [95KR1] where the temperature T is in Kelvin:

$$C_p = 1.045356 \cdot 10^3 - 3.161783 \cdot 10^{-1} T + 7.083814 \cdot 10^{-4} T^2 - 2.705209 \cdot 10^{-7} T^3 \quad (\text{C.5.2})$$

$$C_{pi} = 1006.729 \text{ J/kgK} \quad \text{and:}$$

$$C_{pe} = 1007.456 \text{ J/kgK} \quad \text{which yields an average specific heat at:}$$

$$C_{p \text{ avg}} = 1007.09 \text{ J/kgK}$$

Utilising equation 6.5.3 one can calculate the leakage coefficient as:

$$k = \left(\frac{(T_e - T_i) Q_i \rho_i C_p}{\Delta P} - Q_i \right) / \left(\frac{\Delta P}{\rho_i} \right)^{\frac{1}{2}} \quad (\text{6.5.3})$$

$$k = \left(\frac{19 \cdot 0.1144 \cdot 1.2037 \cdot 1007.09}{20000} - 0.1144 \right) / \left(\frac{20000}{1.2037} \right)^{\frac{1}{2}} = 0.000134 \text{ m}^2$$

Finally equation 6.5.1 is used to determine the swept volume of the blower:

$$V_p = \frac{60(Q_i + k \left(\frac{\Delta P}{\rho_i} \right)^{\frac{1}{2}})}{n} \quad (6.5.1)$$

$$V_p = \frac{60(0.1144 + 0.000134 \left(\frac{20000}{1.2037} \right)^{\frac{1}{2}})}{1800} = 0.00439 \text{ m}^3/\text{rev}$$

This procedure can be carried out for a few data points at varying rotor revolution speed and differential pressures. The results are presented in table C.2 at the end of this appendix. Utilising the average of all data points calculated, the swept volume is determined as:

$$V_p = 0.004516 \text{ m}^3/\text{rev}$$

and the blower leakage coefficient as:

$$k = 0.000170118 \text{ m}^2$$

The leakage coefficient is accurate to within 0.5% of the value stated by the manufacturer and the swept volume is accurate to within 1% of the value given by the manufacturer. The exact values of the leakage coefficient and swept volume may not be stated here as a result of company policy not to allow this information to be divulged.

C.5.2 Roots blower performance prediction

Utilising the blower swept volume and leakage coefficient determined from the performance curves of a HIBON XN 4.5 blower as described in section C.5.1 one can predict the performance curves for the blower at standard conditions to verify that they correspond to the curves published by the manufacturer.

Utilising the following values for the blower swept volume and leakage coefficient respectively:

$$V_p = 0.004516 \text{ m}^3/\text{rev}$$

$$k = 0.0001701 \text{ m}^2$$

one can calculate the air inlet flow rate, exhaust temperature and the shaft power required. As an example using a pressure differential of $\Delta P = 40000$ Pa and a rotor revolution speed of $n = 1400$ rpm in table C.3 and the blower inlet conditions at:

$$T_i = 20 \text{ }^\circ\text{C} = 293.15 \text{ K}$$

$$P_i = 101300 \text{ Pa}$$

one can calculate the inlet density by means of the ideal gas equation C.5.1:

$$\rho_i = 1.2037 \text{ kg/m}^3$$

The air leakage flow rate is determined from equation 6.4.15 as:

$$Q_i = k \left(\frac{\Delta P}{\rho_i} \right)^{\frac{1}{2}} \quad (6.4.15)$$

$$Q_i = 0.0001701 \left(\frac{40000}{1.2037} \right)^{\frac{1}{2}} = 0.03101 \text{ m}^3/\text{s}$$

The theoretical air flow rate can be determined by rearranging equation 6.4.16 to:

$$Q_{th} = \frac{V_p n}{60} \quad (C.5.3)$$

$$Q_{th} = \frac{0.004516 \cdot 1400}{60} = 0.1053 \text{ m}^3/\text{s}$$

This allows the determination of the inlet air flow rate from equation 6.4.6 as:

$$Q_i = Q_{th} - Q_l \quad (C.5.4)$$

$$\begin{aligned} Q_i &= 0.10537 - 0.03101 = 0.07436 \text{ m}^3/\text{s} \\ &= 267.7 \text{ m}^3/\text{h} \end{aligned}$$

Equation 6.4.7 yields the volumetric efficiency as:

$$\eta_{vol} = \frac{Q_i}{Q_{th}} \quad (6.4.7)$$

$$\eta_{vol} = \frac{0.07436}{0.10537} = 0.7057$$

The specific heat of the air can be calculated at inlet conditions utilising equation C.5.2:

$$C_{pi} = 1006.729 \text{ J/kgK}$$

Equation 6.4.17 is used to determine the exhaust temperature as:

$$T_e = \frac{\Delta P}{\rho_i \eta_{vol} C_p} + T_i \quad (6.4.17)$$

$$T_e = \frac{4000}{1.2037 \cdot 0.7057 \cdot 1006.73} + 293.15 = 339.92 \text{ K}$$

$$= 66.77 \text{ }^\circ\text{C}$$

The shaft power required is determined by using equation 6.4.19:

$$\dot{W}_{cv} = Q_{th} \Delta P \quad (6.4.19)$$

$$\dot{W}_{cv} = 0.10537 \cdot 40000 = 4215 \text{ W}$$

The numerical results used to plot figures 6.2 to 6.4 in chapter six are given in table C.3.

C.5.3 Transformation of a standard Roots blower performance curve

To verify the correctness of the performance calculation of roots blower at non-standard inlet conditions, the scaling laws can be used to determine the performance data. This can then be compared to the calculation method described in section 6.4. Assume one wishes to determine the performance curves for an inlet pressure of $P_i = 81300 \text{ Pa}$ and an inlet temperature of $T_i = 40 \text{ }^\circ\text{C}$. From the ideal gas equation C.5.1 the inlet density is at:

$$\rho_i = \frac{81300}{287.07 \cdot 313.15} = 0.9044 \text{ kg/m}^3$$

To determine the scaled differential pressure one first uses equation 6.6.6 to determine the equivalent differential pressure corresponding to the new inlet conditions. The reference conditions (subscript 1 in equation 6.6.6) are taken as those at which the manufacturers performance curves were drawn up namely:

$$T_i = 20 \text{ }^\circ\text{C} = 293.15 \text{ K}$$

$$P_i = 101300 \text{ Pa}$$

Using an example at a differential pressure of $\Delta P = 40000$ Pa at $n = 1800$ rpm one can write:

$$\Delta P_2 = \frac{P_{i2}}{P_{i1}} \Delta P_1 \quad (6.6.6)$$

$$\Delta P_2 = \frac{81300}{101300} 40000 = 32102.665 \text{ Pa}$$

The calculations performed in section C.5.2 can now be repeated using the following variables to determine the inlet volume flow rate, exhaust temperature and shaft power requirements:

$$\rho_i = 0.9044 \text{ kg/m}^3$$

$$T_i = 40 \text{ }^\circ\text{C} = 313.15 \text{ K}$$

$$P_i = 81300 \text{ Pa}$$

$$\Delta P = 32102.665 \text{ Pa}$$

The results are:

$$Q_i = 372.37 \text{ m}^3/\text{h}$$

$$T_e = 86.15 \text{ }^\circ\text{C}$$

$$\dot{W}_{cv} = 4.35 \text{ kW}$$

The same operating point can be predicted by means of the scaling laws. From the blower performance curve the values for the inlet air flow rate, exhaust temperature and power requirements at reference conditions can be read off as:

$$Q_i = 376.48 \text{ m}^3/\text{h}$$

$$T_e = 63 \text{ }^\circ\text{C}$$

$$\dot{W}_{cv} = 5.8 \text{ kW}$$

Applying the scaling laws equations 6.6.5, 6.6.7 and 6.6.8:

$$Q_{i2} = Q_i \quad (6.6.5)$$

$$Q_{i2} = 376.48 \text{ m}^3/\text{h}$$

$$T_{e2} = \frac{T_{i2}}{T_{i1}} T_{e1} \quad (6.6.7)$$

$$T_{e2} = \frac{313.15}{293.15} 336.15 = 359.08 \text{ K}$$
$$= 85.93 \text{ }^\circ\text{C}$$

$$\dot{W}_2 = \frac{P_{i2}}{P_{i1}} \dot{W}_1 \quad (6.6.8)$$

$$\dot{W}_2 = \frac{81300}{101300} 5.8 = 4.65 \text{ kW}$$

These values can now be compared with the values obtained by using the performance calculation method as shown in figures 6.5 To 6.7. The numerical values used to create figures 6.5 to 6.7 are given in table C.4.

Tab. C.2 Determination of leakage coefficient and swept volume: HIBON XN 4.5

Absolute inlet pressure		Air inlet temperature		Air density at inlet		Specific heat of air at inlet	
P_i Pa		T_i K		ρ_i kg/m ³		C_{pi} J/kgK	
101300		293.15		1.2037		1006.73	
Rotor revolution speed n rpm	Differential pressure ΔP Pa	Air inlet flow rate Q_i m ³ /h	Air outlet temperature T_e K	Specific heat of air at outlet C_{pe} J/kgK	Average specific heat of air $C_{p\text{ avg}}$ J/kgK	Leakage coefficient k m ²	Swept volume V_p m ³ /rev
1400	10000	326.47	302.15	1007.03	1006.88	0.0000902	0.004239
	20000	302.93	313.15	1007.50	1007.12	0.0001384	0.004371
	30000	285.29	325.15	1008.14	1007.44	0.0001471	0.004392
	40000	270.59	339.15	1009.05	1007.89	0.0001627	0.004492
	50000	255.88	354.15	1010.21	1008.47	0.0001675	0.004509
	60000	241.18	370.15	1011.66	1009.19	0.0001675	0.004474
	70000	232.36	387.15	1013.43	1010.08	0.0001691	0.004514
1800	10000	435.29	302.15	1007.03	1006.88	0.0001203	0.004396
	20000	411.76	312.15	1007.46	1007.09	0.0001344	0.004390
	30000	391.18	324.15	1008.08	1007.41	0.0001739	0.004537
	40000	376.48	336.15	1008.84	1007.79	0.0001742	0.004544
	50000	364.71	348.15	1009.72	1008.23	0.0001663	0.004506
	60000	352.94	362.15	1010.91	1008.82	0.0001738	0.004562
	70000	341.19	376.15	1012.26	1009.49	0.0001730	0.004550
2200	10000	544.12	302.15	1007.03	1006.88	0.0001504	0.004496
	20000	520.59	312.15	1007.46	1007.09	0.0001699	0.004541
	30000	502.94	322.15	1007.97	1007.35	0.0001521	0.004465
	40000	485.29	333.65	1008.67	1007.70	0.0001685	0.004514
	50000	473.53	345.15	1009.49	1008.11	0.0001689	0.004526
	60000	461.76	357.15	1010.47	1008.60	0.0001692	0.004529
	70000	450.00	370.15	1011.66	1009.19	0.0001740	0.004554
3400	10000	873.53	302.15	1007.03	1006.88	0.0002414	0.004670
	20000	850.00	311.15	1007.41	1007.07	0.0001665	0.004545
	30000	829.41	320.15	1007.86	1007.30	0.0001330	0.004436
	40000	817.64	330.65	1008.48	1007.60	0.0001705	0.004557
	50000	802.94	340.65	1009.16	1007.94	0.0001668	0.004536
	60000	785.29	351.15	1009.96	1008.35	0.0001691	0.004516
	70000	776.47	361.15	1010.82	1008.77	0.0001604	0.004489
4200	10000	1088.24	302.15	1007.03	1006.88	0.0003007	0.004710
	20000	1064.71	311.15	1007.41	1007.07	0.0002085	0.004609
	30000	1047.06	320.65	1007.89	1007.31	0.0002051	0.004618
	40000	1035.29	330.15	1008.45	1007.59	0.0001920	0.004608
	50000	1017.65	340.15	1009.12	1007.93	0.0001945	0.004605
	60000	1005.88	349.15	1009.80	1008.27	0.0001659	0.004521
	70000	1000.00	359.15	1010.64	1008.69	0.0001665	0.004542

Tab. C.3 Roots blower performance prediction: HIBON XN 4.5

Absolute inlet pressure P_i Pa	Air inlet temperature T_i K	Air inlet density ρ_i kg/m ³	Specific heat of air at inlet C_{pi} J/kgK	Swept volume V_p m ³ /rev	Leakage coefficient k m ²		
101300	293.15	1.2037	1006.73	0.004516	0.0001701		
Differential pressure ΔP Pa	Rotor revolution speed n rpm	Air inlet flow rate Q_i m ³ /h	Air outlet temperature T_e °C	Shaft power W kW	Experimental air inlet flow rate Q_i m ³ /h	Experimental air outlet temperature T_e °C	Experimental shaft power W kW
10000	1400	323.54	29.68	1.05	326.47	29.0	1.1
	1800	431.93	29.32	1.35	435.29	29.0	1.3
	2200	540.32	29.10	1.66	544.12	29.0	1.7
	3400	865.49	28.78	2.56	873.53	29.0	2.5
	4200	1082.27	28.68	3.16	1088.24	29.0	3.2
20000	1400	300.42	40.84	2.11	302.93	40.0	2.1
	1800	408.81	39.69	2.71	411.76	39.0	2.8
	2200	517.20	39.02	3.31	520.59	39.0	3.3
	3400	842.37	38.05	5.12	850.00	38.0	5.4
	4200	1059.15	37.73	6.32	1064.71	38.0	6.8
30000	1400	282.68	53.22	3.16	285.29	52.0	3.3
	1800	391.07	50.87	4.06	391.18	51.0	4.2
	2200	499.46	49.55	4.97	502.94	49.0	5.2
	3400	824.63	47.66	7.68	829.41	47.0	8.0
	4200	1041.41	47.05	9.48	1047.06	47.5	10.1
40000	1400	267.72	66.77	4.22	270.59	66.0	4.5
	1800	376.11	62.80	5.42	376.48	63.0	5.8
	2200	484.50	60.61	6.62	485.29	60.5	7.0
	3400	809.67	57.56	10.24	817.64	57.5	10.9
	4200	1026.45	56.60	12.65	1035.29	57.0	13.5
50000	1400	254.55	81.49	5.27	255.88	81.0	5.6
	1800	362.94	75.45	6.77	364.71	75.0	7.2
	2200	471.32	72.18	8.28	473.53	72.0	8.9
	3400	796.49	67.72	12.80	802.94	67.5	13.8
	4200	1013.27	66.34	15.81	1017.65	67.0	16.9
60000	1400	242.63	97.41	6.32	241.18	97.0	6.8
	1800	351.02	88.79	8.13	352.94	89.0	8.6
	2200	459.41	84.24	9.94	461.76	84.0	10.6
	3400	784.58	78.14	15.36	785.29	78.0	16.5
	4200	1001.36	76.27	18.97	1005.88	76.0	20.2
70000	1400	231.68	114.58	7.38	232.36	114.0	7.8
	1800	340.07	102.85	9.48	341.19	103.0	9.9
	2200	448.46	96.78	11.59	450.00	97.0	12.5
	3400	773.62	88.79	17.91	776.47	88.0	19.1
	4200	990.40	86.37	22.13	1000.00	86.0	23.6

Tab. C.4 Scaled and calculated blower performance prediction: HIBON XN 4.5

Rotor revolution speed n rpm	Differential pressure ΔP Pa	Scaled differential pressure ΔP Pa	Predicted air inlet flow rate Q_i m^3/h	Predicted air outlet temperature T_e $^{\circ}C$	Predicted shaft power W kW	Experimental air inlet flow rate Q_i m^3/h
1400	10000	8025.67	321.67	50.39	0.85	326.47
	20000	16051.33	297.77	62.44	1.69	302.93
	30000	24077.00	279.44	75.87	2.54	285.29
	40000	32102.67	263.98	90.63	3.38	270.59
	50000	40128.33	250.36	106.73	4.23	255.88
	60000	48154.00	238.05	124.22	5.07	241.18
	70000	56179.66	226.72	143.16	5.92	232.36
1800	10000	8025.67	430.06	49.99	1.09	435.29
	20000	16051.33	406.16	61.15	2.17	411.76
	30000	24077.00	387.83	73.23	3.26	391.18
	40000	32102.67	372.37	86.15	4.35	376.48
	50000	40128.33	358.75	99.88	5.44	364.71
	60000	48154.00	346.44	114.40	6.52	352.94
	70000	56179.66	335.11	129.74	7.61	341.19
2200	10000	8025.67	538.45	49.75	1.33	544.12
	20000	16051.33	514.55	60.41	2.66	520.59
	30000	24077.00	496.22	71.74	3.99	502.94
	40000	32102.67	480.76	83.69	5.32	485.29
	50000	40128.33	467.14	96.20	6.65	473.53
	60000	48154.00	454.82	109.27	7.97	461.76
	70000	56179.66	443.50	122.87	9.30	450.00
3400	10000	8025.67	863.62	49.40	2.05	873.53
	20000	16051.33	839.72	59.33	4.11	850.00
	30000	24077.00	821.38	69.64	6.16	829.41
	40000	32102.67	805.92	80.28	8.22	817.64
	50000	40128.33	792.31	91.21	10.27	802.94
	60000	48154.00	779.99	102.42	12.32	785.29
	70000	56179.66	768.67	113.90	14.38	776.47
4200	10000	8025.67	1080.40	49.28	2.54	1088.24
	20000	16051.33	1056.50	58.98	5.07	1064.71
	30000	24077.00	1038.16	68.97	7.61	1047.06
	40000	32102.67	1022.70	79.21	10.15	1035.29
	50000	40128.33	1009.08	89.67	12.69	1017.65
	60000	48154.00	996.77	100.34	15.22	1005.88
	70000	56179.66	985.45	111.20	17.76	1000.00

Tab. C.4 continued

Rotor revolution speed n rpm	Differential pressure ΔP Pa	Experimental air outlet temperature T_e °C	Experimental shaft power W kW	Scaled differential pressure ΔP Pa	Scaled air inlet flow rate Q_i m ³ /h	Scaled air outlet temperature T_e °C	Scaled shaft power W kW
1400	10000	29.0	1.1	8025.67	326.47	49.61	0.88
	20000	40.0	2.1	16051.33	302.93	61.36	1.69
	30000	52.0	3.3	24077.00	285.29	74.18	2.65
	40000	66.0	4.5	32102.67	270.59	89.14	3.61
	50000	81.0	5.6	40128.33	255.88	105.16	4.49
	60000	97.0	6.8	48154.00	241.18	122.25	5.46
	70000	114.0	7.8	56179.66	232.36	140.41	6.26
1800	10000	29.0	1.3	8025.67	435.29	49.61	1.04
	20000	39.0	2.8	16051.33	411.76	60.30	2.25
	30000	51.0	4.2	24077.00	391.18	73.11	3.37
	40000	63.0	5.8	32102.67	376.48	85.93	4.65
	50000	75.0	7.2	40128.33	364.71	98.75	5.78
	60000	89.0	8.6	48154.00	352.94	113.71	6.90
	70000	103.0	9.9	56179.66	341.19	128.66	7.95
2200	10000	29.0	1.7	8025.67	544.12	49.61	1.36
	20000	39.0	3.3	16051.33	520.59	60.30	2.65
	30000	49.0	5.2	24077.00	502.94	70.98	4.17
	40000	60.5	7.0	32102.67	485.29	83.26	5.62
	50000	72.0	8.9	40128.33	473.53	95.55	7.14
	60000	84.0	10.6	48154.00	461.76	108.37	8.51
	70000	97.0	12.5	56179.66	450.00	122.25	10.03
3400	10000	29.0	2.5	8025.67	873.53	49.61	2.01
	20000	38.0	5.5	16051.33	850.00	59.23	4.41
	30000	47.0	8.0	24077.00	829.41	68.84	6.42
	40000	57.5	10.9	32102.67	817.64	80.06	8.75
	50000	67.5	13.8	40128.33	802.94	90.74	11.08
	60000	78.0	16.5	48154.00	785.29	101.96	13.24
	70000	88.0	19.1	56179.66	776.47	112.64	15.33
	10000	29.0	3.2	8025.67	1088.24	49.61	2.57
	20000	38.0	6.8	16051.33	1064.71	59.23	5.46
	30000	47.5	10.1	24077.00	1047.06	69.38	8.11
	40000	57.0	13.5	32102.67	1035.29	79.52	10.83
	50000	67.0	16.9	40128.33	1017.65	90.21	13.56
	60000	76.0	20.2	48154.00	1005.88	99.82	16.21
	70000	86.0	23.6	56179.66	1000.00	110.50	18.94

SIMULATION DATA

D.1 Initial conditions for cement conveying

Tab. D.1.1 Pressure ratio vs. initial solids Froude number for cement using λ_{tot} and λ_s^*

Initial solids Froude number Fr_{co} ---	Pressure ratio at $\dot{G} = 273 \text{ kg/h}$ P_i/P_e ---	Pressure ratio at $\dot{G} = 723 \text{ kg/h}$ P_i/P_e ---	Pressure ratio at $\dot{G} = 1002 \text{ kg/h}$ P_i/P_e ---	Pressure ratio at $\dot{G} = 1423 \text{ kg/h}$ P_i/P_e ---
0.2806	1.0159	1.0222	1.0231	1.0246
0.7796	1.0165	1.0242	1.0263	1.0328
3.1183	1.0169	1.0254	1.0280	1.0362
77.9572	1.0172	1.0262	1.0289	1.0379
311.8287	1.0171	1.0261	1.0289	1.0378
1247.3148	1.0171	1.0259	1.0285	1.0374
4989.2591	1.0169	1.0253	1.0278	1.0363
11225.8329	1.0166	1.0248	1.0270	1.0352

Tab. D.1.2 Pressure ratio vs. initial solids Froude number for cement using λ_{tot} and λ_s'

Initial solids Froude number Fr_{co} ---	Pressure ratio at $\dot{G} = 273 \text{ kg/h}$ P_i/P_e ---	Pressure ratio at $\dot{G} = 723 \text{ kg/h}$ P_i/P_e ---	Pressure ratio at $\dot{G} = 1002 \text{ kg/h}$ P_i/P_e ---	Pressure ratio at $\dot{G} = 1423 \text{ kg/h}$ P_i/P_e ---
0.2806	1.0152	1.0206	1.0210	1.0213
0.7796	1.0158	1.0226	1.0242	1.0295
3.1183	1.0162	1.0238	1.0259	1.0330
77.9572	1.0165	1.0245	1.0268	1.0347
311.8287	1.0165	1.0245	1.0268	1.0346
1247.3148	1.0164	1.0242	1.0264	1.0342
4989.2591	1.0162	1.0237	1.0257	1.0331
11225.8329	1.0160	1.0231	1.0249	1.0320

D.2 Results for the conveying simulations with cement using λ_{tot} and λ_s^*

Tab. D.2.1 Results for cement conveying at $\dot{G} = 273$ kg/h with λ_{tot} and λ_s^*

Cement mass flow rate \dot{G} kg/h	Mass flow ratio μ ---	Inlet temperature T °C	Absolute outlet pressure P_e Pa	Initial solids velocity c_o m/s	Pipe roughness ϵ m	Feeder air leakage <i>Leakage</i> %
273	0.291	46.5	87510	0.5	0	0
Distance from feed point L m	Simulated pressure relative to exit ΔP Pa	Simulated average air velocity v m/s	Simulated solids velocity c m/s	Experimental pressure relative to exit [89LA1] ΔP Pa	Experimental average air velocity [89LA1] v m/s	Experimental solids velocity [89LA1] c m/s
-2.00	1502.50	33.13	0.00			
-1.00	1417.44	33.17	0.00			
-0.60	1383.39	33.18	0.00			
0.00	1332.28	33.20	0.00			
0.02	1108.65	33.28	24.61			
0.05	1079.73	33.29	27.47			
0.07	1065.02	33.30	28.83			
0.09	1055.47	33.30	29.65			
0.12	1048.45	33.30	30.20			
0.14	1042.88	33.31	30.60			
0.16	1038.21	33.31	30.90			
0.19	1034.16	33.31	31.14			
0.21	1030.55	33.31	31.33			
0.40	1008.76	33.32	32.10			
0.61	989.48	33.33	32.41			
0.81	972.47	33.33	32.55			
1.21	940.40	33.35	32.67			
1.50	917.54	33.35	32.71			
1.79	894.82	33.36	32.73	878.00	33.39	26.20
2.29	855.68	33.38	32.75			
2.79	816.59	33.39	32.77			
3.29	777.50	33.41	32.78			
3.79	738.40	33.42	32.80	408.00	33.57	26.35
4.29	699.28	33.44	32.81			
4.79	660.15	33.45	32.83	678.00	33.49	26.28
5.29	621.00	33.47	32.84			
5.79	581.83	33.48	32.85	528.00	33.55	26.33
6.29	542.64	33.50	32.87			
6.79	503.43	33.51	32.88	398.00	33.60	26.37
7.29	464.20	33.53	32.90			
7.79	424.96	33.54	32.91	448.00	33.57	26.35
8.29	385.70	33.56	32.92			
8.79	346.42	33.57	32.94	308.00	33.62	26.38
9.29	307.12	33.59	32.95			
9.79	267.81	33.60	32.97	238.00	33.64	26.40
10.32	225.85	33.62	32.98			
10.79	189.12	33.63	32.99	118.00	33.68	26.43
11.49	134.00	33.65	33.01			
12.19	78.84	33.67	33.03	8.00	33.72	26.46
12.69	39.42	33.69	33.05			
13.19	-0.02	33.70	33.06	68.00	33.71	26.46

Tab. D.2.2 Results for cement conveying at $\dot{G} = 723$ kg/h with λ_{tot} and λ_s^*

Cement mass flow rate \dot{G} kg/h	Mass flow ratio μ ---	Inlet temperature T °C	Absolute outlet pressure P_e Pa	Initial solids velocity c_o m/s	Pipe roughness ϵ m	Feeder air leakage <i>Leakage</i> %
723	0.777	41	87615	0.5	0	0
Distance from feed point L m	Simulated pressure relative to exit ΔP Pa	Simulated average air velocity v m/s	Simulated solids velocity c m/s	Experimental pressure relative to exit [89LA1] ΔP Pa	Experimental average air velocity [89LA1] v m/s	Experimental solids velocity [89LA1] c m/s
-2.00	2291.85	31.98	0.00			
-1.00	2210.55	32.01	0.00			
-0.60	2178.00	32.02	0.00			
0.00	2129.17	32.04	0.00			
0.02	1555.95	32.24	23.93			
0.05	1484.32	32.27	26.70			
0.07	1449.04	32.28	28.01			
0.09	1426.94	32.29	28.80			
0.12	1411.29	32.30	29.33			
0.14	1399.33	32.30	29.71			
0.16	1389.69	32.30	30.00			
0.19	1381.62	32.31	30.23			
0.21	1374.66	32.31	30.41			
0.40	1337.13	32.32	31.15			
0.61	1308.25	32.33	31.45			
0.81	1284.35	32.34	31.59			
1.21	1240.93	32.36	31.70			
1.50	1210.52	32.37	31.74			
1.79	1180.46	32.38	31.76	1092.00	32.42	26.01
2.29	1128.83	32.40	31.79			
2.79	1077.33	32.42	31.81			
3.29	1025.84	32.44	31.83			
3.79	974.33	32.45	31.85	892.00	32.49	26.07
4.29	922.79	32.47	31.86			
4.79	871.22	32.49	31.88	882.00	32.51	26.08
5.29	819.62	32.51	31.90			
5.79	767.99	32.53	31.92	812.00	32.54	26.11
6.29	716.33	32.55	31.94			
6.79	664.64	32.57	31.95	612.00	32.61	26.16
7.29	612.91	32.59	31.97			
7.79	561.15	32.61	31.99	642.00	32.58	26.14
8.29	509.37	32.63	32.01			
8.79	457.54	32.64	32.02	532.00	32.61	26.16
9.29	405.69	32.66	32.04			
9.79	353.81	32.68	32.06	432.00	32.65	26.20
10.32	298.43	32.70	32.08			
10.79	249.94	32.72	32.10	342.00	32.68	26.22
11.49	177.16	32.75	32.12			
12.19	104.32	32.78	32.15	132.00	32.76	26.28
12.69	52.25	32.80	32.17			
13.19	0.15	32.82	32.18	232.00	32.74	26.27

Tab. D.2.3 Results for cement conveying at $\dot{G} = 1002 \text{ kg/h}$ with λ_{tot} and λ_s^*

Cement mass flow rate \dot{G} kg/h	Mass flow ratio μ ---	Inlet temperature T °C	Absolute outlet pressure P_e Pa	Initial solids velocity c_o m/s	Pipe roughness ε m	Feeder air leakage $Leakage$ %
1002	1.111	31.8	87876	0.5	0	0
Distance from feed point L m	Simulated pressure relative to exit ΔP Pa	Simulated average air velocity v m/s	Simulated solids velocity c m/s	Experimental pressure relative to exit [89LA1] ΔP Pa	Experimental average air velocity [89LA1] v m/s	Experimental solids velocity [89LA1] c m/s
-2.00	2542.78	29.92	0.00			
-1.00	2469.01	29.94	0.00			
-0.60	2439.48	29.95	0.00			
0.00	2395.18	29.97	0.00			
0.02	1647.02	30.22	22.59			
0.05	1555.71	30.25	25.16			
0.07	1511.21	30.26	26.37			
0.09	1483.61	30.27	27.09			
0.12	1464.27	30.28	27.58			
0.14	1449.63	30.28	27.93			
0.16	1437.96	30.29	28.20			
0.19	1428.28	30.29	28.41			
0.21	1420.01	30.29	28.58			
0.40	1376.96	30.31	29.26			
0.61	1345.45	30.32	29.54			
0.81	1320.06	30.33	29.66			
1.21	1274.73	30.34	29.77			
1.50	1243.27	30.35	29.81			
1.79	1212.29	30.36	29.83	1157.00	30.37	24.70
2.29	1159.19	30.38	29.86			
2.79	1106.28	30.40	29.88			
3.29	1053.39	30.42	29.90			
3.79	1000.49	30.44	29.91	927.00	30.45	24.76
4.29	947.57	30.45	29.93			
4.79	894.61	30.47	29.95	877.00	30.48	24.79
5.29	841.62	30.49	29.96			
5.79	788.60	30.51	29.98	827.00	30.50	24.80
6.29	735.55	30.53	30.00			
6.79	682.46	30.55	30.02	637.00	30.57	24.86
7.29	629.34	30.56	30.03			
7.79	576.18	30.58	30.05	657.00	30.56	24.85
8.29	522.99	30.60	30.07			
8.79	469.77	30.62	30.08	477.00	30.63	24.91
9.29	416.52	30.64	30.10			
9.79	363.23	30.66	30.12	357.00	30.68	24.95
10.32	306.35	30.68	30.14			
10.79	256.55	30.69	30.15	257.00	30.72	24.98
11.49	181.80	30.72	30.18			
12.19	106.98	30.75	30.20	-13.00	30.81	25.06
12.69	53.49	30.76	30.22			
13.19	-0.03	30.78	30.24	37.00	30.80	25.05

Tab. D.2.4 Results for cement conveying at $\dot{G} = 1423$ kg/h with λ_{tot} and λ_s^*

Cement mass flow rate \dot{G} kg/h	Mass flow ratio μ ---	Inlet temperature T °C	Absolute outlet pressure P_e Pa	Initial solids velocity c_o m/s	Pipe roughness ε m	Feeder air leakage <i>Leakage</i> %
1423	1.407	24.3	88950	0.5	0	0
Distance from feed point L m	Simulated pressure relative to exit ΔP Pa	Simulated average air velocity v m/s	Simulated solids velocity c m/s	Experimental pressure relative to exit [89LA1] ΔP Pa	Experimental average air velocity [89LA1] v m/s	Experimental solids velocity [89LA1] c m/s
-2.00	3370.46	32.05	0.00			
-1.00	3283.97	32.08	0.00			
-0.60	3249.35	32.09	0.00			
0.00	3197.39	32.11	0.00			
0.02	2060.86	32.51	24.19			
0.05	1920.14	32.56	26.98			
0.07	1851.62	32.59	28.31			
0.09	1809.31	32.60	29.11			
0.12	1779.83	32.61	29.65			
0.14	1757.70	32.62	30.04			
0.16	1740.20	32.63	30.34			
0.19	1725.81	32.63	30.57			
0.21	1713.64	32.64	30.76			
0.40	1652.55	32.66	31.53			
0.61	1610.54	32.67	31.86			
0.81	1577.99	32.69	32.02			
1.21	1521.62	32.71	32.16			
1.50	1483.24	32.72	32.22			
1.79	1445.79	32.73	32.25	1213.00	32.94	27.33
2.29	1382.05	32.76	32.29			
2.79	1318.83	32.78	32.32			
3.29	1255.76	32.80	32.34			
3.79	1192.73	32.82	32.37	943.00	33.04	27.41
4.29	1129.68	32.85	32.39			
4.79	1066.59	32.87	32.41	843.00	33.06	27.43
5.29	1003.46	32.89	32.43			
5.79	940.29	32.92	32.46	803.00	33.07	27.44
6.29	877.07	32.94	32.48			
6.79	813.80	32.96	32.50	603.00	33.15	27.50
7.29	750.49	32.99	32.52			
7.79	687.13	33.01	32.54	643.00	33.13	27.49
8.29	623.72	33.03	32.57			
8.79	560.26	33.06	32.59	603.00	33.14	27.49
9.29	496.76	33.08	32.61			
9.79	433.21	33.10	32.63	413.00	33.20	27.54
10.32	365.37	33.13	32.66			
10.79	305.96	33.15	32.68	353.00	33.12	27.48
11.49	216.77	33.18	32.71			
12.19	127.49	33.22	32.74	113.00	33.30	27.63
12.69	63.66	33.24	32.76			
13.19	-0.22	33.27	32.79	103.00	33.30	27.63

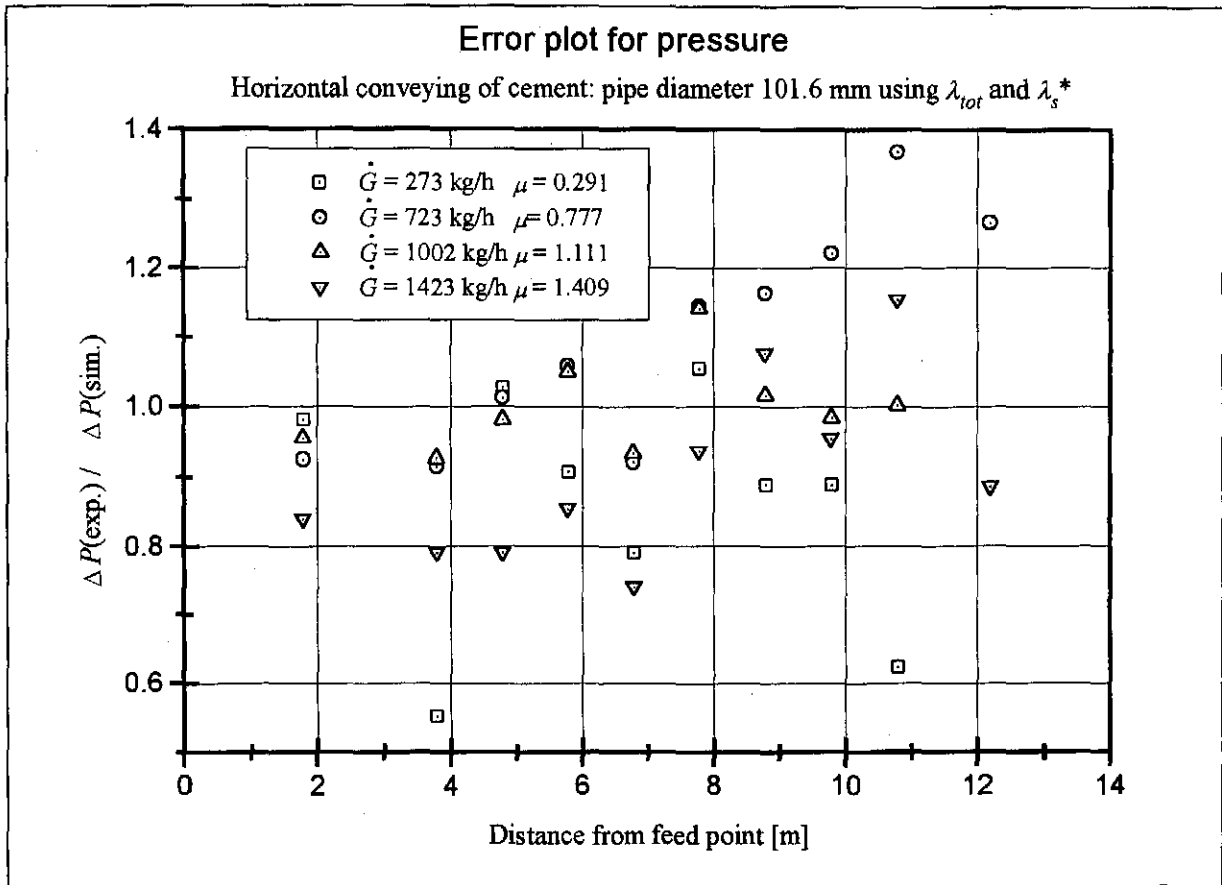


Fig. D.2.1 Cement conveying error plot for the pressure

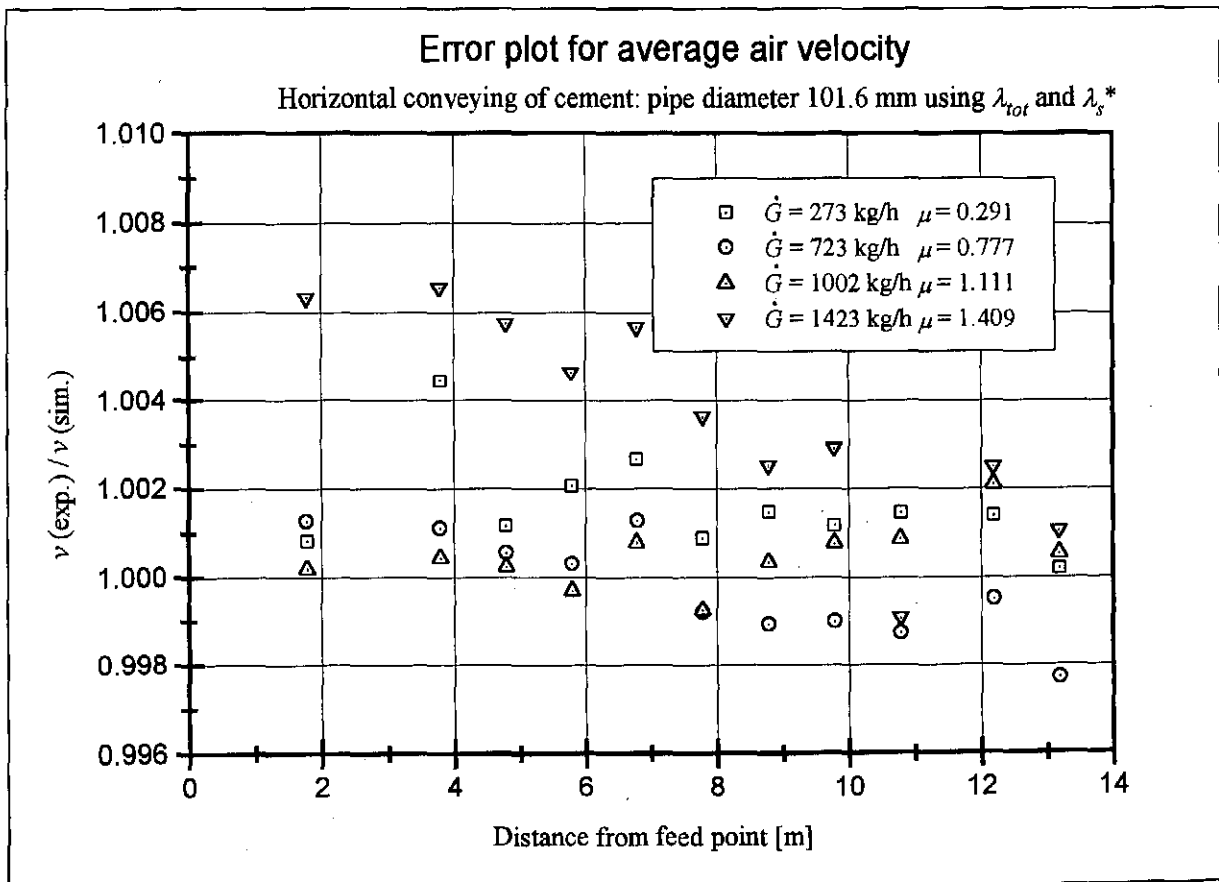


Fig. D.2.2 Cement conveying error plot for the average air velocity

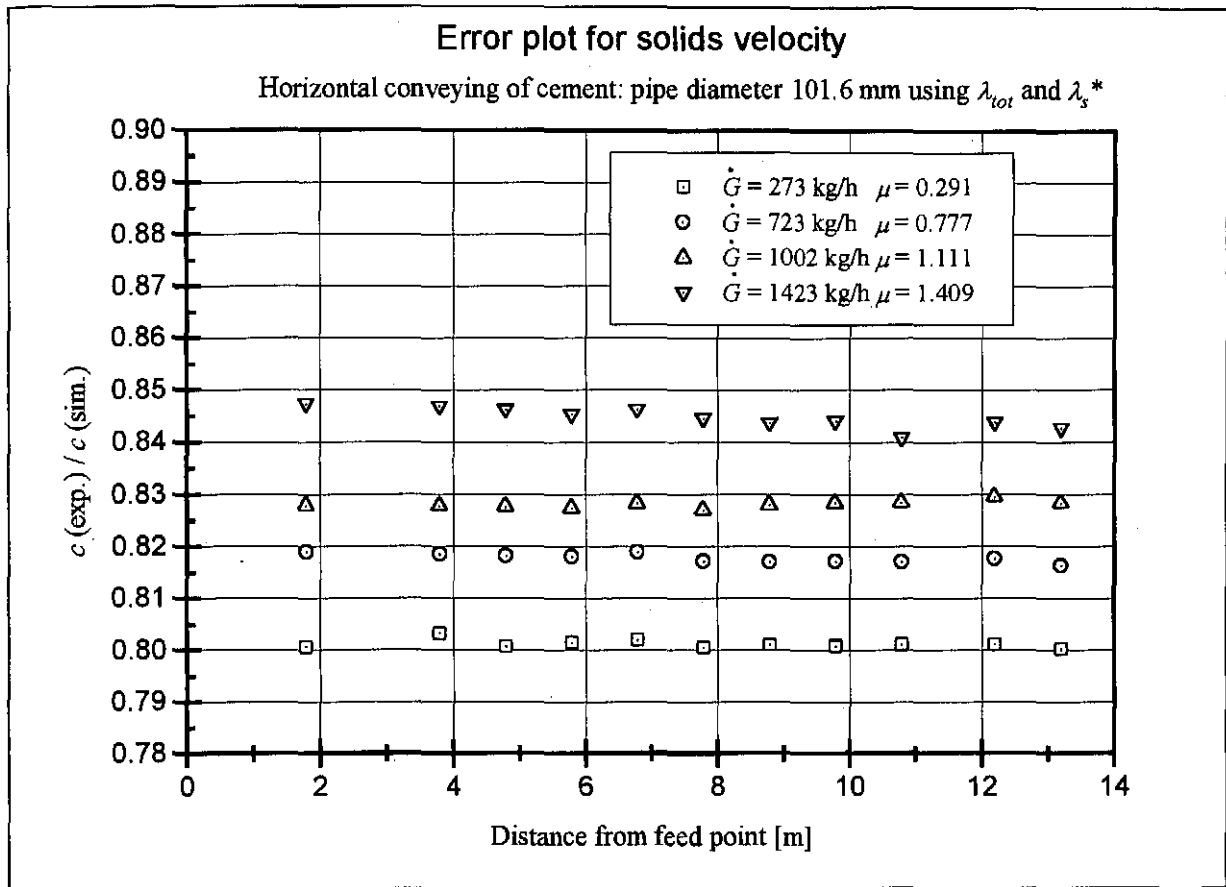


Fig. D.2.3 Cement conveying error plot for the solids velocity

D.3 Results for the conveying simulations with cement using λ_{tot} and λ_s' Tab. D.3.1 Results for cement conveying at $\dot{G} = 273$ kg/h with λ_{tot} and λ_s'

Cement mass flow rate \dot{G} kg/h	Mass flow ratio μ ---	Inlet temperature T °C	Absolute outlet pressure P_e Pa	Initial solids velocity c_o m/s	Pipe roughness ε m	Feeder air leakage <i>Leakage</i> %
273	0.291	46.5	87510	0.5	0	0
Distance from feed point L m	Simulated pressure relative to exit ΔP Pa	Simulated average air velocity v m/s	Simulated solids velocity c m/s	Experimental pressure relative to exit [89LA1] ΔP Pa	Experimental average air velocity [89LA1] v m/s	Experimental solids velocity [89LA1] c m/s
-2.00	1442.26	33.16	0.00			
-1.00	1357.14	33.19	0.00			
-0.60	1323.06	33.20	0.00			
0.00	1271.93	33.22	0.00			
0.02	1057.69	33.30	23.61			
0.05	1038.01	33.31	25.50			
0.07	1030.81	33.31	26.07			
0.09	1027.12	33.31	26.27			
0.12	1024.62	33.31	26.34			
0.14	1022.55	33.31	26.37			
0.16	1020.64	33.31	26.38			
0.19	1018.78	33.32	26.38			
0.21	1016.95	33.32	26.38			
0.40	1002.39	33.32	26.39			
0.61	986.02	33.33	26.40			
0.81	970.28	33.33	26.40			
1.21	939.24	33.35	26.41			
1.50	916.67	33.35	26.42			
1.79	894.08	33.36	26.42	878.00	33.39	26.20
2.29	855.05	33.38	26.44			
2.79	815.99	33.39	26.45			
3.29	776.91	33.41	26.46			
3.79	737.82	33.42	26.47	408.00	33.57	26.35
4.29	698.71	33.44	26.48			
4.79	659.58	33.45	26.50	678.00	33.49	26.28
5.29	620.43	33.47	26.51			
5.79	581.27	33.48	26.52	528.00	33.55	26.33
6.29	542.09	33.50	26.53			
6.79	502.89	33.51	26.55	398.00	33.60	26.37
7.29	463.67	33.53	26.56			
7.79	424.43	33.54	26.57	448.00	33.57	26.35
8.29	385.17	33.56	26.58			
8.79	345.90	33.57	26.59	308.00	33.62	26.38
9.29	306.61	33.59	26.61			
9.79	267.30	33.60	26.62	238.00	33.64	26.40
10.32	225.35	33.62	26.63			
10.79	188.63	33.63	26.64	118.00	33.68	26.43
11.49	133.51	33.65	26.66			
12.19	78.36	33.67	26.68	8.00	33.72	26.46
12.69	38.95	33.69	26.69			
13.19	-0.49	33.70	26.70	68.00	33.71	26.46

Tab. D.3.2 Results for cement conveying at $\dot{G} = 723$ kg/h with λ_{tot} and λ_s'

Cement mass flow rate \dot{G} kg/h	Mass flow ratio μ ---	Inlet temperature T °C	Absolute outlet pressure P_e Pa	Initial solids velocity c_o m/s	Pipe roughness ε m	Feeder air leakage <i>Leakage</i> %
723	0.777	41	87615	0.5	0	0
Distance from feed point L m	Simulated pressure relative to exit ΔP Pa	Simulated average air velocity v m/s	Simulated solids velocity c m/s	Experimental pressure relative to exit [89LA1] ΔP Pa	Experimental average air velocity [89LA1] v m/s	Experimental solids velocity [89LA1] c m/s
-2.00	2149.79	32.03	0.00			
-1.00	2068.35	32.06	0.00			
-0.60	2035.76	32.07	0.00			
0.00	1986.84	32.09	0.00			
0.02	1434.00	32.29	23.12			
0.05	1383.20	32.31	25.05			
0.07	1365.27	32.31	25.67			
0.09	1357.08	32.31	25.91			
0.12	1352.41	32.32	26.00			
0.14	1349.10	32.32	26.04			
0.16	1346.34	32.32	26.05			
0.19	1343.80	32.32	26.06			
0.21	1341.35	32.32	26.06			
0.40	1322.16	32.33	26.07			
0.61	1300.62	32.34	26.07			
0.81	1279.91	32.34	26.08			
1.21	1239.07	32.36	26.09			
1.50	1209.35	32.37	26.10			
1.79	1179.63	32.38	26.11	1092.00	32.42	26.01
2.29	1128.24	32.40	26.13			
2.79	1076.82	32.42	26.14			
3.29	1025.37	32.44	26.16			
3.79	973.89	32.45	26.17	892.00	32.49	26.07
4.29	922.37	32.47	26.19			
4.79	870.83	32.49	26.21	882.00	32.51	26.08
5.29	819.25	32.51	26.22			
5.79	767.64	32.53	26.24	812.00	32.54	26.11
6.29	716.00	32.55	26.25			
6.79	664.33	32.57	26.27	612.00	32.61	26.16
7.29	612.63	32.59	26.28			
7.79	560.90	32.61	26.30	642.00	32.58	26.14
8.29	509.13	32.63	26.32			
8.79	457.34	32.64	26.33	532.00	32.61	26.16
9.29	405.51	32.66	26.35			
9.79	353.65	32.68	26.37	432.00	32.65	26.20
10.32	298.30	32.70	26.38			
10.79	249.83	32.72	26.40	342.00	32.68	26.22
11.49	177.09	32.75	26.42			
12.19	104.28	32.78	26.44	132.00	32.76	26.28
12.69	52.23	32.80	26.46			
13.19	0.16	32.82	26.48	232.00	32.74	26.27

Tab. D.3.3 Results for cement conveying at $\dot{G} = 1002$ kg/h with λ_{tot} and λ_s'

Cement mass flow rate \dot{G} kg/h	Mass flow ratio μ ---	Inlet temperature T °C	Absolute outlet pressure P_e Pa	Initial solids velocity c_o m/s	Pipe roughness ε m	Feeder air leakage <i>Leakage</i> %
1002	1.111	31.8	87876	0.5	0	0
Distance from feed point L m	Simulated pressure relative to exit ΔP Pa	Simulated average air velocity v m/s	Simulated solids velocity c m/s	Experimental pressure relative to exit [89LA1] ΔP Pa	Experimental average air velocity [89LA1] v m/s	Experimental solids velocity [89LA1] c m/s
-2.00	2359.21	29.98	0.00			
-1.00	2285.29	30.00	0.00			
-0.60	2255.70	30.01	0.00			
0.00	2211.30	30.03	0.00			
0.02	1489.63	30.27	21.83			
0.05	1425.45	30.29	23.61			
0.07	1403.44	30.30	24.17			
0.09	1393.79	30.30	24.38			
0.12	1388.54	30.30	24.46			
0.14	1384.99	30.31	24.50			
0.16	1382.09	30.31	24.51			
0.19	1379.46	30.31	24.51			
0.21	1376.94	30.31	24.52			
0.40	1357.23	30.32	24.52			
0.61	1335.11	30.32	24.53			
0.81	1313.85	30.33	24.54			
1.21	1271.92	30.34	24.55			
1.50	1241.41	30.35	24.56			
1.79	1210.89	30.36	24.57	1157.00	30.37	24.70
2.29	1158.13	30.38	24.58			
2.79	1105.33	30.40	24.60			
3.29	1052.50	30.42	24.61			
3.79	999.64	30.44	24.63	927.00	30.45	24.76
4.29	946.74	30.46	24.64			
4.79	893.81	30.47	24.66	877.00	30.48	24.79
5.29	840.85	30.49	24.67			
5.79	787.86	30.51	24.69	827.00	30.50	24.80
6.29	734.83	30.53	24.70			
6.79	681.77	30.55	24.72	637.00	30.57	24.86
7.29	628.68	30.56	24.73			
7.79	575.55	30.58	24.75	657.00	30.56	24.85
8.29	522.39	30.60	24.76			
8.79	469.20	30.62	24.78	477.00	30.63	24.91
9.29	415.97	30.64	24.79			
9.79	362.71	30.66	24.81	357.00	30.68	24.95
10.32	305.86	30.68	24.83			
10.79	256.09	30.69	24.84	257.00	30.72	24.98
11.49	181.38	30.72	24.86			
12.19	106.60	30.75	24.88	-13.00	30.81	25.06
12.69	53.14	30.76	24.90			
13.19	-0.35	30.78	24.92	37.00	30.80	25.05

Tab. D.3.4 Results for cement conveying at $\dot{G} = 1423$ kg/h with λ_{tot} and λ_s'

Cement mass flow rate \dot{G} kg/h	Mass flow ratio μ ---	Inlet temperature T °C	Absolute outlet pressure P_s Pa	Initial solids velocity c_o m/s	Pipe roughness ϵ m	Feeder air leakage <i>Leakage</i> %
1423	1.409	24.3	87950	0.5	0	0
Distance from feed point L m	Simulated pressure relative to exit ΔP Pa	Simulated average air velocity v m/s	Simulated solids velocity c m/s	Experimental pressure relative to exit [89LA1] ΔP Pa	Experimental average air velocity [89LA1] v m/s	Experimental solids velocity [89LA1] c m/s
-2.00	3084.88	32.15	0.00			
-1.00	2998.11	32.18	0.00			
-0.60	2963.38	32.19	0.00			
0.00	2911.25	32.21	0.00			
0.02	1812.73	32.60	23.42			
0.05	1712.25	32.64	25.40			
0.07	1677.58	32.65	26.04			
0.09	1662.60	32.65	26.29			
0.12	1654.86	32.66	26.39			
0.14	1649.97	32.66	26.43			
0.16	1646.24	32.66	26.44			
0.19	1642.98	32.66	26.45			
0.21	1639.92	32.66	26.46			
0.40	1616.45	32.67	26.46			
0.61	1590.15	32.68	26.47			
0.81	1564.86	32.69	26.48			
1.21	1515.00	32.71	26.50			
1.50	1478.71	32.72	26.51			
1.79	1442.41	32.73	26.52	1213.00	32.94	27.33
2.29	1379.65	32.76	26.54			
2.79	1316.84	32.78	26.56			
3.29	1253.98	32.80	26.57			
3.79	1191.07	32.83	26.59	943.00	33.04	27.41
4.29	1128.12	32.85	26.61			
4.79	1065.13	32.87	26.63	843.00	33.06	27.43
5.29	1002.08	32.89	26.65			
5.79	938.99	32.92	26.67	803.00	33.07	27.44
6.29	875.86	32.94	26.69			
6.79	812.67	32.96	26.71	603.00	33.15	27.50
7.29	749.44	32.99	26.73			
7.79	686.17	33.01	26.75	643.00	33.13	27.49
8.29	622.84	33.03	26.77			
8.79	559.47	33.06	26.79	603.00	33.14	27.49
9.29	496.05	33.08	26.81			
9.79	432.58	33.10	26.83	413.00	33.20	27.54
10.32	364.83	33.13	26.85			
10.79	305.50	33.15	26.87	353.00	33.12	27.48
11.49	216.43	33.18	26.89			
12.19	127.27	33.22	26.92	113.00	33.30	27.63
12.69	63.53	33.24	26.94			
13.19	-0.26	33.27	26.96	103.00	33.30	27.63

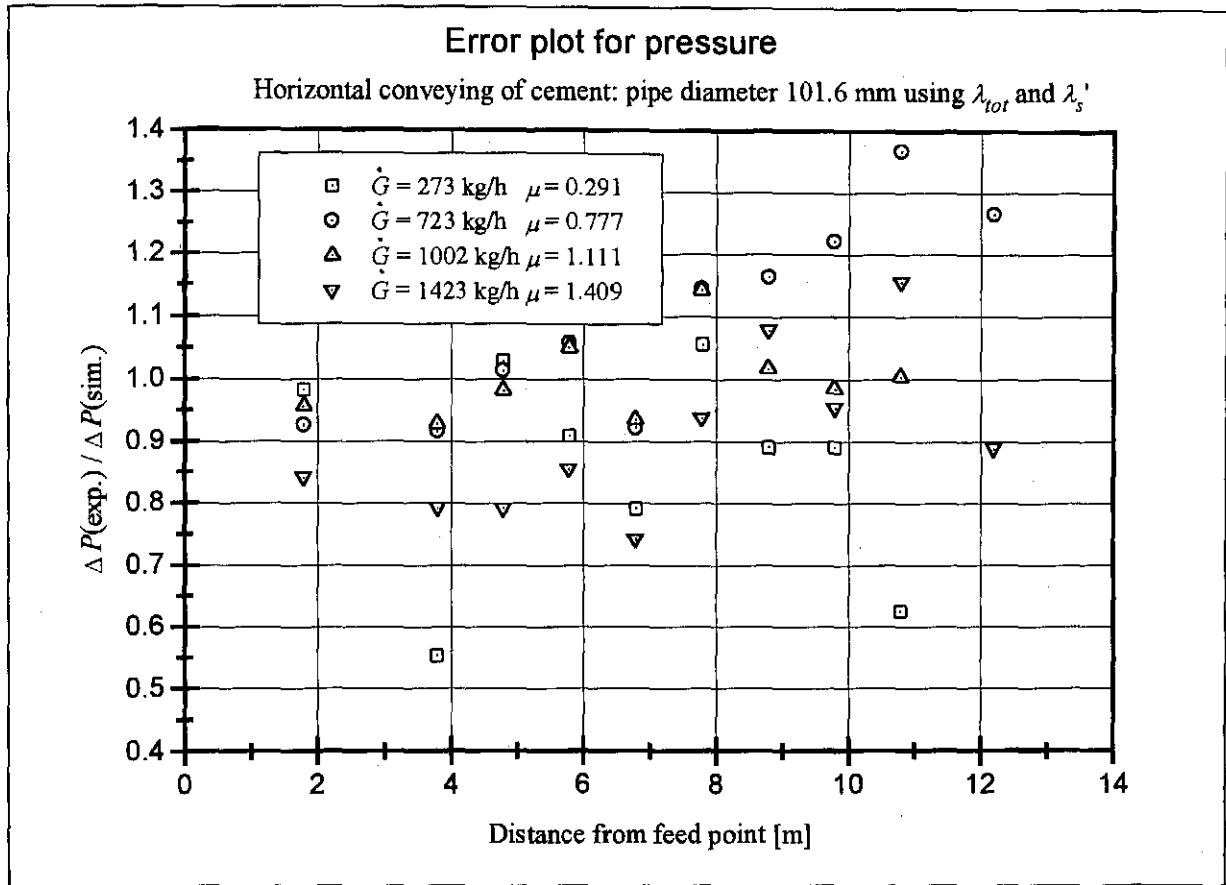


Fig. D.3.1 Cement conveying error plot for the pressure

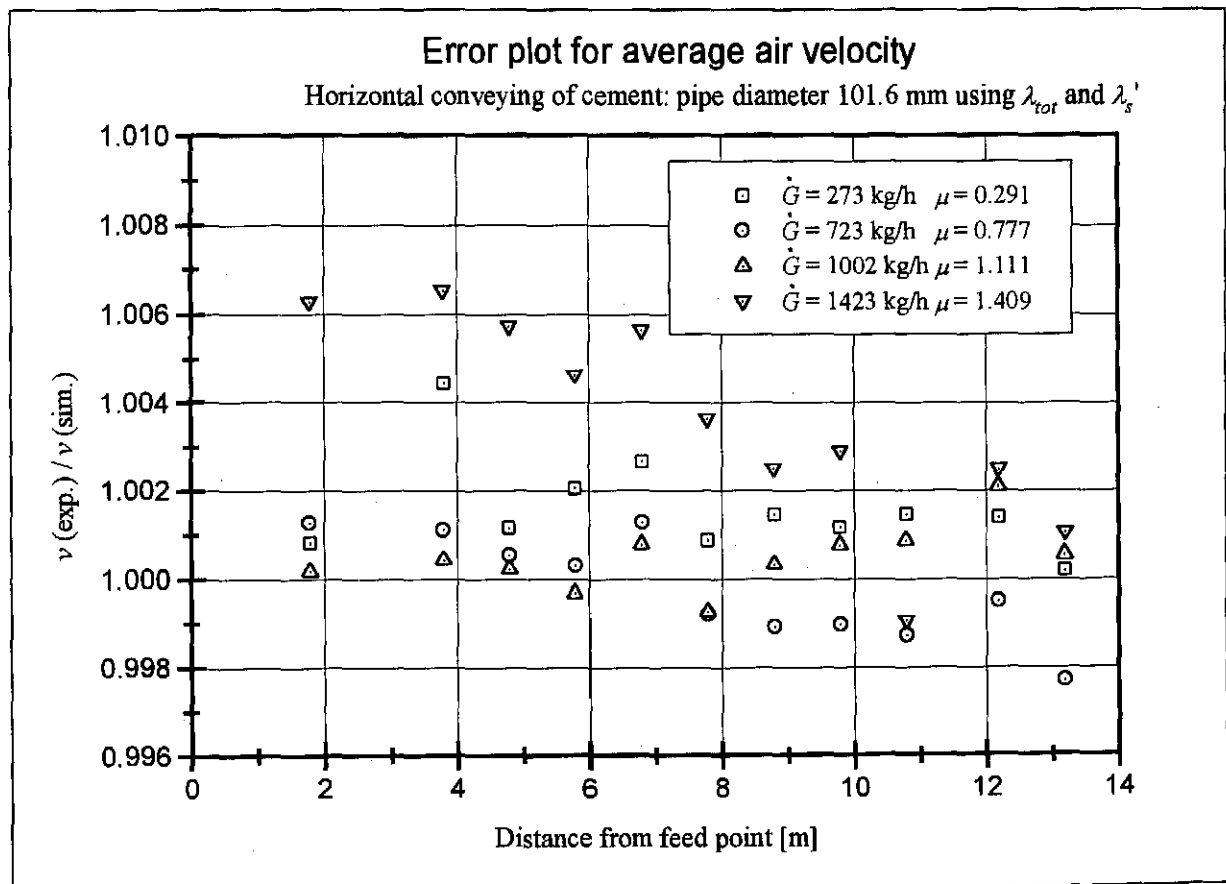


Fig. D.3.2 Cement conveying error plot for the average air velocity

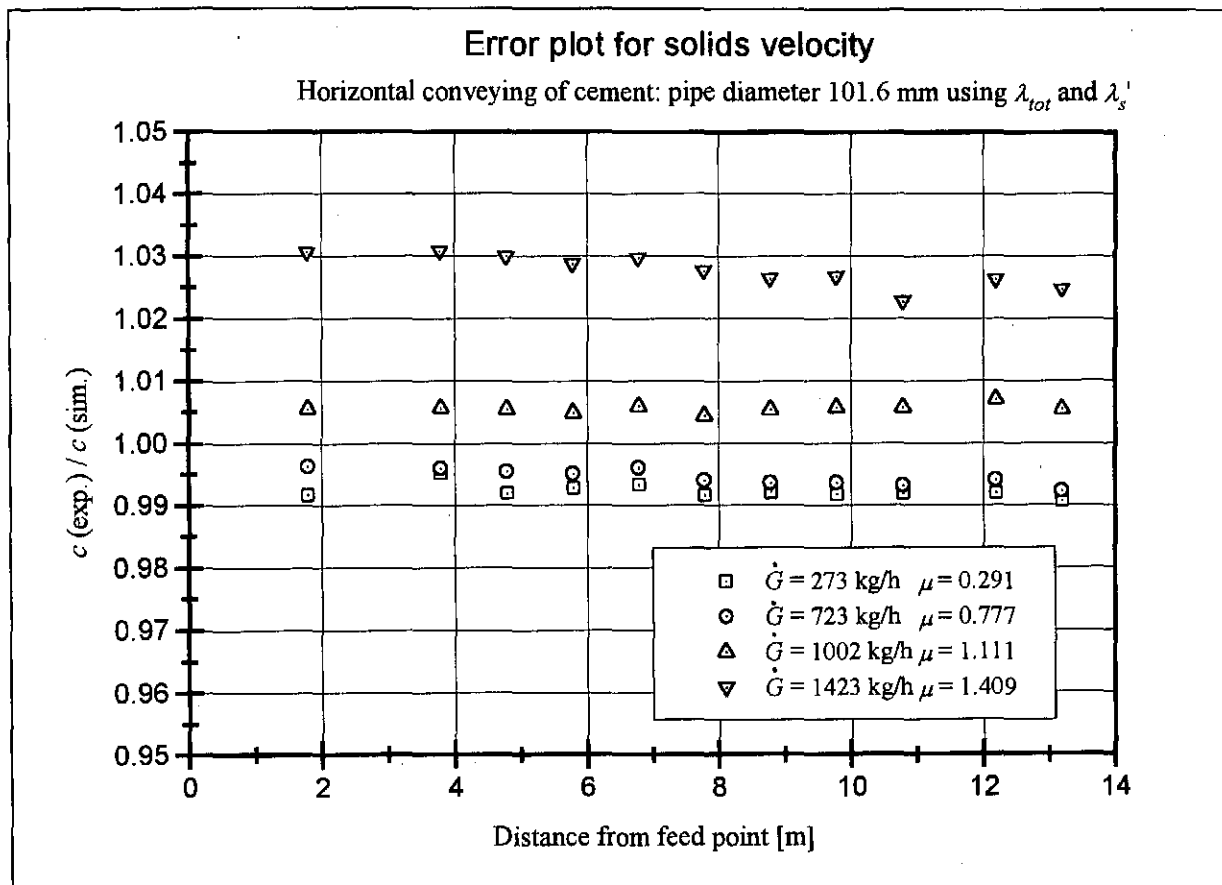


Fig. D.3.3 Cement conveying error plot for the solids velocity

D.4 State diagram data for cement

Tab. D.4.1 Normalised and non-dimensional state diagram data for cement using λ_{tot} and λ_s^*

Mass flow rate \dot{G} kg/h	Mass flow ratio μ ---	Average density ρ_s kg/m ³	Average air velocity v m/s	Dynamic pressure P_{dyn} Pa	Pressure drop per unit length $\Delta P/\Delta L$ Pa/m	$\log(\mu)$ ---	$\log(Fr)$ ---
257	0.2	0.9941	44.29	974.96	98.14	3.29	-0.6990
	0.25	0.9934	35.46	624.41	78.83	3.10	-0.6021
	0.3	0.9929	29.56	433.83	66.07	2.94	-0.5229
	0.35	0.9926	25.35	318.84	56.97	2.81	-0.4559
	0.375	0.9925	23.66	277.78	53.34	2.75	-0.4260
	0.38	0.9925	23.35	270.52	52.66	2.74	-0.4202
788	0.5	0.9969	54.17	1462.57	173.45	3.47	-0.3010
	0.75	0.9948	36.19	651.38	115.63	3.12	-0.1249
	0.8	0.9945	33.94	572.66	108.55	3.06	-0.0969
	0.9	0.9941	30.18	452.66	96.81	2.96	-0.0458
	0.95	0.9939	28.59	406.34	91.88	2.91	-0.0223
	1.02	0.9937	26.64	352.56	85.80	2.85	0.0086
950	0.6	0.9973	54.40	1475.55	185.50	3.47	-0.2218
	0.7	0.9963	46.67	1085.14	158.56	3.34	-0.1549
	0.9	0.9951	36.35	657.27	123.51	3.12	-0.0458
	1	0.9946	32.73	532.62	111.41	3.03	0.0000
	1.1	0.9943	29.76	440.34	101.55	2.95	0.0414
	1.15	0.9941	28.47	402.95	97.28	2.91	0.0607
	1.2	0.9939	27.29	370.12	93.36	2.87	0.0792
1300	1	0.9967	44.69	995.30	168.69	3.30	0.0000
	1.1	0.9961	40.65	823.02	153.32	3.22	0.0414
	1.2	0.9957	37.28	691.88	140.63	3.14	0.0792
	1.3	0.9953	34.43	589.76	129.96	3.08	0.1139
	1.4	0.9950	31.98	508.69	120.86	3.01	0.1461
	1.5	0.9947	29.85	443.25	113.00	2.95	0.1761
	1.58	0.9945	28.35	399.58	107.45	2.91	0.1987

Tab. D.4.2 Normalised and non-dimensional state diagram data for cement using λ_{tot} and λ_s'

Mass flow rate \dot{G} kg/h	Mass flow ratio μ ---	Average density ρ_s kg/m ³	Average air velocity v m/s	Dynamic pressure P_{dyn} Pa	Pressure drop per unit length $\Delta P/\Delta L$ Pa/m	$\log(\mu)$ ---	$\log(Fr)$ ---
257	0.2	0.9941	44.29	974.96	98.08	3.29	-0.6990
	0.25	0.9934	35.46	624.41	78.81	3.10	-0.6021
	0.3	0.9929	29.56	433.83	66.07	2.94	-0.5229
	0.35	0.9926	25.35	318.83	56.99	2.81	-0.4559
	0.375	0.9925	23.66	277.78	53.35	2.75	-0.4260
	0.38	0.9925	23.35	270.52	52.68	2.74	-0.4202
788	0.5	0.9969	54.17	1462.59	173.06	3.47	-0.3010
	0.75	0.9948	36.19	651.39	115.52	3.12	-0.1249
	0.8	0.9945	33.94	572.66	108.47	3.06	-0.0969
	0.9	0.9941	30.18	452.66	96.78	2.96	-0.0458
	0.95	0.9939	28.59	406.34	91.86	2.91	-0.0223
	1.02	0.9937	26.64	352.56	85.80	2.85	0.0086
950	0.6	0.9973	54.40	1475.58	185.00	3.47	-0.2218
	0.7	0.9963	46.67	1085.15	158.24	3.34	-0.1549
	0.9	0.9951	36.35	657.28	123.37	3.12	-0.0458
	1	0.9946	32.73	532.63	111.33	3.03	0.0000
	1.1	0.9943	29.76	440.34	101.51	2.95	0.0414
	1.15	0.9941	28.47	402.95	97.26	2.91	0.0607
	1.2	0.9940	27.29	370.12	93.36	2.87	0.0792
1300	1	0.9967	44.69	995.31	168.27	3.30	0.0000
	1.1	0.9961	40.65	823.03	153.01	3.22	0.0414
	1.2	0.9957	37.28	691.88	140.40	3.14	0.0792
	1.3	0.9953	34.43	589.77	129.79	3.08	0.1139
	1.4	0.9950	31.98	508.69	120.75	3.01	0.1461
	1.5	0.9947	29.85	443.25	112.93	2.95	0.1761
	1.58	0.9945	28.35	399.58	107.41	2.91	0.1987

D.5 Initial conditions for tube ice conveyingTab. D.5.1 Pressure ratio vs. initial solids Froude number for tube ice using λ_{tot} and λ_s'

Initial solids Froude number Fr_{co} ---	Pressure ratio at $\dot{G} = 9360$ kg/h P_i/P_e ---	Pressure ratio at $\dot{G} = 13100$ kg/h P_i/P_e ---	Pressure ratio at $\dot{G} = 16200$ kg/h P_i/P_e ---	Pressure ratio at $\dot{G} = 22300$ kg/h P_i/P_e ---
0.7713	1.3931	1.4858	1.6125	
1.7355	1.3959	1.4942	1.6359	1.7211
3.0853	1.3963	1.4960	1.6408	1.7330
6.9418	1.3951	1.4959	1.6427	1.7377
12.3410	1.3930	1.4942	1.6420	1.7376
49.3641	1.3828	1.4838	1.6337	1.7284
111.0692	1.3725	1.4723	1.6234	1.7159

D.6 Bend friction coefficient data

Tab. D.6.1 Sliding friction coefficients for bend flow in a 136 mm diameter uPVC pipe

Sliding friction coefficient f ---	Ice mass flow rate G kg/s
0.3	2.56
0.2	3.64
0.125	4.51
0.075	6.19

D.7 Results for the conveying simulations with tube using λ_{tot} and λ_s' Tab. D.7.1 Results for tube ice conveying at $\dot{G} = 9360$ kg/h using λ_{tot} and λ_s'

Tube ice mass flow rate \dot{G} kg/h	Mass flow ratio μ ---	Inlet temperature T °C	Absolute outlet pressure P_e Pa	Initial solids velocity c_o m/s	Pipe roughness ϵ m	Feeder air leakage $Leakage$ %
9360	4.09	0	88500	1	$1 \cdot 10^{-4}$	9.86
Distance from feed point L m	Simulated pressure relative to exit ΔP Pa	Simulated average air velocity v m/s	Simulated solids velocity c m/s	Experimental pressure relative to exit [91SH1] ΔP Pa	Experimental average air velocity [91SH1] v m/s	Experimental solids velocity [91SH1] c m/s
-2.00	35070.02	30.81	0.00	35000.00	31.00	0.00
-1.00	34963.60	30.83	0.00			
0.00	34857.08	30.86	0.00			
0.86	32484.17	28.36	6.33			
2.58	31031.55	28.71	9.17			
3.44	30552.35	28.82	10.05			
5.16	29790.71	29.01	11.36			
6.88	29179.33	29.16	12.32			
8.60	28657.26	29.29	13.07			
12.04	27775.28	29.51	14.17			
17.20	26680.93	29.79	15.26			
22.36	25735.53	30.04	15.98			
24.08	25441.30	30.12	16.17			
25.80	25154.93	30.19	16.35	25800.00	30.40	17.27
55.10	20864.39	31.38	17.95			
84.40	16965.33	32.54	18.87	17800.00	32.60	18.72
92.72	15884.49	32.87	19.12			
101.73	14722.46	33.24	19.38			
102.43	14633.41	33.27	19.40			
103.12	14544.40	33.30	19.42			
103.81	14455.43	33.33	19.44			
104.51	14366.51	33.36	19.46			
105.20	14277.63	33.39	19.48			
105.38	14230.12	33.40	18.62			
105.56	14179.48	33.42	17.85			
105.74	14125.72	33.44	17.15			
105.92	14068.76	33.45	16.52			
106.10	14008.45	33.47	15.94			
110.75	13046.32	33.79	17.11			
115.09	12257.13	34.06	17.92			
115.40	12203.60	34.07	17.97			
115.58	12149.06	34.09	17.27			
115.75	12091.12	34.11	16.65			
115.93	12029.98	34.13	16.08			
116.11	11965.62	34.15	15.56			
116.29	11898.03	34.18	15.09			
118.93	11237.45	34.40	16.08			
158.57	4878.67	36.75	21.31			
195.56	0.49	38.77	23.09	0.00	39.20	23.09

Tab. D.7.2 Results for tube ice conveying at $\dot{G} = 13100$ kg/h using λ_{tot} and λ_s'

Tube ice mass flow rate \dot{G} kg/h	Mass flow ratio μ ---	Inlet temperature T °C	Absolute outlet pressure P_e Pa	Initial solids velocity c_0 m/s	Pipe roughness ϵ m	Feeder air leakage <i>Leakage</i> %
13100	5.19	0	91300	1	$1 \cdot 10^{-4}$	10.26
Distance from feed point L m	Simulated pressure relative to exit ΔP Pa	Simulated average air velocity v m/s	Simulated solids velocity c m/s	Experimental pressure relative to exit [91SH1] ΔP Pa	Experimental average air velocity [91SH1] v m/s	Experimental solids velocity [91SH1] c m/s
-2.00	45282.77	30.89	0.00	46100.00	30.50	0.00
-1.00	45165.00	30.91	0.00			
0.00	45047.13	30.94	0.00			
0.86	42268.65	28.34	6.87			
2.58	40466.93	28.73	9.77			
3.44	39869.16	28.86	10.66			
5.16	38917.31	29.07	11.96			
6.88	38151.98	29.24	12.90			
8.60	37497.45	29.39	13.62			
12.04	36388.91	29.65	14.67			
17.20	35005.78	29.97	15.69			
22.36	33801.57	30.26	16.36			
24.08	33424.79	30.35	16.54			
25.80	33057.13	30.44	16.69	31200.00	30.20	17.13
55.10	27454.10	31.88	18.25			
84.40	22274.66	33.33	19.31	23600.00	33.00	18.99
92.72	20830.98	33.76	19.61			
101.73	19275.22	34.24	19.94			
102.43	19155.82	34.27	19.97			
103.12	19036.46	34.31	19.99			
103.81	18917.13	34.35	20.02			
104.51	18797.84	34.39	20.04			
105.20	18678.57	34.42	20.07			
105.38	18619.08	34.44	19.49			
105.56	18556.68	34.46	18.96			
105.74	18491.47	34.48	18.46			
105.92	18423.41	34.50	18.00			
106.10	18352.50	34.53	17.57			
110.75	17215.42	34.89	18.51			
115.09	16250.63	35.20	19.18			
115.40	16184.30	35.22	19.22			
115.58	16118.72	35.24	18.72			
115.75	16050.20	35.27	18.26			
115.93	15978.85	35.29	17.83			
116.11	15904.67	35.31	17.43			
116.29	15827.65	35.34	17.05			
118.93	15075.43	35.59	17.84			
158.57	6911.32	38.55	22.52			
195.56	0.10	41.47	24.70	0.00	41.60	24.68

Tab. D.7.3 Results for tube ice conveying at $\dot{G} = 16200$ kg/h using λ_{tot} and λ_s'

Tube ice mass flow rate \dot{G} kg/h	Mass flow ratio μ ---	Inlet temperature T °C	Absolute outlet pressure P_e Pa	Initial solids velocity c_o m/s	Pipe roughness ϵ m	Feeder air leakage <i>Leakage</i> %
16200	5.12	0	97000	1.5	$1 \cdot 10^{-4}$	10.2
Distance from feed point L m	Simulated pressure relative to exit ΔP Pa	Simulated average air velocity v m/s	Simulated solids velocity c m/s	Experimental pressure relative to exit [91SH1] ΔP Pa	Experimental average air velocity [91SH1] v m/s	Experimental solids velocity [91SH1] c m/s
-2.00	62344.72	33.23	0.00	62300.00	33.60	0.00
-1.00	62186.58	33.26	0.00			
0.00	62028.27	33.30	0.00			
0.86	59007.53	30.48	7.89			
2.58	57022.53	30.87	11.11			
3.44	56364.98	31.00	12.07			
5.16	55319.64	31.22	13.45			
6.88	54479.94	31.39	14.43			
8.60	53761.44	31.54	15.17			
12.04	52539.59	31.80	16.20			
17.20	50997.71	32.13	17.17			
22.36	49631.41	32.43	17.78			
24.08	49198.50	32.52	17.94			
25.80	48773.45	32.62	18.08	48400.00	32.80	18.85
55.10	41988.08	34.21	19.55			
84.40	35263.45	35.95	20.75	35000.00	36.10	21.04
92.72	33309.66	36.49	21.12			
101.73	31160.14	37.10	21.53			
102.43	30993.15	37.15	21.56			
103.12	30825.92	37.20	21.59			
103.81	30658.42	37.25	21.62			
104.51	30490.67	37.29	21.66			
105.20	30322.65	37.34	21.69			
105.38	30248.80	37.37	21.33			
105.56	30172.70	37.39	20.99			
105.74	30094.50	37.41	20.67			
105.92	30014.20	37.43	20.36			
106.10	29931.81	37.46	20.07			
110.75	28535.77	37.88	20.85			
115.09	27293.65	38.25	21.43			
115.40	27206.39	38.28	21.46			
115.58	27128.29	38.31	21.13			
115.75	27047.97	38.33	20.82			
115.93	26965.58	38.36	20.52			
116.11	26881.11	38.38	20.23			
116.29	26794.61	38.41	19.96			
118.93	25903.14	38.69	20.59			
158.57	13899.89	42.87	25.08			
195.56	0.60	49.02	28.71	0.00	49.10	29.64

Tab. D.7.4 Results for tube ice conveying at $\dot{G} = 22300$ kg/h using λ_{tot} and λ_s'

Tube ice mass flow rate \dot{G} kg/h	Mass flow ratio μ ---	Inlet temperature T °C	Absolute outlet pressure P_e Pa	Initial solids velocity c_o m/s	Pipe roughness ϵ m	Feeder air leakage <i>Leakage</i> %
22300	7.01	0	98200	1.5	$1 \cdot 10^{-4}$	10.2
Distance from feed point L m	Simulated pressure relative to exit ΔP Pa	Simulated average air velocity v m/s	Simulated solids velocity c m/s	Experimental pressure relative to exit [91SH1] ΔP Pa	Experimental average air velocity [91SH1] v m/s	Experimental solids velocity [91SH1] c m/s
-2.00	73180.33	30.79	0.00	70200.00	31.30	0.00
-1.00	73033.74	30.82	0.00			
0.00	72887.03	30.85	0.00			
0.86	69102.50	28.32	8.10			
2.58	66630.97	28.74	11.11			
3.44	65814.85	28.88	11.98			
5.16	64520.47	29.11	13.21			
6.88	63482.52	29.30	14.07			
8.60	62594.57	29.46	14.70			
12.04	61081.69	29.74	15.57			
17.20	59160.79	30.10	16.36			
22.36	57444.58	30.43	16.86			
24.08	56898.24	30.53	17.00			
25.80	56360.84	30.64	17.12	54200.00	31.10	17.73
55.10	47764.54	32.43	18.53			
84.40	39425.50	34.38	19.85	39300.00	34.40	19.91
92.72	37049.32	34.98	20.25			
101.73	34459.30	35.66	20.70			
102.43	34259.14	35.71	20.74			
103.12	34058.81	35.77	20.77			
103.81	33858.33	35.82	20.81			
104.51	33657.68	35.88	20.84			
105.20	33456.87	35.93	20.88			
105.38	33365.27	35.96	20.70			
105.56	33271.79	35.98	20.54			
105.74	33176.73	36.01	20.37			
105.92	33080.12	36.03	20.22			
106.10	32981.95	36.06	20.07			
110.75	31431.09	36.49	20.63			
115.09	30032.67	36.88	21.07			
115.40	29933.97	36.91	21.10			
115.58	29840.03	36.94	20.93			
115.75	29744.25	36.97	20.76			
115.93	29646.91	36.99	20.61			
116.11	29548.05	37.02	20.46			
116.29	29447.67	37.05	20.31			
118.93	28493.35	37.33	20.74			
158.57	15155.96	41.68	24.50			
195.56	-0.38	48.05	28.23	0.00	48.10	28.98

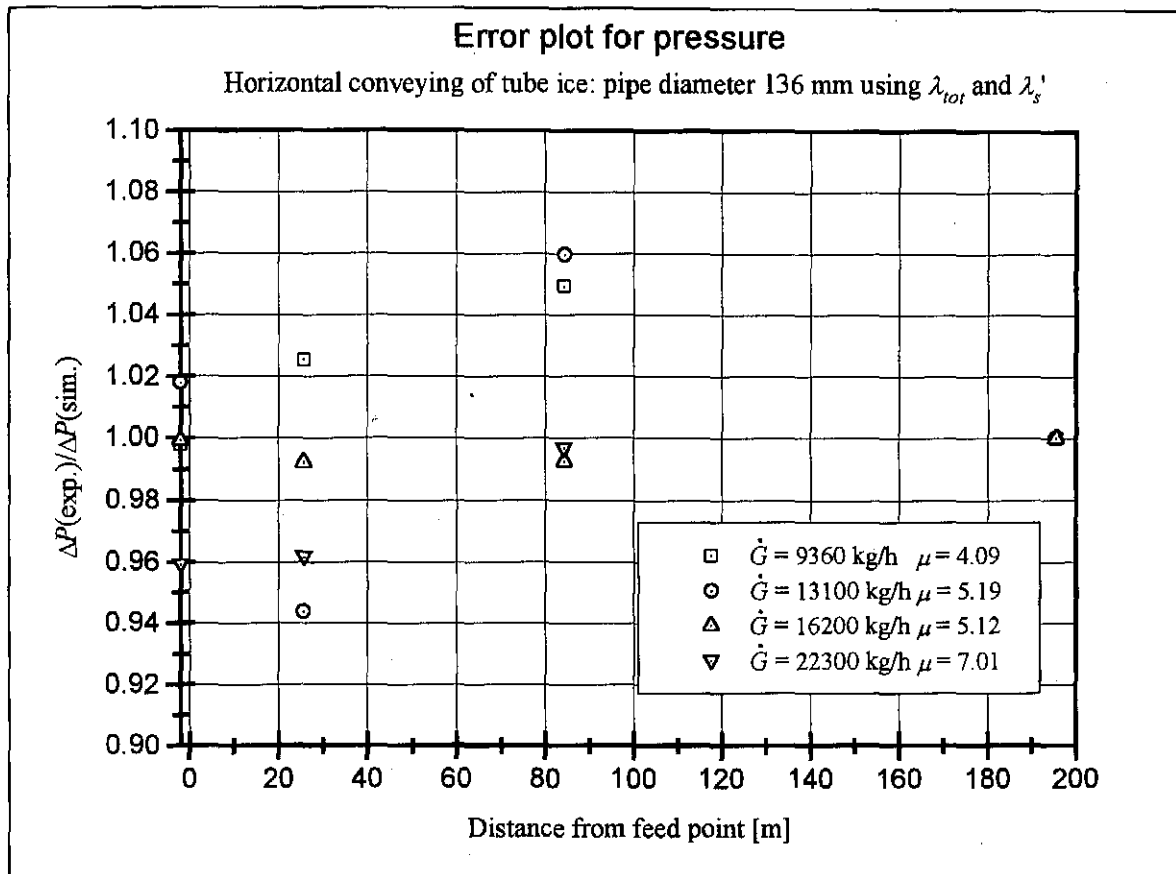


Fig. D.7.1 Tube ice conveying error plot for the pressure

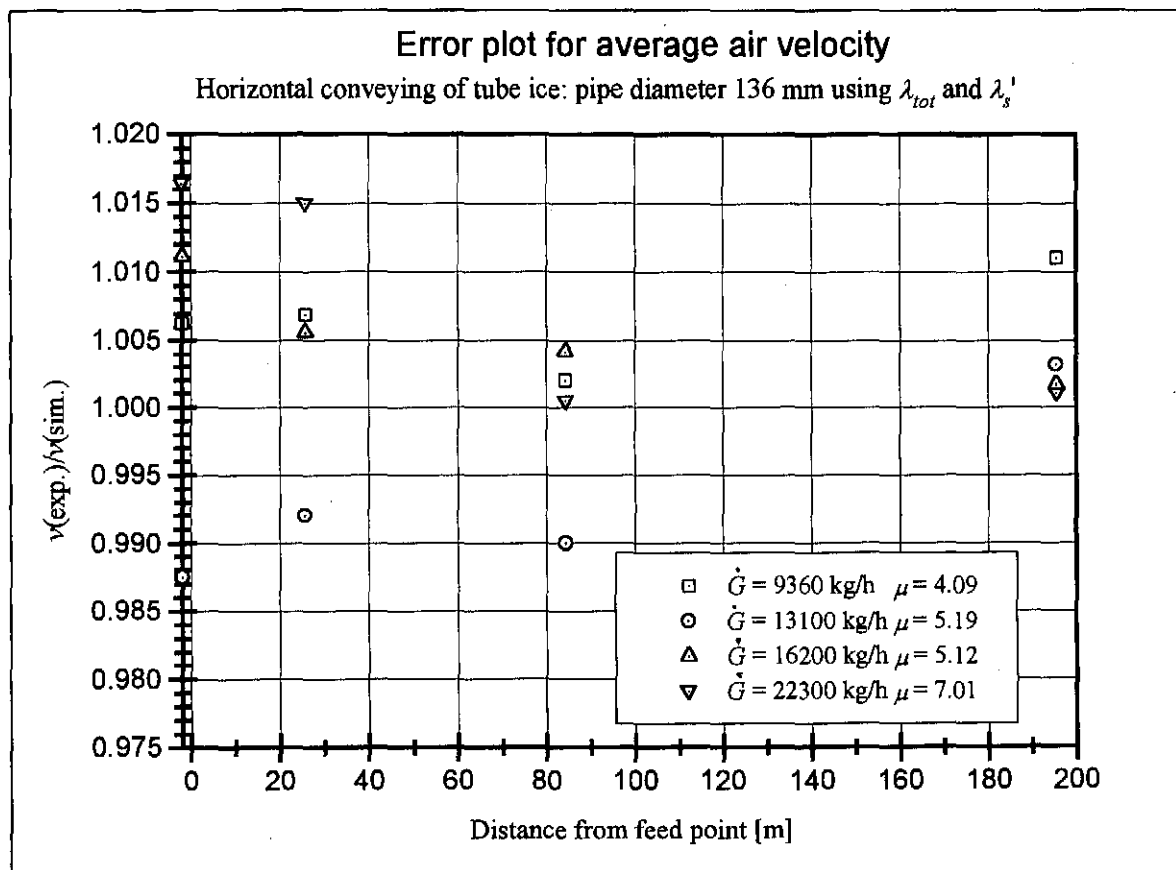


Fig. D.7.2 Tube ice conveying error plot for the average air velocity

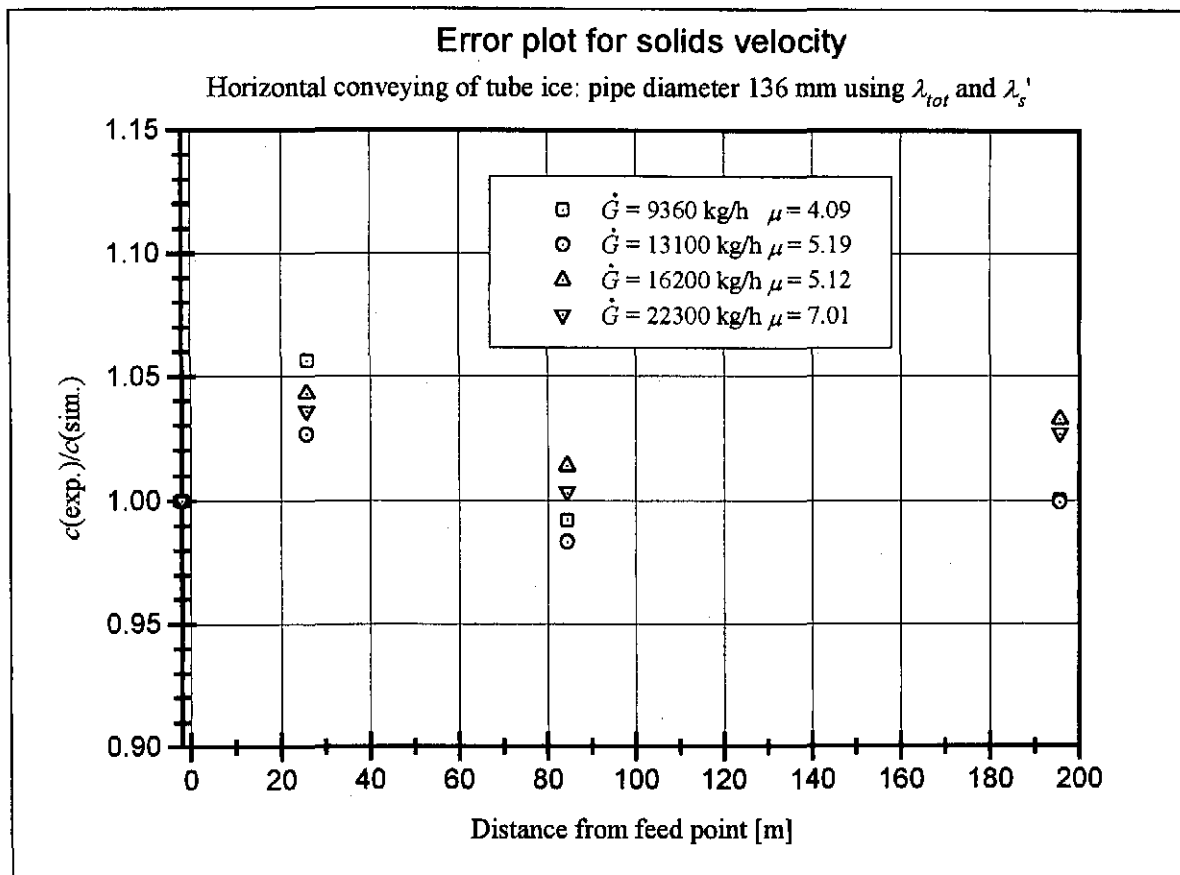


Fig. D.7.3 Tube ice conveying error plot for the solids velocity

D.8 State diagram data for tube ice

Tab. D.8.1 Normalised and non-dimensional simulated state diagram for ice using λ_{tot} and λ_s'

Mass flow rate \dot{G} kg/h	Mass flow ratio μ ---	Average density ρ_s kg/m ³	Average air velocity v m/s	Dynamic pressure P_{dyn} Pa	Pressure drop per unit length $\Delta P/\Delta L$ Pa/m	$\log(\mu)$ ---	$\log(Fr)$ ---
9200	2.5	1.4648	48.86	1748.17	507.27	3.25	0.3979
	2.9	1.3786	44.25	1349.74	276.38	3.17	0.4624
	3	1.3656	43.13	1270.10	241.56	3.14	0.4771
	3.2	1.3468	40.93	1128.34	191.29	3.10	0.5051
	3.5	1.3316	37.81	952.01	150.56	3.03	0.5441
	4	1.3255	33.23	731.72	134.25	2.92	0.6021
	4.5	1.3307	29.43	576.21	148.36	2.81	0.6532
15400	4	1.5210	49.70	1878.33	657.56	3.27	0.6021
	4.5	1.4356	46.16	1529.31	428.99	3.20	0.6532
	5	1.3866	42.75	1266.98	297.98	3.14	0.6990
	5.5	1.3621	39.47	1060.84	232.40	3.07	0.7404
	6	1.3528	36.40	896.15	207.37	3.00	0.7782
	6.5	1.3524	33.61	763.73	206.46	2.93	0.8129
21600	6	1.4861	47.27	1660.54	564.06	3.22	0.7782
	6.5	1.4375	44.77	1440.87	434.18	3.18	0.8129
	7	1.4062	42.33	1259.66	350.33	3.13	0.8451
	7.5	1.3878	39.94	1107.15	301.18	3.08	0.8751
	8	1.3788	37.66	977.59	277.13	3.03	0.9031
	8.5	1.3765	35.49	867.04	270.76	2.98	0.9294
	9	1.3787	33.47	772.46	276.79	2.92	0.9542
27800	7.8	1.4963	46.56	1622.05	591.53	3.21	0.8921
	8.5	1.4476	43.82	1390.02	461.21	3.16	0.9294
	9	1.4253	41.91	1251.42	401.37	3.12	0.9542
	9.5	1.4110	40.03	1130.33	363.27	3.08	0.9777
	10	1.4032	38.20	1023.87	342.25	3.04	1.0000
	10.5	1.4002	36.45	929.99	334.40	3.00	1.0212
Air alone		1.3871	55.11	2106.09	299.22		
		1.3446	44.04	1304.19	185.54		
		1.3225	36.59	885.21	126.26		
		1.3049	29.11	552.99	79.35		

PROGRAMME USER MANUAL

Contents:	Page:
E.1 Introduction.....	E1
E.2 Main program window.....	E1
E.3 Pipeline geometry definition.....	E2
E.4 Entry of conveying properties.....	E5
E.5 Entry and selection of the conveying material.....	E7
E.6 Pneumatic conveyor simulation.....	E9
E.7 Display of results.....	E10
E.8 Blower selection.....	E12
E.9 Error messages and calculation feedback messages.....	E18
E.10 Computer requirements and programme installation procedure.....	E20

E.1 Introduction

PNEUSIM runs under Windows 3.1, Windows '95 or Windows '97. To make provision for users without a mouse pointer all buttons or menu selections can be accessed by pressing the 'Alt' button in combination with the underlined letter in the menu or button caption. The 'Tab' key in combination with the arrow keys can also be used to scroll through the button and input window selections.

Access to help files is through the 'Help' selection in the menu bar at the top of each screen.

E.2 Main program window

The main programme window appears on startup of PNEUSIM and allows the selection of the respective sub-programmes. These are the pipeline geometry definition under 'Geometry' and 'Define', the entry of the required conveying parameters and type of material under 'Simulation' and the visualisation of the output data from the two-phase flow simulation under 'Results' and 'Display'. Roots blower selection can be done under 'Blower'. The options 'Feeder' and 'Separator' are currently not available.

E.3 Pipeline geometry definition

The pipeline geometry is created in the window entitled 'Pipe Layout Design' which can be accessed by selecting the 'Geometry' and 'Define' option in the menu bar of the main programme screen as explained in section E.2.

On selecting 'Define' a screen is displayed requiring definition of a file name for the geometry data file. The default extension for this file is .LYT. On exiting this screen by using the 'OK' button, the Pipe Layout Design screen appears as shown in figure E.1.

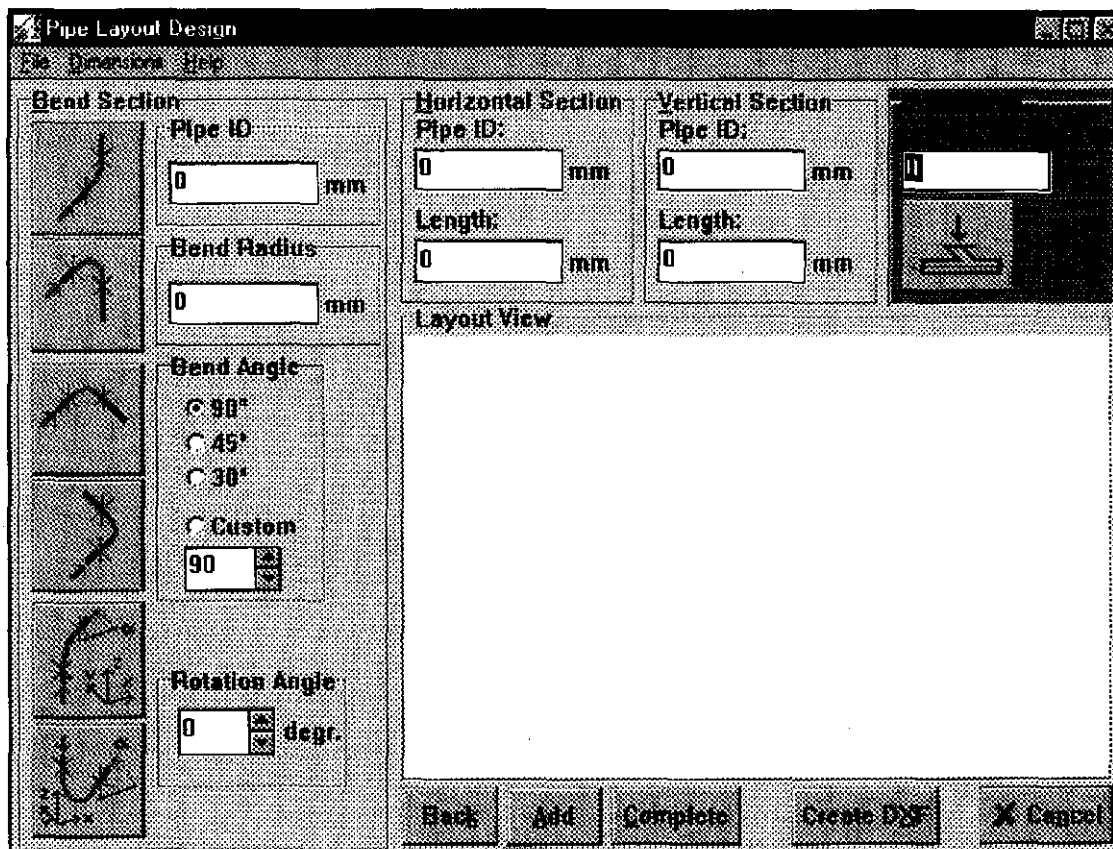


Fig. E.1 Pipeline Layout Design screen

The default unit of dimension is millimeter. This can be changed to meters, inches or feet by selecting the 'Dimensions' menu item. The units of dimension can be changed at any time during program execution.

The layout of the pipeline is defined by joining horizontal, vertical and bend sections and a feed point in the correct sequence. These can be selected from the four separate window frames under the headings of Bend Section, Horizontal Section, Vertical Section and Feed Point. For the horizontal and vertical sections the pipeline inner diameter, *Pipe ID*, and section length, *Length*, requires definition. On completing this and selecting the 'Add' button, the geometry is represented in graphical form in the Layout View window and the corresponding

data stored in the data file. For pneumatic conveying sloping pipe sections are avoided and thus not included as a selection option in the programme.

A selection of six bend types covers the range of possible bend geometries. These are depicted as icon boxes on the left hand side of the screen in figure E.1. The top two icons define bends in the vertical plane with flow from the horizontal to the vertical. The two center icons define left hand and right hand bends in the horizontal plane looking in direction of the flow. The bend angle for a horizontal bend can be chosen between 0° to 90° .

The bottom two icons define bends with flow from the vertical to the horizontal. Definition of the rotation angle allows for a change in direction of the pipeline. After entering the bend section dimensions, the required icon box must be selected by clicking on it with the left hand mouse button and then selecting the 'Add' button.

The programme can simulate air alone flows for sections of pipe with large radius bends. For an air alone analysis, no feed point is added to the pipe layout. For pure two-phase flow the feed point must be the first component selected on starting the pipe layout geometry.

Combined air and two-phase flow simulation is possible by first generating the air supply line geometry and adding the feed point where the material is fed into the pipeline before completing the geometry of the conveying line. Note that the feed tee pipe diameter must be the same as the pipe leading up to the feeding tee.

Stepped pipelines are generated by increasing the diameter of the horizontal or vertical pipe section. The expansion is modelled by a sine function shaped expansion with an expansion half angle of 15° . It is automatically generated during the simulation. For this reason the horizontal and vertical pipe with the increased diameter must be long enough to accommodate the expansion. The pipes are colour coded for easier identification where horizontal pipes are black, vertical pipes are blue, bends are red and the feed point is shown as a thick red line perpendicular to the conveying line. A completed example pipe layout is shown in figure E.2.

Errors in the component definition can be rectified by selecting the 'Back' button which removes the last generated component.

By choosing the 'File' menu item, 'New' option, the current geometry is overwritten and a new data file created. On executing this option, the current layout is removed from the Layout View window and the generation of a new layout can commence.

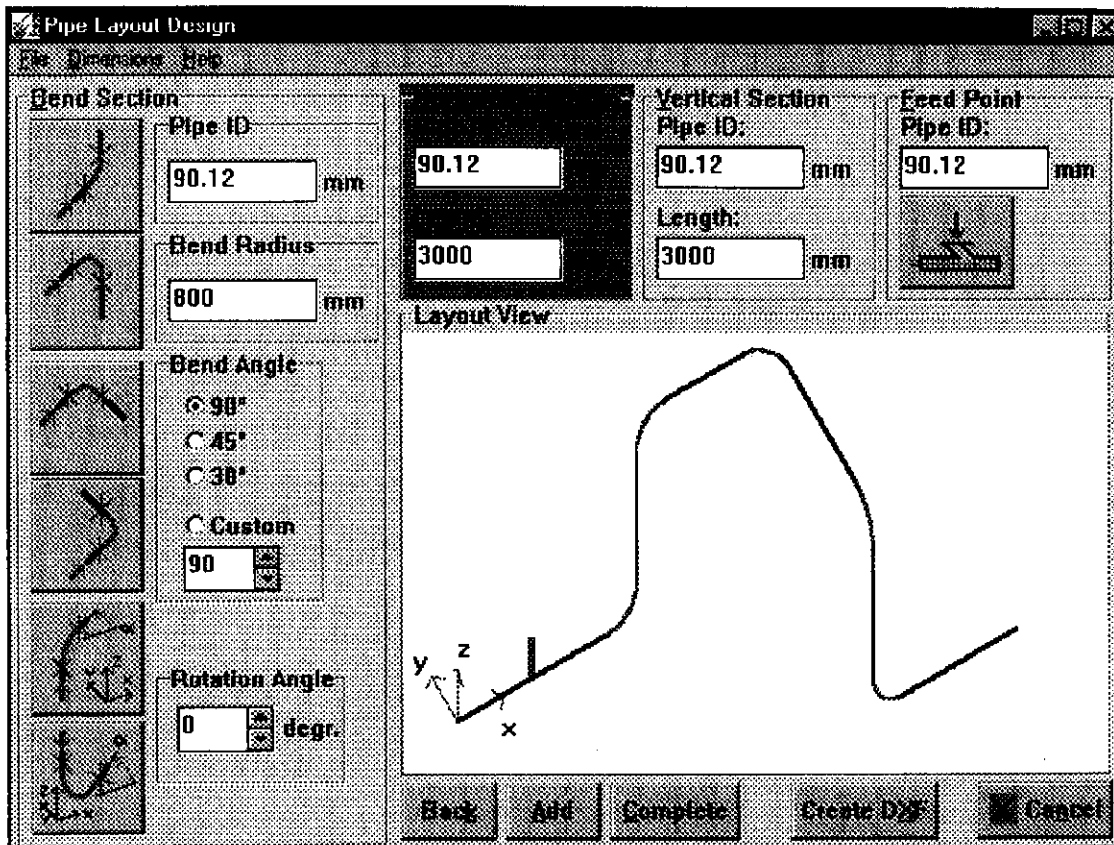


Fig. E.2 Example of a completed pipe layout

As an additional option the pipeline geometry can be converted into a DXF file (Data Exchange File) that can be imported into a drawing programme such as AutoCAD for further

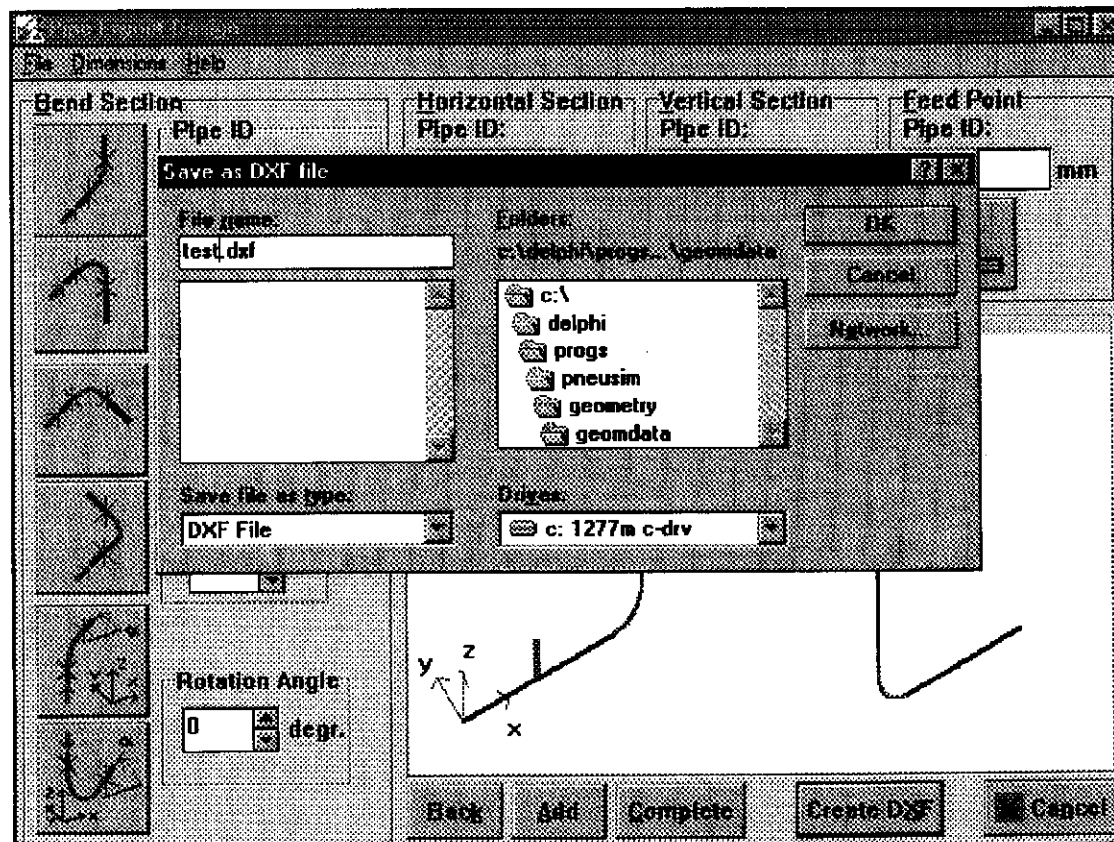


Fig. E.3 Saving the pipeline geometry as a DXF file

use in systems layout design. On selecting the 'Create DXF' button the user is prompted to supply the DXF file name and destination directory of the file as shown in figure E.3. After choosing the OK button, the DXF file is generated and the window returns to its previous display.

The 'File', 'Exit' menu selection or the 'Complete' or 'Cancel' buttons can be used to exit the pipe layout design screen and return to the main program menu.

E.4 Entry of conveying properties

The Conveying Conditions and Material Properties windows are accessed by selecting 'Simulation' in the main programme window. This window is split into two sections as shown in figure E.4. The top section Conveying Conditions contains the details pertaining to the

Conveying Conditions		Conveying Type	
Solids mass flow rate:	4.1667 kg/s	<input checked="" type="radio"/> Positive pressure conveying	
Required mass flow ratio:	6	<input type="radio"/> Vacuum conveying	
Inlet air temperature:	0 deg. C		
Initial solids velocity:	2.5 m/s	Pipe absolute outlet pressure:	101325 Pa
Pipe roughness:	0.0001 m	Estimated absolute inlet pressure:	200000 Pa
Feeder air leakage:	10 %		

Conveying Material Properties	
Name:	OPC (Lamda star)
	Tube Ice (Non Simp)
	OPC (Lamda accent)
Particle density:	921 kg/m ³
Particle diameter:	33040 µm
Sphericity:	0.68331
Friction coefficient:	0.17858
Pipe inner diameter:	0.136 m

Fig. E.4 Conveying Conditions and Material Properties screen

required conveying parameters. Following are the parameters that require specification by the user:

Solids mass flow rate: The required material mass flow rate must be entered in kg/s.

Required mass flow ratio: The required mass flow ratio is assumed constant throughout the pipeline for two-phase flow. Where air leakage through the feeding device is taken into account, the mass flow ratio is adjusted automatically to provide an increased air mass flow in

the clean air section before the feed point according to the leakage specified in the *Feeder air leakage* window.

Inlet air temperature: The conveyor air inlet temperature is entered in °C. The conveying process is assumed isothermal so that the temperature remains constant throughout the conveying pipeline.

Initial solids velocity: The initial solids velocity is required to initialise the calculation procedure. If the initial solids velocity is unknown for a certain material, the simulation should be run for a range of initial velocities (approx. range: 0.1 - 6 m/s) and the resultant pressure drop versus the initial solids velocity plotted. This curve shows a maximum pressure drop corresponding to an initial solids velocity. This solids velocity is then used for all subsequent simulations for the specific material that it was determined for.

Pipe roughness: The pipe roughness is used for air alone pressure drop determination and in the bend flow model. The unit for the surface roughness is meters. The roughness ratio is automatically calculated utilising the pipe diameter from the pipe layout file.

Feeder air leakage: The estimated feeder leakage is defined as a fraction of the inlet air mass flow rate where:

$$\% \text{ leakage} = 100 \left(1 - \frac{\text{Conveying air mass flow rate}}{\text{Inlet air mass flow rate}} \right) \quad (\text{E.1})$$

For rotary vane feeders a rough estimate lies at 10%. The mass flow ratio entered in the *Required mass flow ratio* entry is automatically adjusted to provide the increased inlet air mass flow rate in the clean air simulation before the feed point where the air leakage occurs.

The type of conveying to be modelled is selected in the Conveying Type window. Selecting the appropriate button changes the required windows for the pressure. For positive pressure conveying the *pipe absolute outlet pressure* is required. This is usually atmospheric pressure plus the pressure drop expected over the solids and air separation equipment. An estimate of the absolute conveyor pipe inlet pressure is also required to give the program a reference value for starting the simulation. Should this be too low, the programme will indicate this during the simulation process and return to the current window. For vacuum conveying only the conveyor inlet pressure is required.

During the simulation process for positive pressure conveying the programme uses an iteration procedure to obtain the correct inlet pressure. The calculation for vacuum conveying is completed in one step without iteration.

E.5 Entry and selection of the conveying material

The Conveying Conditions and Material Properties window which is accessed from 'Simulation' menu in the main programme window also contains a material database and allows the user to define or erase materials from the database. This is found at the bottom of the screen under the heading Conveying Material Properties as depicted in figure E.4

Available materials from the database are shown by name in the display window on the left hand side of this section. The material is selected by highlighting the material name with a click on the left hand mouse button while pointing at the name. Materials can also be added or deleted by depressing the 'Insert Material' or 'Delete Material' buttons respectively. The 'Insert Material' button brings up the Insert New Material window in which the material properties are defined as shown in figure E.5. The following properties are required:

Material name: A descriptive name for the material is entered in this field.

Particle true density: The true particle density is used by the simulation programme. This should not be confused with the bulk density. The unit required is in kg/m^3 .

Particle mean diameter: The particle equivalent spherical diameter is entered in this field in μm .

Particle sphericity: The particle sphericity defines the shape of the particle and is defined as the ratio of the surface area of a particle of equivalent spherical diameter of the true particle (i.e. a

The screenshot shows a dialog box titled "Insert New Material". It contains the following fields and controls:

- Material name:** A text box containing "Hydrated lime".
- Particle true density:** A text box with the unit "kg/m³".
- Particle mean diameter:** A text box with the unit "µm".
- Particle sphericity:** A text box.
- Sliding friction coefficient:** A text box.
- Pipe inner diameter:** A text box with the unit "m".
- Mixture friction coefficient:** Five text boxes labeled a, b, c, d, and e.
- Solids friction coefficient:** Five text boxes labeled a, b, c, d, and e.
- Pressure minimum curve correlation:** Two text boxes labeled a and b.
- Buttons:** "Insert" and "Cancel" buttons at the bottom right.

Fig. E.5 Adding a conveying material to the database

sphere with an equivalent diameter so that the spherical particle has the same volume as a true particle) to the true surface area of the particle. Valid entries in this field range between 0 and 1 only.

Sliding friction coefficient: The dynamic friction coefficient is used in the bend flow model and is equivalent to the dynamic friction coefficient of the conveying material sliding over the pipe material. Note that this model is not accurate at this time and bend friction coefficients may have to be adjusted according to the material mass flow rate through the conveyor.

Pipe inner diameter: The pipe diameter for which the friction coefficient correlations is valid is required in this field. This serves as a reference for the designer to ensure that the correlations are correctly applied.

Mixture friction coefficient: The mixture friction coefficient or total friction coefficient is correlated according to the following equation:

$$\lambda_{tot} = \exp(a)\mu^b Fr^c Re_d^d \left(\frac{d_s}{d}\right)^e \quad (E.2)$$

where a , b , c , d , e are the constants that are entered into the respective fields in the mixture friction coefficient window. If a constant value of the friction coefficient is required, the natural logarithm of the friction coefficient is entered as constant a . Constants b , c , d and e are entered as zero.

Solids friction coefficient: The mixture friction coefficient or total friction coefficient is correlated according to the following equation:

$$\lambda_s' = \exp(a)\mu^b Fr^c Re_d^d \left(\frac{d_s}{d}\right)^e \quad (E.3)$$

where a , b , c , d , e are the constants that are entered into the respective boxes in the mixture friction coefficient window. If a constant value of the friction coefficient is required, the natural logarithm of the friction coefficient is entered as constant a . Constants b , c , d and e are entered as zero

Pressure minimum correlation: This field currently has no function. Any value can be entered here.

The 'Start Simulation' button opens the Conveyor Simulation Progress window and is used once all data has been entered for the conveying conditions and the required material has been selected. The Cancel button returns the programme to the main programme window.

E.6 Pneumatic conveyor simulation

Once the Start simulation button has been pressed in the Conveying Conditions and Material Properties window the programme will request a file name for the output data. This file has a standard .TXT extension and its default location is in the PNEUSIM/RESULTS directory. This file contains all the output data in space delimited form (i.e. a space between subsequent entries) and can be imported into a spreadsheet if required. Headings for the data columns are automatically included and self explanatory. Once the data output file has been specified the programme requires the selection of the pipe layout file to be used for the simulation. This is chosen from the layout file dialogue box by clicking on the required file with the left hand mouse button. Once this is done the Conveyor Simulation Progress window appears as shown in figure E.6. The Start button is used to start the simulation. During the process a progress bar will indicate the percentage of the simulation that is completed. The Calculation feedback messages give an indication of the status of the integration process. The *Conveyor outlet pressure*, *Conveyor inlet pressure* and *System pressure drop* will indicate values once the simulation process is complete. Cancel will end the simulation process and return to the Conveying Conditions and Material Properties window.

Any errors occurring during integration will be indicated in separate error message boxes. These indicate the nature of the error and terminate integration. Help files attached to the error

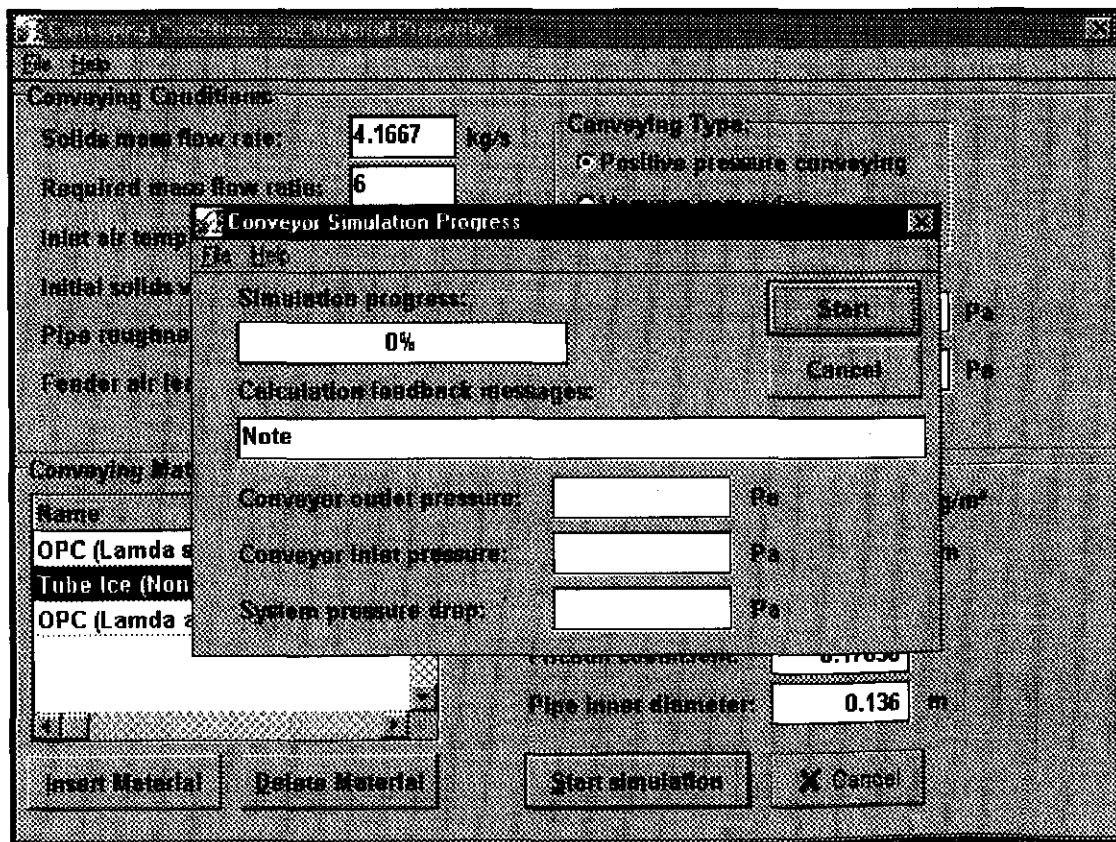


Fig. E.6 Conveyor Simulation Progress screen

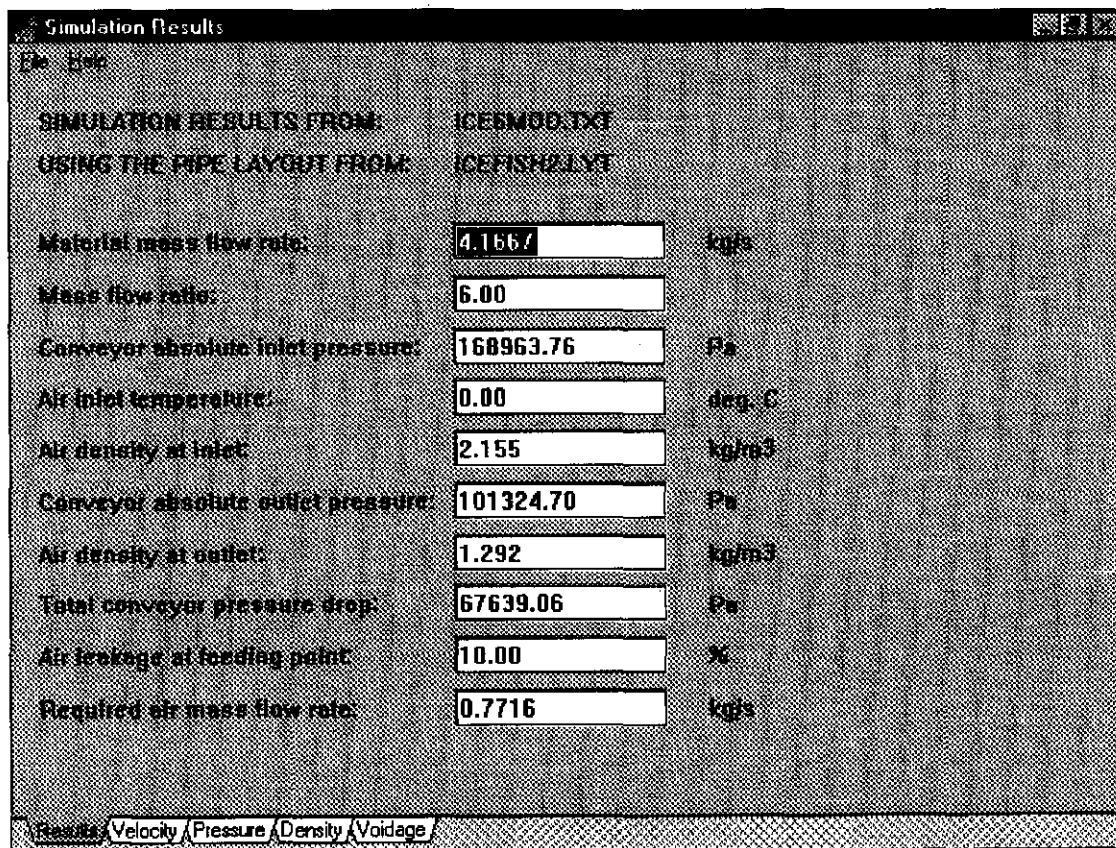
message boxes can be accessed to determine corrective action to solve the encountered problems. Section E.9 of the user manual outlines the possible error messages and the calculation feedback messages that may be encountered. On clicking the OK button on the error message box the programme returns to the Conveying Conditions and Material Properties window where changes to the conveying conditions can be made

E.7 Display of results

The Display Results window is accessed from the 'Results' and 'Display' menus in the main programme window. This programme module displays and prints the main results of the two-phase flow simulation. The window consists of five tabs that are visible at the bottom of the screen. The first tab to be displayed is the one containing the main results as shown in figure E.7. The others are: *Velocity*, *Pressure*, *Density* and *Voidage*.

Results: Displays the most important conveyor parameters required for the subsequent design of the solids and air separation units and the selection of the prime air mover.

Velocity: Displays the solids velocity and the average and interstitial air velocity profiles along the pipeline. The x-axis value is the stretched distance of the pipeline. An example of the screen



The screenshot shows a window titled "Simulation Results" with a menu bar containing "File Edit". The main area displays simulation parameters and their values. At the bottom, there are five tabs: "Results", "Velocity", "Pressure", "Density", and "Voidage", with "Results" being the active tab.

Parameter	Value	Unit
SIMULATION RESULTS FROM:	ICESM06.TXT	
USING THE PIPE LAYOUT FROM:	ICEFISH2.LYT	
Material mass flow rate:	4.1567	kg/s
Mass flow ratio:	6.00	
Conveyor absolute inlet pressure:	168963.76	Pa
Air inlet temperature:	0.00	deg. C
Air density at inlet:	2.155	kg/m ³
Conveyor absolute outlet pressure:	101324.70	Pa
Air density at outlet:	1.292	kg/m ³
Total conveyor pressure drop:	67639.06	Pa
Air leakage at loading point:	10.00	%
Required air mass flow rate:	0.7716	kg/s

Fig. E.7 Displaying numerical conveyor results

when choosing this tab is depicted in figure E.8.

Pressure: The absolute conveying pressure trace is displayed in this window.

Density: The air density trace along the pipeline is displayed in this window.

Voidage: The voidage trace is displayed in this window.

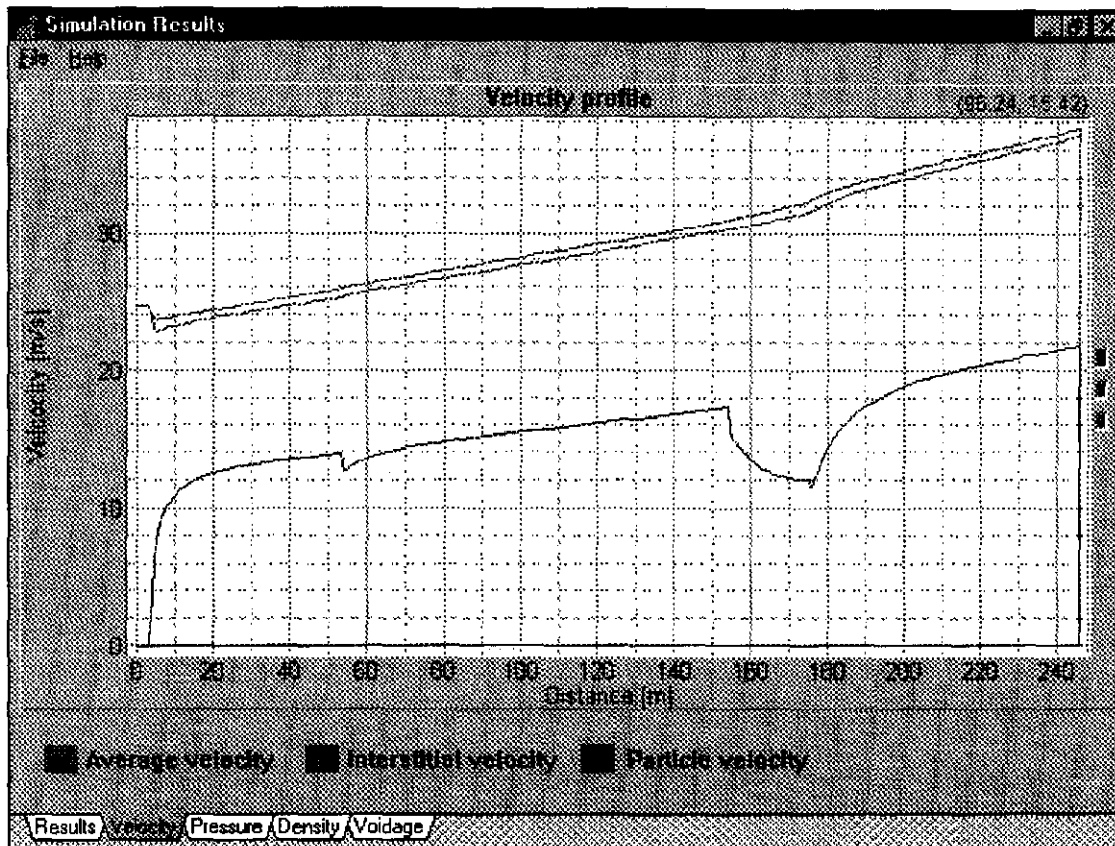


Fig. E.8 Graphical display of the solids velocity and air velocities

The following menus are available for each tab. The 'File' and 'Open' menu discards the old data and loads a new data file according to the file chosen in the file dialogue editor. The 'File' and 'Print' menu is selected to print the results displayed in the *Results* tab. 'File' and 'Exit' returns to the PNEUSIM programme main menu.

Graphs can be printed by clicking on the graph heading with the right hand button of the mouse and choosing the print command. Additional help files are available for the graph explaining features such as zooming and shifting. These are accessed by clicking the graph heading with the right hand mouse button.

E.8 Blower selection

The blower selection main menu is displayed after choosing 'Blower' in the main programme screen as shown in figure E.9. This allows the user to input details pertaining to the project.

These details are used as identifying headings when the blower selection results are printed or stored as a file. The date is automatically generated.

Blower Characteristic Data section: The 'Specify blower characteristics' button allows the user to create a custom blower data file. This button opens the Blower Characteristic Data Input

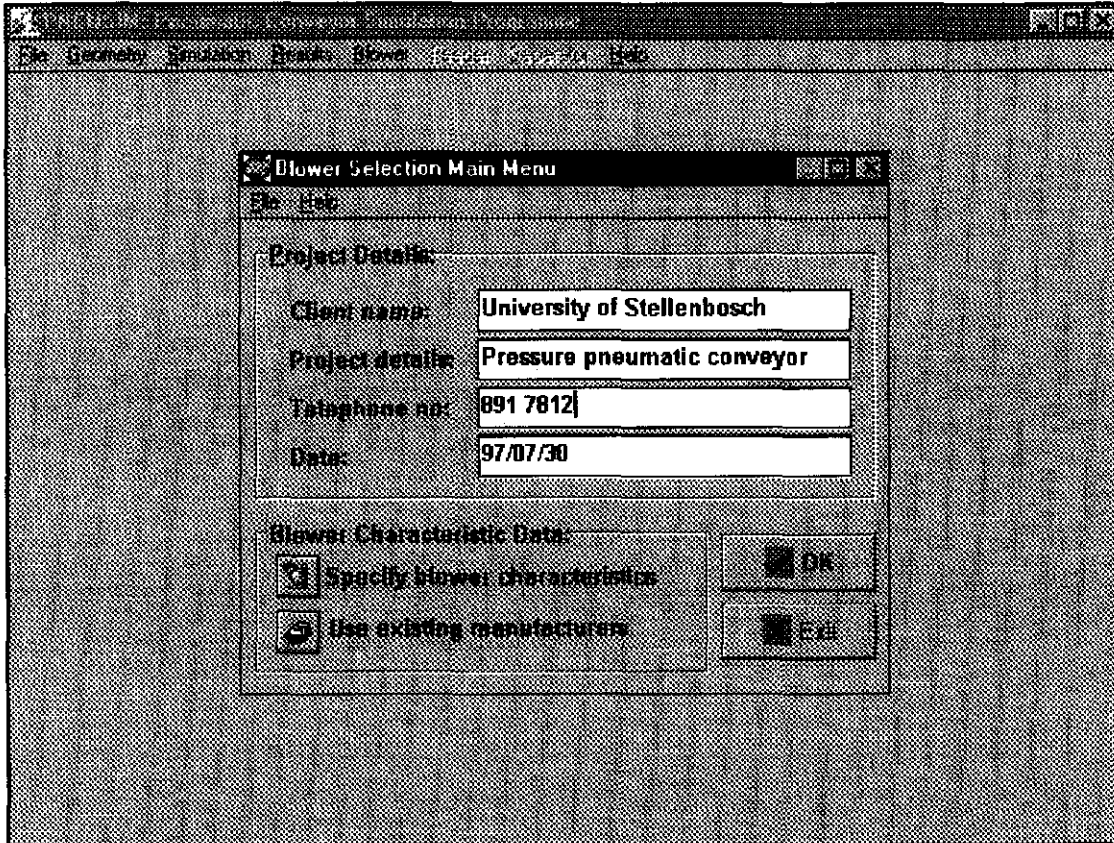


Fig. E.9 Blower main menu screen

window as shown in figure E.10. Details on the use of this feature are given below under the heading: Specifying Blower Characteristics.

The button with the caption 'Use existing manufacturers' refers to the data files containing manufacturer specifications for their range of blowers. When choosing this option the manufacturer data file must already have been generated previously. These data files are used to calculate and select appropriate blowers for the blower performance required by the user.

The 'Use existing manufacturers' button has the same function as the 'OK' button and advances the screen to the Blower Data Input Menu window where the required blower performance is entered by the user. The 'Exit' button returns control to the programme main window.

Specifying Blower Characteristics:

The Blower Characteristic Data Input window is accessed from the 'Specify blower characteristics' button in the blower main menu and is shown in figure E10. This window can be used to input the blower characteristics of a single blower or create a complete file for a full range of blowers. The following details are required to build a blower data file:

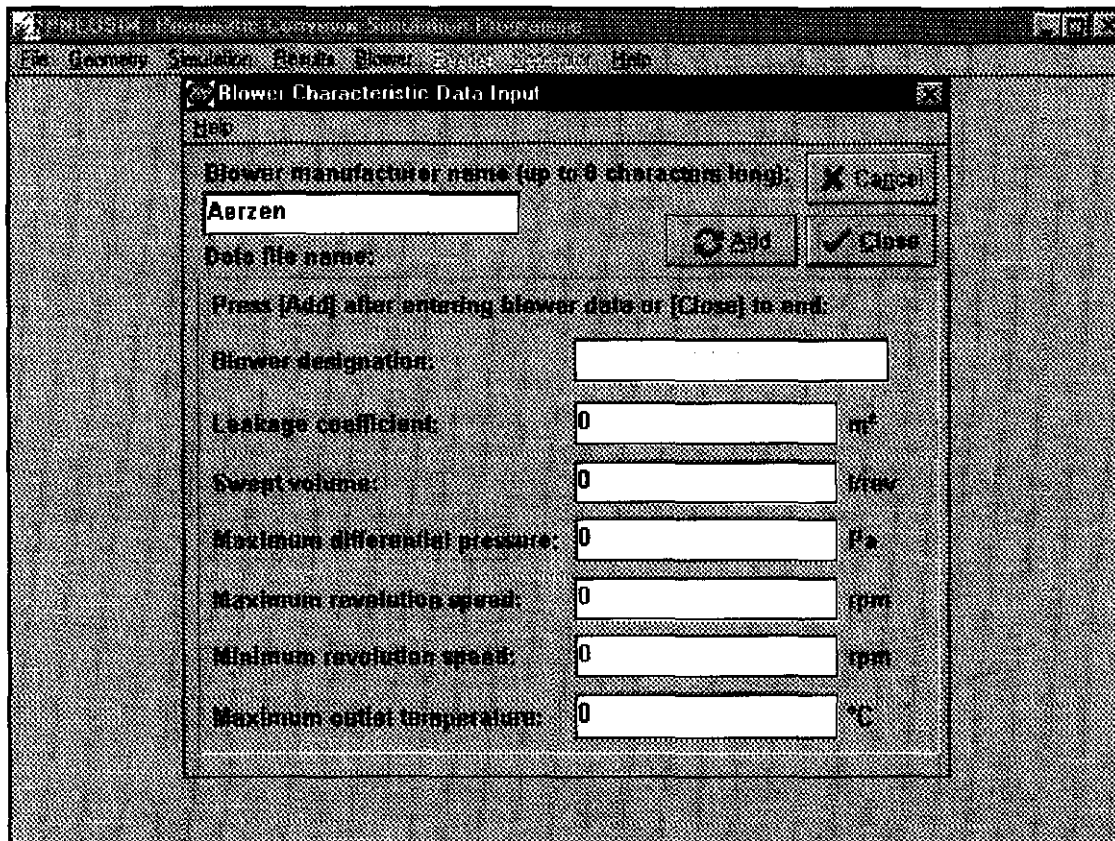


Fig. E.10 Defining blower characteristics

Blower manufacturer name: This name can contain characters a..z, A..Z, the underscore `_`, or numbers from 0..9. The name is also used to select the appropriate manufacturer or blower during the blower selection calculation. For this reason it is important that a descriptive name be used. If a complete range of blowers from a single manufacturer is to be generated it is advisable to use the manufacturer name to identify the data file i.e. [manufacturers name].DAT. This file is stored in the PNEUSIM/BLOWER/BLOWMANF subdirectory as a text file and can be viewed in any text editor.

Blower Designation: The blower designation is typically an abbreviation used to describe the blower type and size.

Leakage coefficient: The leakage coefficient is defined in standard SI format given by the following equation:

$$\text{Leakage coeff. [m}^2\text{]} = \text{Volumetric leakage flow} \left[\frac{\text{m}^3}{\text{s}} \right] \times \left(\frac{\text{Blower inlet density} \left[\frac{\text{kg}}{\text{m}^3} \right]}{\text{Differential pressure [Pa]}} \right)^2 \quad (\text{E.4})$$

It may be necessary to convert in-house company definitions to the above format.

Swept volume: The swept volume is the volume that the blower displaces during one revolution of the rotor. The dimension is in litres per revolution.

Maximum differential pressure: This is the maximum positive differential pressure in Pa that the blower can handle at reference conditions of an atmospheric pressure of 101300 Pa absolute and an inlet temperature of 20 °C. This pressure differential is used to determine the maximum pressure ratio which is enforced for altitude calculations as well as for vacuum applications.

Maximum revolution speed: This specifies the maximum revolution speed in revolutions per minute for which the blower is designed.

Minimum revolution speed: This specifies the minimum revolution speed in revolutions per minute that the blower may run at.

Maximum outlet temperature: The maximum allowable outlet temperature in °C for the given blower.

The buttons at the top right of the window have the following functions:

'Add' adds the given specifications to the data file and clears all data input boxes so that data for the next blower can be entered. The 'Close' closes the data file, closes the current window and returns the controls to the Blower Selection Main Menu.

The 'Cancel' button terminates the data input, removes the data file if one has been created during the current session and returns the controls to the Blower Selection Main Menu.

Specifying the required blower performance:

The Blower Data Input window is accessed by choosing the 'Use existing manufacturers' or the 'OK' button in the Blower Selection Main Menu window. Figure E.11 shows an example of the Blower Data Input Window. This window is used to specify the required performance of the blower which includes flow rates, differential pressure, temperature and safety factors.

Fig. E.11 Entering the required blower performance data

Dimensions are customisable from the top of the menu. Any of the units topics can be chosen to display the different dimensions supported in this window. This window is divided into seven subsections which are in part linked. This means that the values of some of the entries will change in accordance to user input in a different window. Following are the main inputs that are required:

AMBIENT CONDITIONS section: These are the prevailing atmospheric conditions around the blower during operation. Changing the *Altitude* automatically adjusts the *Ambient absolute pressure* according to the Standard US Atmosphere. When the ambient absolute pressure is entered manually the *Altitude* window will not reflect the changes and remains zero.

BLOWER INLET CONDITIONS section: When the **APPLICATION TYPE** is set to *Positive pressure blower*, the inlet conditions will automatically be set to the same as the values in the **AMBIENT CONDITIONS** section. For the **APPLICATION TYPE** set to *Exhauster Application*, the inlet conditions can be set by the user, either changing the *Blower absolute inlet pressure*, the *Blower gauge inlet pressure* or the *Blower differential pressure*. Note that gauge pressure for vacuum conditions must be entered as a negative value.

For the **APPLICATION TYPE** section set to *Pressure/Exhauster combination* both the blower inlet and outlet conditions can be specified. Note that the *Blower absolute outlet pressure* must always be higher than the *Blower absolute inlet pressure*.

BLOWER OTLET PRESSURE section: For an **APPLICATION TYPE** section set to *Positive pressure blower*, the outlet conditions can be set by the user, either changing the *Blower absolute outlet pressure*, *Blower gauge outlet pressure* or the *Blower differential pressure*. The *user defined* button will be checked.

For the **APPLICATION TYPE** section set to *Exhauster Application*, the outlet conditions will be at ambient conditions. The *at ambient condition* button will be checked.

For the **APPLICATION TYPE** section set to *Pressure/Exhauster combination* both the blower inlet and outlet conditions can be specified. Note that the *Blower absolute outlet pressure* must always be higher than the *Blower absolute inlet pressure*.

APPLICATION TYPE section: The application type can be chosen according to the function of the blower in question. Selecting the application simplifies the data input as the inlet conditions for the *Positive pressure blower* are automatically set to ambient conditions. The outlet conditions for the *Exhauster Application* are set to ambient conditions. Where none of the two above apply, choose the *Pressure/Exhauster combination*.

INLET FLOW RATE section: The inlet flow rate can be entered as a volume or mass flow rate. The current inlet conditions are used for the conversion from one to the other. The 'Flow Rate' button on the top menu bar can be used to change from a volume flow rate to a mass flow rate or vice versa.

DIFFERENTIAL PRESSURE section: This section provides an alternative to changing the Blower absolute inlet pressure, the Blower absolute outlet pressure, the Blower gauge inlet pressure or the Blower gauge outlet pressure.

POWER LOSSES: The power loss terms containing the *Transmission loss* and the *Motor safety factor* are used to determine the size of the motor required for the blower. The transmission losses for belt drives are typically 5 % and for flexible direct coupling they are in the region of 3 %. Motor safety factors can be taken between 10-15 %.

Two buttons are available on the bottom left of the screen. The 'Select' button opens up the Blower Selection Results screen after having entering the required blower performance. The 'Cancel' button return to the Blower Selection Main Menu without processing information provided in the current window.

Selecting a blower manufacturer:

The Blower Selection Results window is displayed on choosing the 'Select' button in the Blower Data Input Window. The manufacturers are selected from the list in the *Select blower manufacturer/s* section in the top left hand corner. A single manufacturer is chosen with the click of the left hand mouse button. If more than one manufacturer is desired depress the 'Ctrl' key on the keyboard while selecting the required manufacturers with the mouse. Selecting the 'OK' button below the manufacturers list will result in the blower selection being displayed in the window at the bottom of the screen as shown in figure E.12. If the window is filled, a scroll bar appears next to the right border and additional results can be made visible by scrolling down the window.

Blower Selection Results: University of Stellenbosch

Select blower manufacturer/s:

- AERZEN
- HIBON
- ROBUSCHI

OK Cancel

Compatible blowers:

Blower Type:	Volumetric efficiency:	Temp. rise:	Outlet temp.:	Outlet density:	Outlet volume flow rate:	Shaft power:	Coupling power:	Motor power:	Rev. speed:
	%	°C	°C	kg/m ³	m ³ /s	kW	kW	kW	rpm
HIBON									
SNH40	92.2	27.2	47.2	1.4120	0.8295	32.124	32.124	32.124	1606
SNH50	89.8	28.0	48.0	1.4088	0.8314	32.979	32.979	32.979	1326
SNH60	88.4	28.4	48.4	1.4069	0.8325	33.481	33.481	33.481	1132
SNH70	88.4	28.4	48.4	1.4069	0.8325	33.481	33.481	33.481	947
SNH90	85.5	29.4	49.4	1.4027	0.8351	34.638	34.638	34.638	770
SNH100	81.6	30.8	50.8	1.3966	0.8387	36.297	36.297	36.297	729
SNH110	82.5	30.4	50.4	1.3980	0.8378	35.895	35.895	35.895	653
SNH140	79.5	31.6	51.6	1.3931	0.8408	37.252	37.252	37.252	528
SNH170	75.6	33.2	53.2	1.3862	0.8430	39.163	39.163	39.163	461
SNH200	73.7	34.1	54.1	1.3826	0.8472	40.169	40.169	40.169	404
SNH210	78.6	31.9	51.9	1.3916	0.8417	37.655	37.655	37.655	378
SNH280	74.6	33.6	53.6	1.3844	0.8461	38.666	38.666	38.666	282

Fig. E.12 Selecting a blower

The input data and any additional constant properties are displayed in two sections in the top right hand part of the screen. Choose the 'Cancel' button to return to the Blower Data Input Menu window.

The 'File' selection from the top menu bar allows saving or printing of the selection results.

'File' and 'Save As' saves the results as a text file. Specify a file name in the Save Blower Data File dialogue box. The default extension for this file is .TXT. To view the results, the data file can be imported into a word processor such as for example Word for Windows as a text file and the font changed to 'Courier new' to display the columns correctly. The 'File' and 'Print' selection will print the results.

E.9 Error messages and calculation feedback messages

This section contains a short description of error messages that may occur during the two-phase flow simulation. The *Calculation feedback messages* are explained in the second part of this section. Both are listed in alphabetical order.

Error messages:

- *Air velocity exceeding 200 m/s. Check input data:* The mass flow ratio is too low or the pipeline too long. In the second case a decrease in pressure along the pipeline may cause the velocity to become too high towards the end of the pipeline. To solve this problem: i.) Adjust the conveyor inlet pressure estimate or ii.) Increase the mass flow ratio or iii.) Redefine the pipeline layout using stepped pipelines.
- *Expansion length longer than pipe section. Increase the pipe section length after the expansion:* The length of the pipe containing an expansion is shorter than the expansion itself. The minimum horizontal or vertical pipeline length required when increasing the diameter of the pipe to include an expansion is calculated from:

$$\text{Minimum pipe length} = \frac{d_2 - d_1}{2 \tan 15^\circ} \quad (\text{E.5})$$

where d_2 is the larger pipe diameter and d_1 is the smaller pipe diameter. Regenerate the pipe layout file and ensure that the pipe length at the increased diameter meets the specification of the equation above. Expansions are not physically added as components and are generated automatically at the start of the increased diameter pipe by the programme.

- *Expansion not allowed into a bend or feed point. Ending analysis:* During the generation of the pipe layout file a change in diameter has been specified going into a bend or into the feeding tee. These expansions are not allowable from a practical point of view. Redefine the pipe layout file and restart the simulation.

- *Particle Reynolds number is out of bounds: The particle Reynolds number is too high.* This may be as a result of too high air velocities. Try increasing the mass flow ratio to reduce the air velocity.
- *Pipe Reynolds number out of bounds: The Reynolds number based on the pipe diameter is too high.* This is usually as a result of too high an air velocity. This problem can be solved by increasing the mass flow ratio to reduce the air velocity.
- *Power of negative number. Result set to zero. Error in Power function:* This error may occur if the initial solids velocity is chosen too low or the mass flow ratio is specified too low. Check and adjust these parameters.
- *Temperature out of range for air abs. viscosity calculation:* The conveying air temperature is out of limits for the calculation of the absolute viscosity. The ranges must be within a range of 220K to 380K. Check and correct the air temperature in the Conveying Conditions and Material Properties window.
- *Too many steps after each other. Terminating program:* See the calculation feedback message: *Too many steps at x = ?. IFLAG = 4* below. This message will appear if no solution can be attained due to an unrealistic specification of friction coefficients. Check the conveyor and material input data carefully before retrying the simulation.
- *Unable to open 'data file name':* There is an error with the specified data file. Check if the file name is correctly spelt and that it is available.

Calculation feedback messages:

- *Adjusting relative error. IFlag = 3:* The relative error tolerance was adjusted in the Runge-Kutta-Fehlberg routine to complete the integration. This is an informative message only.
- *Changing Abs. error to 1e-9. IFLAG = 5:* The absolute local error tolerance in the Runge-Kutta-Fehlberg routine has been changed from 0 to 1e-9. This is an informative message only.
- *Increasing Rel. error by 10%. IFLAG = 6:* The accuracy of the integration could not be achieved by using the smallest available step size. The relative local error tolerance is increased by 10% in an attempt to complete the integration. The initial error tolerance is set at 1e-6 for two-phase flow and at 1e-8 for single phase flow. This is an informative message only.
- *Pipe Reynolds number out of bounds for drag coefficient calculation:* The Reynolds number based on the pipe diameter is too high. This is most likely as a result of a too high air velocity. This problem can be solved by increasing the mass flow ratio to reduce the air velocity.

- *Too many steps at x = ?*. *IFLAG = 4*: The Runge-Kutta-Fehlberg integration routine is carrying out excessive derivative evaluations at a point x meters down the pipeline. This may occur at points where variables such as friction coefficients show a rapid change in value due to for example the flow running into a bend where the friction coefficients are modified. This is an informative message but may in excessive cases terminate the integration. This problem is usually associated with the friction coefficient definition. Check this carefully and retry the simulation.
- *Too much output*: This indicates that the automatic step size choice during integration is longer than the step size defined for the output of the data along the pipeline. This is an informative message only.

E.10 Computer requirements and programme installation procedure

The computer programme PNEUSIM was run on a Pentium 60 computer with 16 Mb RAM with Delphi 1.0 and Windows '95 installed. Screen resolution is set to 480x640 pixels for optimum display of the user interface windows. Higher screen resolutions can be utilised but will result in a smaller interface windows. The programme can be run through Windows 3.1, Windows '95 and should also be compatible with Windows '97. A prerequisite is that either the Borland Database Engine (BDE) must be installed either separately or as part of DELPHI 1.0 on the computer so that the conveying material database can be utilised. Two 1.44MB, 3¹/₂ inch computer discs are included at the back of this thesis. Disc 1 contains the executable file of the pneumatic conveyor simulation programme which can be run on a computer conforming to the criteria given above. Disc 2 contains the source code for the pneumatic conveyor simulation programme PNEUSIM in form of a compressed executable file.

For initial evaluation purposes the programme can be run from the first included 1.44 MB, 3¹/₂ inch computer disc. Place disc 1 in the drive of the computer that it is to be run on and run the executable PNEUSIM.EXE that can be found on the disk in the directory PNEUSIM/. Programme execution is slow as a result of running from the 3¹/₂ inch computer disc

For faster programme execution copy the complete PNEUSIM directory from the 3¹/₂ inch computer disc to the root directory of the destination computer and run PNEUSIM.EXE that is found in the PNEUSIM directory. The PNEUSIM directory must be placed in the root directory for the computer programme to run correctly.

The second included 1.44 MB, 3¹/₂ inch computer disc contains the complete source code of the pneumatic conveyor simulation programme which has been compressed in the file SOURCE.EXE. All directories as set out in section F.1 in appendix F can be extracted. To do this, create a directory PNEUSIM in the root directory of the destination computer (usually the C: drive). Copy the file SOURCE.EXE to the PNEUSIM directory of the computer that it is to be installed on. Run the file SOURCE.EXE from DOS or through the 'run' command in Windows 3.1 or Windows '95. In the command line type C:/PNEUSIM/SOURCE.EXE -d if the file has been placed in the PNEUSIM directory in the root directory C:. The '-d' extension must be added to the command line to ensure that all directories including sub-directories are correctly extracted. Do not run the SOURCE.EXE file directly by double clicking with the mouse. Once the files and directories have been extracted they should conform with the directory structure presented in section F.1 in appendix F. The files can now be accessed, modified, compiled and run using DELPHI 1.0.

Note that the computer programme uses separate files for the help function, material database, pipe layout and results. To ensure these can be correctly accessed by the programme the directory locations must conform with the directory structure on the destination computer. Two source code files can be inspected and modified if required. These are PNEUSIM.DPR for the help file locations and MAINMENU.PAS for the location of the remaining files. The file locations can be found at the end of the two files given above.

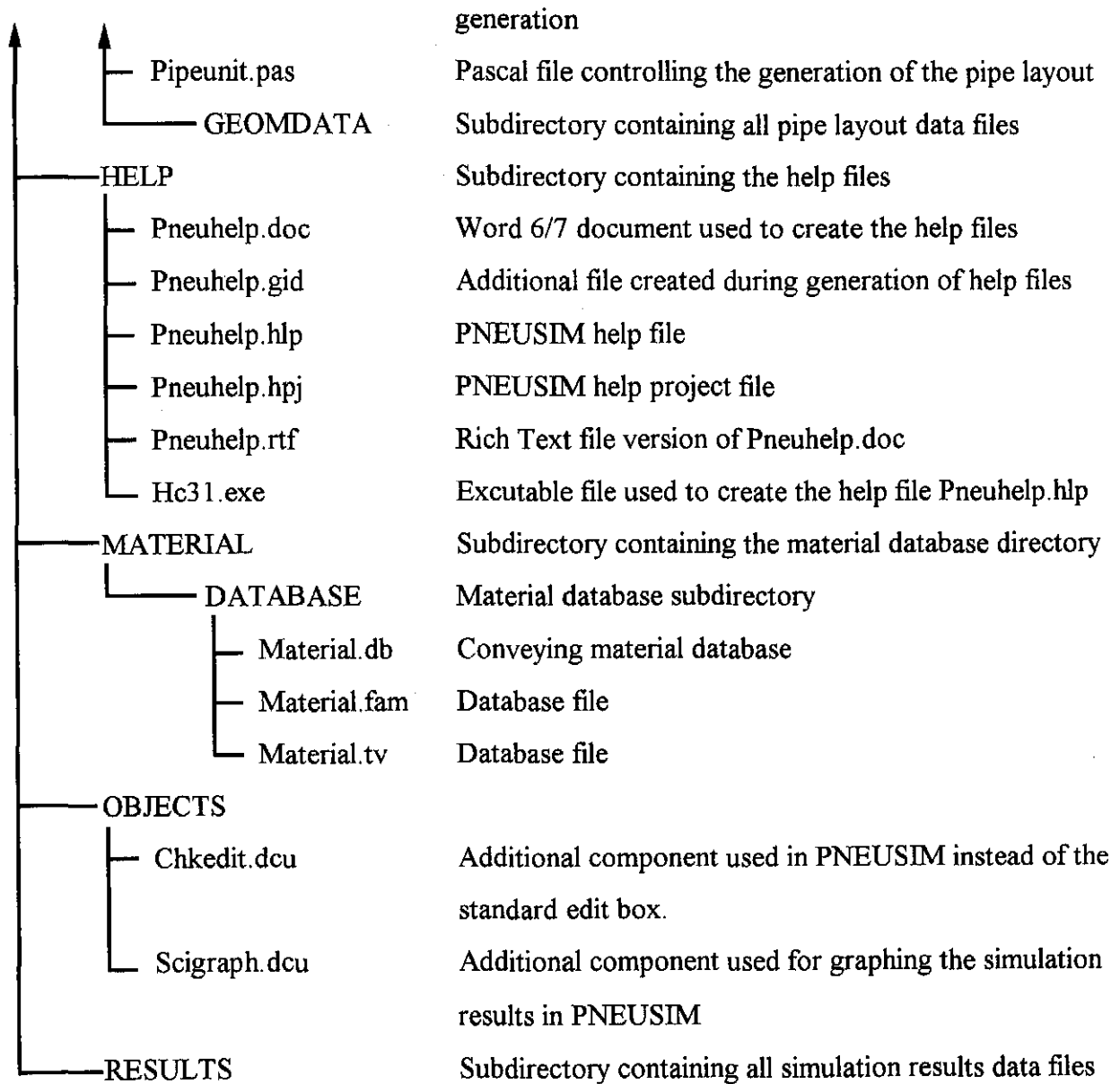
DIRECTORY STRUCTURE AND PROGRAMME FLOWCHART

F.1 File directory structure

The structure and contents of the directories of the programme PNEUSIM are given below as a reference for future users. The files can be accessed through DELPHI 1.0 or any appropriate text editor including PASCAL editors. For DELPHI programmers two non-standard objects require loading into the DELPHI object library before the programme can be modified or compiled. These can be found under the directory named Objects.

PNEUSIM	Main directory
— About.dfm	Form for the About PNEUSIM information window
— About.pas	Pascal file controlling the About form
— FileLoca.pas	Pascal file containing all file locations used by PNEUSIM
— Mainmenu.dfm	Main programme menu form for PNEUSIM
— Mainmenu.pas	Pascal file controlling the Mainmenu form
— Pneusim.dpr	Project file
— Pneusim.dsk	Desktop setting file
— Pneusim.dsm	Additional Delphi file
— Pneusim.opt	Additional Delphi file
— Pneusim.res	Delphi resource file
— Pneusim.exe	PNEUSIM executable file
— Blower.ico	Blower icon
— Pneu.ico	Pneumatic conveyor icon
— BLOWER	Blower subdirectory
— Aboutbl.dfm	Form for the About Blower information window
— Aboutbl.pas	Pascal file controlling the Aboutbl form
— Blowcalc.dfm	Form for blower selection results
— Blowcalc.pas	Pascal file which calculates and selects the blowers from the blower data files and displays the results in the Blowcalc form

Blowchar.dfm	Form for the input blower characteristic data
Blowchar.pas	Pascal file controlling the blower characteristic data input
Blowdata.dfm	Form for the input of the required blower performance
Blowdata.pas	Pascal file controlling the Blowdata form
Blowmain.dfm	Main blower form displaying the project details
Blowmain.pas	Pascal file controlling the Blowmain form
Conversn.pas	Pascal file controlling unit conversions i.e. mm to m etc.
BLOWMANF	Subdirectory containing all blower data files
CALCULAT	Subdirectory for the two-phase flow simulation
Calcunit.dfm	Form displaying simulation progress
Calcunit.pas	This is the core programme file that implements the Runge-Kutta-Fehlberg integration procedure of the two-phase flow differential equations. The STARTANALYSIS procedure for which the flow diagram is presented in the next section is found in this file.
Insunit.dfm	Form for the insertion of a new conveying material
Insunit.pas	Pascal file controlling the Insunit form
Simuunit.dfm	Form used to input conveying material data and the required conveyor parameters
Simuunit.pas	Pascal file controlling the Simuunit form
DISPLAY	Subdirectory containing files used to display simulation results
Display.dfm	Display results form
Display.pas	Pascal file controlling the Display form
Scirun.gid	Additional file created during generation of help files
Scirun.hlp	Help file for the SciGraph object used for graphs in Display.dfm
GEOMETRY	Subdirectory containing all files for the pipe layout generation
Dxfunit.dfm	Form for creating a DXF file from the pipe layout data file
Dxfunit.pas	Pascal file for the DXF conversion
Pipeunit.dfm	Form for the pipe layout generation and pipe layout file



RUNGE-KUTTA-FEHLBERG PROGRAMME LISTING

D.1 Runge-Kutta-Fehlberg differential equation solver programme listing

Program RKF45PAS;

```
(*****)
(* Programme to implement the Runge-Kutta-Fehlberg subroutine for solving two *)
(* differential equations. Based on the FORTRAN programme RKF45 given      *)
(* in Computer Methods for Mathematical Computations 1977 Prentice Hall    *)
(* Forsythe, George E.                                                    *)
(* Malcolm, Michael A.                                                    *)
(* Moler, Cleve B.                                                         *)
(* The algorithm implements self adjusting step size. Refer to Forsythe, Malcolm ... *)
(* & Moler for details pertaining the variables and implementation        *)
(* Translated into Pascal (Delphi) 29.08.96 by K. Wodrich                 *)
(* For the definition, derivation and implementation of the differential equations for *)
(* flat-plate flow refer to White [91WH1] pages 233-237                  *)
(*****)
```

uses

winCRT;

type

```
YVector = array[1..3] of double; {Change the number according to the number of
differential equations to be solved}
```

type

```
WorkRec = {Storage record equivalent to the Fortran Work}
record {and IWork array}
```

```
  a1 : YVector;
  a2 : double;
  a3 : YVector;
  a4 : YVector;
  a5 : YVector;
  a6 : YVector;
  a7 : YVector;
  a8 : double;
  a9 : double;
  a10 : integer;
  a11 : integer;
  a12 : integer;
  a13 : integer;
  a14 : integer;
end;
```

var

```
Work : WorkRec;
```

```

    Y : Yvector; {Dependent variable}
    T : double;  {Independent variable}
NEQN : integer; {Number of differential equations to solve}
    Tout : double; {Final value of the independent variable}
    RelErr : double;
    AbsErr : double;
    IFlag : integer;
    EPS : double;
    U26 : double;
```

```
TFinal : double;
```

```
TPrint : double;
```

```

(*****
(*          POWER FUNCTION double type variable          *)
(*****
function Power(x,a:double): double;
{Function to raise double variable x to the double power of a ie. x^a}
begin;
  IF x > 0 THEN
    Power := EXP(a*LN(x))
  ELSE IF x = 0 THEN
    Power := 0;
  IF x < 0 THEN
    begin
      Writeln('Power of negative number. Result set to zero. Error in Power function');
      Power := 0;
    end;
end; {function Power}
```

```

(*****
(*          MAX FUNCTION double type variable          *)
(*****
function MAX(Value1, Value2 : double): double;
{Function to determine the maximum of two values passed to the function}
begin
  If Value1 >= Value2 THEN
    MAX := Value1
  ELSE
    MAX := Value2;
end; {function MAX}
```

```

(*****
(*          MIN FUNCTION double type variable          *)
(*****
function MIN(Value1, Value2 : double): double;
{Function to determine the maximum of two values passed to the function}
begin
  If Value1 <= Value2 THEN
```

```

    MIN := Value1
ELSE
    MIN := Value2;
end; {function MIN}

```

```

(*****)
(*          SIGNR FUNCTION double type variable          *)
(*****)
function SIGNR(Value1, Value2 : double): double;
{Function equivalent to Fortran Sign function. Checks Value2 for its sign:
If Value2 >= 0 then Value1 = abs(Value1)
If Value2 < 0 then Value1 = -abs(Value1) Variable types: double }
begin
IF Value2 >= 0.0 THEN
    SIGNR := ABS(Value1)
ELSE IF Value2 < 0.0 THEN
    SIGNR := -ABS(Value1);
end; {function SIGN} .

```

```

(*****)
(*          SIGNI FUNCTION Integer type variable          *)
(*****)
function SIGNI(Value1, Value2 : Integer): Integer;
{Function equivalent to Fortran Sign function. Checks Value2 for its sign:
If Value2 >= 0 then Value1 = abs(Value1)
If Value2 < 0 then Value1 = -abs(Value1) Variable types: Integer }
begin
IF Value2 >= 0.0 THEN
    SIGNI := ABS(Value1)
ELSE IF Value2 < 0.0 THEN
    SIGNI := -ABS(Value1);
end; {function SIGNI}

```

```

procedure FEval(T: double; Y: YVector; var YP: YVector);
(*****)
{Procedure to evaluate the derivative of the differential equations
that have to be solved. Use this procedure to define the differential equations}
begin
    YP[1] := -Y[1]*Y[3];
    YP[2] := Y[1];
    YP[3] := Y[2];
end; {procedure FEval}

```

```

procedure FEHL(Neqn: integer; var Y: YVector; var T: double; var H: double; var YP: YVector;
    var F1: YVector; var F2: YVector; var F3: YVector; var F4: YVector;
    var F5: YVector; var S: YVector);
(*****)
{Fehlberg Fourth-Fifth order Runge Kutta method calculates new values for the following:
F1[Neqn], F2[Neqn], F3[Neqn], F4[Neqn], F5[Neqn], S[Neqn] and passes the new values
back to the calling routine. Checked for correct functioning 12.09.96}
{Define variables used only in FEHL subroutine}

```

```

var
  CH : double;
  K : integer;

begin
  CH := H/4.0;
  FOR K := 1 TO NEQN DO
    F5[K] := Y[K] + CH*YP[K];
    FEval(T + CH,F5,F1);

  CH := 3.0*H/32.0;
  FOR K := 1 to NEqn DO
    F5[K] := Y[K]+CH*(YP[K]+3.0*F1[K]);
    FEval(T + 3.0*H/8.0,F5,F2);

  CH := H/2197.0;
  FOR K := 1 TO NEqn DO
    F5[K] := Y[K]+CH*(1932.0*YP[K]+(7296.0*F2[K]-7200.0*F1[K]));
    FEval(T + 12.0*H/13.0,F5,F3);

  CH := H/4104.0;
  FOR K := 1 TO NEqn DO
    F5[K]:=Y[K]+CH*((8341.0*YP[K]-845.0*F3[K])+(29440.0*F2[K]-32832.0*F1[K]));
    FEval(T + H,F5,F4);

  CH := H/20520.0;
  FOR K := 1 TO NEQN DO
    F1[K]:=Y[K]+CH*((-6080.0*YP[K]+(9295.0*F3[K]-5643.0*F4[K]))
      +(41040.0*F1[K]-28352.0*F2[K]));
    FEval(T + H/2.0,F1,F5);

  {Compute approximate solution at T+H: Y(T+H)}
  CH := H/7618050.0;
  FOR K := 1 TO NEQN DO

    S[K]:=Y[K]+CH*((902880.0*YP[K]+(3855735.0*F3[K]
      -1371249.0*F4[K]))+(3953664.0*F2[K]+277020.0*F5[K]));
end; {procedure FEHL}
(*****)

procedure RKFS(NEQN:integer;var Y:YVector;var T:double;var Tout:double;
  var RelErr:double;var AbsErr:double;var IFlag:integer;
  var YP:YVector;var H:double;var F1:YVector;var F2:YVector;
  var F3:YVector;var F4:YVector;var F5:YVector;var SAVRE:double;
  var SAVAE:double;var NFE:integer;var KOP:integer;var INIT:integer;
  var JFlag:integer;var KFlag:integer);
(*****)
{Fehlberg Fourth-Fifth order Runge-Kutta method}
{Define variables}

var

```

```

HFAILD : boolean;
OUTPUT : boolean;
  A : double;
  AE : double;
  DT : double;
  EE : double;
EEOET : double;
ESTTOL : double;
  ET : double;
  HMin : double;
  RER : double;
  S : double;
SCALE : double;
  TOL : double;
  TOLN : double;
EPSP1 : double;
  YPK : double;
  K : integer;
MFLag : integer;

```

Const

```

  REMIN : double = 1E-12;  {minimum acceptable value of Relative Error}
  MaxNFE : double = 3000;  {restrict function evaluations to approx. MaxNFE}

```

Label

```

  5,10,20,25,30,40,45,50,55,60,65,70,80,85,90,95,100,150,200,220,250,260,270,300;

```

begin

```

{Check input parameters}
IF NEqn < 1 THEN GOTO 10;
IF (RelErr < 0.0) OR (AbsErr < 0.0) THEN GOTO 10;
MFlag := IFlag;
IF (MFlag = 0) OR (MFlag > 8) THEN GOTO 10;
IF MFlag <> 1 THEN GOTO 20;

{Compute machine epsilon}
  EPS := 1.0;
5:  EPS := EPS/2.0;
  EPSP1 := EPS + 1.0;
  IF EPSP1 > 1.0 THEN GOTO 5;
  U26 := 26.0 * EPS;
  GOTO 50;

{Invalid input parameters}
10: IFlag := 8;
  Exit;

{Check continuation possibilities}
20: IF (T = TOut) AND (KFlag <> 3) THEN GOTO 10;
  IF MFlag <> 2 THEN GOTO 25;
{IFlag = 2 or -2}
  IF (KFlag = 3) OR (INIT = 0) THEN GOTO 45;
  IF KFlag = 4 THEN GOTO 40;

```

```

    IF (KFlag = 5) AND (AbsErr = 0.0) THEN GOTO 30;
    IF (KFlag = 6) AND (RelErr <= SAVRE) AND (AbsErr <= SAVAE) THEN GOTO 30;
    GOTO 50;
{IFlag = 3,4,5,6,7 or 8}
25: IF IFlag = 3 THEN GOTO 45;
    IF IFlag = 4 THEN GOTO 40;
    IF (IFlag = 5) AND (AbsErr > 0.0) THEN GOTO 45;
{Integration cannot be continued: IFlag = 5,6,7 or 8}
30: halt;
{Reset function evaluation counter}
40: NFE := 0;
    IF MFlag = 2 THEN GOTO 50;
{Reset Flag value from previous call}
45: IFlag := JFlag;
    IF KFlag = 3 THEN
        MFlag := IFlag;
{Save input IFlag and set continuation flag for subsequent input checking}
50: JFlag := IFlag;
    KFlag := 0;
{Save error estimates}
    SAVRE := RelErr;
    SAVAE := AbsErr;
    RER := 2.0*EPS + ReMin;
    IF RelErr >= RER THEN GOTO 55;
{Relative error tolerance too small}
    RelErr := RER;
    Iflag := 3;
    KFlag := 3;
    exit;
55: DT := TOut - T;
    IF MFlag = 1 THEN GOTO 60;
    IF INIT = 0 THEN GOTO 65;
    GOTO 80;
{Initialization}
60: INIT := 0;
    KOP := 0;
    A := T;
    FEval(A, Y, YP);
    NFE := 1;
    IF T <> TOut THEN GOTO 65;
    IFlag := 2;
    Exit;
65: Init := 1;
    H := Abs(DT);
    TOLN := 0.0;
    FOR K := 1 TO NEQN DO
        begin
            TOL := RelErr*ABS(Y[K])+AbsErr;
            IF TOL <= 0.0 THEN GOTO 70;
            TOLN := TOL;
            YPK := ABS(YP[K]);

```

```

    IF YPK*POWER(H, 5) > TOL THEN
      H := Power((TOL/YPK),0.2);
    end;
70: IF TOLN <= 0.0 THEN H := 0.0;
    {Check maximum of Abs(T) and Abs(DT)}
    H := Max(H, U26*Max(ABS(T),ABS(DT)));
    {Check sign of IFLAG}
    JFlag := SIGNI(2,IFLAG);
    {Set stepsize for integration in the direction from T to TOUT}
80: H := SIGNR(H,DT);
    {Test if RKF severely impacted}
    IF ABS(H) >= 2.0*ABS(DT) THEN KOP := KOP + 1;
    IF KOP <> 100 THEN GOTO 85;
    {Unnecessary frequency of output}
    KOP := 0;
    IFlag := 7;
    Exit;
85: IF Abs(DT) > U26*ABS(T) THEN GOTO 95;
    {If too close to output point, extrapolate and return}
    FOR K := 1 TO NEqn DO
      begin
        Y[K] := Y[K] + DT*YP[K];
      end;
    A := TOUT;
    FEval(A,Y,YP);
    NFE := NFE + 1;
    GOTO 300;
    {Initialize output point indicator}
95: Output := false;
    {Avoid premature underflow}
    Scale := 2.0/RelErr;
    AE := Scale*AbsErr;
    {Step by step integration}
100: HFaild := false;
    {Set smallest allowable step size}
    HMIN := U26*Abs(T);
    {Adjust step to reach output point}
    DT := Tout-T;
    IF ABS(DT) >= 2.0*ABS(H) THEN GOTO 200;
    IF ABS(DT) > ABS(H) THEN GOTO 150;
    OUTPUT := True;
    H := DT;
    GOTO 200;
150: H := 0.5*DT;
200: IF NFE <= MAXNFE THEN GOTO 220;
    {Too much work}
    IFlag := 4;
    KFlag := 4;
    Exit;
    {Advance an approximate solution over one step of length H}
220: FEHL(NEQN,Y,T,H,YP,F1,F2,F3,F4,F5,F1);

```



```

NFE := NFE + 5;
EEOET := 0.0;
FOR K := 1 TO NEQN DO
  begin
    ET := ABS(Y[K]) + ABS(F1[K]) + AE;
    IF ET <= 0.0 THEN
      begin
        IFlag := 5;
        exit;
      end;
    EE := ABS((-2090.0*YP[K]+(21970.0*F3[K]-15048.0*F4[K]))+
      (22528.0*F2[K]-27360.0*F5[K]));
    EEOET := MAX(EEOET, EE/ET);
  end; {For K := 1 TO NEQN DO}
ESTTOL := ABS(H)*EEOET*SCALE/752400.00;
IF ESTTOL <= 1.0 THEN GOTO 260;
{Unsuccessful step}
HFAILD := true;
OUTPUT := false;
S := 0.1;
IF ESTTOL < 59049.0 THEN S := 0.9/Power(ESTTOL,0.2);
H := S*H;
IF ABS(H) > HMIN THEN GOTO 200;
{Requested error unattainable at smallest allowable step size}
IFlag := 6;
KFlag := 6;
exit;
260: T := T + H;
FOR K := 1 TO NEQN DO
  begin
    Y[K] := F1[K];
  end;
A := T;
FEval(A,Y,YP);
NFE := NFE + 1;
S := 5.0;
IF ESTTOL > 1.889568e-4 THEN S := 0.9/Power(ESTTOL,0.2);
IF HFAILD = true THEN S := MIN(S, 1.0);
H := SIGNR(MAX(S*ABS(H),HMIN), H);
IF Output = true THEN GOTO 300;
IF IFlag > 0 THEN GOTO 100;
IFLag := -2;
exit;
300: T := Tout;
IFlag := 2;
Exit;
end; {procedure RKFS}

```

```
{START MAIN PROGRAMME}
```

```
label 10;
```

```
begin
```

```
{Define the initial conditions}
```

```
Y[1] := 0.46960; {Dependent variable initial condition equivalent to Y1}
```

```
Y[2] := 0; {Dependent variable initial condition equivalent to Y3}
```

```
Y[3] := 0; {Dependent variable initial condition equivalent to Y3}
```

```
NEQN := 3; {Number of equations}
```

```
T := 0.0; {Initial value of the independent variable}
```

```
TFinal := 6; {Final value of the independent variable}
```

```
TPrint := 0.2; {Interval used to print solution to screen}
```

```
RelErr := 1.0E-9;
```

```
AbsErr := 0.0;
```

```
IFlag := 1;
```

```
Tout := T;
```

```
Writeln('T: Y[3] Y[2] Y[1]');
```

```
{Call Runge-Kutta-Fehlberg routine}
```

```
10:
```

```
RKFS(NEQN,Y,T,TOUT,RelErr,AbsErr,IFlag,Work.a1,Work.a2,Work.a3,Work.a4,Work.a5,  
Work.a6,Work.a7,Work.a8,Work.a9,Work.a10,Work.a11,Work.a12,Work.a13,Work.a14);
```

```
CASE IFlag OF
```

```
1: begin
```

```
writeln('Improper call');
```

```
halt;
```

```
end;
```

```
2: begin
```

```
Writeln('T:5:1, ',Y[3]:8:5,' ',Y[2]:8:5,' ',Y[1]:8:5);
```

```
Tout := T + TPrint;
```

```
IF T < TFinal THEN GOTO 10
```

```
ELSE halt;
```

```
end;
```

```
3: begin
```

```
Writeln('AbsErr: ', AbsErr:0:10);
```

```
Writeln('RelErr: ', RelErr:0:10);
```

```
GOTO 10;
```

```
end;
```

```
4: begin
```

```
writeln('Too many steps');
```

```
GOTO 10;
```

```
end;
```

```
5: begin
```

```
AbsErr := 1.0E-9;
```

```
Writeln('AbsErr: ', AbsErr:0:10);
```

```
Writeln('RelErr: ', RelErr:0:10);
```

```
GOTO 10;
```

```
end;
```

```
6: begin
  RelErr := 10.0*RelErr;
  Writeln('AbsErr: ', AbsErr:0:10);
  Writeln('RelErr: ', RelErr:0:10, ' Option Iflag 6');
  IFlag := 2;
  GOTO 10;
end;
7: begin
  writeln('Too much output');
  IFlag := 2;
  GOTO 10;
end;
8: begin
  writeln('Improper call');
  halt;
end;
end; {CASE IFlag OF}

end.
```